
بسم الله الرحمن الرحيم

Three dimensional nonlinear flow problems in the presence of nanoparticles

By

Taseer Muhammad

Department of Mathematics
Quaid-i-Azam University
Islamabad, Pakistan
2018

Three dimensional nonlinear flow problems in the presence of nanoparticles

By

Taseer Muhammad

Supervised By

Prof. Dr. Tasawar Hayat

Department of Mathematics
Quaid-i-Azam University
Islamabad, Pakistan
2018

Three dimensional nonlinear flow problems in the presence of nanoparticles

By

Taseer Muhammad

A THESIS SUBMITTED IN THE PARTIAL FULFILLMENT OF THE REQUIREMENT FOR THE DEGREE OF

DOCTOR OF PHILOSOPHY

IN

MATHEMATICS

Supervised By

Prof. Dr. Tasawar Hayat

Department of Mathematics
Quaid-i-Azam University
Islamabad, Pakistan
2018

Author's Declaration

I, **Taseer Muhammad** hereby state that my PhD thesis titled **Three dimensional nonlinear flow problems in the presence of nanoparticles** is my own work and has not been submitted previously by me for taking any degree from the Quaid-I-Azam University Islamabad, Pakistan or anywhere else in the country/world.

At any time if my statement is found to be incorrect even after my graduation the university has the right to withdraw my PhD degree.

Name of Student: **Taseer Muhammad**

Date: **25-01-2018**

Plagiarism Undertaking

I solemnly declare that research work presented in the thesis titled "**Three dimensional nonlinear flow problems in the presence of nanoparticles**" is solely my research work with no significant contribution from any other person. Small contribution/help wherever taken has been duly acknowledged and that complete thesis has been written by me.

I understand the zero tolerance policy of the HEC and **Quaid-I-Azam University** towards plagiarism. Therefore, I as an Author of the above titled thesis declare that no portion of my thesis has been plagiarized and any material used as reference is properly referred/cited.

I undertake that if I found guilty of any formal plagiarism in the above titled thesis even afterward of PhD degree, the university reserves the rights to withdraw/revoke my PhD degree and that HEC and the university has the right to publish my name on the HEC/University website on which names of students are placed who submitted plagiarized thesis.

Student/Author Signature:

Name: Taseer Muhammad

Three dimensional nonlinear flow problems in the presence of nanoparticles

By

Taseer Muhammad

CERTIFICATE

A DISSERTATION SUBMITTED IN THE PARTIAL FULFILLMENT OF THE REQUIREMENTS FOR THE DEGREE OF THE DOCTOR OF PHILOSOPHY

We accept this dissertation as conforming to the required standard

1. _____
Prof. Dr. Muhammad Yousaf Malik
(Chairman)

2. _____
Prof. Dr. Tasawar Hayat
(Supervisor)

3. Saleem Asghar
Prof. Dr. Saleem Asghar
Department of Mathematics
COMSATS Institute of Information Technology
Park Road Chak Shahzad
Islamabad
(External Examiner)

4. _____
Dr. Tariq Javed
Associate Professor
Department of Mathematics & Statistics
International Islamic University
H-10 Sector, Islamabad

(External Examiner)

Department of Mathematics
Quaid-i-Azam University
Islamabad, Pakistan
2018

Certificate of Approval

This is to certify that the research work presented in this thesis entitled **Three dimensional nonlinear flow problems in the presence of nanoparticles** was conducted by Mr. **Taseer Muhammad** under the kind supervision of **Prof. Dr. Tasawar Hayat**. No part of this thesis has been submitted anywhere else for any other degree. This thesis is submitted to the Department of Mathematics, Quaid-I-Azam University, Islamabad in partial fulfillment of the requirements for the degree of Doctor of Philosophy in field of Mathematics from Department of Mathematics, Quaid-i-Azam University Islamabad, Pakistan.

Student Name: **Taseer Muhammad** Signature: _____

External committee:

a) **External Examiner 1**: Signature: _____
Name: **Dr. Saleem Asghar**
Designation: Professor
Office Address: Department of Mathematics, COMSATS Institute of Information Technology, Park Road, Chak Shahzad, Islamabad.

b) **External Examiner 2**: Signature: _____
Name: **Dr. Tariq Javed**
Designation: Associate Professor
Office Address: Department of Mathematics & Statistics, International Islamic University, H-10 Sector, Islamabad.

c) **Internal Examiner** : Signature: _____
Name: **Dr. Tasawar Hayat**
Designation: Professor
Office Address: Department of Mathematics, Quaid-I-Azam University, Islamabad.

Supervisor Name: Signature: _____
Prof. Dr. Tasawar Hayat

Name of Dean/ HOD Signature: _____

Prof. Dr. Muhammad Yousuf Malik

DEDICATED TO

MY BELOVED PARENTS

AND

MY SUPERVISOR

Acknowledgements

I begin by praising the “Almighty Allah”, the Lord of the whole world who has expertized me the potential and ability to complete this dissertation. I invoke peace for Hazrat Muhammad (PBUH) the last prophet of Allah, who is forever a torch bearer of guidance for humanity as a whole.

I express my sincere and respectful admiration to my worthy supervisor **Prof. Dr. Tasawar Hayat (National Distinguished Professor)** for his scholarly guidance, mentorship and vast knowledge that helped me to embark upon this highly important work. He sets high standards for his students and he not only encourages but also guides them to meet those standards. It was a great privilege and honor for me to work under his kind supervision. I am ever indebted and obliged to him.

I would like to convey my sincere and respectful gratitude to my HOD **Mrs. Raheela Sohail** for his kind support and guidance that helped me to complete this important work. I would also like to extend my gratitude to my co-advisors **Dr. Sabir Ali Shehzad, Dr. Muhammad Farooq, Dr. Meraj Mustafa and Dr. Abdul Qayyum** for providing me useful suggestions. The discussions with them helped me to sort out the technical details of my work. I am thankful to them for being so cooperative, kind and helpful.

I want to convey my deepest thanks and compliments to my father **Javaid Asghar**, my mother **Nasreen Asghar**, my brothers **Sagheer Muhammad**, **Safeer Muhammad**, **Sameer Muhammad**, **Touqeer Muhammad** and my sister **Vardah Javaid** for their endless love, prayers, encouragement, cordial cooperation and continuous support. Their efforts and prayers

flourished me throughout my life. I would never be able to pay back the love and affection showered upon me by them. I cannot forget their kind care and their interest in my success.

At this great occasion I want to remember my these teachers Dr. Ahmed Zeeshan, Dr. Arshad Zia, Dr. Ahmer Mehmood, Dr. Muhammad Ayub, Dr. Malik Yousaf, Dr. Masood Khan, Dr. Nasir Ali, Dr. Rahmat Ellahi, Dr. Sohail Nadeem, Dr. Tayyab Kamran, Dr. Tariq Javed, Dr. Tahir Mehmood, Dr. Zaheer Abbas and Mr. Niaz Ahmad.

I have been lucky enough to have good friends in my academic and social life, and cannot forget their role in my education and university life. I want to express my unbound thanks to all my friends and colleagues especially Dr. Ashfaq Ahmad, Kamal Badshah (Late), Rana Anjum Saeed, Arsalan Aziz, Bilal Ahmad, Hamad Kiyani, Muhammad Rizwan, Zafar Ali Bhatti, Dr. Umer Farooq, Dr. Fahim Ud din, Dr. Muhammad Usman, Dr. Tehseen Abbas, Dr. Muhammad Zubair, Dr. Muhammad Waqas, Dr. Shahid Farooq, Dr. Zakir Hussain, Dr. Muhammad Azam, Dr. Anum Tanveer, Hina Zahir, Sadia Ayub, Farwa Haider, Kiran Rafique, Khalil Choudhary, Asad Hussain, Sohail Ahmad, Mumtaz Khan, Sajid Qayyum, Muhammad Ijaz Khan, Ikram Ullah, Muhammad Waleed Khan, Faisal Shah, Zahid Nisar, Tayyab Ilyas, Rana Danish Aslam, Capt. Shahzad Ali, Muhammad Muti and Atif Naveed. Thank you for the good time we have all together.

Taseer Muhammad

Preface

Nanofluids are engineered colloids made of base fluid and nanoparticles (1-100 nm). The nanoparticles colloids have certain physical characteristics that enhance their importance in industrial applications like ceramics, paints, coatings, food industries and drug delivery systems. These colloids are made of ultrafine nanoparticles. The ultra-high performance cooling is one of the major requirements of present industrial technologies. Metals (Cu, Fe, Al and Au), oxide ceramics (CuO and Al_2O_3), carbide ceramics (TiC and SiC), single, double or multiple wall nanotubes (SWCNT, DWCNT and MWCNT), semiconductors (SiO and TiO_2) and various composite materials are implemented in the production of nanoparticles and are submerged in a working fluid to make them nanofluids. The nanofluids are usually used to overcome the poor thermal performance of ordinary fluids like propylene glycol, water, oil and ethylene glycol. Nanotechnology is very useful in the development of better lubricants and oils. Such consideration is successfully implemented now in field of biomedical engineering like cancer therapy and safer surgery.

The boundary-layer flows due to stretching surface are prominent in plastic and metal industries like annealing and thinning of copper wires, drawing of stretching sheets through quiescent fluids, polymer filament or sheet extruded from a dye, manufacturing of plastic and rubber sheets, continuous cooling of fiber spinning, boundary layer along a liquid film condensation process and aerodynamic extrusion of plastic films. There is no doubt that nanofluids have vital role in the heat transfer enhancement. Thus we intend to study the boundary-layer flows in the presence of nanoparticles. It is further noted that two-dimensional flow problems in literature are much studied when compared with the three-dimensional flow problems. Keeping such facts in

mind the prime objective of present thesis is to analyze three-dimensional flow problems of nanofluids due to stretching surface. The present thesis is structured as follows.

Chapter one contains literature survey of relevant previous published works and laws of conservation of mass, momentum, energy and concentration transport. Mathematical formulation and boundary-layer expressions of Maxwell, Oldroyd-B, Jeffrey and Sisko fluids are provided. Basic concept of optimal homotopy analysis method is also included.

Chapter two addresses three-dimensional flow of viscous nanofluid in the presence of Cattaneo-Christov double diffusion. Thermal and concentration diffusions are considered by introducing Cattaneo-Christov fluxes. Novel features of Brownian motion and thermophoresis are retained. The conversion of nonlinear partial differential system to nonlinear ordinary differential system is done through suitable transformations. The obtained nonlinear systems are solved. Graphs are plotted in order to analyze that how the temperature and concentration profiles are affected by distinct physical parameters. Skin friction coefficients and rates of heat and mass transfer are numerically computed and addressed. The contents of this chapter are published in **Results in Physics 6 (2016) 897-903.**

Chapter three explores three-dimensional flow of viscous nanofluid characterizing porous space by Darcy-Forchheimer relation. Both thermal convective and zero nanoparticles mass flux conditions are utilized. The modeled systems are reduced into dimensionless expressions. The governing mathematical system is solved by optimal homotopy analysis method (OHAM). Importance of physical parameters is described through the plots. Numerical computations are presented to study skin-friction coefficients and Nusselt number. The outcomes of this chapter are published in **Results in Physics 7 (2017) 2791-2797.**

Chapter four examines three-dimensional flow of Maxwell nanofluid. Flow is generated due to a bidirectional stretching surface. Mathematical formulation is performed subject to boundary layer approach. Heat source/sink, Brownian motion and thermophoresis effects are considered. Newly developed boundary condition requiring zero nanoparticle mass flux at boundary is employed. The governing nonlinear boundary layer expressions are reduced to nonlinear ordinary differential system through appropriate transformations. The resulting nonlinear system has been solved. Graphs are plotted to examine the contributions of various physical parameters on velocities, temperature and concentration fields. Local Nusselt number is computed and examined numerically. The results of this chapter are published in **Applied Mathematics and Mechanics-English Edition 36 (2015) 747-762.**

Chapter five describes magnetohydrodynamic (MHD) three-dimensional flow of Maxwell nanofluid subject to convective boundary condition. Flow induced is by a bidirectional stretching surface. Effects of thermophoresis and Brownian motion are present. Unlike the previous cases even in the absence of nanoparticles, the correct formulation for the flow of MHD Maxwell fluid is established. Newly suggested boundary condition having zero nanoparticles mass flux is utilized. The resulting nonlinear ordinary differential systems are solved for the velocities, temperature and concentration distributions. Effects of physical parameters on temperature and concentration are plotted and examined. Numerical values of local Nusselt number are computed and analyzed. The contents of this chapter are published in **Journal of Magnetism and Magnetic Materials 389 (2015) 48-55.**

Chapter six presents three-dimensional flow of Maxwell nanofluid subject to rotating frame. Flow is induced by uniform stretching of boundary surface in one direction. Novel aspects of Brownian diffusion and thermophoresis are accounted. Boundary layer approach is invoked to

simplify the governing system of partial differential equations. Suitable variables are introduced to non-dimensionalize the relevant boundary layer expressions. Newly proposed boundary condition associated with zero nanoparticles mass flux is imposed. Uniformly valid convergent solution expressions are developed through optimal homotopy analysis method (OHAM). Graphs have been sketched in order to explore the role of embedded flow parameters. Heat transfer rate has been computed and analyzed. The outcomes of this chapter are published in **Journal of Molecular Liquids 229 (2017) 541-547.**

Chapter seven examines three-dimensional rotating flow of Maxwell fluid in the presence of nanoparticles. Flow is induced due to an exponentially stretching sheet. Optimal homotopic approach is employed for the solution of governing system. The optimal values of auxiliary parameters are computed. The optimal solution expressions of temperature and concentration are elaborated via plots by employing various values of involved parameters. Moreover the local Nusselt and Sherwood numbers are characterized by numerical data. The results of this chapter are published in **Journal of Molecular Liquids 229 (2017) 495-500.**

Chapter eight addresses three-dimensional flow of MHD Oldroyd-B nanofluid. Flow is induced by a bidirectional stretching surface. Novel attributes of Brownian motion and thermophoresis are considered. Newly developed boundary condition requiring zero nanoparticles mass flux is employed. The governing nonlinear boundary layer equations through appropriate transformations are reduced into the nonlinear ordinary differential systems. The obtained nonlinear system has been solved for the velocities, temperature and concentration profiles. The contributions of various physical parameters are studied graphically. The local Nusselt number is tabulated and discussed. The contents of this chapter are published in **Journal of Molecular Liquids 212 (2015) 272-282.**

Chapter nine explores magnetohydrodynamic (MHD) three-dimensional stretching flow of an Oldroyd-B nanofluid in the presence of heat generation/absorption and convective boundary condition. A condition associated with nanoparticles mass flux at the surface is utilized. The strong nonlinear differential equations are solved through optimal homotopy analysis method (OHAM). Effects of various physical parameters on temperature and concentration are studied. The local Nusselt number is also computed and analyzed. The outcomes of this chapter are published in **International Journal of Thermal Sciences 111 (2017) 274-288.** Chapter ten extends the analysis of chapter eight for Jeffrey nanofluid. The results of this chapter are published in **Zeitschrift für Naturforschung A 70 (2015) 225-233.** Chapter eleven presents bidirectional stretched flow of Jeffrey nanofluid subject to convective boundary condition. Modeling and computations are prepared subject to thermophoresis, Brownian motion and zero nanoparticles mass flux. Computational results for the velocities, temperature, concentration and Nusselt number are presented. The contents of this chapter are published in **Journal of Aerospace Engineering 29 (2016) 04015054.**

Chapter twelve examines combined effects of magnetic field and nanoparticles in three-dimensional flow of Sisko fluid. Nanofluid for Brownian motion, thermophoresis and zero nanoparticles mass flux at surface is adopted. Nonlinear differential systems are solved first for the convergent solutions and then analyzed. The outcomes of this chapter are published in **Advanced Powder Technology 27 (2016) 504-512.** Chapter thirteen is prepared to extend the flow analysis of previous chapter in presence of convective condition. The results of this chapter are published in **Journal of Magnetism and Magnetic Materials 413 (2016) 1-8.**

Chapter fourteen presents the major findings and some possible extensions of presented research work.

Contents

Chapter 1

Basics of liquid mechanics

1.1 Introduction

The current chapter contains survey of literature corresponding to nanoliquid, magnetohydrodynamics, extending surface, non-Newtonian fluids and Darcy-Forchheimer porous medium. Constitutive expressions of Maxwell, Oldroyd-B, Jeffrey and Sisko fluids are included. Boundary-layer expressions for three dimensional (3D) flows of non-Newtonian fluids (Sisko, Maxwell, Oldroyd-B and Jeffrey) are also given.

1.2 Background

Dilute suspensions of fibers and particles of nano-sized submerged in liquids are designated as "nanoliquids". The nanoliquids completely variation the thermal performance of these mixtures which arises e.g. density, viscosity, diffusivity and thermal conductivity. In all these physical features, thermal conductivity is the most important one because of its importance in various physical implications. The nanoparticles in generally are made of metal oxides (TiO_2, ZnO_2, Al_2O_3, SiO_2), metallic (Au, Cu), carbon (nanotubes, diamond) or any other materials. Ordinary liquid has poor conductivity. This poor conductivity can be improved greatly with the use of nanoparticles. In fact, the Brownian motion factor of nanoparticles in base liquid is important in this direction. A great amount of heat is produced in heat exchangers and microelectro mechanical processes to reduce the framework performance. Liquid thermal

conductivity is improved by nanoparticles addition just to cool such industrial processes. The nanoparticles have superficial importance in biological and engineering applications like medicine, solar cells, catalysts, electronics, optics, materials, manufacturing, glass industry, turbine blades cooling, plasma and laser cutting processes etc. Choi and Eastman [1] tentatively investigated the framework of nanoparticles and they inferred that the inclusion of nanoparticles into common base fluids is exceedingly helpful method to improve the cooling ability of ordinary fluids. Buongiorno [2] built up a two-component relation for investigating thermal energy transport in nanoliquids. The relation is based on two important slip mechanisms namely Brownian motion and thermophoresis. A sizeable information on nanoliquids have been presented in the literature. Here we present some important researches which have been reported by considering the features of thermophoretic and Brownian motion (see $[3-25]$ and several investigations therein).

The centrality of magneto nanoliquids has redesigned strikingly in biomedical industry. Such liquids have potential applications in gastric meds, cleaned devices, adroit biomaterials for wound treatment and various others. An associated alluring field can be considered for control of electrically coordinating nanoliquids to achieve the most astonishing quality thing in present day amassing. Particular examinations have been made in the past to review the enormous execution of magneto nanoliquids suspension in which the nanoparticles are in a vague demand from proteins or DNA. The magneto nanoparticles have been similarly utilized for transfer of tumor through hyperthermia, appealing resonation imaging, concentrating on sedate release, synergistic effects in immunology, asthma treatment and so forth [26] . Lin et al. [27] examined the sufficiency of MHD in unsteady pseudo-plastic nanoliquid flow past a thin film by employing heat source. Free-convective flow of MHD nanoliquid is considered by Sheikholeslami et al. [28] . Abbasi et al. [29] depicted effect of MHD in thermally and solutally stratified Maxwell nanoliquid flow by a moving surface. Hayat et al. [30] discussed MHD Sisko nanoliquid flow with magnetic field. They considered that flow generation is because of bidirectional extending surface. Heysiattalab et al. [31] dissected anisotropic conduct of magnetic nanoliquids (MNFs) at filmwise condensation by vertical surface subject to parameter directional magnetic field impact. MHD three dimensional (3D) flow of nanoliquid by convectively heated nonlinear extending surface is considered by Hayat et al. [32] . Hayat et al. [33] likewise analyzed doubly

stratified thixotropic nanoliquid flow subject to magnetic field impact. Malvandi et al. [34] examined thermal attributes in hydro-magnetic nanoliquid flow inside vertical micro-annular tube. Hayat et al. [35] investigated MHD three dimensional (3D) Oldroyd-B nanoliquid flow with heat source/sink.

The examinations of boundary-layer flows bounded by extending surface are fundamentally expanded all through the previous couple of decades because of their useful enormity in modern and innovative frameworks. Such flows incorporate into wire drawing, paper generation, expulsion of plastic sheets, drawing of plastic movies, glass fiber creation, hot rolling and various others. Thus Sakiadis [36] presented an examination to take a gander at the flow caused by continuously moving surface. At that point Crane [37] continued crafted by Sakiadis [36] for extending surface and gave a correct answer for velocity field. After innovative examination of Crane, a couple of experts have examined particular issues of extending surface. Many of examinations in literature manage two dimensional (2D) flow by extending sheet. There are uncommon examinations available in literature with respect to three-dimension (3D) flow by extending sheet. In this way Wang [38] talked about three dimensional (3D) flow bounded by extending surface. He demonstrated that established issues of axisymmetric and two dimensional (2D) flows actuated by extending surface can be viably proficient from this examination. At that point Ariel [39] inspected three dimension flow by extending surface. He gave exact and homotopic perturbation arrangements of representing framework. Hydro-magnetic unsteady three dimensional (3D) extending flow is examined by Xu et al. [40]. MHD three dimension (3D) flow saturating porous media by extending surface is analyzed by Hayat et al. [41]. Liu et al. [42] explored three dimension viscous liquid flow by exponential extending surface. Recently Hayat et al. [43] reported three dimension viscous nanoliquid flow by extending surface subject to Cattaneo-Christov double diffusion.

Recently the flow analysis of non-Newtonian fluids has gained considerable attention. Especially such fluids are experienced in the foodstuffs, plastic and metal industries, nuclear and chemical industries, bioengineering and polymeric liquids etc. All the non-Newtonian liquid expressions by means of their different properties cannot be made distinct by employing one relationship. Thus various relations are suggested in agreement with the characteristics of non-Newtonian fluids. The procedure of stress retardation and relaxation is portrayed by rate-type

non-Newtonian expressions. The most straightforward subclass of rate-type non-Newtonian liquid is named as Maxwell liquid [44] . This relation analyzed striking qualities of relaxation time. Maxwell liquid can't foresee the effect of retardation time. To anticipate the effects of both retardation and relaxation times, the Oldroyd-B liquid relation [45] has been recommended. The vast majority of organic and polymeric materials more often than not show the qualities of both retardation and relaxation times. Further the Jeffrey liquid relation [46] is a subclass of rate type non-Newtonian fluids. This liquid relation exhibits the properties of ratio of relaxation to retardation and retardation times. Then again, Sisko liquid relation [47] portrays both pseudoplastic and dilatant fluids relying upon their shear thinning and shear thickening highlights. Sisko liquid relation is a more summed up adaptation of power law relation. It comprises of both power law and viscous models. Further Sisko liquid can depict many typical properties of viscous and non-Newtonian liquids through selection of the various material variables.

The phenomenon of flow transport in porous space is a subject of recent advancements in geophysical and engineering processes. These processes are encountered in the applications like frameworks of ground water, grain storage, gas-cleaning filtration, vessels of gas-cooled reactors, insulation of granular and fiber, machines of high power density, petroleum reservoirs, porous bearings, porous pipes, blood flow via arteries or lungs, casting solidification, fossil fuel beds etc. These applications have attained the potential interest of engineers and scientists from different fields. Much works corresponding to porous media problems are dealt with by utilizing the Darcy's theory [48]. The main disadvantage of this theory is that it works only for those problems which are modeled by accounting low porosity and smaller velocities. Many of practical implications involve the non-uniform porous distribution and higher flow transport. In such circumstances, the Darcy's theory fails to describe the exact nature of physical phenomenon. For this purpose, the involvement of non-Darcian effects is accounted to describe the exact conduct of physical problem. Forchheimer [49] considered such factors by using the additional term through square velocity in Darcian velocity expression. Muskat [50] verified that this law holds for higher Reynolds parameter. Seddeek [51] utilized the Darcy-Forchheimer theory to explore the mixed convective thermophoretic flow saturated in porous space. Convective flow with radiation and temperature-dependent viscosity in non-Darcian porous space has been disclosed by Pal and Mondal [52]. Pal and Chatterjee [53] elaborated the features of

micropolar liquid flow in non-Darcy porous space with radiation and temperature-dependent heat source. Singh et al. [54] developed an analysis of hydro-magnetic time-dependent flow in porous channel by employing the Darcy-Brinkman-Forchheimer expression. Gireesha et al. [55] numerically computed the problem of liquid-particle submersion in viscous liquid flow saturated in non-Darcy porous medium. Hayat et al. [56] described properties of temperature-dependent conductivity in Darcy-Forchheimer porous space. Shehzad et al. [57] analytically explored the features of non-linear convective flow of Oldroyd-B liquid in non-Darcian space with Cattaneo-Christov theory of heat diffusion. Further relevant investigations on Darcy-Forchheimer flow can be quoted through the studies [58 – 66] and various attempts therein.

1.3 Basic laws

1.3.1 Law of mass conservation

It is stated that the total mass in any closed framework is conserved. Differential form of law of mass conservation is

$$\frac{\partial \rho}{\partial t} + \boldsymbol{\nabla} \cdot (\rho \mathbf{V}) = 0, \tag{1.1}$$

here $\mathbf{V}$ exhibits liquid velocity and ρ represents liquid density. The above expression for an incompressible liquid is

$$\boldsymbol{\nabla} \cdot \mathbf{V} = 0. \tag{1.2}$$

1.3.2 Law of momentum conservation

It is stated that the total linear momentum of a closed framework is conserved. Differential form of law of momentum conservation is given by

$$\rho \frac{d\mathbf{V}}{dt} = \boldsymbol{\nabla} \cdot \boldsymbol{\tau} + \rho \mathbf{b}. \tag{1.3}$$

Here $\boldsymbol{\tau} = -p\mathbf{I} + \mathbf{S}$ stands for Cauchy stress tensor, $\mathbf{I}$ for identity tensor, p for pressure, $\mathbf{b}$ for body force, $\mathbf{S}$ for extra stress tensor and d/dt for material time derivative. Velocity field and

Cauchy stress tensor for three-diemensional (3D) flow are given by

$$\mathbf{V} = [u(x,y,z), v(x,y,z), w(x,y,z)], \tag{1.4}$$

$$\boldsymbol{\tau} = \begin{bmatrix} \sigma_{xx} & \tau_{xy} & \tau_{xz} \\ \tau_{yx} & \sigma_{yy} & \tau_{yz} \\ \tau_{zx} & \tau_{zy} & \sigma_{zz} \end{bmatrix}, \tag{1.5}$$

in which u, v, w stand for velocity components along $x-$, $y-$ and $z-$directions respectively, τ_{xy}, τ_{xz}, τ_{yx}, τ_{yz}, τ_{zx} and τ_{zy} depict shear stresses and σ_{xx}, σ_{yy} and σ_{zz} represent normal stresses. Expression (1.3) in scalar form is expressed by

$$\rho\left(\frac{\partial u}{\partial t} + u\frac{\partial u}{\partial x} + v\frac{\partial u}{\partial y} + w\frac{\partial u}{\partial z}\right) = \frac{\partial(\sigma_{xx})}{\partial x} + \frac{\partial(\tau_{xy})}{\partial y} + \frac{\partial(\tau_{xz})}{\partial z} + \rho b_x, \tag{1.6}$$

$$\rho\left(\frac{\partial v}{\partial t} + u\frac{\partial v}{\partial x} + v\frac{\partial u}{\partial y} + w\frac{\partial v}{\partial z}\right) = \frac{\partial(\tau_{yx})}{\partial x} + \frac{\partial(\sigma_{yy})}{\partial y} + \frac{\partial(\tau_{yz})}{\partial z} + \rho b_y, \tag{1.7}$$

$$\rho\left(\frac{\partial w}{\partial t} + u\frac{\partial w}{\partial x} + v\frac{\partial w}{\partial y} + w\frac{\partial w}{\partial z}\right) = \frac{\partial(\tau_{zx})}{\partial x} + \frac{\partial(\tau_{zy})}{\partial y} + \frac{\partial(\sigma_{zz})}{\partial z} + \rho b_z, \tag{1.8}$$

where b_x, b_y and b_z depict components of body force in $x-$, $y-$ and $z-$axes respectively.

1.3.3 Law of energy conservation

The energy expression for a nanoliquid can be written as

$$\rho c_p \frac{dT}{dt} = -\boldsymbol{\nabla}\cdot\mathbf{q} + h_p \boldsymbol{\nabla}\cdot\mathbf{j}_p, \tag{1.9}$$

where c_p stands for specific heat, h_p for specific enthalpy of nanoparticles, T for temperature, $\mathbf{j}_p$ for nanoparticles diffusion mass flux and $\mathbf{q}$ for energy flux. The energy and nanoparticles diffusion mass fluxes are

$$\mathbf{q} = -k\boldsymbol{\nabla}T + h_p\mathbf{j}_p, \tag{1.10}$$

$$\mathbf{j}_p = \rho_p D_B \boldsymbol{\nabla}C - \rho_p D_T \frac{\boldsymbol{\nabla}T}{T_\infty}, \tag{1.11}$$

where k stands for thermal conductivity, ρ_p for nanoparticle mass density, D_B for Brownian movement coefficient, D_T for thermophoretic diffusion coefficient and C for nanoparticle con-

centration. Now Eq. (1.9) becomes

$$\rho c_p \frac{dT}{dt} = k\boldsymbol{\nabla}^2 T + \rho_p c_p \left[D_B \boldsymbol{\nabla} C.\boldsymbol{\nabla} T + D_T \frac{\boldsymbol{\nabla} T.\boldsymbol{\nabla} T}{T_\infty} \right], \tag{1.12}$$

which is the energy expression for nanoliquid.

1.3.4 Law of concentration conservation

The concentration expression for nanoliquid is

$$\frac{dC}{dt} = -\frac{1}{\rho_p} \boldsymbol{\nabla}.\mathbf{j}_p, \tag{1.13}$$

After employing Eq. (1.11) , we have

$$\frac{dC}{dt} = D_B \boldsymbol{\nabla}^2 C + D_T \frac{\boldsymbol{\nabla}^2 T}{T_\infty}, \tag{1.14}$$

which is the concentration expression for nanoliquid.

1.4 Boundary-layer expressions of non-Newtonian fluids

1.4.1 Maxwell liquid

Extra stress tensor $\mathbf{S}$ for Maxwell liquid is

$$\left(1 + \lambda_1 \frac{D}{Dt}\right) \mathbf{S} = \mathbf{S} + \lambda_1 \frac{D\mathbf{S}}{Dt} = \mu \mathbf{A}_1, \tag{1.15}$$

where λ_1 stands for relaxation time, D/Dt for covariant differentiation, μ for dynamic viscosity and $\mathbf{A}_1$ for first Rivlin-Erickson tensor. First Rivlin-Erickson tensor is

$$\mathbf{A}_1 = (\operatorname{grad} \mathbf{V})^{T'} + \operatorname{grad} \mathbf{V}, \tag{1.16}$$

in which T' exhibits matrix transpose. For three dimensional (3D) flow, we get

$$\mathbf{A}_1 = \begin{bmatrix} 2\frac{\partial u}{\partial x} & \frac{\partial u}{\partial y}+\frac{\partial v}{\partial x} & \frac{\partial u}{\partial z}+\frac{\partial w}{\partial x} \\ \frac{\partial u}{\partial y}+\frac{\partial v}{\partial x} & 2\frac{\partial v}{\partial y} & \frac{\partial v}{\partial z}+\frac{\partial w}{\partial y} \\ \frac{\partial u}{\partial z}+\frac{\partial w}{\partial x} & \frac{\partial v}{\partial z}+\frac{\partial w}{\partial y} & 2\frac{\partial w}{\partial z} \end{bmatrix}. \tag{1.17}$$

For tensor $\mathbf{S}$ for rank two, vector $\mathbf{b_1}$ and scalar φ, we have

$$\frac{D\mathbf{S}}{Dt} = \frac{\partial \mathbf{S}}{\partial t} + (\mathbf{V}\cdot\boldsymbol{\nabla})\mathbf{S} - \mathbf{S}(\operatorname{grad}\mathbf{V})^{T'} - (\operatorname{grad}\mathbf{V})\mathbf{S}, \tag{1.18}$$

$$\frac{D\mathbf{b_1}}{Dt} = \frac{\partial \mathbf{b_1}}{\partial t} + (\mathbf{V}\cdot\boldsymbol{\nabla})\mathbf{b_1} - (\operatorname{grad}\mathbf{V})\mathbf{b_1}, \tag{1.19}$$

$$\frac{D\varphi}{Dt} = \frac{\partial \varphi}{\partial t} + (\mathbf{V}\cdot\boldsymbol{\nabla})\varphi. \tag{1.20}$$

Application of $\left(1+\lambda_1\frac{D}{Dt}\right)$ on Eq. (1.3), we get following expression in absence of body forces

$$\rho\left(1+\lambda_1\frac{D}{Dt}\right)\frac{d\mathbf{V}}{dt} = -\left(1+\lambda_1\frac{D}{Dt}\right)\nabla p + \left(1+\lambda_1\frac{D}{Dt}\right)(\nabla\cdot\mathbf{S}). \tag{1.21}$$

By using the process as in ref. [67], we get

$$\frac{D}{Dt}(\nabla\cdot) = \nabla\cdot\left(\frac{D}{Dt}\right). \tag{1.22}$$

Hence above expression in the absence of pressure gradient becomes

$$\rho\left(1+\lambda_1\frac{D}{Dt}\right)\frac{d\mathbf{V}}{dt} = \mu\left(\nabla\cdot\mathbf{A}_1\right). \tag{1.23}$$

Thus above expression for steady Maxwell liquid flow is expressed by

$$u\frac{\partial u}{\partial x}+v\frac{\partial u}{\partial y}+w\frac{\partial u}{\partial z}+\lambda_1\begin{pmatrix} u^2\frac{\partial^2 u}{\partial x^2}+v^2\frac{\partial^2 u}{\partial y^2}+w^2\frac{\partial^2 u}{\partial z^2} \\ +2uv\frac{\partial^2 u}{\partial x\partial y}+2vw\frac{\partial^2 u}{\partial y\partial z}+2uw\frac{\partial^2 u}{\partial x\partial z}\end{pmatrix} = \nu\left(\frac{\partial^2 u}{\partial x^2}+\frac{\partial^2 u}{\partial y^2}+\frac{\partial^2 u}{\partial z^2}\right), \tag{1.24}$$

$$u\frac{\partial v}{\partial x}+v\frac{\partial v}{\partial y}+w\frac{\partial v}{\partial z}+\lambda_1\begin{pmatrix} u^2\frac{\partial^2 v}{\partial x^2}+v^2\frac{\partial^2 v}{\partial y^2}+w^2\frac{\partial^2 v}{\partial z^2} \\ +2uv\frac{\partial^2 v}{\partial x\partial y}+2vw\frac{\partial^2 v}{\partial y\partial z}+2uw\frac{\partial^2 v}{\partial x\partial z}\end{pmatrix} = \nu\left(\frac{\partial^2 v}{\partial x^2}+\frac{\partial^2 v}{\partial y^2}+\frac{\partial^2 v}{\partial z^2}\right), \tag{1.25}$$

$$u\frac{\partial w}{\partial x}+v\frac{\partial w}{\partial y}+w\frac{\partial w}{\partial z}+\lambda_1\left(\begin{array}{c}u^2\frac{\partial^2 w}{\partial x^2}+v^2\frac{\partial^2 w}{\partial y^2}+w^2\frac{\partial^2 w}{\partial z^2}\\+2uv\frac{\partial^2 w}{\partial x\partial y}+2vw\frac{\partial^2 w}{\partial y\partial z}+2uw\frac{\partial^2 w}{\partial x\partial z}\end{array}\right)=\nu\left(\frac{\partial^2 w}{\partial x^2}+\frac{\partial^2 w}{\partial y^2}+\frac{\partial^2 w}{\partial z^2}\right). \tag{1.26}$$

By employing the boundary-layer approach [68], orders for u, v, x and y and w and z are 1 and δ. Then $w-$momentum expression vanishes automatically because it has order δ. Thus expressions of boundary-layer for 3D Maxwell liquid flow are

$$u\frac{\partial u}{\partial x}+v\frac{\partial u}{\partial y}+w\frac{\partial u}{\partial z}+\lambda_1\left(\begin{array}{c}u^2\frac{\partial^2 u}{\partial x^2}+v^2\frac{\partial^2 u}{\partial y^2}+w^2\frac{\partial^2 u}{\partial z^2}\\+2uv\frac{\partial^2 u}{\partial x\partial y}+2vw\frac{\partial^2 u}{\partial y\partial z}+2uw\frac{\partial^2 u}{\partial x\partial z}\end{array}\right)=\nu\frac{\partial^2 u}{\partial z^2}, \tag{1.27}$$

$$u\frac{\partial v}{\partial x}+v\frac{\partial v}{\partial y}+w\frac{\partial v}{\partial z}+\lambda_1\left(\begin{array}{c}u^2\frac{\partial^2 v}{\partial x^2}+v^2\frac{\partial^2 v}{\partial y^2}+w^2\frac{\partial^2 v}{\partial z^2}\\+2uv\frac{\partial^2 v}{\partial x\partial y}+2vw\frac{\partial^2 v}{\partial y\partial z}+2uw\frac{\partial^2 v}{\partial x\partial z}\end{array}\right)=\nu\frac{\partial^2 v}{\partial z^2}. \tag{1.28}$$

1.4.2 Oldroyd-B liquid

Extra stress tensor $\mathbf{S}$ for an Oldroyd-B liquid is expressed by

$$\left(1+\lambda_1\frac{D}{Dt}\right)\mathbf{S}=\mathbf{S}+\lambda_1\frac{D\mathbf{S}}{Dt}=\mu\left(1+\lambda_2\frac{D}{Dt}\right)\mathbf{A}_1, \tag{1.29}$$

in which λ_2 exhibits retardation time and law of momentum conservation in the absence of body force and pressure gradient can be written by

$$\rho\left(1+\lambda_1\frac{D}{Dt}\right)\frac{d\mathbf{V}}{dt}=\mu\left(1+\lambda_2\frac{D}{Dt}\right)(\nabla\cdot\mathbf{A}_1). \tag{1.30}$$

Scalar forms of expressions of boundary-layer in present situation are

$$\begin{aligned}&u\frac{\partial u}{\partial x}+v\frac{\partial u}{\partial y}+w\frac{\partial u}{\partial z}+\lambda_1\left(\begin{array}{c}u^2\frac{\partial^2 u}{\partial x^2}+v^2\frac{\partial^2 u}{\partial y^2}+2uv\frac{\partial^2 u}{\partial x\partial y}\\+w^2\frac{\partial^2 u}{\partial z^2}+2vw\frac{\partial^2 u}{\partial y\partial z}+2uw\frac{\partial^2 u}{\partial x\partial z}\end{array}\right)\\ =\;&\nu\left(\frac{\partial^2 u}{\partial z^2}+\lambda_2\left(\begin{array}{c}u\frac{\partial^3 u}{\partial x\partial z^2}+v\frac{\partial^3 u}{\partial y\partial z^2}-\frac{\partial u}{\partial x}\frac{\partial^2 u}{\partial z^2}\\+w\frac{\partial^3 u}{\partial z^3}-\frac{\partial u}{\partial y}\frac{\partial^2 v}{\partial z^2}-\frac{\partial u}{\partial z}\frac{\partial^2 w}{\partial z^2}\end{array}\right)\right),\end{aligned} \tag{1.31}$$

$$u\frac{\partial v}{\partial x}+v\frac{\partial v}{\partial y}+w\frac{\partial v}{\partial z}+\lambda_1\left(\begin{array}{c}u^2\frac{\partial^2 v}{\partial x^2}+v^2\frac{\partial^2 v}{\partial y^2}+w^2\frac{\partial^2 v}{\partial z^2}\\+2uv\frac{\partial^2 v}{\partial x\partial y}+2vw\frac{\partial^2 v}{\partial y\partial z}+2uw\frac{\partial^2 v}{\partial x\partial z}\end{array}\right)$$
$$=\quad \nu\left(\frac{\partial^2 u}{\partial z^2}+\lambda_2\left(\begin{array}{c}u\frac{\partial^3 v}{\partial x\partial z^2}+v\frac{\partial^3 v}{\partial y\partial z^2}+w\frac{\partial^3 v}{\partial z^3}\\-\frac{\partial v}{\partial x}\frac{\partial^2 v}{\partial z^2}-\frac{\partial v}{\partial y}\frac{\partial^2 v}{\partial z^2}-\frac{\partial v}{\partial z}\frac{\partial^2 w}{\partial z^2}\end{array}\right)\right). \tag{1.32}$$

1.4.3 Jeffrey liquid

Extra stress tensor for Jeffrey liquid can be mentioned as follows:

$$\mathbf{S}=\frac{\mu}{1+\lambda^*}\left(\mathbf{A}_1+\lambda_2\frac{d\mathbf{A}_1}{dt}\right). \tag{1.33}$$

Here λ^* stands for relaxation to retardation times ratio. Moreover tensor of extra stress $\mathbf{S}$ gives

$$S_{xx}=\frac{\mu}{1+\lambda^*}\left(2\frac{\partial u}{\partial x}+\lambda_2\left(u\frac{\partial}{\partial x}+v\frac{\partial}{\partial y}+w\frac{\partial}{\partial z}\right)2\frac{\partial u}{\partial x}\right), \tag{1.34}$$

$$S_{xy}=\frac{\mu}{1+\lambda^*}\left(\left(\frac{\partial u}{\partial y}+\frac{\partial v}{\partial x}\right)+\lambda_2\left(u\frac{\partial}{\partial x}+v\frac{\partial}{\partial y}+w\frac{\partial}{\partial z}\right)\left(\frac{\partial u}{\partial y}+\frac{\partial v}{\partial x}\right)\right)=S_{yx}, \tag{1.35}$$

$$S_{xz}=\frac{\mu}{1+\lambda^*}\left(\left(\frac{\partial u}{\partial z}+\frac{\partial w}{\partial x}\right)+\lambda_2\left(u\frac{\partial}{\partial x}+v\frac{\partial}{\partial y}+w\frac{\partial}{\partial z}\right)\left(\frac{\partial u}{\partial z}+\frac{\partial w}{\partial x}\right)\right)=S_{zx}, \tag{1.36}$$

$$S_{yy}=\frac{\mu}{1+\lambda^*}\left(2\frac{\partial v}{\partial y}+\lambda_2\left(u\frac{\partial}{\partial x}+v\frac{\partial}{\partial y}+w\frac{\partial}{\partial z}\right)2\frac{\partial v}{\partial y}\right), \tag{1.37}$$

$$S_{yz}=\frac{\mu}{1+\lambda^*}\left(\left(\frac{\partial v}{\partial z}+\frac{\partial w}{\partial y}\right)+\lambda_2\left(u\frac{\partial}{\partial x}+v\frac{\partial}{\partial y}+w\frac{\partial}{\partial z}\right)\left(\frac{\partial v}{\partial z}+\frac{\partial w}{\partial y}\right)\right)=S_{zy}, \tag{1.38}$$

$$S_{zz}=\frac{\mu}{1+\lambda^*}\left(2\frac{\partial w}{\partial z}+\lambda_2\left(u\frac{\partial}{\partial x}+v\frac{\partial}{\partial y}+w\frac{\partial}{\partial z}\right)2\frac{\partial w}{\partial z}\right). \tag{1.39}$$

The law of momentum conservation for Jeffrey liquid provides

$$\rho\left(u\frac{\partial u}{\partial x}+v\frac{\partial u}{\partial y}+w\frac{\partial u}{\partial z}\right)=\frac{\partial}{\partial x}S_{xx}+\frac{\partial}{\partial y}S_{xy}+\frac{\partial}{\partial z}S_{xz}, \tag{1.40}$$

$$\rho\left(u\frac{\partial v}{\partial x}+v\frac{\partial v}{\partial y}+w\frac{\partial v}{\partial z}\right)=\frac{\partial}{\partial x}S_{yx}+\frac{\partial}{\partial y}S_{yy}+\frac{\partial}{\partial z}S_{yz}, \tag{1.41}$$

$$\rho\left(u\frac{\partial w}{\partial x}+v\frac{\partial w}{\partial y}+w\frac{\partial w}{\partial z}\right)=\frac{\partial}{\partial x}S_{zx}+\frac{\partial}{\partial y}S_{zy}+\frac{\partial}{\partial z}S_{zz}, \tag{1.42}$$

where body forces and pressure gradient are absent. By putting S_{xx}, S_{xy}, S_{xz}, S_{yx}, S_{yy}, S_{yz}, S_{zx}, S_{zy} and S_{zz} in expressions $(1.40)-(1.42)$ and then employing boundary layer approximations one has

$$u\frac{\partial u}{\partial x}+v\frac{\partial u}{\partial y}+w\frac{\partial u}{\partial z}=\frac{\nu}{1+\lambda^*}\left(\frac{\partial^2 u}{\partial z^2}+\lambda_2\left(\begin{array}{l}\frac{\partial u}{\partial z}\frac{\partial^2 u}{\partial x\partial z}+\frac{\partial v}{\partial z}\frac{\partial^2 u}{\partial y\partial z}+\frac{\partial w}{\partial z}\frac{\partial^2 u}{\partial z^2}\\ +u\frac{\partial^3 u}{\partial x\partial z^2}+v\frac{\partial^3 u}{\partial y\partial z^2}+w\frac{\partial^3 u}{\partial z^3}\end{array}\right)\right), \tag{1.43}$$

$$u\frac{\partial v}{\partial x}+v\frac{\partial v}{\partial y}+w\frac{\partial v}{\partial z}=\frac{\nu}{1+\lambda^*}\left(\frac{\partial^2 v}{\partial z^2}+\lambda_2\left(\begin{array}{l}\frac{\partial u}{\partial z}\frac{\partial^2 v}{\partial x\partial z}+\frac{\partial v}{\partial z}\frac{\partial^2 v}{\partial y\partial z}+\frac{\partial w}{\partial z}\frac{\partial^2 v}{\partial z^2}\\ +u\frac{\partial^3 v}{\partial x\partial z^2}+v\frac{\partial^3 v}{\partial y\partial z^2}+w\frac{\partial^3 v}{\partial z^3}\end{array}\right)\right). \tag{1.44}$$

1.4.4 Sisko liquid

The extra stress tensor for Sisko liquid can be defined below:

$$\mathbf{S}=\left[a+b\left|\sqrt{\frac{1}{2}tr(\mathbf{A}_1^2)}\right|^{n-1}\right]\mathbf{A}_1. \tag{1.45}$$

Here a, b and n $(n\geq 0)$ are the material constants of the Sisko liquid. Moreover extra stress tensor $\mathbf{S}$ in components form is defined by

$$S_{xx}=\left(a+b\left|\frac{1}{2}tr(\mathbf{A}_1^2)\right|^{\frac{n-1}{2}}\right)\left(2\frac{\partial u}{\partial x}\right), \tag{1.46}$$

$$S_{xy}=\left(a+b\left|\frac{1}{2}tr(\mathbf{A}_1^2)\right|^{\frac{n-1}{2}}\right)\left(\frac{\partial u}{\partial y}+\frac{\partial v}{\partial x}\right)=S_{yx}, \tag{1.47}$$

$$S_{xz}=\left(a+b\left|\frac{1}{2}tr(\mathbf{A}_1^2)\right|^{\frac{n-1}{2}}\right)\left(\frac{\partial u}{\partial z}+\frac{\partial w}{\partial x}\right)=S_{zx}, \tag{1.48}$$

$$S_{yy}=\left(a+b\left|\frac{1}{2}tr(\mathbf{A}_1^2)\right|^{\frac{n-1}{2}}\right)\left(2\frac{\partial v}{\partial y}\right), \tag{1.49}$$

$$S_{yz}=\left(a+b\left|\frac{1}{2}tr(\mathbf{A}_1^2)\right|^{\frac{n-1}{2}}\right)\left(\frac{\partial v}{\partial z}+\frac{\partial w}{\partial y}\right)=S_{zy}, \tag{1.50}$$

$$S_{zz}=\left(a+b\left|\frac{1}{2}tr(\mathbf{A}_1^2)\right|^{\frac{n-1}{2}}\right)\left(2\frac{\partial w}{\partial z}\right), \tag{1.51}$$

where

$$\left|\frac{1}{2}tr(\mathbf{A}_1^2)\right|^{\frac{n-1}{2}} = \left|2\left(\frac{\partial u}{\partial x}\right)^2+2\left(\frac{\partial v}{\partial y}\right)^2+2\left(\frac{\partial w}{\partial z}\right)^2 + \left(\frac{\partial u}{\partial y}+\frac{\partial v}{\partial x}\right)^2+\left(\frac{\partial u}{\partial z}+\frac{\partial w}{\partial x}\right)^2+\left(\frac{\partial v}{\partial z}+\frac{\partial w}{\partial y}\right)^2\right|. \tag{1.52}$$

Law of momentum conservation for Sisko liquid provides

$$\rho\left(u\frac{\partial u}{\partial x}+v\frac{\partial u}{\partial y}+w\frac{\partial u}{\partial z}\right)=\frac{\partial}{\partial x}S_{xx}+\frac{\partial}{\partial y}S_{xy}+\frac{\partial}{\partial z}S_{xz}, \tag{1.53}$$

$$\rho\left(u\frac{\partial v}{\partial x}+v\frac{\partial v}{\partial y}+w\frac{\partial v}{\partial z}\right)=\frac{\partial}{\partial x}S_{yx}+\frac{\partial}{\partial y}S_{yy}+\frac{\partial}{\partial z}S_{yz}, \tag{1.54}$$

$$\rho\left(u\frac{\partial w}{\partial x}+v\frac{\partial w}{\partial y}+w\frac{\partial w}{\partial z}\right)=\frac{\partial}{\partial x}S_{zx}+\frac{\partial}{\partial y}S_{zy}+\frac{\partial}{\partial z}S_{zz}, \tag{1.55}$$

where body forces and pressure gradient have been omitted. By putting the estimations of S_{xx}, S_{xy}, S_{xz}, S_{yx}, S_{yy}, S_{yz}, S_{zx}, S_{zy} and S_{zz} in expressions (1.53) $-$ (1.55) and then employing approximations of boundary-layer we finally get

$$u\frac{\partial u}{\partial x}+v\frac{\partial u}{\partial y}+w\frac{\partial u}{\partial z}=\frac{a}{\rho}\frac{\partial^2 u}{\partial z^2}+\frac{b}{\rho}\frac{\partial}{\partial z}\left[\frac{\partial u}{\partial z}\left|\frac{\partial u}{\partial z}\right|^{n-1}\right], \tag{1.56}$$

$$u\frac{\partial v}{\partial x}+v\frac{\partial v}{\partial y}+w\frac{\partial v}{\partial z}=\frac{a}{\rho}\frac{\partial^2 v}{\partial z^2}+\frac{b}{\rho}\frac{\partial}{\partial z}\left[\frac{\partial v}{\partial z}\left|\frac{\partial v}{\partial z}\right|^{n-1}\right]. \tag{1.57}$$

1.5 Solutions by OHAM

The optimal homotopic analysis technique (OHAM) is utilized to find the approximate arrangements of highly nonlinear problems. The optimal homotopy analysis technique gives us a convenient way to control the convergence of approximation homotopy arrangements and adjust convergence regions. For the fundamental concept of optimal homotopy analysis technique, we assume a nonlinear differential expression

$$\mathcal{N}\left[u\left(x\right)\right]=0, \tag{1.58}$$

in which $\mathcal{N}$ stands for nonlinear operator, $u(x)$ for unknown function and x for independent parameter.

1.5.1 Zeroth-order deformation problems

$$(1-p)\,\mathcal{L}\left[\hat{u}(x;p)-u_0(x)\right]=p\hbar\mathcal{N}\left[\hat{u}(x;p)\right], \tag{1.59}$$

in which $u_0(x)$ stands for the initial approximation, $\mathcal{L}$ for auxiliary linear operator, $p\in[0,1]$ for embedding parameter, $\hbar$ for nonzero auxiliary parameter and $\hat{u}(x;p)$ for the unknown function of x and p.

1.5.2 mth-order deformation problems

Differentiating m times zeroth approximation i.e., Eq. (1.59) w.r.t. p then dividing via $m!$ and finally inserting $p=0$ we have expression for mth-order

$$\mathcal{L}\left[u_m(x)-\chi_m u_{m-1}(x)\right]=\hbar\mathcal{R}_m(x), \tag{1.60}$$

$$\mathcal{R}_m(x)=\frac{1}{(m-1)!}\frac{\partial^m\mathcal{N}\left[\hat{u}(x;p)\right]}{\partial p^m}\bigg|_{p=0}, \tag{1.61}$$

where

$$\chi_m=\begin{cases}0, & m\leq 1\\ 1, & m>1\end{cases}. \tag{1.62}$$

Setting $p=0$ and $p=1$ one has

$$\hat{u}(x;0)=u_0(x)\quad\text{and}\quad\hat{u}(x;1)=u(x). \tag{1.63}$$

The arrangement $\hat{u}(x;p)$ varies from initial deformation $u_0(x)$ to desired final arrangement $u(x)$ when p goes from 0 to 1. Using Taylor series expansion one has

$$\hat{u}(x;p)=u_0(x)+\sum_{m=1}^{\infty}u_m(x)\,p^m,\quad u_m(x)=\frac{1}{m!}\frac{\partial^m\hat{u}(x;p)}{\partial p^m}\bigg|_{p=0}. \tag{1.64}$$

For $p=1$ we get

$$u(x)=u_0(x)+\sum_{m=1}^{\infty}u_m(x). \tag{1.65}$$

1.5.3 Optimal convergence control parameter

The nonzero auxiliary parameter $\hbar$ in homotopy arrangements control area of convergence and also homotopy arrangements rate. To find optimal data of convergence control parameter $\hbar$, we employed minimization idea by defining squared residual errors as proposed by Liao [69] .

$$\varepsilon_m = \frac{1}{k+1}\sum_{j=0}^{k}\left[\mathcal{N}\left(\sum_{i=0}^{m} u_m(\zeta)\right)_{\zeta=j\delta\zeta}\right]^2, \tag{1.66}$$

where ε_m is the total residual square error.

Chapter 2

Three-dimensional flow of nanofluid with Cattaneo-Christov double diffusion

Three dimensional (3D) flow of viscous nanoliquid by extending surface has been explored subject to Cattaneo-Christov double diffusion. Concentration and thermal diffusions are described by presenting Cattaneo-Christov fluxes. The novel characteristics in regards to Brownian dispersion and thermophoresis are retained. The variation in partial differential framework (PDEs) to nonlinear ordinary differential framework (ODEs) is done through reasonable transformations. The subsequent nonlinear frameworks are solved. Plots have been shown keeping in mind the end goal to examine that how concentration and temperature profiles are influenced by distinct relevant flow variables. Besides skin frictions and rates of mass and heat transfer are numerically figured and addressed. Our findings delineate that concentration and temperature distributions are diminishing elements of concentration and temperature relaxation variables respectively.

2.1 Formulation

We elaborate three dimensional (3D) flow of viscous nanoliquid by linear extending surface subject to constant wall concentration and temperature. The Brownian movement and ther-

mophoresis perspectives are accounted. Here $x-$ and $y-$axes are along the extending surface while $z-$axis is normal to surface. Let $U_w(x) = ax$ and $V_w(y) = by$ indicate extending velocities along the $x-$ and $y-$directions respectively. Mass and heat transfer are examined by means of Cattaneo-Christov double diffusion articulations. Resulting expressions for boundary-layer considerations are

$$\frac{\partial u}{\partial x} + \frac{\partial v}{\partial y} + \frac{\partial w}{\partial z} = 0, \tag{2.1}$$

$$u\frac{\partial u}{\partial x} + v\frac{\partial u}{\partial y} + w\frac{\partial u}{\partial z} = \nu\frac{\partial^2 u}{\partial z^2}, \tag{2.2}$$

$$u\frac{\partial v}{\partial x} + v\frac{\partial v}{\partial y} + w\frac{\partial v}{\partial z} = \nu\frac{\partial^2 v}{\partial z^2}. \tag{2.3}$$

Note that u, v and w depict velocities in $x-$, $y-$ and $z-$directions while $\nu(=\mu/\rho_f)$, ρ_f and μ stand for kinematic viscosity, density and dynamic viscosity respectively. Cattaneo-Christov double diffusion hypothesis has been proposed in portraying concentration and temperature diffusions with mass and heat fluxes relaxations respectively. At that point frame indifferent generalization with respect to Fourier's and Fick's laws (which are termed as Cattaneo-Christov anomalous diffusion expressions) are

$$\mathbf{q} + \lambda_E\left(\frac{\partial \mathbf{q}}{\partial t} + \mathbf{V}.\nabla\mathbf{q} - \mathbf{q}.\nabla\mathbf{V} + (\nabla.\mathbf{V})\,\mathbf{q}\right) = -k\nabla T, \tag{2.4}$$

$$\mathbf{J} + \lambda_C\left(\frac{\partial \mathbf{J}}{\partial t} + \mathbf{V}.\nabla\mathbf{J} - \mathbf{J}.\nabla\mathbf{V} + (\nabla.\mathbf{V})\,\mathbf{J}\right) = -D_B\nabla C, \tag{2.5}$$

in which k stands for thermal conductivity, D_B for Brownian diffusivity, $\mathbf{J}$ and $\mathbf{q}$ for mass and heat fluxes respectively, λ_C and λ_E for relaxation time of mass and heat fluxes respectively. Fundamental Fourier's and Fick's laws are deduced by putting $\lambda_E = \lambda_C = 0$ in Eqs. (2.4) and (2.5). By using incompressibility condition ($\nabla.\mathbf{V} = 0$) and steady flow with ($\frac{\partial \mathbf{q}}{\partial t} = 0$) and ($\frac{\partial \mathbf{J}}{\partial t} = 0$), Eqs. (2.4) and (2.5) are diminished by

$$\mathbf{q} + \lambda_E\left(\mathbf{V}.\nabla\mathbf{q} - \mathbf{q}.\nabla\mathbf{V}\right) = -k\nabla T, \tag{2.6}$$

$$\mathbf{J} + \lambda_C\left(\mathbf{V}.\nabla\mathbf{J} - \mathbf{J}.\nabla\mathbf{V}\right) = -D_B\nabla C. \tag{2.7}$$

The three dimension (3D) temperature and concentration expressions provide

$$u\frac{\partial T}{\partial x}+v\frac{\partial T}{\partial y}+w\frac{\partial T}{\partial z}+\lambda_E\Phi_E=\alpha_m\left(\frac{\partial^2 T}{\partial z^2}\right)+\frac{(\rho c)_p}{(\rho c)_f}\left(D_B\left(\frac{\partial T}{\partial z}\frac{\partial C}{\partial z}\right)+\frac{D_T}{T_\infty}\left(\frac{\partial T}{\partial z}\right)^2\right), \quad (2.8)$$

$$u\frac{\partial C}{\partial x}+v\frac{\partial C}{\partial y}+w\frac{\partial C}{\partial z}+\lambda_C\Phi_C=D_B\left(\frac{\partial^2 C}{\partial z^2}\right)+\frac{D_T}{T_\infty}\left(\frac{\partial^2 T}{\partial z^2}\right). \quad (2.9)$$

Here one has the following prescribed conditions:

$$u=U_w(x)=ax,\ v=V_w(y)=by,\ w=0,\ T=T_w,\ C=C_w \text{ at } \ z=0, \quad (2.10)$$

$$u\to 0,\ v\to 0,\ T\to T_\infty,\ C\to C_\infty \text{ as } z\to\infty, \quad (2.11)$$

where

$$\begin{aligned}\Phi_E &= u^2\frac{\partial^2 T}{\partial x^2}+v^2\frac{\partial^2 T}{\partial y^2}+w^2\frac{\partial^2 T}{\partial z^2}+2uv\frac{\partial^2 T}{\partial x\partial y}\\ &+2vw\frac{\partial^2 T}{\partial y\partial z}+2uw\frac{\partial^2 T}{\partial x\partial z}+\left(u\frac{\partial u}{\partial x}+v\frac{\partial u}{\partial y}+w\frac{\partial u}{\partial z}\right)\frac{\partial T}{\partial x}\\ &+\left(u\frac{\partial v}{\partial x}+v\frac{\partial v}{\partial y}+w\frac{\partial v}{\partial z}\right)\frac{\partial T}{\partial y}+\left(u\frac{\partial w}{\partial x}+v\frac{\partial w}{\partial y}+w\frac{\partial w}{\partial z}\right)\frac{\partial T}{\partial z}, \quad (2.12)\end{aligned}$$

and

$$\begin{aligned}\Phi_C &= u^2\frac{\partial^2 C}{\partial x^2}+v^2\frac{\partial^2 C}{\partial y^2}+w^2\frac{\partial^2 C}{\partial z^2}+2uv\frac{\partial^2 C}{\partial x\partial y}\\ &+2vw\frac{\partial^2 C}{\partial y\partial z}+2uw\frac{\partial^2 C}{\partial x\partial z}+\left(u\frac{\partial u}{\partial x}+v\frac{\partial u}{\partial y}+w\frac{\partial u}{\partial z}\right)\frac{\partial C}{\partial x}\\ &+\left(u\frac{\partial v}{\partial x}+v\frac{\partial v}{\partial y}+w\frac{\partial v}{\partial z}\right)\frac{\partial C}{\partial y}+\left(u\frac{\partial w}{\partial x}+v\frac{\partial w}{\partial y}+w\frac{\partial w}{\partial z}\right)\frac{\partial C}{\partial z}, \quad (2.13)\end{aligned}$$

in which $\alpha_m=k/(\rho c)_f$, $(\rho c)_p$ and $(\rho c)_f$ stand for thermal diffusivity, effective heat potential of nanoparticles and heat potential of liquid respectively, T for temperature, D_B for Brownian diffusivity, C for concentration, D_T for thermophoretic diffusion coefficient, C_w and T_w for constant wall concentration and temperature and C_∞ and T_∞ represent ambient liquid

concentration and temperature respectively. Selecting

$$\left.\begin{array}{c} u = axf'(\zeta),\ v = ayg'(\zeta),\ w = -(a\nu)^{1/2}(f(\zeta)+g(\zeta)), \\ \theta(\zeta) = \frac{T-T_\infty}{T_w-T_\infty},\ \phi(\zeta) = \frac{C-C_\infty}{C_w-C_\infty},\ \zeta = \left(\frac{a}{\nu}\right)^{1/2} z. \end{array}\right\} \tag{2.14}$$

Expression (2.1) is identically verified and Eqs. (2.2), (2.3) and (2.8) − (2.13) have been diminished to

$$f''' + (f+g)f'' - f'^2 = 0, \tag{2.15}$$

$$g''' + (f+g)g'' - g'^2 = 0, \tag{2.16}$$

$$\frac{1}{\mathrm{Pr}}\theta'' + N_b\theta'\phi' + N_t\theta'^2 + (f+g)\theta' - \delta_t\left((f+g)\left(f'+g'\right)\theta' + (f+g)^2\theta''\right) = 0, \tag{2.17}$$

$$\frac{1}{Sc}\phi'' + \frac{N_t}{N_b}\frac{1}{Sc}\theta'' + (f+g)\phi' - \delta_c\left((f+g)\left(f'+g'\right)\phi' + (f+g)^2\phi''\right) = 0, \tag{2.18}$$

$$f(0) = g(0) = 0,\ f'(0) = 1,\ g'(0) = \alpha,\ \theta(0) = 1,\ \phi(0) = 1, \tag{2.19}$$

$$f'(\infty) \to 0,\ g'(\infty) \to 0,\ \theta(\infty) \to 0,\ \phi(\infty) \to 0. \tag{2.20}$$

Here α stands for ratio number, N_b for Brownian movement number, Pr denotes Prandtl parameter, δ_t stands for nondimensional thermal relaxation number, N_t for thermophoresis number, δ_c for nondimensional concentration relaxation number and Sc for Schmidt parameter. These variables can be specified by employing the definitions given below:

$$\left.\begin{array}{c} \alpha = \frac{b}{a},\ \mathrm{Pr} = \frac{\nu}{\alpha_m},\ \delta_t = a\lambda_E,\ \delta_c = a\lambda_C, \\ N_b = \frac{(\rho c)_p D_B(C_w-C_\infty)}{(\rho c)_f \nu},\ N_t = \frac{(\rho c)_p D_T(T_w-T_\infty)}{(\rho c)_f \nu T_\infty},\ Sc = \frac{\nu}{D_B}. \end{array}\right\} \tag{2.21}$$

Dimensionless expressions of skin frictions are as follows:

$$\left.\begin{array}{c} \mathrm{Re}_x^{1/2} C_{fx} = -f''(0), \\ \mathrm{Re}_y^{1/2} C_{fy} = -\alpha^{-3/2} g''(0), \end{array}\right\} \tag{2.22}$$

where $\mathrm{Re}_x = U_w x/\nu$ and $\mathrm{Re}_y = V_w y/\nu$ depict local Reynolds parameters.

2.2 Solutions by OHAM

The optimal series arrangements of Eqs. (2.15) – (2.18) through (2.19) and (2.20) have been developed by utilizing optimal homotopic analysis technique (OHAM). The linear operators and initial deformations have been selected as follows:

$$\left.\begin{array}{c} f_0(\zeta) = 1 - \exp(-\zeta),\ g_0(\zeta) = \alpha(1 - \exp(-\zeta)), \\ \theta_0(\zeta) = \exp(-\zeta),\ \phi_0(\zeta) = \exp(-\zeta), \end{array}\right\} \tag{2.23}$$

$$\left.\begin{array}{c} \mathcal{L}_f = \frac{d^3 f}{d\zeta^3} - \frac{df}{d\zeta},\quad \mathcal{L}_g = \frac{d^3 g}{d\zeta^3} - \frac{dg}{d\zeta}, \\ \mathcal{L}_\theta = \frac{d^2\theta}{d\zeta^2} - \theta,\quad \mathcal{L}_\phi = \frac{d^2\phi}{d\zeta^2} - \phi. \end{array}\right\} \tag{2.24}$$

The above linear operators obey

$$\left.\begin{array}{c} \mathcal{L}_f\left[F_1^* + F_2^*\exp(\zeta) + F_3^*\exp(-\zeta)\right] = 0, \\ \mathcal{L}_g\left[F_4^* + F_5^*\exp(\zeta) + F_6^*\exp(-\zeta)\right] = 0, \\ \mathcal{L}_\theta\left[F_7^*\exp(\zeta) + F_8^*\exp(-\zeta)\right] = 0, \\ \mathcal{L}_\phi\left[F_9^*\exp(\zeta) + F_{10}^*\exp(-\zeta)\right] = 0, \end{array}\right\} \tag{2.25}$$

in which F_j^* $(j = 1 - 10)$ stand for arbitrary constants. Problems for zeroth and mth-order deformations are easily formulated in the view of above operators. The deformation issues are solved by BVPh2.0 of Mathematica software.

2.3 Convergence analysis

We have solved the momentum, energy and concentration expressions with the help of BVPh2.0. These expressions contain unknown variables $\hbar_f$, $\hbar_g$, $\hbar_\theta$ and $\hbar_\phi$. We can compute the minimum estimation of these variables by taking total error small. In the frame of HAM, these variables play a vital role. That is why these variables refer to as convergence-control parameter which differs HAM from other analytical approximation methods. In order to reduce the CPU time, we have employed average residual errors at the mth-oder of approximation which are defined

by

$$\varepsilon_m^f = \frac{1}{k+1}\sum_{j=0}^{k}\left[\mathcal{N}_f\left(\sum_{i=0}^{m}\hat{f}(\zeta),\ \sum_{i=0}^{m}\hat{g}(\zeta)\right)_{\zeta=j\delta\zeta}\right]^2, \tag{2.26}$$

$$\varepsilon_m^g = \frac{1}{k+1}\sum_{j=0}^{k}\left[\mathcal{N}_g\left(\sum_{i=0}^{m}\hat{f}(\zeta),\ \sum_{i=0}^{m}\hat{g}(\zeta)\right)_{\zeta=j\delta\zeta}\right]^2, \tag{2.27}$$

$$\varepsilon_m^\theta = \frac{1}{k+1}\sum_{j=0}^{k}\left[\mathcal{N}_\theta\left(\sum_{i=0}^{m}\hat{f}(\zeta),\ \sum_{i=0}^{m}\hat{g}(\zeta),\ \sum_{i=0}^{m}\hat{\theta}(\zeta),\ \sum_{i=0}^{m}\hat{\phi}(\zeta),\right)_{\zeta=j\delta\zeta}\right]^2, \tag{2.28}$$

$$\varepsilon_m^\phi = \frac{1}{k+1}\sum_{j=0}^{k}\left[\mathcal{N}_\phi\left(\sum_{i=0}^{m}\hat{f}(\zeta),\ \sum_{i=0}^{m}\hat{g}(\zeta),\ \sum_{i=0}^{m}\hat{\theta}(\zeta),\ \sum_{i=0}^{m}\hat{\phi}(\zeta),\right)_{\zeta=j\delta\zeta}\right]^2. \tag{2.29}$$

Here $\mathcal{N}_f$, $\mathcal{N}_g$, $\mathcal{N}_\theta$ and $\mathcal{N}_\phi$ denote the non-linear operators corresponding to Eqs. $(2.15)-(2.18)$ respectively. Following Liao [69] :

$$\varepsilon_m^t = \varepsilon_m^f + \varepsilon_m^g + \varepsilon_m^\theta + \varepsilon_m^\phi, \tag{2.30}$$

where ε_m^t represents total residual square error, $k = 20$ and $\delta\zeta = 0.5$. Optimal data for auxiliary variables at 2nd order of deformations is $\hbar_f = -1.64104$, $\hbar_g = -1.02624$, $\hbar_\theta = -0.933309$ and $\hbar_\phi = -0.946239$ and $\varepsilon_m^t = 2.61 \times 10^{-4}$. Table 2.1 presents average square residual error at different order of deformations. It has been analyzed that the average residual square errors reduce with higher order deformations.

Table 2.1. Individual average residual square errors employing optimal data of auxiliary variables.

m	ε_m^f	ε_m^g	ε_m^θ	ε_m^ϕ
2	4.27×10^{-6}	1.29×10^{-7}	1.40×10^{-4}	1.17×10^{-4}
6	4.47×10^{-8}	1.35×10^{-10}	4.69×10^{-7}	1.11×10^{-6}
10	7.13×10^{-10}	3.77×10^{-13}	4.43×10^{-9}	7.21×10^{-8}
16	1.83×10^{-12}	6.35×10^{-16}	4.41×10^{-11}	9.87×10^{-10}
20	3.73×10^{-14}	1.63×10^{-17}	4.75×10^{-12}	7.80×10^{-11}
26	1.18×10^{-16}	5.18×10^{-20}	6.96×10^{-14}	1.41×10^{-12}
30	2.62×10^{-18}	1.20×10^{-21}	3.47×10^{-15}	9.38×10^{-14}

2.4 Discussion

This portion explores the impacts of various pertinent variables like ratio number α, Prandtl parameter Pr, Schmidt parameter Sc, Brownian movement number N_b, thermophoresis number N_t, thermal relaxation number δ_t and concentration relaxation number δ_c on temperature $\theta(\zeta)$ and concentration $\phi(\zeta)$ distributions. Fig. 2.1 presents that bigger estimations of ratio number α give lower temperature $\theta(\zeta)$ and layer of thermal. Furthermore two dimension (2D) flow situation is acquired when $\alpha = 0$. Fig. 2.2 exhibits that how temperature field $\theta(\zeta)$ is get affected by Prandtl parameter Pr. It is watched that by upgrading Prandtl parameter Pr, the temperature $\theta(\zeta)$ and layer of thermal diminishes. Physically, as Prandtl parameter Pr is a basic piece of thermal diffusivity, in this way, thermal diffusivity is in charge of lower temperature. Higher estimations of Prandtl parameter Pr provide poor thermal diffusivity which compares to bring down temperature field and less layer of thermal. Fig. 2.3 exhibits the variety in temperature field $\theta(\zeta)$ for distinct estimations of Brownian movement number N_b. It has been clearly watched that by expanding Brownian movement number N_b, an upgrade showed up in temperature $\theta(\zeta)$ and its corresponding layer of thermal. Fig. 2.4 is attracted to portray the impact of thermophoreis parameter N_t on temperature field $\theta(\zeta)$. expanding estimations of thermophoresis number N_t constitutes a elevated temperature and more layer of thermal. The purpose for this contention is that an improvement in N_t provide a more grounded thermophoretic force which permits further movement of nanoparticles in the liquid which is far from the surface structures a elevated temperature and layer of thermal. Fig. 2.5 presents variety in temperature $\theta(\zeta)$ for various estimations of thermal relaxation number δ_t. It has been obviously analyzed that an upgrade in the estimation of thermal relaxation number δ_t exhibits diminishing conduct for temperature $\theta(\zeta)$ and layer of thermal. Here $\delta_t = 0$ speaks to that the present relation is lessened to basic Fourier's law. Fig. 2.6 portrays that expanding estimations of ratio number α presents a poor concentration distribution $\phi(\eta)$ and less layer of concentration. Fig. 2.7 presents that more prominent Schmidt parameter Sc shapes a diminishment in concentration field $\phi(\zeta)$. Physically Schmidt parameter depends on Brownian diffusivity. An expansion in Schmidt parameter Sc provide poor Brownian diffusivity. Such poor Brownian diffusivityrelates to bring down concentration field $\phi(\zeta)$. From Fig. 2.8, it is clearly inspected that a poor concentration field $\phi(\zeta)$ is created by utilizing bigger Brownian

movement number N_b. Fig. 2.9 exhibits that higher thermophoresis number N_t create a more grounded concentration field $\phi(\zeta)$. Fig. 2.10 presents how concentration relaxation number δ_c affects concentration field $\phi(\zeta)$. By expanding δ_c, both concentration $\phi(\zeta)$ and layer of concentration diminishes. Here $\delta_c = 0$ represents that present relation is diminished to basic Fick's law. Table 2.2 exhibits the comparison for different estimations of α with exact arrangement. Table 2.2 presents an excellent agreement of OHAM arrangement with the existing exact arrangement in a limiting situation. Table 2.3 is developed to analyze skin frictions $-C_{fx}\,\mathrm{Re}_x^{1/2}$ and $-C_{fy}\,\mathrm{Re}_y^{1/2}$ for several estimations of α. It is watched that skin frictions show opposite conduct for bigger ratio number α. Numeric estimations of transfer of heat rate $-\theta'(0)$ for distinct thermal relaxation δ_t are presented in Table 2.4. Here we examined that transfer of heat rate has higher estimations for bigger δ_t. Table 2.5 exhibits numerical estimations of transfer of mass rate $-\phi'(0)$ for distinct estimations of concentration relaxation δ_c. It is watched that estimations of transfer of mass rate are greater when bigger estimations of δ_c are considered.

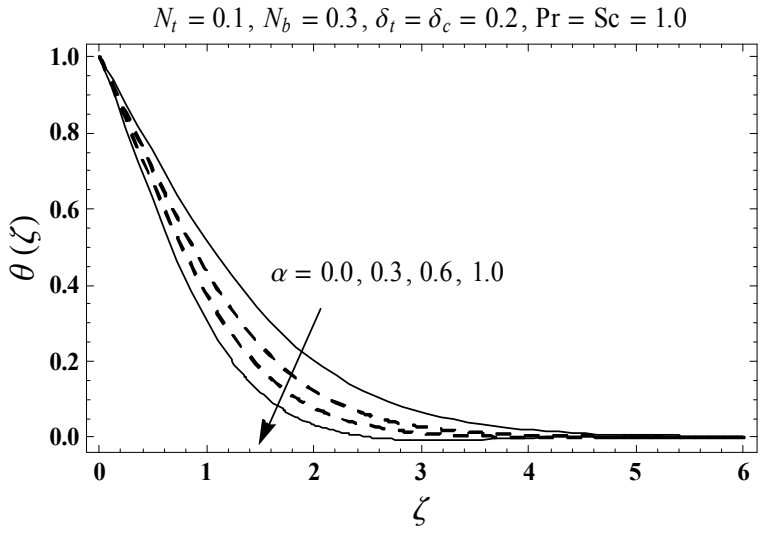

Fig. 2.1. Plots of $\theta(\zeta)$ for α.

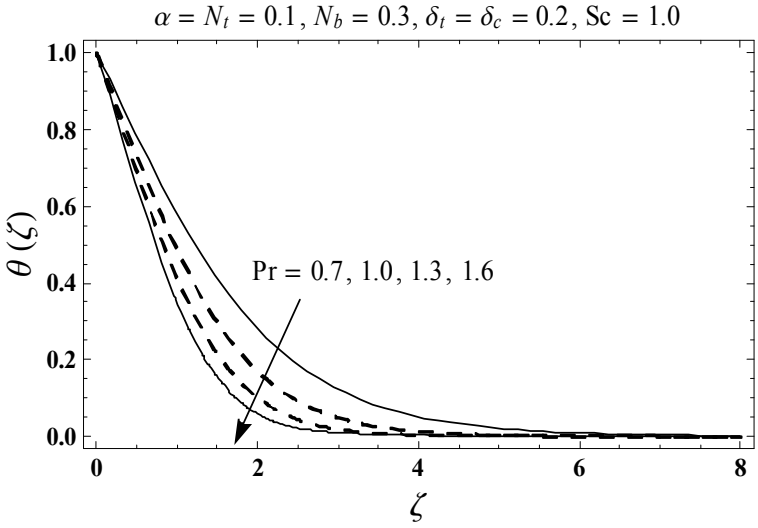

Fig. 2.2. Plots of $\theta(\zeta)$ for Pr.

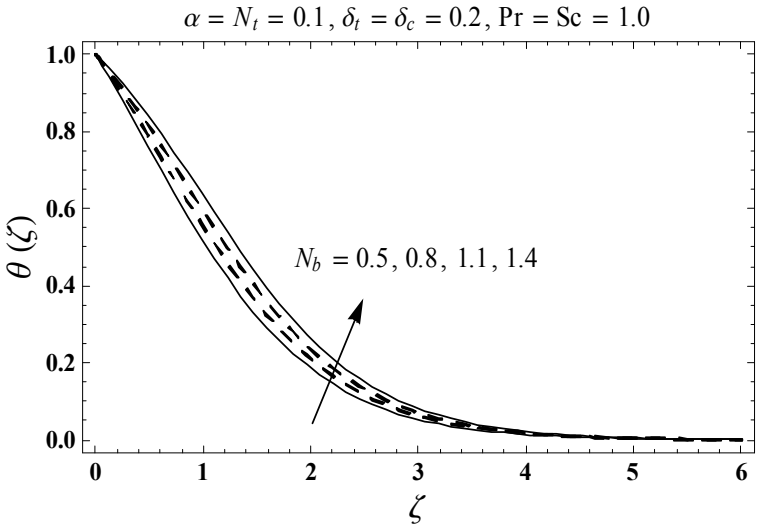

Fig. 2.3. Plots of $\theta(\zeta)$ for N_b.

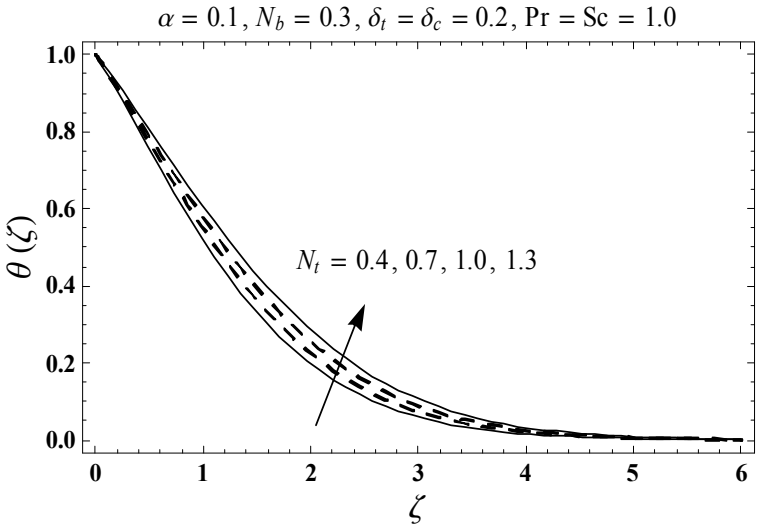

Fig. 2.4. Plots of $\theta(\zeta)$ for N_t.

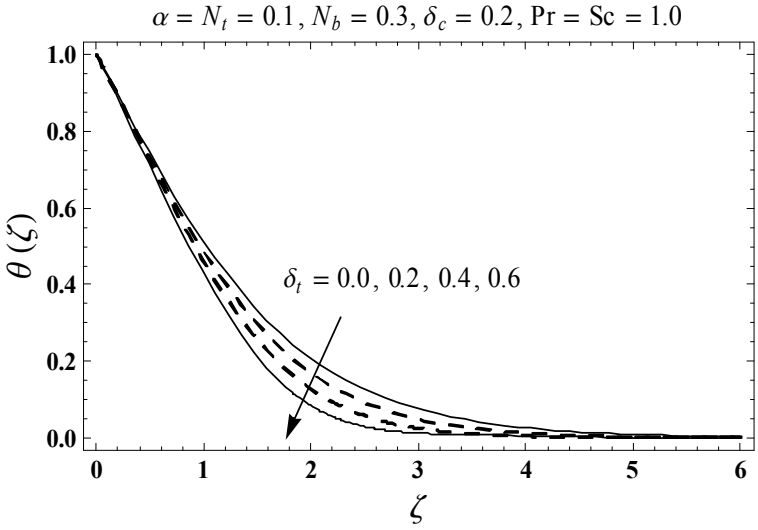

Fig. 2.5. Plots of $\theta(\zeta)$ for δ_t.

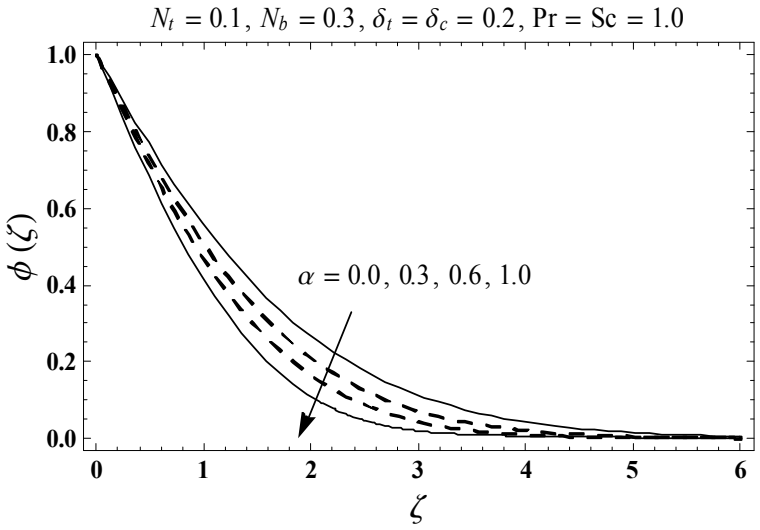

Fig. 2.6. Plots of $\phi(\zeta)$ for α.

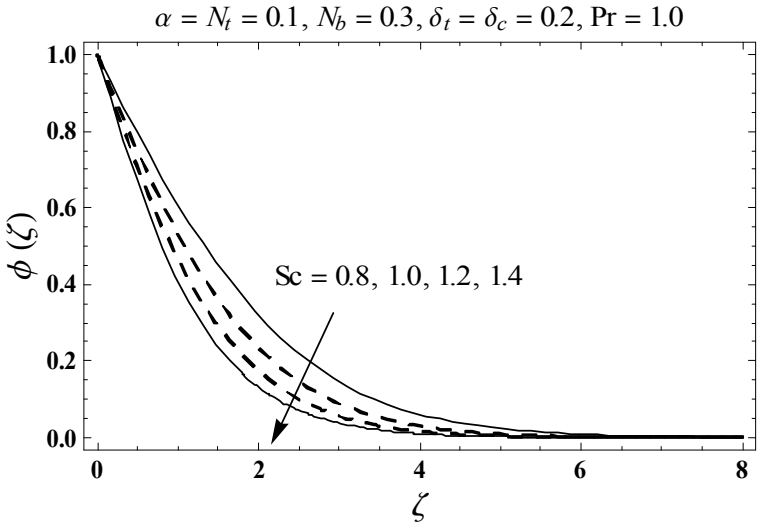

Fig. 2.7. Plots of $\phi(\zeta)$ for Sc.

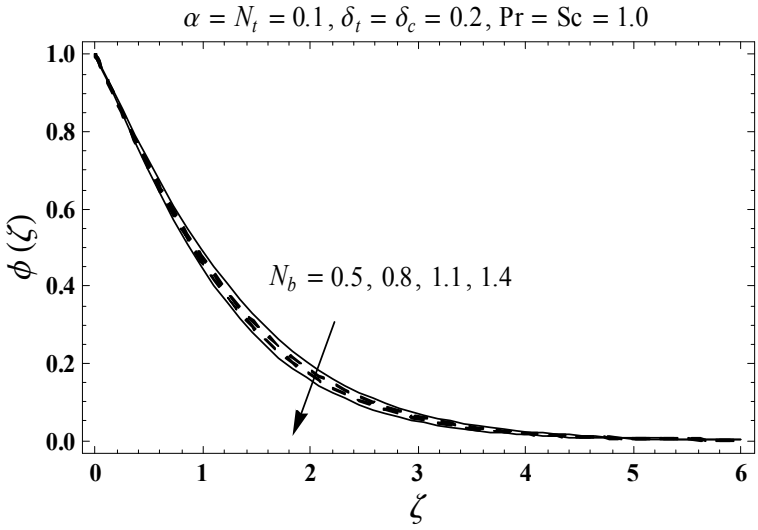

Fig. 2.8. Plots of $\phi(\zeta)$ for N_b.

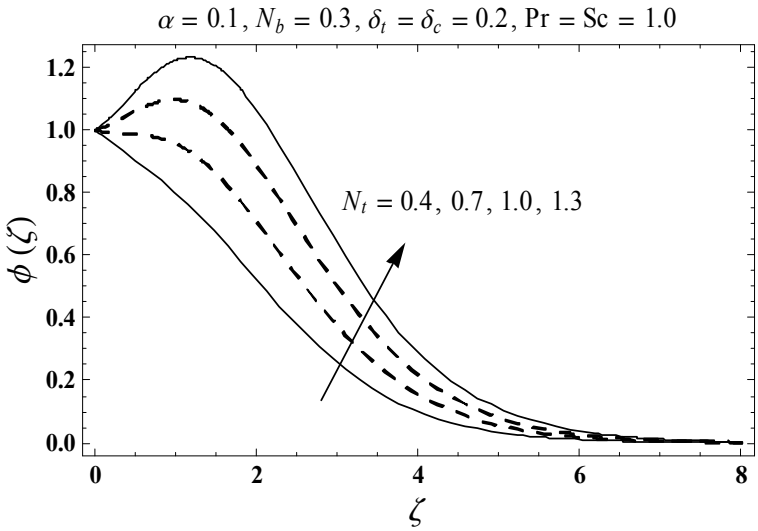

Fig. 2.9. Plots of $\phi(\zeta)$ for N_t.

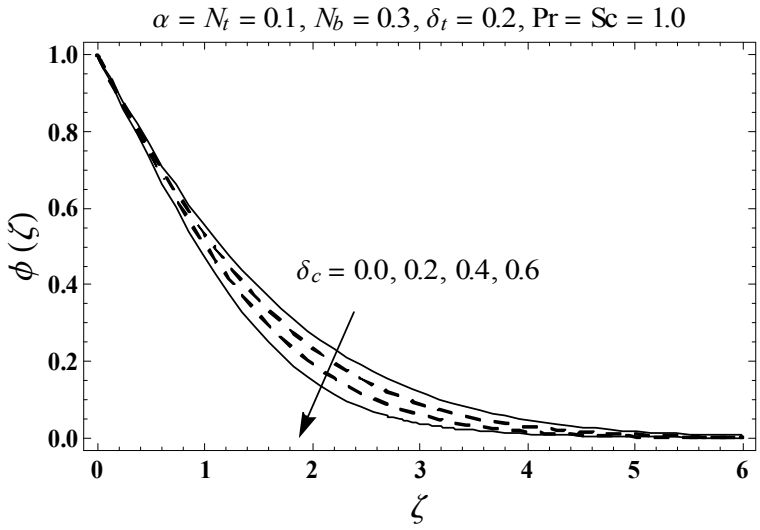

Fig. 2.10. Plots of $\phi(\zeta)$ for δ_c.

Table 2.2. Comparative estimations of $-f''(0)$ and $-g''(0)$ for several estimations of α.

α	$-f''(0)$		$-g''(0)$	
	OHAM	Exact [38]	OHAM	Exact [38]
0	1	1	0	0
0.25	1.048811	1.048813	0.194564	0.194564
0.50	1.093095	1.093097	0.465205	0.465205
0.75	1.134486	1.134485	0.794618	0.794622
1.0	1.173722	1.173720	1.173722	1.173720

Table 2.3. Numeric data for skin frictions $-C_{fx}\,\mathrm{Re}_x^{1/2}$ and $-C_{fy}\,\mathrm{Re}_y^{1/2}$ for distinct estimations of α.

α	0.1	0.4	0.7	1.0
$-\mathrm{Re}_x^{1/2}\,C_{fx}$	1.02026	1.07579	1.12640	1.17372
$-\mathrm{Re}_y^{1/2}\,C_{fy}$	2.11389	1.38037	1.23711	1.17372

Table 2.4. Numeric data for transfer of heat rate $-\theta'(0)$ for distinct estimations of δ_t when $\alpha = N_t = 0.1$, $N_b = 0.3$, $\delta_c = 0.2$ and $\mathrm{Pr} = Sc = 1.0$.

δ_t	0.0	0.1	0.2	0.3
$-\theta'(0)$	0.51107	0.51884	0.52697	0.53541

Table 2.5. Numeric data for transfer of mass rate $-\phi'(0)$ for distinct estimations of δ_c when $\alpha = N_t = 0.1$, $N_b = 0.3$, $\delta_t = 0.2$ and $\mathrm{Pr} = Sc = 1.0$.

δ_c	0.0	0.1	0.2	0.3
$-\phi'(0)$	0.50540	0.51536	0.52574	0.53673

Chapter 3

A revised model for Darcy-Forchheimer three dimensional flow of nanofluid subject to convective boundary condition

Three dimensional flow of nanoliquid characterizing porous space by Darcy-Forchheimer expression is studied. Zero nanoparticles mass flux and thermal convective conditions are implemented at the boundary. The modeled expressions are diminished into dimensionless quantities. The governing mathematical phenomenon is tackled via optimal homotopic procedure. Importance of physical constraints is described through plots. Numerical benchmark is presented to study skin frictions and local Nusselt number. Skin frictions are declared expanding functions of porosity and Forchheimer variables. Moreover the local Nusselt number is diminished for bigger estimations of porosity and Forchheimer variables.

3.1 Formulation

Three dimensional flow of nanoliquid filling porous space by Darcy-Forchheimer relation is studied. Flow is by a bidirectional extending surface. Nanoliquid relation describes attributes

of thermophoresis and Brownian movement. Thermal convection and zero nanoparticles flux constraints are implemented at boundary. We consider Cartesian coordinate framework such that $x-$ and $y-$axes are picked along and normal to extending surface. Let $U_w(x) = ax$ and $V_w(y) = by$ be the extending velocities along the $x-$ and $y-$directions. The surface temperature is controlled by a convective heating procedure which is portrayed by heat exchange coefficient h_f and temperature of hot liquid T_f under the surface. The boundary-layer expressions for flow under consideration are

$$\frac{\partial u}{\partial x} + \frac{\partial v}{\partial y} + \frac{\partial w}{\partial z} = 0, \tag{3.1}$$

$$u\frac{\partial u}{\partial x} + v\frac{\partial u}{\partial y} + w\frac{\partial u}{\partial z} = \nu\frac{\partial^2 u}{\partial z^2} - \frac{\nu}{K}u - Fu^2, \tag{3.2}$$

$$u\frac{\partial v}{\partial x} + v\frac{\partial v}{\partial y} + w\frac{\partial v}{\partial z} = \nu\frac{\partial^2 v}{\partial z^2} - \frac{\nu}{K}v - Fv^2, \tag{3.3}$$

$$u\frac{\partial T}{\partial x} + v\frac{\partial T}{\partial y} + w\frac{\partial T}{\partial z} = \alpha_m\frac{\partial^2 T}{\partial z^2} + \frac{(\rho c)_p}{(\rho c)_f}\left(D_B\left(\frac{\partial T}{\partial z}\frac{\partial C}{\partial z}\right) + \frac{D_T}{T_\infty}\left(\frac{\partial T}{\partial z}\right)^2\right), \tag{3.4}$$

$$u\frac{\partial C}{\partial x} + v\frac{\partial C}{\partial y} + w\frac{\partial C}{\partial z} = D_B\left(\frac{\partial^2 C}{\partial z^2}\right) + \frac{D_T}{T_\infty}\left(\frac{\partial^2 T}{\partial z^2}\right). \tag{3.5}$$

Here one has the following prescribed conditions:

$$u = ax,\ v = by,\ w = 0,\ -k\frac{\partial T}{\partial z} = h_f(T_f - T),\ D_B\frac{\partial C}{\partial z} + \frac{D_T}{T_\infty}\frac{\partial T}{\partial z} = 0 \text{ at } z = 0, \tag{3.6}$$

$$u \to 0,\ \ v \to 0,\ \ T \to T_\infty,\ \ C \to C_\infty \ \text{ as } z \to \infty. \tag{3.7}$$

Here u, v and w represent velocities in $x-$, $y-$ and $z-$directions, $\nu = \mu/\rho_f$ stands for kinematic viscosity, μ for dynamic viscosity, ρ_f for density, K for permeability of porous medium, $F = C_b/xK^{1/2}$ for nonuniform inertia coefficient, C_b for drag coefficient, T for temperature, $\alpha_m = k/(\rho c)_f$ for thermal diffusivity, k for thermal conductivity, $(\rho c)_p$ for effective heat potential of nanoparticles, $(\rho c)_f$ for heat potential of liquid, C for concentration, D_B for Brownian movement coefficient, D_T for thermophoretic diffusion coefficient, T_∞ for ambient temperature,

C_∞ for ambient concentration and a and b for positive constants. Selecting

$$\left.\begin{array}{c} u = axf'(\zeta),\ v = ayg'(\zeta),\ w = -\left(a\nu\right)^{1/2}(f+g), \\ \theta(\zeta) = \frac{T-T_\infty}{T_f-T_\infty},\ \phi(\zeta) = \frac{C-C_\infty}{C_\infty},\ \zeta = \left(\frac{a}{\nu}\right)^{1/2} z. \end{array}\right\} \tag{3.8}$$

Now Eq. (3.1) is identically verified while Eqs. $(3.2)-(3.7)$ are

$$f''' + (f+g)f'' - f'^2 - \lambda f' - F_r f'^2 = 0, \tag{3.9}$$

$$g''' + (f+g)g'' - g'^2 - \lambda g' - F_r g'^2 = 0, \tag{3.10}$$

$$\theta'' + \Pr\left((f+g)\theta' + N_b\theta'\phi' + N_t\theta'^2\right) = 0, \tag{3.11}$$

$$\phi'' + Sc(f+g)\phi' + \frac{N_t}{N_b}\theta'' = 0, \tag{3.12}$$

$$f(0) = g(0) = 0,\ f'(0) = 1,\ g'(0) = \alpha,\ \theta'(0) = -\gamma\left(1-\theta\left(0\right)\right),\ N_b\phi'(0) + N_t\theta'(0) = 0, \tag{3.13}$$

$$f'(\infty) \to 0,\ g'(\infty) \to 0,\ \theta(\infty) \to 0,\ \phi(\infty) \to 0. \tag{3.14}$$

Here λ stands for porosity number, α for ratio number, Sc for Schmidt parameter, F_r for Forchheimer parameter, Pr for Prandtl parameter, γ for Biot parameter, N_b for Brownian movement number and N_t for thermophoresis number. These variables can be specified by employing the definitions given below:

$$\left.\begin{array}{c} \lambda = \frac{\nu}{Ka},\ F_r = \frac{C_b}{K^{1/2}},\ \alpha = \frac{b}{a},\ \Pr = \frac{\nu}{\alpha_m},\ Sc = \frac{\nu}{D_B}, \\ \gamma = \frac{h_f}{k}\sqrt{\frac{\nu}{a}},\ N_t = \frac{(\rho c)_p D_T\left(T_f-T_\infty\right)}{(\rho c)_f \nu T_\infty},\ N_b = \frac{(\rho c)_p D_B C_\infty}{(\rho c)_f \nu}. \end{array}\right\} \tag{3.15}$$

Dimensionless relations of skin frictions and Nusselt number are

$$\left.\begin{array}{c} \mathrm{Re}_x^{1/2}\, C_{fx} = -f''(0), \\ \mathrm{Re}_y^{1/2}\, C_{fy} = -\alpha^{-3/2} g''(0), \\ \mathrm{Re}_x^{-1/2}\, Nu_x = -\theta'\left(0\right), \end{array}\right\} \tag{3.16}$$

where $\mathrm{Re}_x = U_w x/\nu$ and $\mathrm{Re}_y = V_w y/\nu$ depict local Reynolds parameters. It is additionally watched that Sherwood number is now identically vanishes.

3.2 Solutions by OHAM

The optimal series arrangements of Eqs. $(3.9)-(3.12)$ through (3.13) and (3.14) have been developed by utilizing optimal homotopic analysis technique (OHAM). The linear operators and initial deformations have been selected as follows:

$$\left.\begin{array}{c} f_0(\zeta)=1-\exp(-\zeta),\ g_0(\zeta)=\alpha(1-\exp(-\zeta)), \\ \theta_0(\zeta)=\frac{\gamma}{1+\gamma}\exp(-\zeta),\ \phi_0(\zeta)=-\frac{\gamma}{1+\gamma}\frac{N_t}{N_b}\exp(-\zeta), \end{array}\right\} \tag{3.17}$$

$$\left.\begin{array}{c} \mathcal{L}_f=\frac{d^3f}{d\zeta^3}-\frac{df}{d\zeta},\quad \mathcal{L}_g=\frac{d^3g}{d\zeta^3}-\frac{dg}{d\zeta}, \\ \mathcal{L}_\theta=\frac{d^2\theta}{d\zeta^2}-\theta,\quad \mathcal{L}_\phi=\frac{d^2\phi}{d\zeta^2}-\phi. \end{array}\right\} \tag{3.18}$$

The above linear operators obey

$$\left.\begin{array}{c} \mathcal{L}_f\left[F_1^*+F_2^*\exp(\zeta)+F_3^*\exp(-\zeta)\right]=0, \\ \mathcal{L}_g\left[F_4^*+F_5^*\exp(\zeta)+F_6^*\exp(-\zeta)\right]=0, \\ \mathcal{L}_\theta\left[F_7^*\exp(\zeta)+F_8^*\exp(-\zeta)\right]=0, \\ \mathcal{L}_\phi\left[F_9^*\exp(\zeta)+F_{10}^*\exp(-\zeta)\right]=0, \end{array}\right\} \tag{3.19}$$

where F_j^* $(j=1-10)$ stand for arbitrary constants. Problems for zeroth and mth-order deformations are easily formulated in the view of above operators. The deformation issues are solved by BVPh2.0 of Mathematica software.

3.3 Convergence analysis

We have solved the momentum, energy and concentration expressions with the help of BVPh2.0. These expressions contain unknown variables $\hbar_f$, $\hbar_g$, $\hbar_\theta$ and $\hbar_\phi$. We can compute the minimum estimation of these variables by taking total error small. In the frame of HAM, these variables play a vital role. That is why these variables refer to as convergence-control parameter which differs HAM from other analytical approximation methods. In order to reduce the CPU time, we have employed average residual errors at the mth-oder of approximation which are defined

by

$$\varepsilon_m^f = \frac{1}{k+1}\sum_{j=0}^{k}\left[\mathcal{N}_f\left(\sum_{i=0}^{m}\hat{f}(\zeta),\sum_{i=0}^{m}\hat{g}(\zeta)\right)_{\zeta=j\delta\zeta}\right]^2, \tag{3.20}$$

$$\varepsilon_m^g = \frac{1}{k+1}\sum_{j=0}^{k}\left[\mathcal{N}_g\left(\sum_{i=0}^{m}\hat{f}(\zeta),\sum_{i=0}^{m}\hat{g}(\zeta)\right)_{\zeta=j\delta\zeta}\right]^2, \tag{3.21}$$

$$\varepsilon_m^\theta = \frac{1}{k+1}\sum_{j=0}^{k}\left[\mathcal{N}_\theta\left(\sum_{i=0}^{m}\hat{f}(\zeta),\sum_{i=0}^{m}\hat{g}(\zeta),\sum_{i=0}^{m}\hat{\theta}(\zeta),\sum_{i=0}^{m}\hat{\phi}(\zeta),\right)_{\zeta=j\delta\zeta}\right]^2, \tag{3.22}$$

$$\varepsilon_m^\phi = \frac{1}{k+1}\sum_{j=0}^{k}\left[\mathcal{N}_\phi\left(\sum_{i=0}^{m}\hat{f}(\zeta),\sum_{i=0}^{m}\hat{g}(\zeta),\sum_{i=0}^{m}\hat{\theta}(\zeta),\sum_{i=0}^{m}\hat{\phi}(\zeta),\right)_{\zeta=j\delta\zeta}\right]^2. \tag{3.23}$$

Here $\mathcal{N}_f$, $\mathcal{N}_g$, $\mathcal{N}_\theta$ and $\mathcal{N}_\phi$ denote the non-linear operators corresponding to Eqs. (3.9) – (3.12) respectively. Following Liao [69] :

$$\varepsilon_m^t = \varepsilon_m^f + \varepsilon_m^g + \varepsilon_m^\theta + \varepsilon_m^\phi, \tag{3.24}$$

where ε_m^t exhibits total residual square error, $k = 20$ and $\delta\zeta = 0.5$. Optimal data for auxiliary variables at 2nd order of deformations is $\hbar_f = -1.36269$, $\hbar_g = -1.21974$, $\hbar_\theta = -1.34638$ and $\hbar_\phi = -1.22194$ and $\varepsilon_m^t = 2.69 \times 10^{-4}$. Table 3.1 presents average square residual error at different order of deformations. It has been analyzed that the average residual square errors reduce with higher order deformations.

Table 3.1. Individual average residual square errors employing optimal data of auxiliary variables.

m	ε_m^f	ε_m^g	ε_m^θ	ε_m^ϕ
2	1.41×10^{-4}	3.22×10^{-6}	4.80×10^{-5}	7.71×10^{-5}
6	1.60×10^{-5}	8.21×10^{-7}	2.80×10^{-6}	2.42×10^{-5}
10	5.53×10^{-6}	3.67×10^{-7}	5.47×10^{-7}	1.24×10^{-5}
16	2.00×10^{-6}	1.53×10^{-7}	1.06×10^{-7}	5.79×10^{-6}
20	1.22×10^{-6}	9.75×10^{-8}	4.71×10^{-8}	3.86×10^{-6}
26	6.79×10^{-7}	5.62×10^{-8}	1.78×10^{-8}	2.33×10^{-6}
30	4.92×10^{-7}	4.12×10^{-8}	1.06×10^{-8}	1.76×10^{-6}

3.4 Discussion

This section has been arranged to explore the effects of various pertinent variables like porosity parameter λ, Forchheimer parameter F_r, Schmidt parameter Sc, ratio number α, Prandtl parameter Pr, Biot parameter γ, Brownian movement number N_b and thermophoresis number N_t on temperature $\theta(\zeta)$ and concentration $\phi(\zeta)$ distributions. Impact of porosity number λ on temperature $\theta(\zeta)$ is shown in Fig. 3.1. Here temperature profile $\theta(\zeta)$ and layer of thermal are higher with an expansion in porosity parameter λ. Physically the nearness of permeable media is to upgrade the protection from liquid flow which prompts a more grounded temperature $\theta(\zeta)$ and more layer of thermal. Fig. 3.2 presents impact of Forchheimer parameter F_r on $\theta(\zeta)$. An improvement in Forchheimer parameter F_r corresponds to a stronger temperature profile $\theta(\zeta)$ and more layer of thermal. Fig. 3.3 exhibits that bigger estimations of ratio number α correspond to poor temperature profile $\theta(\zeta)$ and less layer of thermal. Moreover two dimension (2D) flow situation is recovered when $\alpha = 0$. Fig. 3.4 illustrates that how temperature field $\theta(\zeta)$ gets affected with the variation in Prandtl parameter Pr. It is watched that by upgrading Prandtl parameter Pr, temperature $\theta(\zeta)$ and layer of thermal decrease. Physically, as Prandtl parameter Pr has converse connection with thermal diffusivity, subsequently, an addition in Pr prompts poor thermal diffusion and accordingly more thinner penetration depth of $\theta(\zeta)$. Fig. 3.5 displays that an improvement in Biot parameter γ causes an improvement in temperature $\theta(\zeta)$ and corresponding layer of thermal. Higher estimations of Biot parameter γ lead to stronger convection which produces a elevated temperature profile and more layer of thermal. Fig. 3.6 is outlined to investigate effect of thermophoreis parameter N_t on temperature $\theta(\zeta)$. Bigger thermophoresis number N_t prompts a elevated temperature $\theta(\zeta)$ and thicker thermal boundary-layer. The purpose for this result is that an upgrade in N_t compares to a more grounded thermophoretic constrain on nanoparticles in heading inverse to forced temperature gradient. This movements nanoparticles towards the icy surrounding liquid because of which layer of thermal upgrades. Fig. 3.7 presents impact of porosity parameter λ on concentration profile $\phi(\zeta)$. Here concentration profile $\phi(\zeta)$ and corresponding layer thickness are expanding functions of porosity parameter λ. Impact of Forchheimer parameter F_r on concentration profile $\phi(\zeta)$ is shown in Fig. 3.8. Large Forchheimer parameter F_r indicates an improvement in concentration profile and corresponding layer of concentration. Fig. 3.9 exhibits that expanding

estimation of ratio number α produces a poor concentration distribution $\phi(\zeta)$ and associated layer of concentration. Fig. 3.10 exhibits that how the variation in Schmidt parameter Sc affects concentration field $\phi(\zeta)$. It has been watched that expanding estimations of Schmidt parameter prompt a poor concentration field $\phi(\zeta)$. Physically Schmidt parameter depends on Brownian diffusivity. An expansion in Schmidt parameter Sc provides poor Brownian diffusivity. Such poor Brownian diffusivity relates to bring down concentration field $\phi(\zeta)$ and thinner layer of concentration. Fig. 3.11 indicates that higher Brownian movement number N_b leads to a diminishment in concentration field $\phi(\zeta)$ and corresponding layer thickness. Fig. 3.12 plots the concentration field $\phi(\zeta)$ for varying estimations of thermophoreis parameter N_t. It has been watched that higher thermophoresis number N_t prompts a more grounded concentration field $\phi(\zeta)$ and associated layer thickness. Table 3.2 exhibits the comparison for different estimations of α with exact arrangement. Table 3.2 presents an excellent agreement of OHAM arrangement with the existing exact arrangement in a limiting situation. Table 3.3 is arranged to examine skin frictions $-C_{fx}\,\mathrm{Re}_x^{1/2}$ and $-C_{fy}\,\mathrm{Re}_y^{1/2}$ for several estimations of F_r, λ and α. It has been watched that skin frictions show reverse trend for bigger ratio number α. Table 3.4 provides numerical computations of local Nusselt number $\mathrm{Re}_x^{-1/2}\,Nu_x$ for several estimations of λ, F_r, α, γ, N_t, N_b, Pr and Sc. Local Nusselt number has higher esteems for bigger Prandtl Pr and Biot γ numbers while inverse conduct is watched for porosity λ and Forchheimer F_r variables. Also

the local Nusselt number stays constant when the Brownian movement number N_b is shifted.

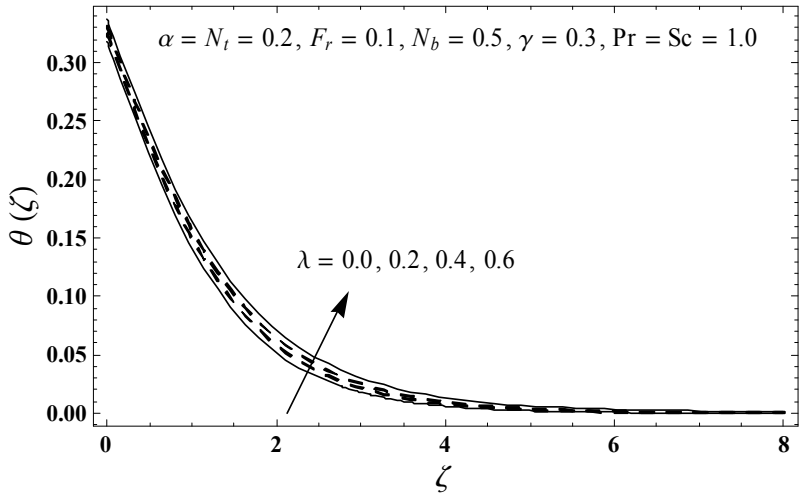

Fig. 3.1. Plots of $\theta(\zeta)$ for λ.

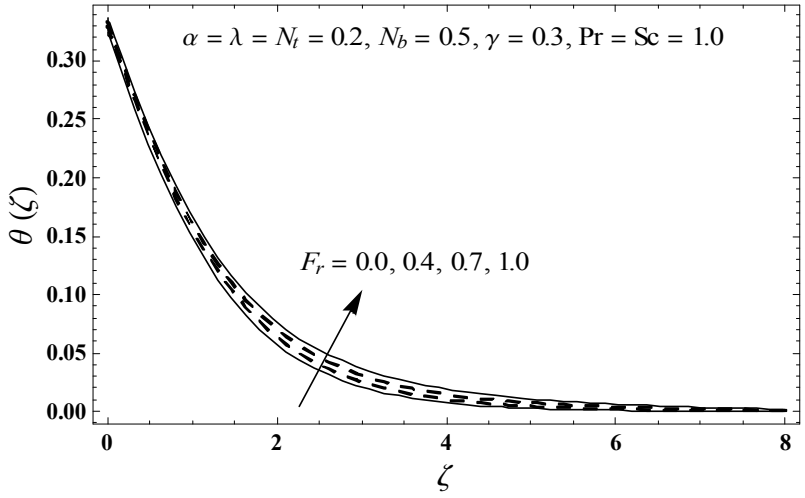

Fig. 3.2. Plots of $\theta(\zeta)$ for F_r.

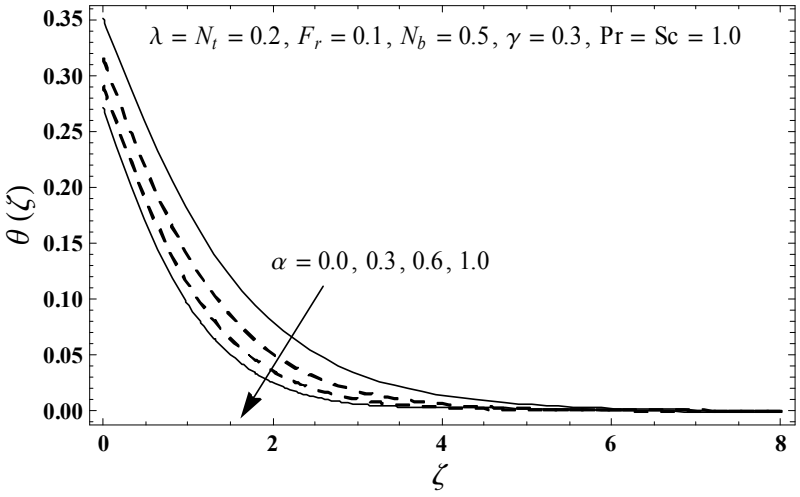

Fig. 3.3. Plots of $\theta(\zeta)$ for α.

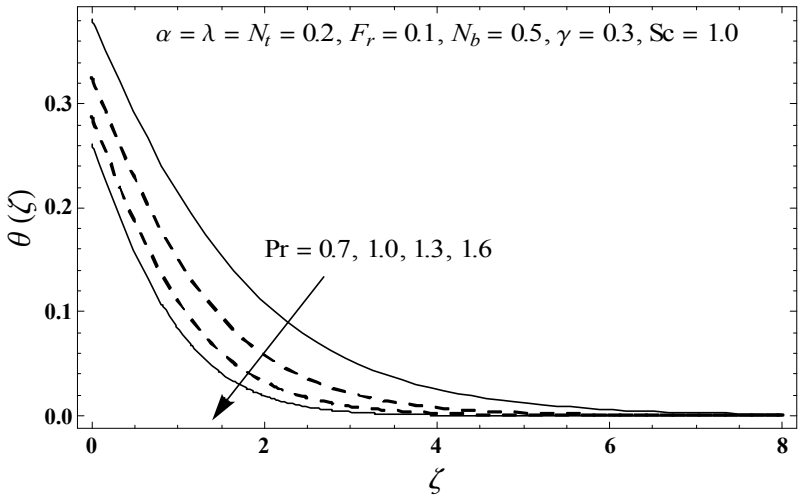

Fig. 3.4. Plots of $\theta(\zeta)$ for Pr.

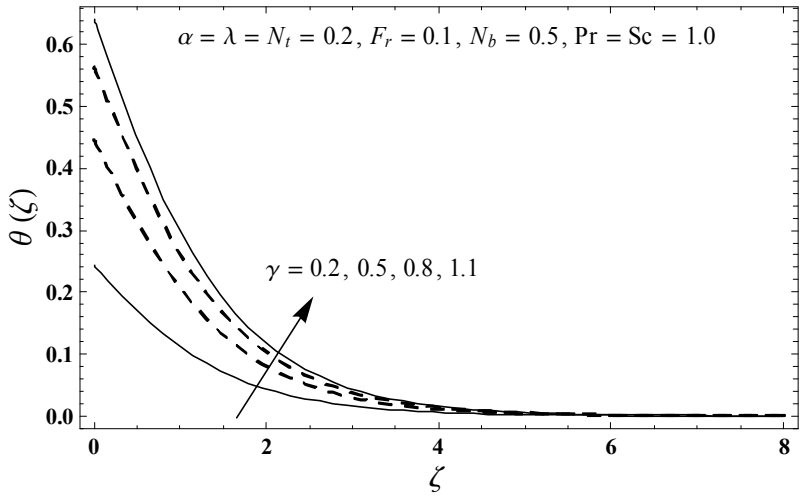

Fig. 3.5. Plots of $\theta(\zeta)$ for γ.

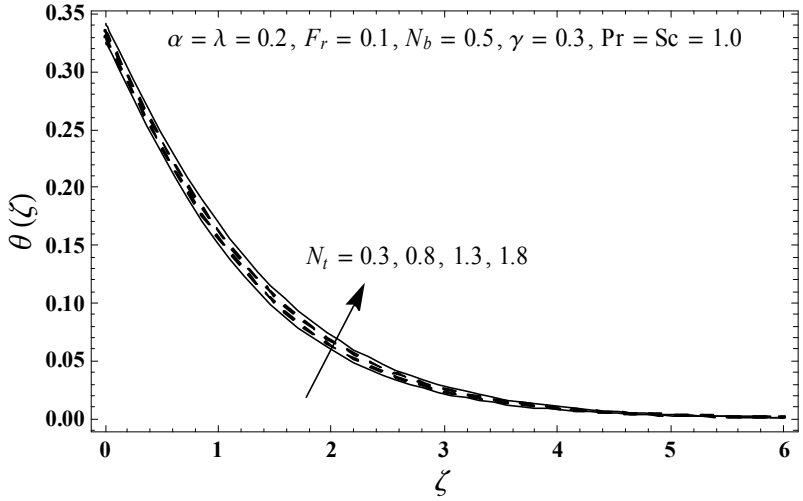

Fig. 3.6. Plots of $\theta(\zeta)$ for N_t.

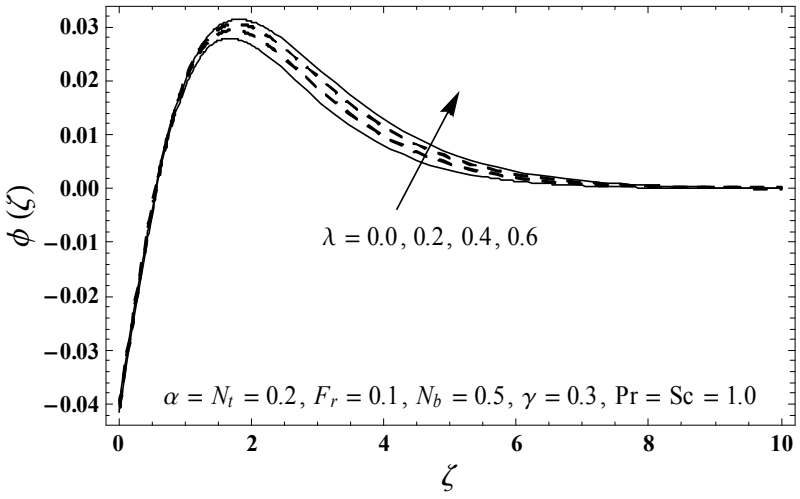

Fig. 3.7. Plots of $\phi(\zeta)$ for λ.

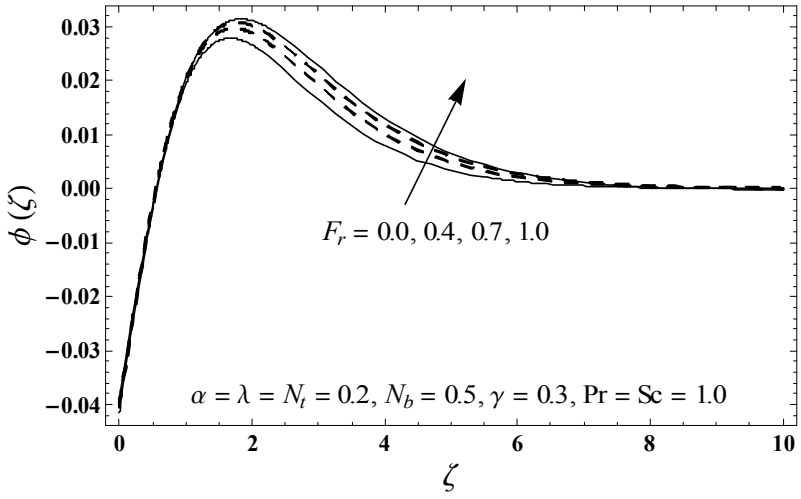

Fig. 3.8. Plots of $\phi(\zeta)$ for F_r.

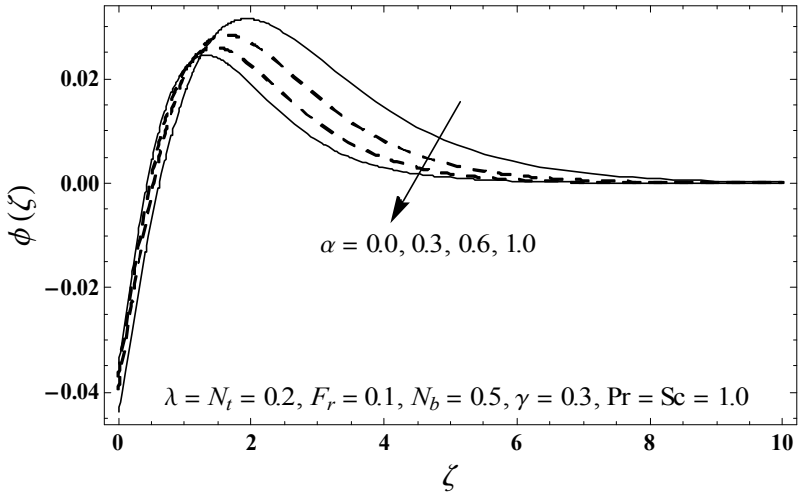

Fig. 3.9. Plots of $\phi(\zeta)$ for α.

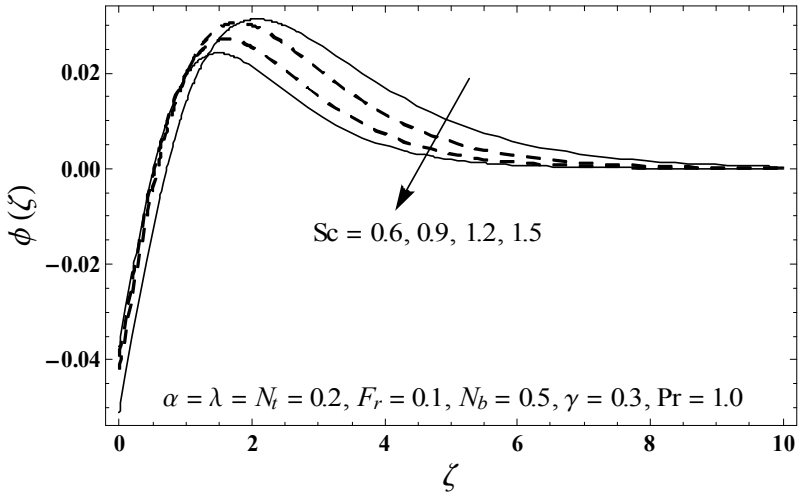

Fig. 3.10. Plots of $\phi(\zeta)$ for Sc.

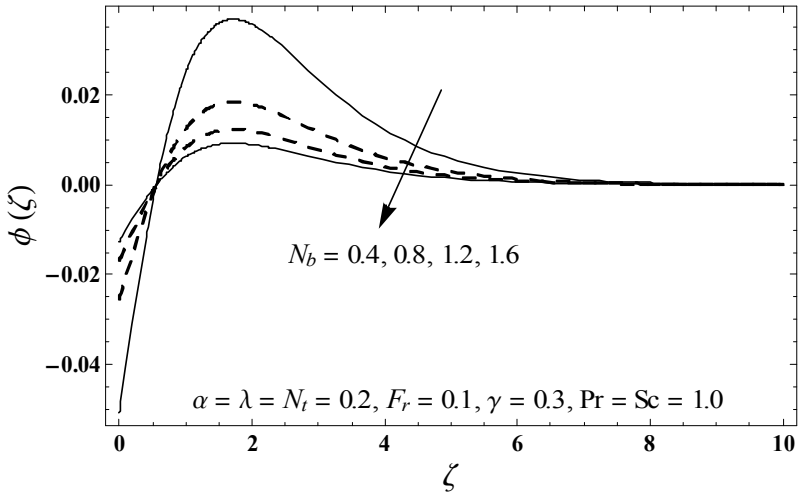

Fig. 3.11. Plots of $\phi(\zeta)$ for N_b.

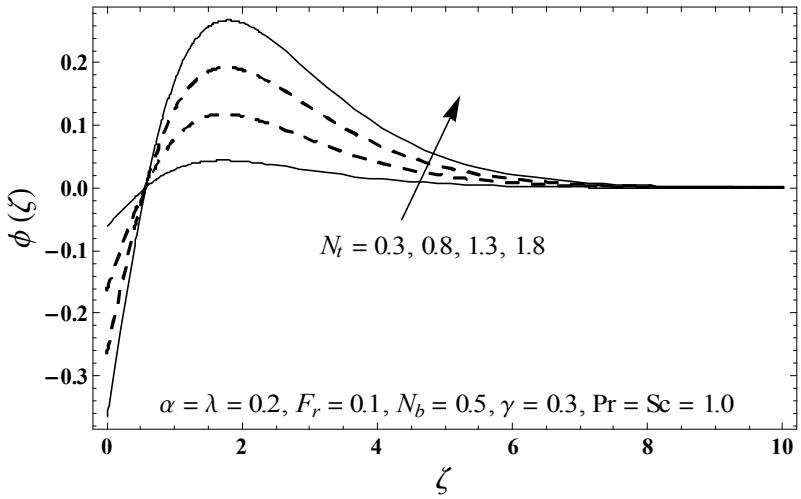

Fig. 3.12. Plots of $\phi(\zeta)$ for N_t.

Table 3.2. Comparative estimations of $-f''(0)$ and $-g''(0)$ for several estimations of α when $\lambda = F_r = 0$.

α	$-f''(0)$		$-g''(0)$	
	OHAM	Exact [38]	OHAM	Exact [38]
0	1	1	0	0
0.25	1.048811	1.048813	0.194564	0.194564
0.50	1.093095	1.093097	0.465205	0.465205
0.75	1.134486	1.134485	0.794618	0.794622
1.0	1.173722	1.173720	1.173722	1.173720

Table 3.3. Numeric data for skin frictions $-C_{fx}\,\mathrm{Re}_x^{1/2}$ and $-C_{fy}\,\mathrm{Re}_y^{1/2}$ for several estimations of F_r, λ and α.

λ	F_r	α	$-\mathrm{Re}_x^{1/2}\,C_{fx}$	$-\mathrm{Re}_y^{1/2}\,C_{fy}$
0.0	0.1	0.2	1.06945	1.67684
0.1			1.11471	1.81669
0.2			1.15830	1.94722
0.2	0.0	0.2	1.13041	1.93414
	0.1		1.15830	1.94722
	0.2		1.18561	1.96037
0.2	0.1	0.1	1.14160	2.54234
		0.3	1.17449	1.70234
		0.5	1.20563	1.47621

Table 3.4. Numeric data for transfer of heat rate $\mathrm{Re}_x^{-1/2} Nu_x$ for various estimations of λ, F_r, α, γ, N_t, N_b, Pr and Sc.

λ	F_r	α	γ	N_t	N_b	Pr	Sc	$\mathrm{Re}_x^{-1/2} Nu_x$
0.0	0.1	0.2	0.3	0.2	0.5	1.0	1.0	0.20448
0.2								0.20248
0.5								0.19970
0.2	0.0	0.2	0.3	0.2	0.5	1.0	1.0	0.20278
	0.2							0.20220
	0.4							0.20164
0.2	0.1	0.0	0.3	0.2	0.5	1.0	1.0	0.19458
		0.3						0.20560
		0.5						0.21080
0.2	0.1	0.2	0.2	0.2	0.5	1.0	1.0	0.15148
			0.5					0.27696
			1.0					0.38194
0.2	0.1	0.2	0.3	0.0	0.5	1.0	1.0	0.20306
				0.5				0.20159
				1.0				0.20004
0.2	0.1	0.2	0.3	0.2	0.5	1.0	1.0	0.20248
					1.0			0.20248
					1.5			0.20248
0.2	0.1	0.2	0.3	0.2	0.5	0.5	1.0	0.16685
						1.0		0.20248
						1.5		0.21949
0.2	0.1	0.2	0.3	0.2	0.5	1.0	0.5	0.20271
							1.0	0.20248
							1.5	0.20234

Chapter 4

Three-dimensional boundary layer flow of Maxwell nanofluid: A mathematical model

This chapter explores three dimensional boundary-layer flow of Maxwell nanoliquid. Flow is generated by a bidirectional extending surface. Mathematical formulation is carried out through boundary-layer approach. Heat source/sink, Brownian movement and thermophoresis are accounted. Newly developed constraint requiring zero nanoparticle flux at boundary is employed in flow analysis of Maxwell liquid. The governing nonlinear boundary-layer expressions through appropriate transformations are diminished to coupled nonlinear ordinary differential framework. The resulting nonlinear framework has been solved. Plots are plotted to explore impacts of various interesting variables on velocities, concentration and temperature. Nusselt number is computed and examined numerically.

4.1 Formulation

We consider the steady three dimensional flow of an incompressible Maxwell nanoliquid. Flow caused is due to linear extending surface. The flow possesses the space $z > 0$. Heat source/sink, Brownian movement and thermophoresis impacts are explored. Thermophysical properties of

liquid are taken constant. The subjected boundary-layer expressions in Maxwell liquid flow are

$$\frac{\partial u}{\partial x}+\frac{\partial v}{\partial y}+\frac{\partial w}{\partial z}=0, \tag{4.1}$$

$$u\frac{\partial u}{\partial x}+v\frac{\partial u}{\partial y}+w\frac{\partial u}{\partial z}+\lambda_1\left(\begin{array}{c}u^2\frac{\partial^2 u}{\partial x^2}+v^2\frac{\partial^2 u}{\partial y^2}+w^2\frac{\partial^2 u}{\partial z^2}\\+2uv\frac{\partial^2 u}{\partial x\partial y}+2vw\frac{\partial^2 u}{\partial y\partial z}+2uw\frac{\partial^2 u}{\partial x\partial z}\end{array}\right)=\nu\frac{\partial^2 u}{\partial z^2}, \tag{4.2}$$

$$u\frac{\partial v}{\partial x}+v\frac{\partial v}{\partial y}+w\frac{\partial v}{\partial z}+\lambda_1\left(\begin{array}{c}u^2\frac{\partial^2 v}{\partial x^2}+v^2\frac{\partial^2 v}{\partial y^2}+w^2\frac{\partial^2 v}{\partial z^2}\\+2uv\frac{\partial^2 v}{\partial x\partial y}+2vw\frac{\partial^2 v}{\partial y\partial z}+2uw\frac{\partial^2 v}{\partial x\partial z}\end{array}\right)=\nu\frac{\partial^2 v}{\partial z^2}, \tag{4.3}$$

$$\begin{aligned}u\frac{\partial T}{\partial x}+v\frac{\partial T}{\partial y}+w\frac{\partial T}{\partial z} &= \alpha\frac{\partial^2 T}{\partial z^2}+\frac{Q}{(\rho c)_f}(T-T_\infty)\\ &\quad+\frac{(\rho c)_p}{(\rho c)_f}\left(D_B\left(\frac{\partial T}{\partial z}\frac{\partial C}{\partial z}\right)+\frac{D_T}{T_\infty}\left(\frac{\partial T}{\partial z}\right)^2\right),\end{aligned} \tag{4.4}$$

$$u\frac{\partial C}{\partial x}+v\frac{\partial C}{\partial y}+w\frac{\partial C}{\partial z}=D_B\left(\frac{\partial^2 C}{\partial z^2}\right)+\frac{D_T}{T_\infty}\left(\frac{\partial^2 T}{\partial z^2}\right). \tag{4.5}$$

Here one has the following prescribed conditions:

$$u=U_w(x)=ax,\ v=V_w(y)=by,\ T=T_w(x),\ D_B\frac{\partial C}{\partial z}+\frac{D_T}{T_\infty}\frac{\partial T}{\partial z}=0 \text{ at } z=0, \tag{4.6}$$

$$u\to 0,\quad v\to 0,\quad T\to T_\infty,\quad C\to C_\infty \quad \text{as } z\to\infty, \tag{4.7}$$

where u, v and w stand for velocities in $x-$, $y-$ and $z-$directions, λ_1 for relaxation time, $\nu\left(=\mu/\rho_f\right)$ for kinematic viscosity, ρ_f for density, μ for dynamic viscosity, T for temperature, $\alpha=k/(\rho c)_f$ for thermal diffusivity, k for thermal conductivity, $(\rho c)_f$ for heat potential of liquid, Q for heat generation/absorption coefficient, $(\rho c)_p$ for effective heat potential of nanoparticles, D_B for Brownian diffusivity, C for concentration, D_T for thermophoretic diffusion, T_w and T_∞ for surface and ambient temperatures and C_∞ for ambient concentration. Here we assumes that surface extending velocities and temperature are

$$U_w(x)=ax,\ V_w(y)=by,\ T_w(x)=T_\infty+T_0x, \tag{4.8}$$

where a, b and T_0 are the positive constants. Selecting

$$\left.\begin{array}{c} u = axf'(\eta),\ v = ayg'(\eta),\ w = -\left(a\nu\right)^{1/2}\left(f(\eta)+g(\eta)\right), \\ \theta(\eta) = \frac{T-T_\infty}{T_w-T_\infty},\ \phi(\eta) = \frac{C-C_\infty}{C_\infty},\ \eta = \left(\frac{a}{\nu}\right)^{1/2} z. \end{array}\right\} \tag{4.9}$$

Eq. (4.1) is automatically verified while Eqs. $(4.2)-(4.8)$ have the following forms:

$$f''' + (f+g)f'' - f'^2 + \beta\left(2\left(f+g\right)f'f'' - \left(f+g\right)^2 f'''\right) = 0, \tag{4.10}$$

$$g''' + (f+g)g'' - g'^2 + \beta\left(2\left(f+g\right)g'g'' - \left(f+g\right)^2 g'''\right) = 0, \tag{4.11}$$

$$\theta'' + \Pr\left((f+g)\theta' - f'\theta + S\theta + Nb\theta'\phi' + Nt\theta'^2\right) = 0, \tag{4.12}$$

$$\phi'' + Le\,\Pr(f+g)\phi' + \frac{Nt}{Nb}\theta'' = 0, \tag{4.13}$$

$$f = 0,\ g = 0,\ f' = 1,\ g' = c,\ \theta = 1,\ Nb\phi' + Nt\theta' = 0 \text{ at } \eta = 0, \tag{4.14}$$

$$f' \to 0,\ g' \to 0,\ \theta \to 0,\ \phi \to 0 \text{ as } \eta \to \infty. \tag{4.15}$$

Here Pr stands for Prandtl parameter, β for Deborah parameter, c for ratio of extending rates, S for heat source/sink parameter, Nb for Brownian movement number, Le for Lewis parameter and Nt for thermophoresis number. These variables can be specified by employing the definitions given below:

$$\left.\begin{array}{c} \beta = \lambda_1 a,\ c = \frac{b}{a},\ \Pr = \frac{\nu}{\alpha},\ S = \frac{Q}{a(\rho c)_f}, \\ Nb = \frac{(\rho c)_p D_B C_\infty}{(\rho c)_f \nu},\ Nt = \frac{(\rho c)_p D_T (T_w - T_\infty)}{(\rho c)_f \nu T_\infty},\ Le = \frac{\alpha}{D_B}. \end{array}\right\} \tag{4.16}$$

The local Nusselt number Nu_x is defined as

$$Nu_x = -\frac{x}{(T_w - T_\infty)}\left.\frac{\partial T}{\partial z}\right|_{z=0} = -\left(\mathrm{Re}_x\right)^{1/2}\theta'(0). \tag{4.17}$$

It is watched that dimensionless mass flux represented by Sherwood number is now automatically zero and $\mathrm{Re}_x = U_w x/\nu$ is local Reynolds parameter.

4.2 Solutions by HAM

The series arrangements of Eqs. $(4.10)-(4.13)$ through (4.14) and (4.15) have been developed by utilizing homotopy analysis technique (HAM). The linear operators and initial deformations have been selected as follows:

$$f_0(\eta)=1-e^{-\eta},\quad g_0(\eta)=c(1-e^{-\eta}),\quad \theta_0(\eta)=e^{-\eta},\quad \phi_0(\eta)=-\frac{Nt}{Nb}e^{-\eta}, \tag{4.18}$$

$$\mathcal{L}_f=f'''-f',\quad \mathcal{L}_g=g'''-g',\quad \mathcal{L}_\theta=\theta''-\theta,\quad \mathcal{L}_\phi=\phi''-\phi. \tag{4.19}$$

The above linear operators obey

$$\left.\begin{array}{cc}\mathcal{L}_f\left[F_1^{**}+F_2^{**}e^{\eta}+F_3^{**}e^{-\eta}\right]=0, & \mathcal{L}_g\left[F_4^{**}+F_5^{**}e^{\eta}+F_6^{**}e^{-\eta}\right]=0,\\ \mathcal{L}_\theta\left[F_7^{**}e^{\eta}+F_8^{**}e^{-\eta}\right]=0, & \mathcal{L}_\phi\left[F_9^{**}e^{\eta}+F_{10}^{**}e^{-\eta}\right]=0,\end{array}\right\} \tag{4.20}$$

in which F_j^{**} $(j=1-10)$ stand for arbitrary constants. Problems for zeroth and mth-order deformations are easily formulated in the view of above operators. The deformation issues are computed by Mathematica software.

4.3 Convergence analysis

The homotopic arrangements have auxiliary variables $\hbar_f$, $\hbar_g$, $\hbar_\theta$ and $\hbar_\phi$. These variables are helpful for convergence of series arrangements. Proper estimations of such variables is quite essential to construct convergent arrangements through homotopic analysis technique (HAM). To get proper estimations of $\hbar_f$, $\hbar_g$, $\hbar_\theta$ and $\hbar_\phi$, the $\hbar-$plots are displayed at 15th order of deformations. Figs. 4.1 and 4.2 clearly show that convergence area lies within the ranges $-1.95\leq\hbar_f\leq-0.25$, $-1.90\leq\hbar_g\leq-0.30$, $-1.85\leq\hbar_\theta\leq-0.80$ and $-1.90\leq\hbar_\phi\leq-0.40$. Table

4.1 exhibits that 32th order of deformations is sufficient for convergent series arrangements.

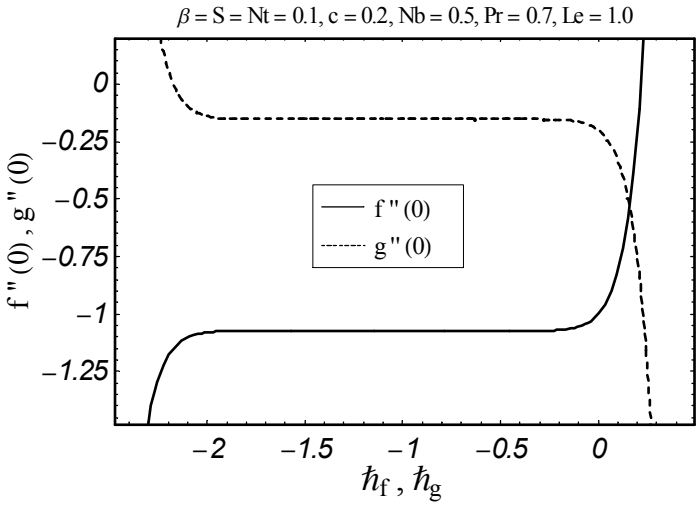

Figs. 4.1. $\hbar-$plots for $f(\eta)$ and $g(\eta)$.

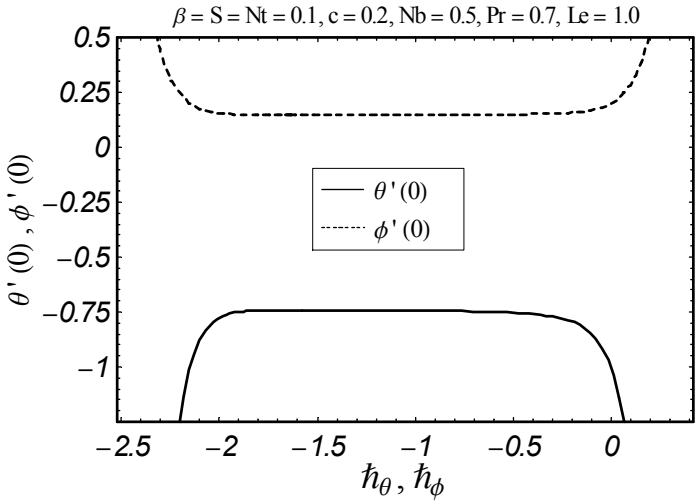

Figs. 4.2. $\hbar-$plots for $\theta(\eta)$ and $\phi(\eta)$.

Table 4.1. HAM arrangements convergence when $\beta = S = Nt = 0.1$, $c = 0.2$, $Nb = 0.5$, $\Pr = 0.7$ and $Le = 1.0$.

Order of deformations	$-f''(0)$	$-g''(0)$	$-\theta'(0)$	$\phi'(0)$
1	1.07840	0.14784	0.80600	0.16120
5	1.07330	0.15325	0.75512	0.15102
10	1.07332	0.15323	0.74481	0.14896
15	1.07332	0.15323	0.74211	0.14842
20	1.07332	0.15323	0.74116	0.14823
25	1.07332	0.15323	0.74078	0.14816
32	1.07332	0.15323	0.74058	0.14811
40	1.07332	0.15323	0.74058	0.14811
50	1.07332	0.15323	0.74058	0.14811

4.4 Discussion

The present section addresses impacts of various influential variables including Deborah parameter β, ratio number c, Prandtl parameter Pr, thermophoresis number Nt, Brownian movement number Nb, heat source/sink parameter S and Lewis parameter Le on temperature $\theta(\eta)$ and concentration $\phi(\eta)$. From Fig. 4.3, we examined that temperature and corresponding layer of thermal are elevated when we improvement the Deborah parameter. Deborah parameter is directly proportional to relaxation time. Relaxation time is bigger for higher Deborah parameter. Hence bigger relaxation time gives rise to temperature and corresponding layer of thermal. Fig. 4.4 exhibits that bigger ratio number give rise to a diminishment in temperature field $\theta(\eta)$. For $c = 0$, two dimensional flow situation is recovered. Here we watched that thermal boundary-layer thickness is more for two dimensional flow in comparison to three dimensional situation. Fig. 4.5 exhibits that temperature field $\theta(\eta)$ is higher for smaller estimations of Prandtl parameter Pr. Physically, bigger Prandtl fluids have weaker thermal diffusivity and small Prandtl fluids have more thermal diffusivity. This variation in thermal diffusivity creates a diminishment in temperature $\theta(\eta)$ and associated layer of thermal. Influence of thermophoresis number Nt on temperature field $\theta(\eta)$ is analyzed in Fig. 4.6. Both temperature and corresponding

layer of thermal are elevated when we improvement thermophoresis number. Fig. 4.7 presents variations of heat source/sink parameter S on temperature field $\theta(\eta)$. Here $S > 0$ is for heat source and $S < 0$ is for heat sink. We watched that temperature and corresponding layer of thermal are elevated in situation of heat source when we compare it with heat sink. Influence of Deborah parameter β on concentration field $\phi(\eta)$ is shown in Fig. 4.8. Here concentration $\phi(\eta)$ and corresponding layer thickness are bigger for higher Deborah parameter β. Fig. 4.9 describes that large c creates decay in concentration $\phi(\eta)$ and associated layer thickness. The variation in concentration field $\phi(\eta)$ for different estimations of Lewis parameter Le is examined in Fig. 4.10. Concentration field is diminished when we improvement Lewis parameter. Lewis parameter is inversely proportional to Brownian movement. Brownian movement is poor for higher Lewis parameter. This poor Brownian movement coefficient creates a diminishment in concentration field. Impact of Prandtl parameter Pr on concentration distribution $\phi(\eta)$ is examined in Fig. 4.11. It is watched that both concentration $\phi(\eta)$ and associated layer thickness are diminishment when we improvement Prandtl parameter Pr. An improvement in thermophoresis number Nt gives rise to concentration $\phi(\eta)$ and its corresponding layer thickness (see Fig. 4.12). Effect of Brownian movement number Nb on concentration field $\phi(\eta)$ is plotted in Fig. 4.13. Here concentration $\phi(\eta)$ and associated layer thickness are diminished for higher Brownian motion. Table 4.2 exhibits the comparison for various estimations of c with exact arrangement. Table 4.2 presents an excellent agreement of HAM arrangement with the existing exact arrangement in a limiting situation. Table 4.3 presents Nusselt number for various estimations of β, c, Pr, S, Nt, Nb and Le. Clearly Nusselt number are diminishment when we improvement the estimations of S, β, Nt and Le. However an improvement is watched

for expanding estimations of c and Pr .

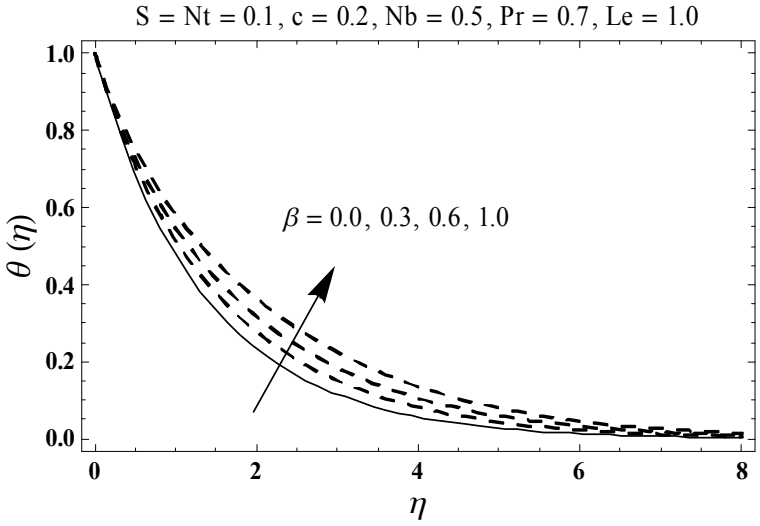

Fig. 4.3. Plots of $\theta(\eta)$ for β.

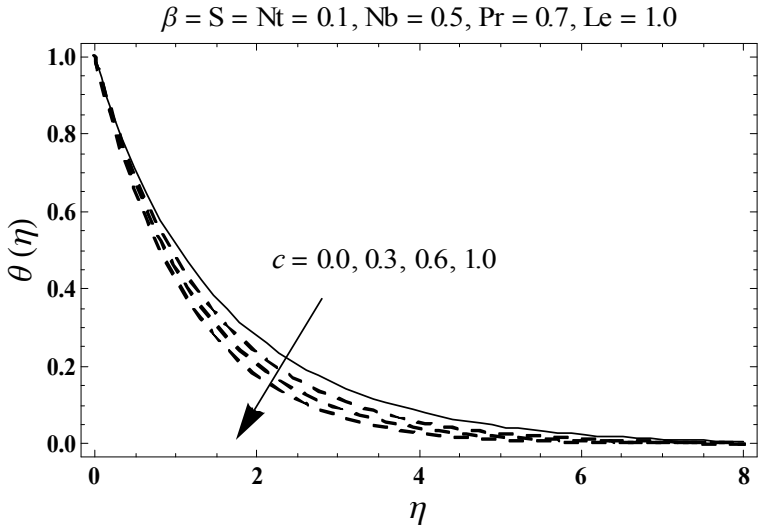

Fig. 4.4. Plots of $\theta(\eta)$ for c.

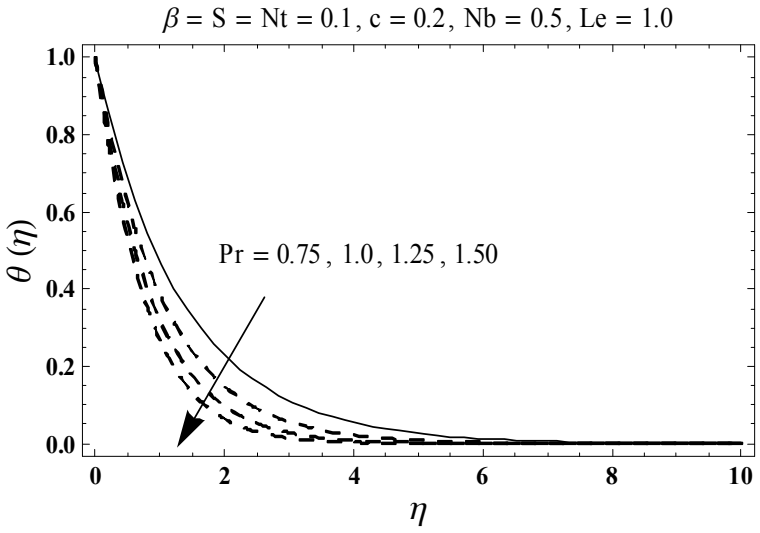

Fig. 4.5. Plots of $\theta(\eta)$ for Pr.

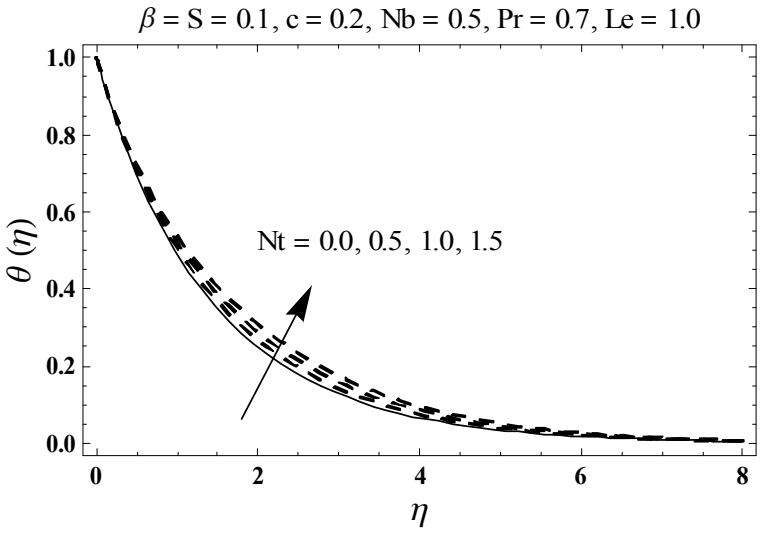

Fig. 4.6. Plots of $\theta(\eta)$ for Nt.

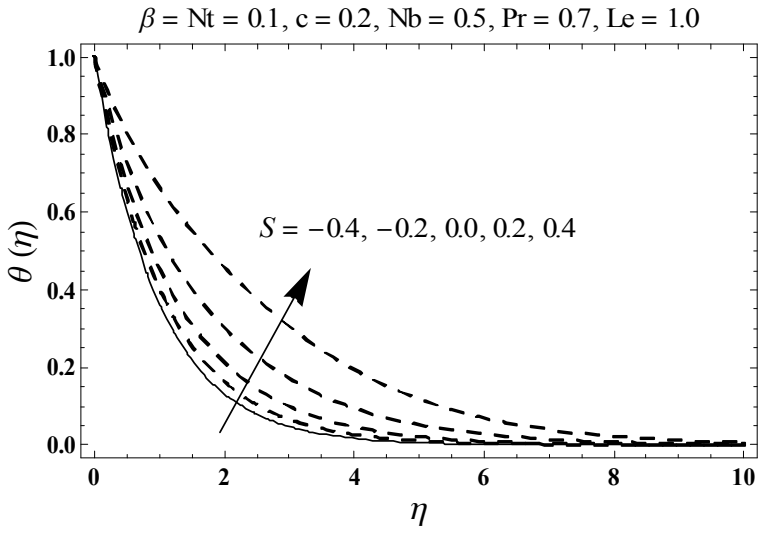

Fig. 4.7. Plots of $\theta(\eta)$ for S.

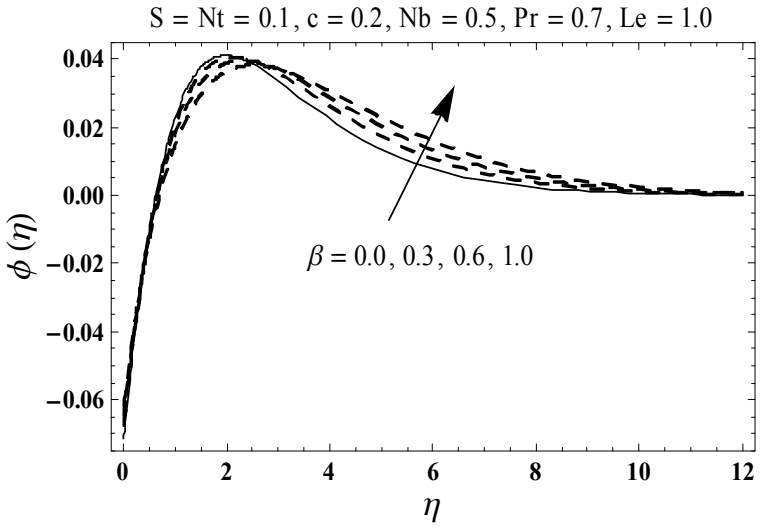

Fig. 4.8. Plots of $\phi(\eta)$ for β.

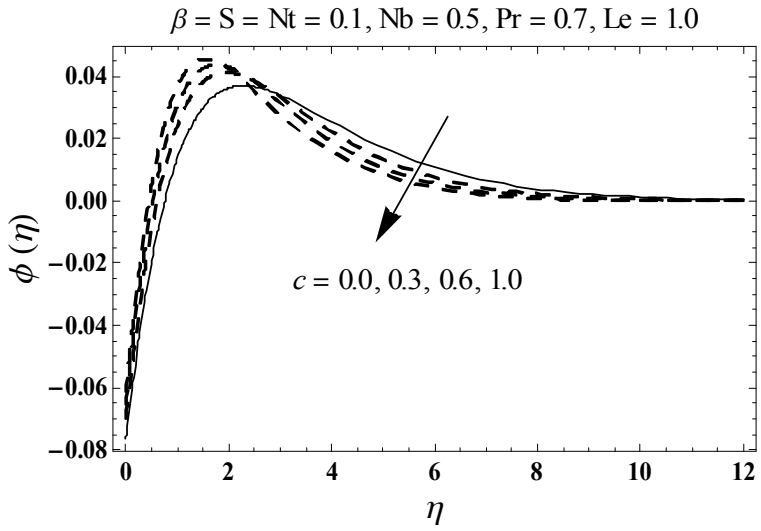

Fig. 4.9. Plots of $\phi(\eta)$ for c.

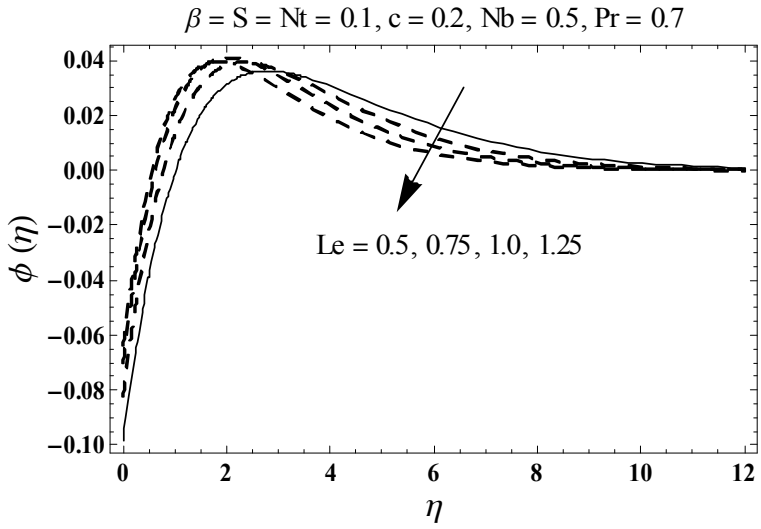

Fig. 4.10. Plots of $\phi(\eta)$ for Le.

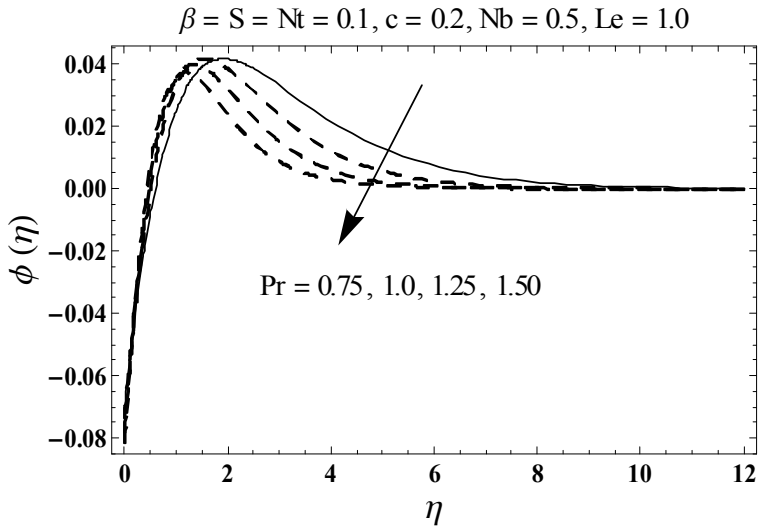

Fig. 4.11. Plots of $\phi(\eta)$ for Pr .

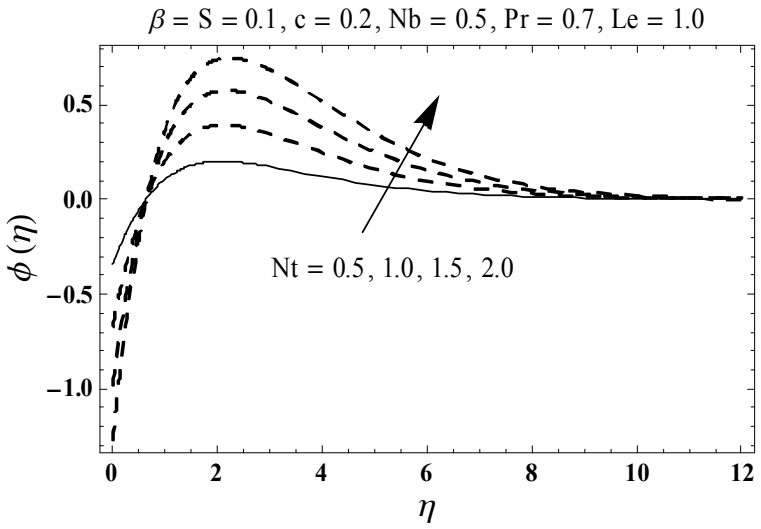

Fig. 4.12. Plots of $\phi(\eta)$ for Nt.

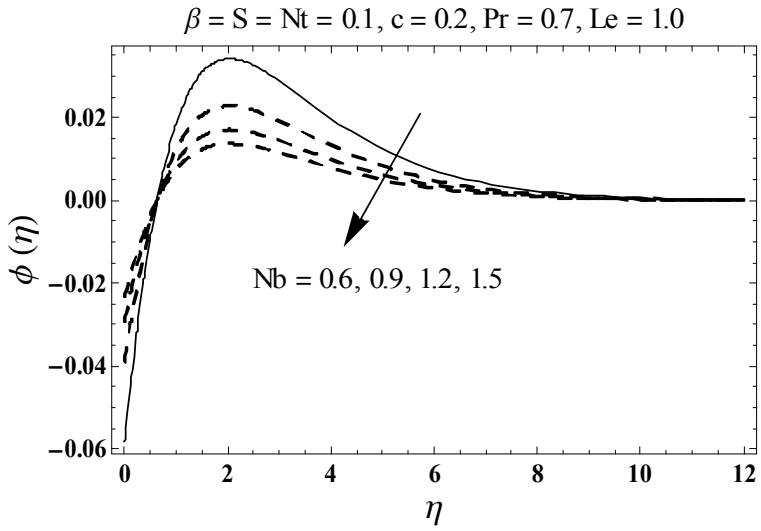

Fig. 4.13. Plots of $\phi(\eta)$ for Nb.

Table 4.2. Comparative estimations of $-f''(0)$ and $-g''(0)$ for several estimations of c when $\beta = 0$.

c	$-f''(0)$		$-g''(0)$	
	HAM	Exact [38]	HAM	Exact [38]
0	1	1	0	0
0.25	1.048811	1.048813	0.194564	0.194564
0.50	1.093095	1.093097	0.465205	0.465205
0.75	1.134486	1.134485	0.794618	0.794622
1.0	1.173722	1.173720	1.173722	1.173720

Table 4.3. Computations of local Nusselt number $(\mathrm{Re}_x)^{-1/2} Nu_x$ against β, c, Pr, S, Nt, Nb and Le.

β	c	Pr	S	Nt	Nb	Le	$-\theta'(0)$
0.0	0.2	0.7	0.1	0.1	0.5	1.0	0.7582
0.2							0.7236
0.5							0.6725
0.1	0.0	0.7	0.1	0.1	0.5	1.0	0.7080
	0.2						0.7408
	0.5						0.7824
0.1	0.2	0.5	0.1	0.1	0.5	1.0	0.5695
		1.0					0.9541
		1.5					1.2417
0.1	0.2	0.7	0.0	0.1	0.5	1.0	0.8077
			0.1				0.7408
			0.2				0.6460
0.1	0.2	0.7	0.1	0.0	0.5	1.0	0.7451
				0.5			0.7247
				1.0			0.7045
0.1	0.2	0.7	0.1	0.1	0.5	1.0	0.7408
					1.0		0.7408
					1.5		0.7408
0.1	0.2	0.7	0.1	0.1	0.5	0.5	0.7426
						1.0	0.7408
						1.5	0.7400

Chapter 5

Interaction of magnetic field in flow of Maxwell nanofluid with convective effect

Magnetohydrodynamic (MHD) three dimensional flow of Maxwell nanoliquid subject to convectively heated boundary is investigated. Flow generated is because of bi-directional extending surface. Thermophoresis and Brownian movement impacts are explored. Unlike the previous cases even in the absence of nanoparticles, the correct formulation for the flow of MHD Maxwell liquid is established. Newly proposed constraint with zero nanoparticles flux at boundary is employed. The governing nonlinear boundary-layer expressions through appropriate transformations are diminished in nonlinear ordinary differential frameworks. The resulting nonlinear frameworks have been solved for velocities, concentration and temperature. Convergence of constructed arrangements is verified. Effects of emerging variables for concentration and temperature are plotted and examined. Numerical estimations of local Nusselt number are computed and analyzed. Clearly effects of magnetic number and Biot parameter on concentration and temperature are quite similar. Both concentration and temperature are elevated for expanding estimation of magnetic number and Biot parameter.

5.1 Formulation

Consider three dimension flow of Maxwell nanoliquid by bi-directional extending surface. A constant magnetic field B_0 parallel to $z-$axis is applied. The electric field and Hall impacts are disregarded. Induced magnetic field is not taken subject to low magnetic Reynolds parameter. Thermophoresis and Brownian motion effects are taken into account. Temperature at surface is controlled by convective heating characterized via coefficient of heat transfer h_f and hot liquid temperature T_f below the surface. The boundary-layer expressions satisfy

$$\frac{\partial u}{\partial x}+\frac{\partial v}{\partial y}+\frac{\partial w}{\partial z}=0, \tag{5.1}$$

$$u\frac{\partial u}{\partial x}+v\frac{\partial u}{\partial y}+w\frac{\partial u}{\partial z}+\lambda_1\left(\begin{array}{c} u^2\frac{\partial^2 u}{\partial x^2}+v^2\frac{\partial^2 u}{\partial y^2}+w^2\frac{\partial^2 u}{\partial z^2} \\ +2uv\frac{\partial^2 u}{\partial x\partial y}+2vw\frac{\partial^2 u}{\partial y\partial z}+2uw\frac{\partial^2 u}{\partial x\partial z}\end{array}\right)=\nu\frac{\partial^2 u}{\partial z^2}-\frac{\sigma B_0^2}{\rho_f}\left(u+\lambda_1 w\frac{\partial u}{\partial z}\right), \tag{5.2}$$

$$u\frac{\partial v}{\partial x}+v\frac{\partial v}{\partial y}+w\frac{\partial v}{\partial z}+\lambda_1\left(\begin{array}{c} u^2\frac{\partial^2 v}{\partial x^2}+v^2\frac{\partial^2 v}{\partial y^2}+w^2\frac{\partial^2 v}{\partial z^2} \\ +2uv\frac{\partial^2 v}{\partial x\partial y}+2vw\frac{\partial^2 v}{\partial y\partial z}+2uw\frac{\partial^2 v}{\partial x\partial z}\end{array}\right)=\nu\frac{\partial^2 v}{\partial z^2}-\frac{\sigma B_0^2}{\rho_f}\left(v+\lambda_1 w\frac{\partial v}{\partial z}\right), \tag{5.3}$$

$$u\frac{\partial T}{\partial x}+v\frac{\partial T}{\partial y}+w\frac{\partial T}{\partial z}=\alpha\frac{\partial^2 T}{\partial z^2}+\frac{(\rho c)_p}{(\rho c)_f}\left(D_B\left(\frac{\partial T}{\partial z}\frac{\partial C}{\partial z}\right)+\frac{D_T}{T_\infty}\left(\frac{\partial T}{\partial z}\right)^2\right), \tag{5.4}$$

$$u\frac{\partial C}{\partial x}+v\frac{\partial C}{\partial y}+w\frac{\partial C}{\partial z}=D_B\left(\frac{\partial^2 C}{\partial z^2}\right)+\frac{D_T}{T_\infty}\left(\frac{\partial^2 T}{\partial z^2}\right). \tag{5.5}$$

Here one has the following prescribed conditions:

$$u=ax,\ v=by,\ w=0,\ -k\frac{\partial T}{\partial z}=h_f\left(T_f-T\right),\ D_B\frac{\partial C}{\partial z}+\frac{D_T}{T_\infty}\frac{\partial T}{\partial z}=0 \text{ at } z=0, \tag{5.6}$$

$$u\to 0,\quad v\to 0,\quad T\to T_\infty,\quad C\to C_\infty \quad \text{as } z\to\infty. \tag{5.7}$$

Here u, v and w stand for velocities in $x-$, $y-$ and $z-$directions, λ_1 for relaxation time, $\nu\left(=\mu/\rho_f\right)$ for kinematic viscosity, k for thermal conductivity, ρ_f for density, μ for dynamic viscosity, $(\rho c)_p$ for effective heat potential of nanoparticles, σ for electrical conductivity, T for temperature, $\alpha=k/(\rho c)_f$ for thermal diffusivity, $(\rho c)_f$ for heat potential of liquid, D_B for Brownian diffusivity, C for concentration, D_T for thermophoretic diffusion, T_∞ for ambient

temperature and C_∞ for ambient concentration. Selecting

$$\left.\begin{array}{c} u = axf'(\eta),\ v = ayg'(\eta),\ w = -\left(a\nu\right)^{1/2}\left(f(\eta)+g(\eta)\right), \\ \theta(\eta) = \frac{T-T_\infty}{T_f-T_\infty},\ \phi(\eta) = \frac{C-C_\infty}{C_\infty},\ \eta = \left(\frac{a}{\nu}\right)^{1/2} z. \end{array}\right\} \tag{5.8}$$

Eq. (5.1) is automatically satisfied while Eqs. $(5.2)-(5.7)$ have the following forms:

$$f''' + \left(M^2\beta + 1\right)(f+g)f'' - f'^2 + \beta\left(2\left(f+g\right)f'f'' - \left(f+g\right)^2 f'''\right) - M^2 f' = 0, \tag{5.9}$$

$$g''' + \left(M^2\beta + 1\right)(f+g)g'' - g'^2 + \beta\left(2\left(f+g\right)g'g'' - \left(f+g\right)^2 g'''\right) - M^2 g' = 0, \tag{5.10}$$

$$\theta'' + \Pr\left((f+g)\theta' + Nb\theta'\phi' + Nt\theta'^2\right) = 0, \tag{5.11}$$

$$\phi'' + Le\Pr(f+g)\phi' + \frac{Nt}{Nb}\theta'' = 0, \tag{5.12}$$

$$f = 0,\ g = 0,\ f' = 1,\ g' = c,\ \theta' = -\gamma\left(1-\theta\left(0\right)\right),\ Nb\phi' + Nt\theta' = 0 \text{ at } \eta = 0, \tag{5.13}$$

$$f' \to 0,\ g' \to 0,\ \theta \to 0,\ \phi \to 0 \text{ as } \eta \to \infty. \tag{5.14}$$

Here Nb stands for Brownian movement number, Le for Lewis parameter, M for magnetic number, Pr for Prandtl parameter, β for Deborah parameter, Nt for thermophoresis number, γ for Biot parameter and c for ratio of extending rates,. These variables can be specified by employing the definitions given below:

$$\left.\begin{array}{c} \beta = \lambda_1 a,\ M^2 = \frac{\sigma B_0^2}{\rho_f a},\ c = \frac{b}{a},\ \Pr = \frac{\nu}{\alpha},\ Nb = \frac{(\rho c)_p D_B C_\infty}{(\rho c)_f \nu}, \\ Nt = \frac{(\rho c)_p D_T\left(T_f - T_\infty\right)}{(\rho c)_f \nu T_\infty},\ \gamma = \frac{h_f}{k}\sqrt{\frac{\nu}{a}},\ Le = \frac{\alpha}{D_B}. \end{array}\right\} \tag{5.15}$$

The local Nusselt number Nu_x is defined as

$$Nu_x = -\frac{x}{(T_w - T_\infty)}\left.\frac{\partial T}{\partial z}\right|_{z=0} = -\left(\mathrm{Re}_x\right)^{1/2}\theta'(0). \tag{5.16}$$

It is watched that dimensionless mass flux represented by Sherwood number is now identically zero while $\mathrm{Re}_x = u_w x/\nu$ for local Reynolds parameter.

5.2 Solutions by HAM

The series arrangements of Eqs. $(5.9)-(5.12)$ through (5.13) and (5.14) have been developed by utilizing homotopic analysis technique (HAM). The linear operators and initial deformations have been selected as follows:

$$f_0(\eta)=1-e^{-\eta},\quad g_0(\eta)=c(1-e^{-\eta}),\quad \phi_0(\eta)=-\frac{\gamma}{1+\gamma}\frac{Nt}{Nb}e^{-\eta},\quad \theta_0(\eta)=\frac{\gamma}{1+\gamma}e^{-\eta}, \tag{5.17}$$

$$\mathcal{L}_f=f'''-f',\quad \mathcal{L}_g=g'''-g',\quad \mathcal{L}_\phi=\phi''-\phi,\quad \mathcal{L}_\theta=\theta''-\theta. \tag{5.18}$$

The above linear operators obey

$$\left.\begin{array}{c}\mathcal{L}_f\left[F_1^{**}+F_2^{**}e^{\eta}+F_3^{**}e^{-\eta}\right]=0,\quad \mathcal{L}_g\left[F_4^{**}+F_5^{**}e^{\eta}+F_6^{**}e^{-\eta}\right]=0,\\ \mathcal{L}_\theta\left[F_7^{**}e^{\eta}+F_8^{**}e^{-\eta}\right]=0,\quad \mathcal{L}_\phi\left[F_9^{**}e^{\eta}+F_{10}^{**}e^{-\eta}\right]=0,\end{array}\right\} \tag{5.19}$$

in which F_j^{**} $(j=1-10)$ stand for arbitrary constants. Problems for zeroth and mth-order deformations are easily formulated in the view of above operators. The deformation issues are computed by Mathematica software.

5.3 Convergence analysis

The series arrangements have auxiliary variables $\hbar_f$, $\hbar_g$, $\hbar_\theta$ and $\hbar_\phi$. These variables are helpful for convergence of acquired series arrangements. Proper estimations of these variables are quite essential to construct homotopic convergent arrangements through homotopic analysis technique (HAM). To choose suitable estimations of $\hbar_f$, $\hbar_g$, $\hbar_\theta$ and $\hbar_\phi$, the $\hbar-$plots are plotted at 15th order of deformations. Figs. 5.1 and 5.2 show that convergence area lies inside the ranges $-1.80\leq\hbar_f\leq-0.35$, $-1.90\leq\hbar_g\leq-0.20$, $-1.65\leq\hbar_\theta\leq-0.15$ and $-1.70\leq\hbar_\phi\leq-0.10$. Table 5.1 exhibits that 8th order of deformations is sufficient for the convergent homotopic

series arrangements.

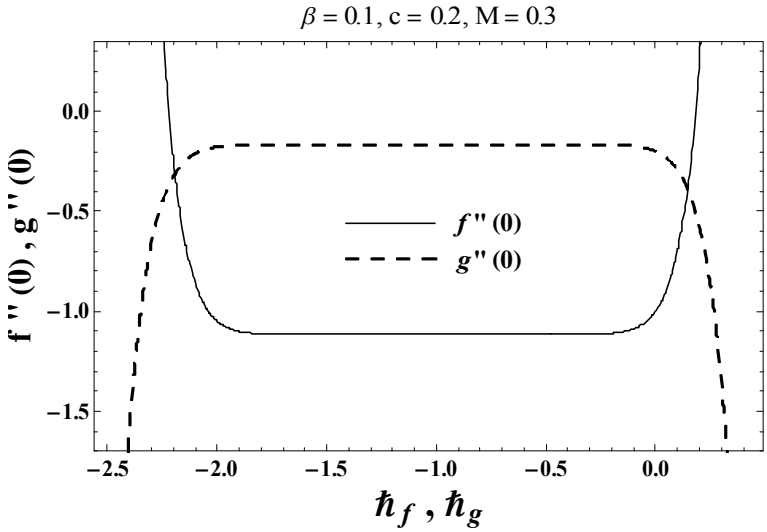

Fig. 5.1. $\hbar-$plots for $f(\eta)$ and $g(\eta)$.

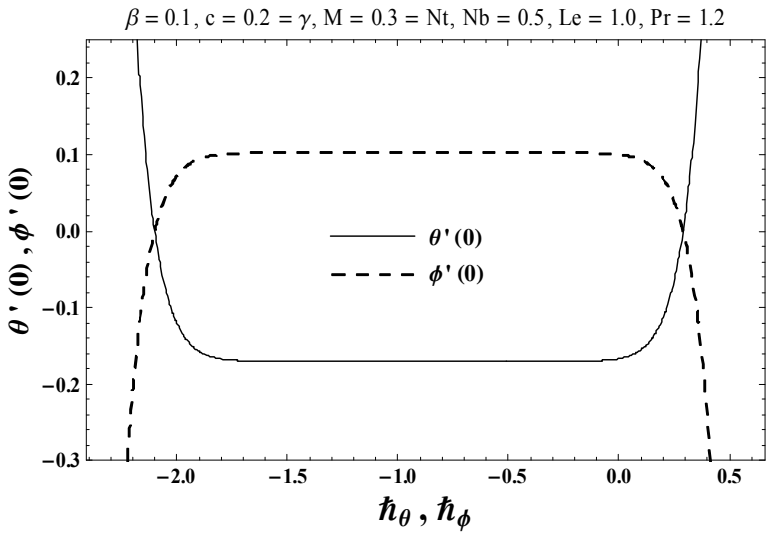

Fig. 5.2. $\hbar-$plots for $\theta(\eta)$ and $\phi(\eta)$.

Table 5.1. HAM arrangements convergence when $\beta = 0.1$, $c = 0.2 = \gamma$, $M = 0.3 = Nt$, $Nb = 0.5$, $Le = 1.0$ and $\Pr = 1.2$.

Order of deformations	$-f''(0)$	$-g''(0)$	$-\theta'(0)$	$\phi'(0)$
1	1.11213	0.16589	0.17056	0.10233
5	1.11540	0.16474	0.17011	0.10206
8	1.11540	0.16473	0.17010	0.10206
15	1.11540	0.16473	0.17010	0.10206
25	1.11540	0.16473	0.17010	0.10206
40	1.11540	0.16473	0.17010	0.10206
50	1.11540	0.16473	0.17010	0.10206

5.4 Discussion

The effects of interesting physical variables like Lewis parameter Le, ratio number c, Prandtl parameter Pr, Deborah parameter β, magnetic number M, Biot parameter γ, thermophoresis number Nt and Brownian movement number Nb on temperature $\theta(\eta)$ and concentration $\phi(\eta)$ are plotted in Figs. $5.3 - 5.16$. Fig. 5.3 presents impact of Deborah parameter β for temperature θ. Here temperature and layer of thermal are elevated when we improvement Deborah parameter. Deborah parameter is directly proportional to relaxation time. Relaxation time is higher for bigger Deborah parameter. Hence higher relaxation time causes to enhance temperature and layer of thermal. Fig. 5.4 presents variations in temperature profile for different estimations of magnetic number M. Here $M > 0$ corresponds to hydro-magnetic flow and $M = 0$ is for hydro-dynamic flow situation. We watched that temperature and layer of thermal are higher for hydro-magnetic flow in comparison to hydro-dynamic flow situation. Fig. 5.5 describes decay in temperature profile and its corresponding layer thickness when c elevates. Here $c = 0$ corresponds to two dimensional flow situation. We watched that layer of thermal is more in two dimension situation when compared with three dimension flow. Fig. 5.6 is displayed to see the influence of Biot parameter γ on temperature profile $\theta(\eta)$. An increment in γ causes a stronger convection which provides elevated temperature and layer of thermal. Fig. 5.7 describes conduct of Prandtl parameter Pr on temperature profile $\theta(\eta)$. We watched

that bigger Prandtl parameter results in a diminishment of temperature profile and layer of thermal. An improvement in Prandtl parameter corresponds to poor thermal diffusivity. Physically bigger Prandtl fluids have poor thermal diffusivity and small Prandtl fluids have stronger thermal diffusivity. This variation in thermal diffusivity creates a diminishment in temperature $\theta(\eta)$ and layer of thermal. Fig. 5.8 presents that bigger estimations of thermophoresis number Nt causes an improvement in temperature profile $\theta(\eta)$. An improvement in Nt producing an improvement in thermophoresis force which tends to shift nanoparticles from hot to cold zone and consequently it elevates the temperature and layer of thermal. Fig. 5.9 presents that an improvement in Deborah parameter β causes an improvement of concentration profile and its corresponding layer thickness. From Fig. 5.10 we watched that concentration field is higher for hydro-magnetic flow ($M > 0$) and lower for hydro-dynamic situation ($M = 0$). It is additionally watched that concentration is improved and leaving from the surface of the surface for hydro-magnetic flow. Impact of ratio number c on concentration profile $\phi(\eta)$ is sketched in Fig. 5.11. Concentration $\phi(\eta)$ and its corresponding layer thickness are diminished when we improvement ratio number. Fig. 5.12 indicates effects of Biot parameter γ on concentration profile $\phi(\eta)$. Here we watched that bigger Biot parameter creates an improvement in concentration profile and its associated layer thickness. Fig. 5.13 exhibits that bigger estimations of Lewis parameter Le causes a diminishment in concentration profile $\phi(\eta)$. Lewis parameter depends on Brownian movement coefficient. Bigger Lewis parameter leads to poor Brownian movement coefficient which exhibits a poor concentration and its corresponding layer thickness. Fig. 5.14 presents variations in concentration $\phi(\eta)$ for different estimations of Prandtl parameter Pr. We watched that bigger Prandtl parameter show a diminishment in concentration $\phi(\eta)$ and its associated layer thickness. Fig. 5.15 exhibits that an improvement in thermophoresis number Nt causes an improvement in concentration $\phi(\eta)$ and its corresponding layer thickness. Fig. 5.16 presents that bigger Brownian movement number Nb creates a diminishment in concentration profile $\phi(\eta)$. In nanoliquid framework, due to existence of nanoparticles, the Brownian movement takes place and with improvement in Nb the Brownian movement is affected and thus layer of concentration diminishes. Table 5.2 exhibits the comparison for different estimations of c with exact arrangement. Table 5.2 presents an excellent agreement of HAM arrangement with the existing exact arrangement in a limiting situation. Table 5.3 is computed to investigate transfer

of heat rate (local Nusselt number) via β, c, M, γ, Le, Pr, Nt and Nb. Transfer of heat rate is an expanding function of Biot parameter γ. Effects of Lewis parameter Le and Brownian movement number Nb on transfer of heat rate are quite similar.

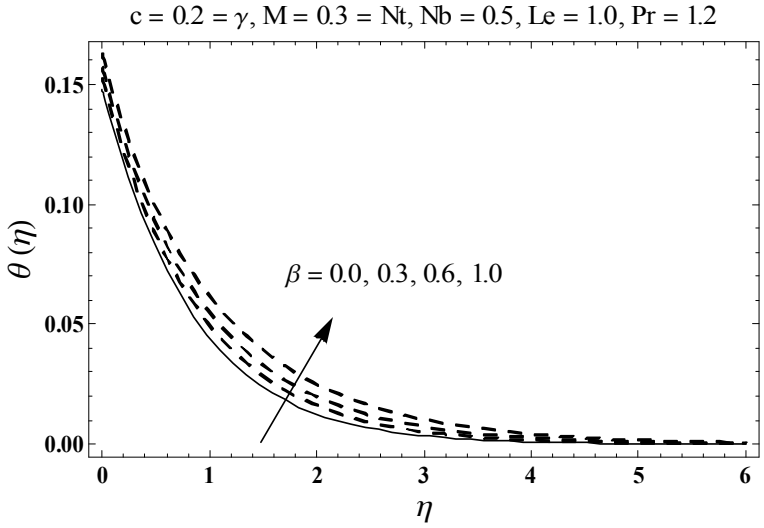

Fig. 5.3. Plots of $\theta(\eta)$ for β.

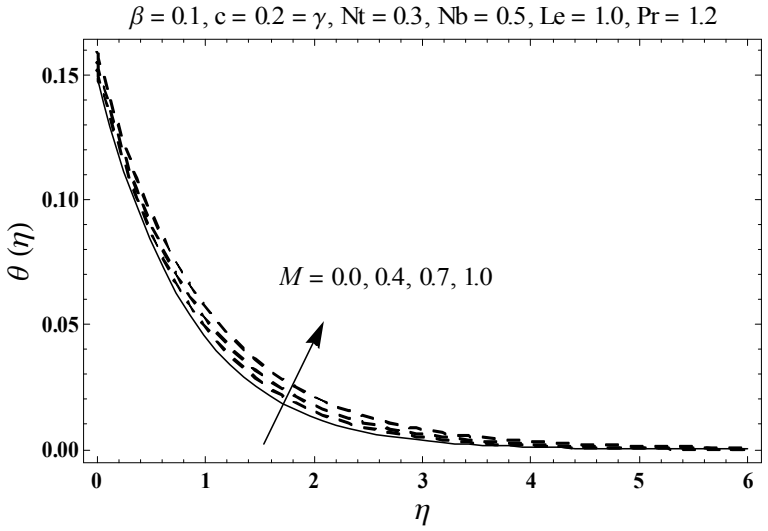

Fig. 5.4. Plots of $\theta(\eta)$ for M.

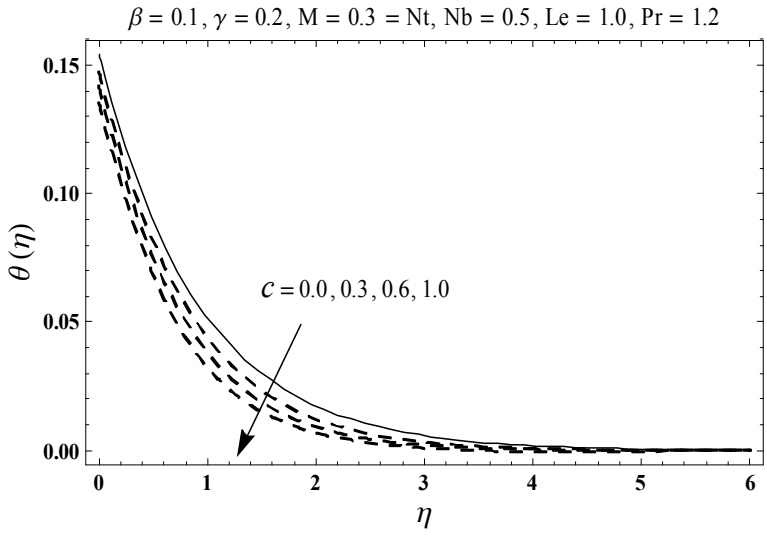

Fig. 5.5. Plots of $\theta(\eta)$ for c.

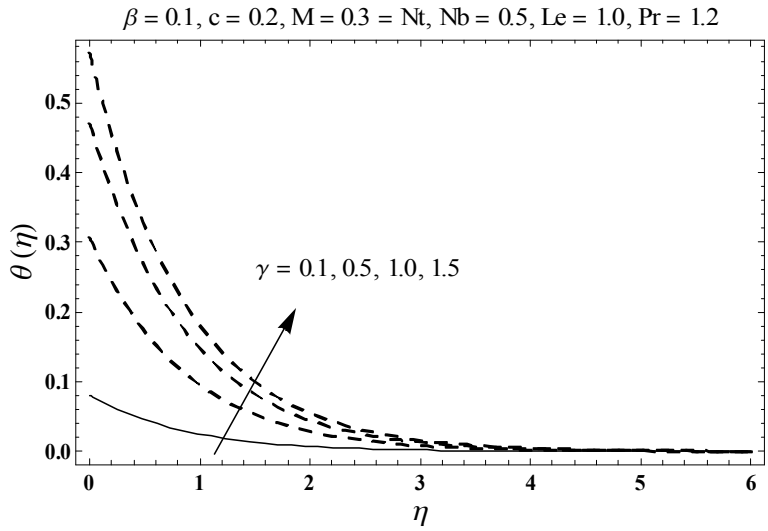

Fig. 5.6. Plots of $\theta(\eta)$ for γ.

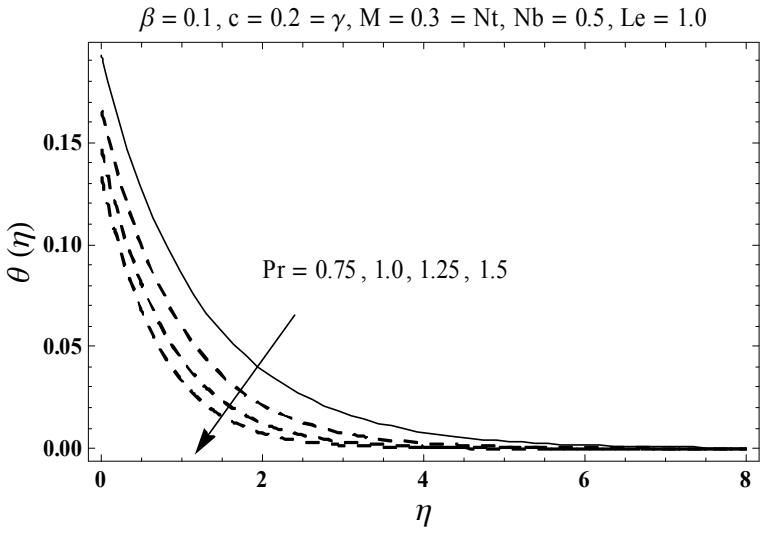

Fig. 5.7. Plots of $\theta(\eta)$ for Pr .

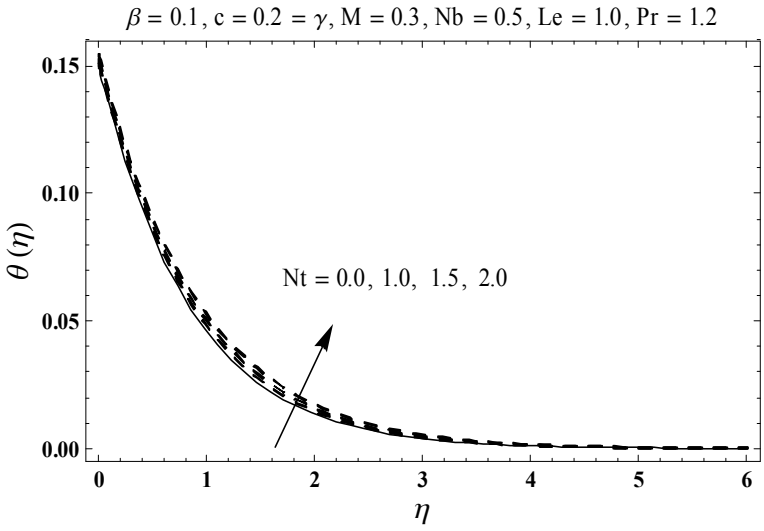

Fig. 5.8. Plots of $\theta(\eta)$ for Nt.

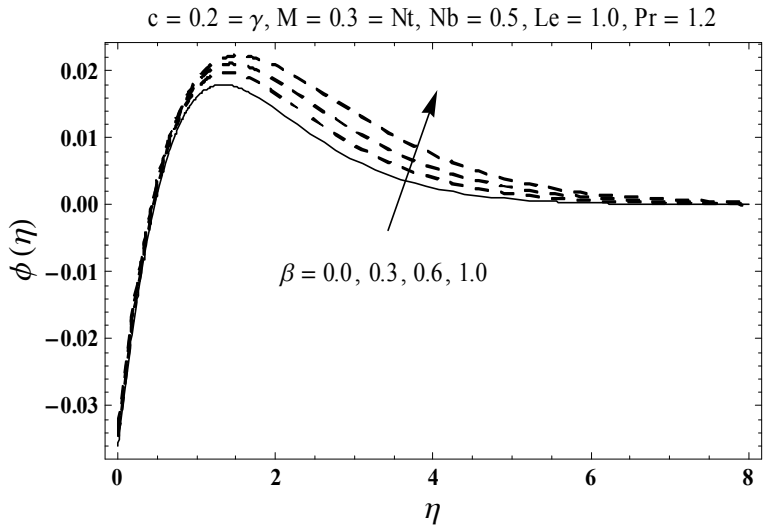

Fig. 5.9. Plots of $\phi(\eta)$ for β.

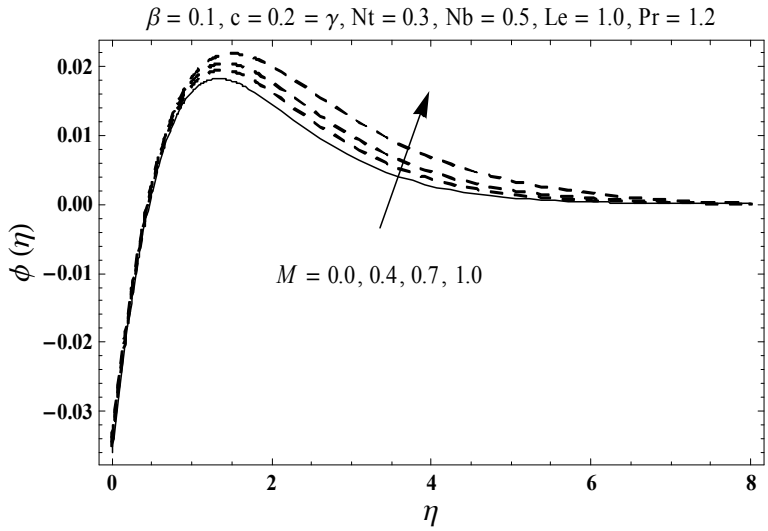

Fig. 5.10. Plots of $\phi(\eta)$ for M.

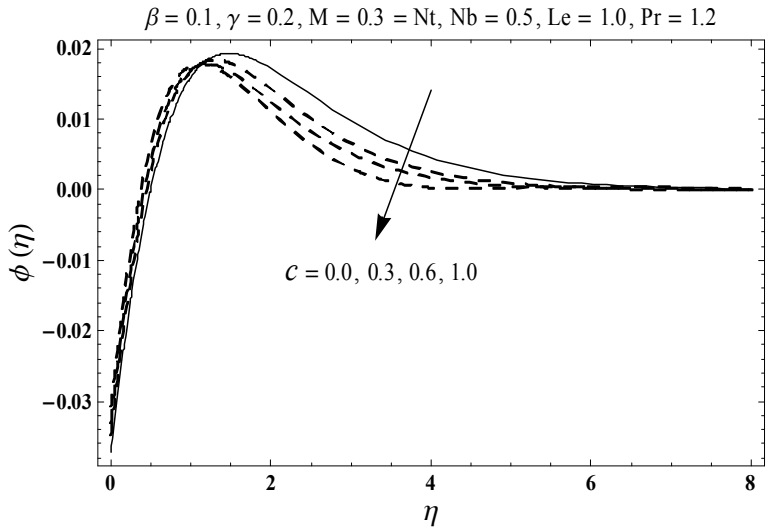

Fig. 5.11. Plots of $\phi(\eta)$ for c.

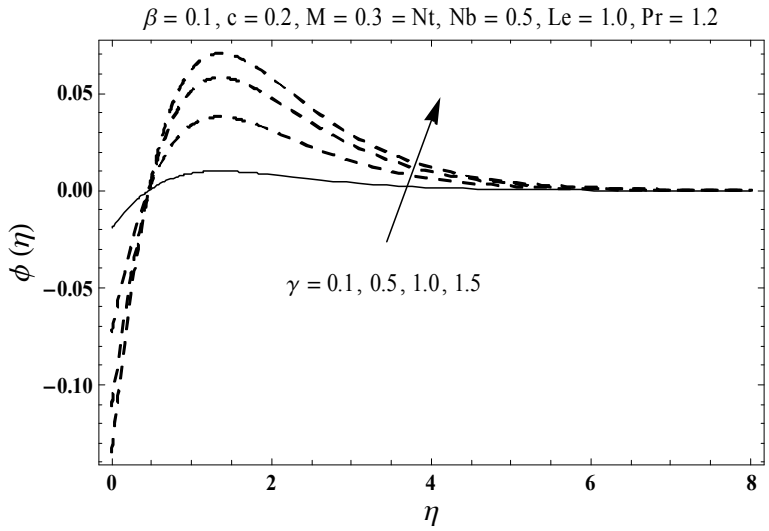

Fig. 5.12. Plots of $\phi(\eta)$ for γ.

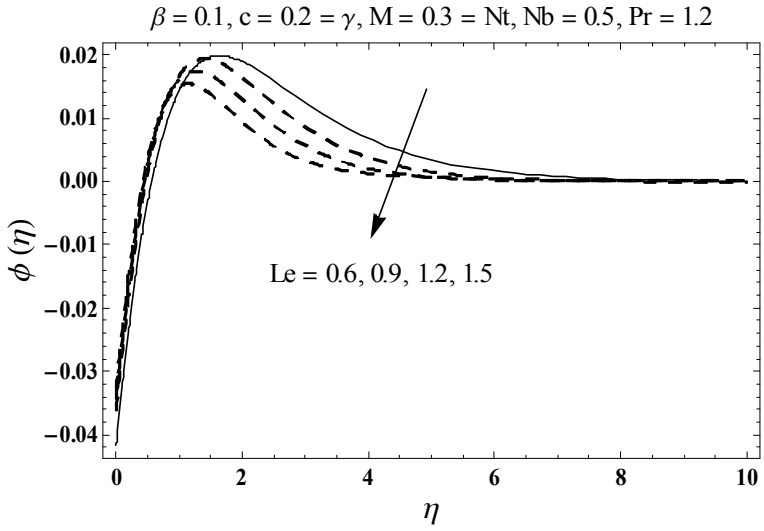

Fig. 5.13. Plots of $\phi(\eta)$ for Le.

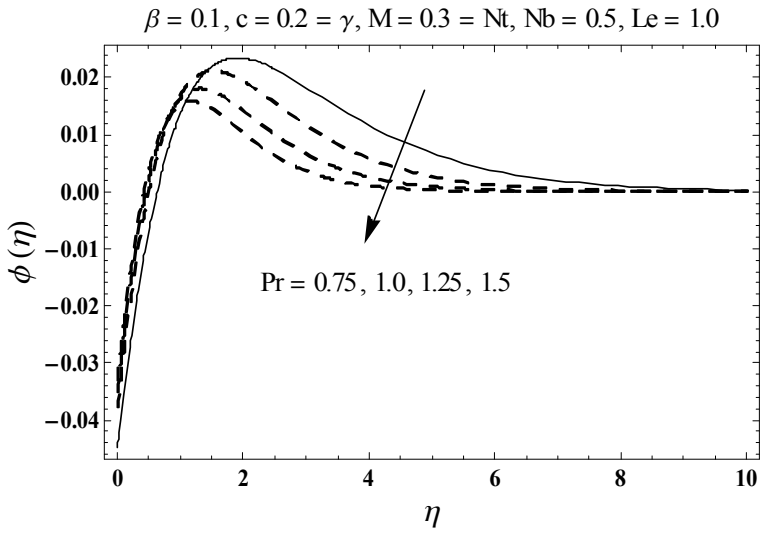

Fig. 5.14. Plots of $\phi(\eta)$ for Pr .

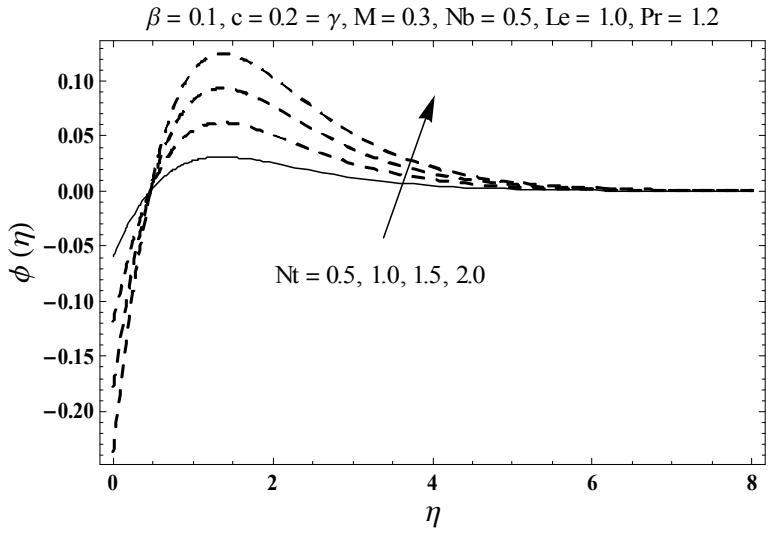

Fig. 5.15. Plots of $\phi(\eta)$ for Nt.

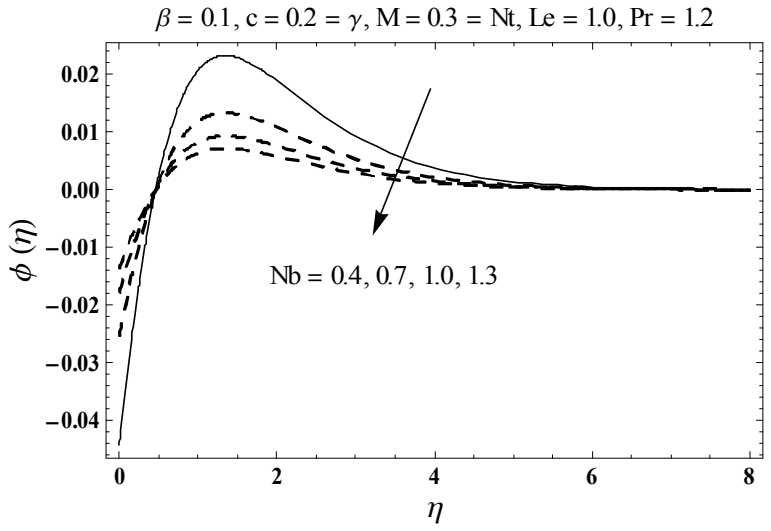

Fig. 5.16. Plots of $\phi(\eta)$ for Nb.

Table 5.2. Comparative estimations of $-f''(0)$ and $-g''(0)$ for various estimations of c when $\beta = M = 0$.

c	$-f''(0)$		$-g''(0)$	
	HAM	Exact [38]	HAM	Exact [38]
0	1	1	0	0
0.25	1.048811	1.048813	0.194564	0.194564
0.50	1.093095	1.093097	0.465205	0.465205
0.75	1.134486	1.134485	0.794618	0.794622
1.0	1.173722	1.173720	1.173722	1.173720

Table 5.3. Numeric data for Nusselt number $\left(-\theta'(0)\right)$ for different estimations of β, c, M, γ, Le, Pr, Nt and Nb.

β	c	M	γ	Le	Pr	Nt	Nb	$-\theta'(0)$
0.0	0.2	0.3	0.2	1.0	1.2	0.3	0.5	0.1704
0.5								0.1689
1.0								0.1675
0.1	0.0	0.3	0.2	1.0	1.2	0.3	0.5	0.1691
	0.5							0.1713
	1.0							0.1730
0.1	0.2	0.0	0.2	1.0	1.2	0.3	0.5	0.1703
		0.5						0.1697
		1.0						0.1678
0.1	0.2	0.3	0.2	1.0	1.2	0.3	0.5	0.1701
			0.7					0.4326
			1.2					0.5817
0.1	0.2	0.3	0.2	0.5	1.2	0.3	0.5	0.1701
				1.0				0.1701
				1.5				0.1701
0.1	0.2	0.3	0.2	1.0	0.5	0.3	0.5	0.1520
					1.0			0.1670
					1.5			0.1735
0.1	0.2	0.3	0.2	1.0	1.2	0.0	0.5	0.1702
						0.5		0.1700
						1.0		0.1699
0.1	0.2	0.3	0.2	1.0	1.2	0.3	0.5	0.1701
							1.0	0.1701
							1.5	0.1701

Chapter 6

An optimal study for three-dimensional flow of Maxwell nanofluid subject to rotating frame

Here we are concerned with optimal homotopy arrangements for three dimensional flow of Maxwell nanoliquid in rotating frame. Flow is induced by uniform extending of boundary surface in one direction. Buongiorno relation is received which includes the novel parts of Brownian movement and thermophoresis. Boundary-layer approximations are conjured to rearrange the governing arrangement of partial differential conditions. Appropriate relations are introduced to nondimensionalize the relevant boundary-layer expressions. Newly suggested condition associated with zero nanoparticles mass flux at boundary is imposed. Uniformly valid convergent arrangement expressions are developed by means of optimal homotopic technique (OHAM). Plots are portrayed in order to explain role of embedded flow variables. Transfer of heat rate has been tabulated and analyzed. Our findings present that concentration and temperature are smaller for Newtonian liquid when compared with upper-convected Maxwell (UCM). Moreover Brownian movement has mild influence of heat flux at boundary. Viscoelastic effect has tendency to reduce transfer of heat rate from the extending boundary.

6.1 Formulation

We explore the three dimensional rotating flow of Maxwell nanoliquid by a linearly extending surface. Nanoliquid relation exhibits the characteristics of Brownian movement and thermophoresis. Cartesian coordinate framework is selected in such a manner that surface is lined up with $xy-$plane and liquid is taken in space $z \geq 0$. Surface deforms linearly in the $x-$direction with rate a. Further the liquid is subjected to uniform rotation about $z-$axis with consistent angular velocity Ω. The associated expressions governing the Maxwell nanoliquid flow in rotating frame are

$$\frac{\partial u}{\partial x}+\frac{\partial v}{\partial y}+\frac{\partial w}{\partial z}=0, \tag{6.1}$$

$$u\frac{\partial u}{\partial x}+v\frac{\partial u}{\partial y}+w\frac{\partial u}{\partial z}-2\Omega v=\nu\frac{\partial^2 u}{\partial z^2}-\lambda_1\left(\begin{array}{c} u^2\frac{\partial^2 u}{\partial x^2}+v^2\frac{\partial^2 u}{\partial y^2}+w^2\frac{\partial^2 u}{\partial z^2} \\ +2uv\frac{\partial^2 u}{\partial x\partial y}+2vw\frac{\partial^2 u}{\partial y\partial z}+2uw\frac{\partial^2 u}{\partial x\partial z} \\ -2\Omega\left(u\frac{\partial v}{\partial x}+v\frac{\partial v}{\partial y}+w\frac{\partial v}{\partial z}\right)+2\Omega\left(v\frac{\partial u}{\partial x}-u\frac{\partial u}{\partial y}\right) \end{array}\right), \tag{6.2}$$

$$u\frac{\partial v}{\partial x}+v\frac{\partial v}{\partial y}+w\frac{\partial v}{\partial z}+2\Omega u=\nu\frac{\partial^2 v}{\partial z^2}-\lambda_1\left(\begin{array}{c} u^2\frac{\partial^2 v}{\partial x^2}+v^2\frac{\partial^2 v}{\partial y^2}+w^2\frac{\partial^2 v}{\partial z^2} \\ +2uv\frac{\partial^2 v}{\partial x\partial y}+2vw\frac{\partial^2 v}{\partial y\partial z}+2uw\frac{\partial^2 v}{\partial x\partial z} \\ +2\Omega\left(u\frac{\partial u}{\partial x}+v\frac{\partial u}{\partial y}+w\frac{\partial u}{\partial z}\right)+2\Omega\left(v\frac{\partial v}{\partial x}-u\frac{\partial v}{\partial y}\right) \end{array}\right), \tag{6.3}$$

$$u\frac{\partial T}{\partial x}+v\frac{\partial T}{\partial y}+w\frac{\partial T}{\partial z}=\alpha_m\frac{\partial^2 T}{\partial z^2}+\frac{(\rho c)_p}{(\rho c)_f}\left(D_B\left(\frac{\partial T}{\partial z}\frac{\partial C}{\partial z}\right)+\frac{D_T}{T_\infty}\left(\frac{\partial T}{\partial z}\right)^2\right), \tag{6.4}$$

$$u\frac{\partial C}{\partial x}+v\frac{\partial C}{\partial y}+w\frac{\partial C}{\partial z}=D_B\left(\frac{\partial^2 C}{\partial z^2}\right)+\frac{D_T}{T_\infty}\left(\frac{\partial^2 T}{\partial z^2}\right). \tag{6.5}$$

Here one has the following prescribed conditions:

$$u=u_w(x)=ax,\ v=0,\ w=0,\ T=T_w,\ D_B\frac{\partial C}{\partial z}+\frac{D_T}{T_\infty}\frac{\partial T}{\partial z}=0 \text{ at } z=0, \tag{6.6}$$

$$u\to 0,\quad v\to 0,\quad T\to T_\infty,\quad C\to C_\infty \text{ as } z\to\infty. \tag{6.7}$$

Here u, v and w stand for velocities in $x-$, $y-$ and $z-$directions, μ for dynamic viscosity, $\nu=\mu/\rho_f$ for kinematic viscosity, ρ_f for density, T for temperature, $\alpha_m=k/(\rho c)_f$ for thermal diffusivity, $(\rho c)_f$ for heat potential of liquid, k for thermal conductivity, $(\rho c)_p$ for effective heat potential of nanoparticles, C for concentration, D_B for Brownian movement coefficient, λ_1 for

liquid relaxation time, D_T for thermophoretic diffusion coefficient, T_w for wall temperature, T_∞ for ambient temperature, C_∞ for ambient concentration and a for positive constant. Selecting

$$\begin{array}{c} u = axf'(\zeta),\ v = axg(\zeta),\ w = -\left(a\nu\right)^{1/2} f\left(\zeta\right), \\ \theta(\zeta) = \frac{T-T_\infty}{T_w-T_\infty},\ \phi(\zeta) = \frac{C-C_\infty}{C_\infty},\ \zeta = \left(\frac{a}{\nu}\right)^{1/2} z. \end{array} \tag{6.8}$$

Expression (6.1) is identically verified while Eqs. $(6.2) - (6.7)$ take to the following forms

$$f''' + ff'' - f'^2 + 2\lambda\left(g - \beta fg'\right) + \beta\left(2ff'f'' - f^2f'''\right) = 0, \tag{6.9}$$

$$g'' + fg' - f'g - 2\lambda\left(f' + \beta\left(f'^2 - ff'' + g^2\right)\right) + \beta\left(2ff'g' - f^2g''\right) = 0, \tag{6.10}$$

$$\theta'' + \Pr\left(f\theta' + Nb\theta'\phi' + Nt\theta'^2\right) = 0, \tag{6.11}$$

$$\phi'' + Scf\phi' + \frac{Nt}{Nb}\theta'' = 0, \tag{6.12}$$

$$f(0) = g(0) = 0,\ f'(0) = 1,\ \theta(0) = 1,\ Nb\phi'(0) + Nt\theta'(0) = 0, \tag{6.13}$$

$$f'(\infty) \to 0,\ g(\infty) \to 0,\ \theta(\infty) \to 0,\ \phi(\infty) \to 0. \tag{6.14}$$

Here Nb stands for Brownian movement number, Pr for Prandtl parameter, β for Deborah parameter, Sc for Schmidt parameter, λ for rotation parameter and Nt for thermophoresis number. These variables can be specified by employing the definitions given below:

$$\left.\begin{array}{c} \lambda = \frac{\Omega}{a},\ \beta = \lambda_1 a,\ \Pr = \frac{\nu}{\alpha_m}, \\ Nb = \frac{(\rho c)_p D_B C_\infty}{(\rho c)_f \nu},\ Nt = \frac{(\rho c)_p D_T (T_w - T_\infty)}{(\rho c)_f \nu T_\infty},\ Sc = \frac{\nu}{D_B}. \end{array}\right\} \tag{6.15}$$

The local Nusselt number Nu_x is defined as

$$\mathrm{Re}_x^{-1/2}\, Nu_x = -\frac{x}{(T_w - T_\infty)}\left.\frac{\partial T}{\partial z}\right|_{z=0} = -\theta'\left(0\right), \tag{6.16}$$

where $\mathrm{Re}_x = u_w x/\nu$ exhibits local Reynolds parameter. It is also watched that Sherwood number is identically zero.

6.2 Solutions by OHAM

The optimal series arrangements of Eqs. $(6.9)-(6.12)$ through (6.13) and (6.14) have been developed by utilizing optimal homotopic analysis technique (OHAM). The linear operators and initial deformations have been selected as follows:

$$\left.\begin{array}{c} f_0(\zeta)=1-\exp(-\zeta),\ g_0(\zeta)=0, \\ \theta_0(\zeta)=\exp(-\zeta),\ \phi_0(\zeta)=-\frac{Nt}{Nb}\exp(-\zeta), \end{array}\right\} \tag{6.17}$$

$$\left.\begin{array}{c} \mathcal{L}_f=\frac{d^3f}{d\zeta^3}-\frac{df}{d\zeta},\quad \mathcal{L}_g=\frac{d^2g}{d\zeta^2}-g, \\ \mathcal{L}_\theta=\frac{d^2\theta}{d\zeta^2}-\theta,\quad \mathcal{L}_\phi=\frac{d^2\phi}{d\zeta^2}-\phi. \end{array}\right\} \tag{6.18}$$

The above linear operators obey

$$\left.\begin{array}{c} \mathcal{L}_f\left[F_1^{**}+F_2^{**}\exp(\zeta)+F_3^{**}\exp(-\zeta)\right]=0, \\ \mathcal{L}_g\left[F_4^{**}\exp(\zeta)+F_5^{**}\exp(-\zeta)\right]=0, \\ \mathcal{L}_\theta\left[F_6^{**}\exp(\zeta)+F_7^{**}\exp(-\zeta)\right]=0, \\ \mathcal{L}_\phi\left[F_8^{**}\exp(\zeta)+F_9^{**}\exp(-\zeta)\right]=0, \end{array}\right\} \tag{6.19}$$

in which F_j^{**} $(j=1-9)$ stand for arbitrary constants. Problems for zeroth and mth-order deformations are easily formulated in the view of above operators. The deformation issues are solved by BVPh2.0 of Mathematica software.

6.3 Convergence analysis

We have solved the momentum, energy and concentration expressions with the help of BVPh2.0. These expressions contain unknown variables $\hbar_f$, $\hbar_g$, $\hbar_\theta$ and $\hbar_\phi$. We can compute the minimum estimation of these variables by taking total error small. In the frame of HAM, these variables play a vital role. That is why these variables refer to as convergence-control parameter which differs HAM from other analytical approximation methods. In order to reduce the CPU time, we have employed average residual errors at the mth-oder of approximation which are defined

by

$$\varepsilon_m^f = \frac{1}{k+1}\sum_{j=0}^{k}\left[\mathcal{N}_f\left(\sum_{i=0}^{m}\hat{f}(\zeta),\ \sum_{i=0}^{m}\hat{g}(\zeta)\right)_{\zeta=j\delta\zeta}\right]^2, \tag{6.20}$$

$$\varepsilon_m^g = \frac{1}{k+1}\sum_{j=0}^{k}\left[\mathcal{N}_g\left(\sum_{i=0}^{m}\hat{f}(\zeta),\ \sum_{i=0}^{m}\hat{g}(\zeta)\right)_{\zeta=j\delta\zeta}\right]^2, \tag{6.21}$$

$$\varepsilon_m^\theta = \frac{1}{k+1}\sum_{j=0}^{k}\left[\mathcal{N}_\theta\left(\sum_{i=0}^{m}\hat{f}(\zeta),\ \sum_{i=0}^{m}\hat{g}(\zeta),\ \sum_{i=0}^{m}\hat{\theta}(\zeta),\ \sum_{i=0}^{m}\hat{\phi}(\zeta),\right)_{\zeta=j\delta\zeta}\right]^2, \tag{6.22}$$

$$\varepsilon_m^\phi = \frac{1}{k+1}\sum_{j=0}^{k}\left[\mathcal{N}_\phi\left(\sum_{i=0}^{m}\hat{f}(\zeta),\ \sum_{i=0}^{m}\hat{g}(\zeta),\ \sum_{i=0}^{m}\hat{\theta}(\zeta),\ \sum_{i=0}^{m}\hat{\phi}(\zeta),\right)_{\zeta=j\delta\zeta}\right]^2. \tag{6.23}$$

Here $\mathcal{N}_f$, $\mathcal{N}_g$, $\mathcal{N}_\theta$ and $\mathcal{N}_\phi$ denote the non-linear operators corresponding to Eqs. (6.9) – (6.12) respectively. Following Liao [69] :

$$\varepsilon_m^t = \varepsilon_m^f + \varepsilon_m^g + \varepsilon_m^\theta + \varepsilon_m^\phi, \tag{6.24}$$

where ε_m^t stands for total residual square error, $k = 20$ and $\delta\zeta = 0.5$. Optimal data for auxiliary variables at 2nd order of deformations is $\hbar_f = -1.50853$, $\hbar_g = -1.17662$, $\hbar_\theta = -1.15433$ and $\hbar_\phi = -1.02305$ and $\varepsilon_m^t = 2.21 \times 10^{-4}$. Table 6.1 presents average square residual error at different order of deformations. It has been analyzed that the average residual square errors reduce with higher order deformations.

Table 6.1. Individual average residual square errors employing optimal data of auxiliary variables.

m	ε_m^f	ε_m^g	ε_m^θ	ε_m^ϕ
2	1.47×10^{-5}	8.14×10^{-6}	1.04×10^{-4}	9.41×10^{-5}
6	3.01×10^{-8}	5.41×10^{-8}	2.34×10^{-6}	6.87×10^{-6}
10	4.52×10^{-10}	1.77×10^{-9}	1.65×10^{-7}	1.14×10^{-6}
16	1.72×10^{-11}	1.61×10^{-11}	4.83×10^{-9}	8.01×10^{-8}
20	6.60×10^{-13}	1.99×10^{-12}	5.72×10^{-10}	1.42×10^{-8}
26	7.19×10^{-14}	7.96×10^{-14}	3.08×10^{-11}	1.10×10^{-9}
30	5.50×10^{-15}	1.62×10^{-14}	4.93×10^{-12}	2.03×10^{-10}

6.4 Discussion

This section explores influences of various pertinent flow variables like Prandtl parameter Pr, Deborah parameter β, Brownian movement number Nb, rotation parameter λ, Schmidt parameter Sc and thermophoresis number Nt on temperature $\theta(\zeta)$ and concentration $\phi(\zeta)$. Fig. 6.1 exhibits curves of temperature field $\theta(\zeta)$ for varying Deborah parameter β. From this Fig. it has been watched that by expanding Deborah parameter β, penetration depth of $\theta(\zeta)$ ends up thicker. Fig. 6.2 plots the temperature $\theta(\zeta)$ for particular estimations of rotation parameter λ. Bigger rotation parameter λ constitutes a elevated temperature and more layer of thermal. Fig. 6.3 exhibits that how temperature $\theta(\zeta)$ gets influenced with variety of Prandtl parameter Pr . It is watched that by upgrading Prandtl parameter Pr, temperature $\theta(\zeta)$ declines and layer of thermal diminishes. Physically as Prandtl parameter Pr has opposite association with thermal diffusivity, thusly, an augmentation in Pr prompts poor thermal diffusion and henceforth less penetration depth of $\theta(\zeta)$. Thicker layer of thermal ascribed to bigger Prandtl parameter is went with higher slope of temperature close to the wall. Fig. 6.4 is plotted to depict impact of thermophoreis parameter Nt for temperature field $\theta(\zeta)$. Bigger thermophoresis number Nt prompt a elevated temperature $\theta(\zeta)$ and thicker layer of thermal. The explanation for this result is that an upgrade in Nt provides a more grounded thermophoretic constrain on nanoparticles in course inverse to forced temperature gradient. This movements nanoparticles towards the chilly surrounding liquid because of which layer of thermal increments. Fig. 6.5 plots the concentration field $\phi(\zeta)$ for wide range of Deborah parameter β. Bigger estimations of Deborah parameter β constitute a bigger concentration field and more layer of concentration. Fig. 6.6 exhibits variation in concentration field $\phi(\zeta)$ for varying rotation parameter λ. From this Fig. it has been watched that by expanding rotation parameter λ, an improvement in concentration $\phi(\zeta)$ and its corresponding layer is taken note. Fig. 6.7 exhibits that how variation of Schmidt parameter Sc affects concentration field $\phi(\zeta)$. It has been watched that the expanding estimations of Schmidt parameter prompt decrease the concentration $\phi(\zeta)$. Schmidt parameter depends on Brownian diffusivity. An expansion in Schmidt parameter Sc provides poor Brownian diffusivity. Such poor Brownian diffusivity relates to bring down concentration $\phi(\zeta)$ and less layer of concentration. Fig. 6.8 plots the concentration $\phi(\zeta)$ for fluctuating estimations of thermophoreis parameter Nt. It has been obviously watched that higher ther-

mophoresis Nt prompts more grounded concentration $\phi(\zeta)$ and associated layer thickness. Fig. 6.9 exhibits that bigger Brownian movement number Nb prompts a diminishment in concentration $\phi(\zeta)$ and its associated layer thickness. Table 6.2 is computed to validate present results with past published outcomes in a limiting sense. From this Table, we inspected that present series arrangements have great concurrence with numerical arrangements of Megahed [70] in a limiting way. Table 6.3 gives numeric calculations of Nusselt number for a few estimations of λ, Nt, β, Pr, Nb and Sc. We found that Nusselt number has higher estimations for bigger Prandtl Pr and Schmidt Sc numbers while inverse pattern is watched for Deborah parameter β and rotation parameter λ. In addition the Nusselt number stays constant when Brownian movement number Nb is shifted.

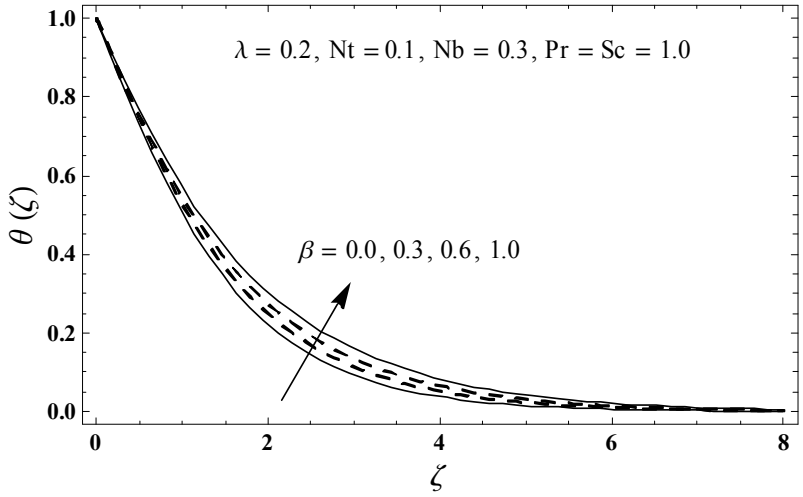

Fig. 6.1. Plots of $\theta(\zeta)$ for β.

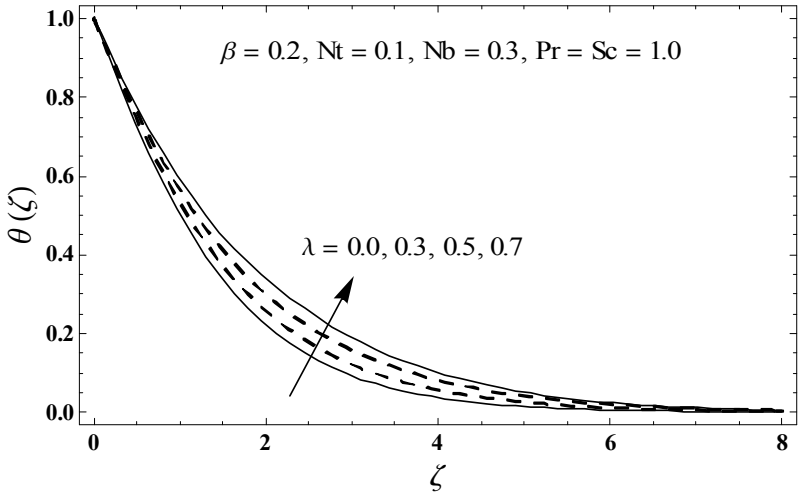

Fig. 6.2. Plots of $\theta(\zeta)$ for λ.

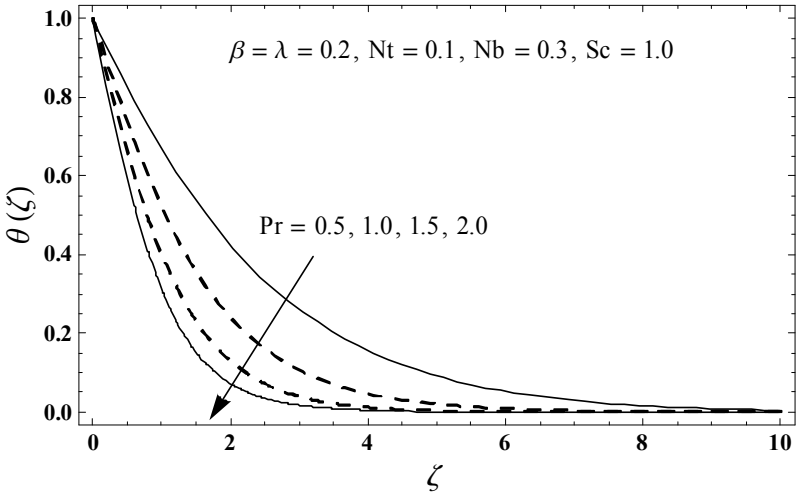

Fig. 6.3. Plots of $\theta(\zeta)$ for Pr .

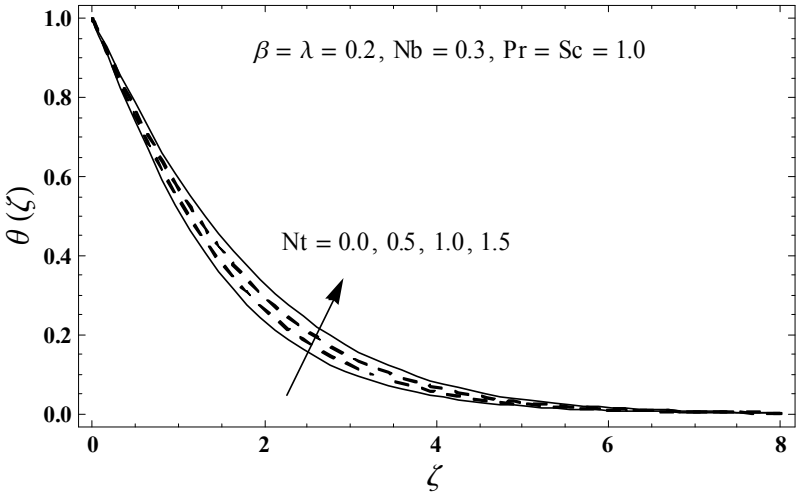

Fig. 6.4. Plots of $\theta(\zeta)$ for Nt.

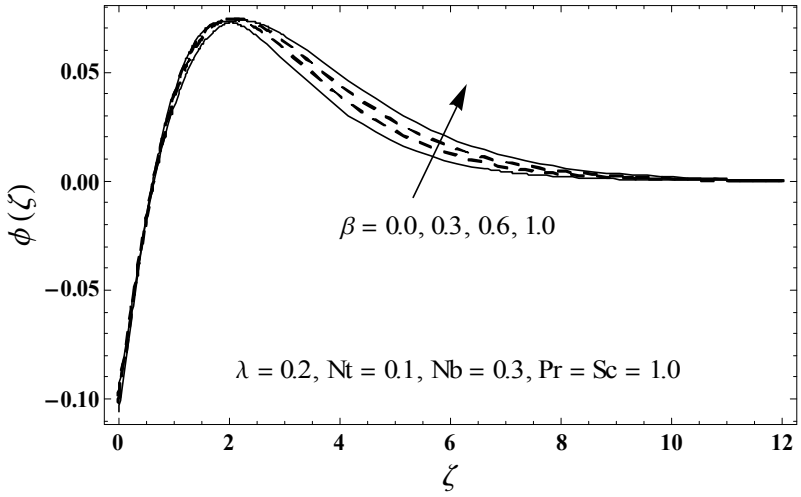

Fig. 6.5. Plots of $\phi(\zeta)$ for β.

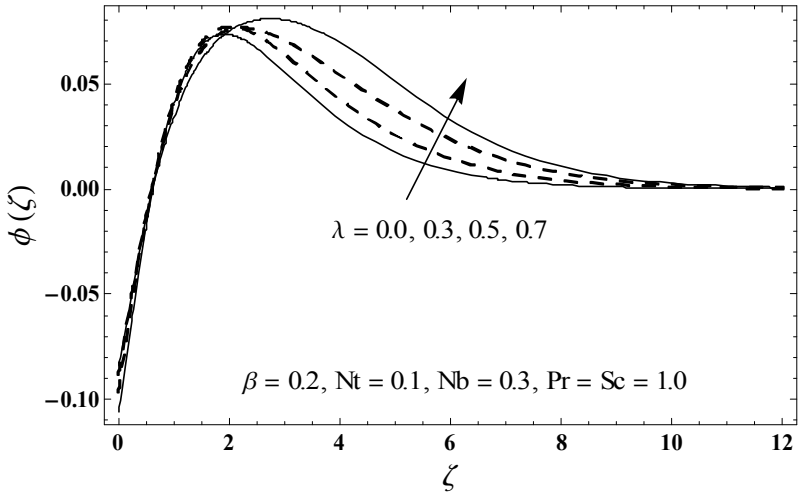

Fig. 6.6. Plots of $\phi(\zeta)$ for λ.

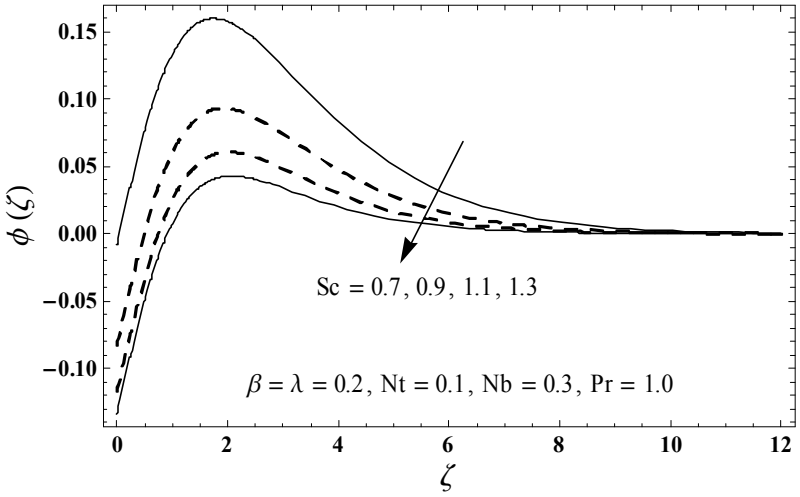

Fig. 6.7. Plots of $\phi(\zeta)$ for Sc.

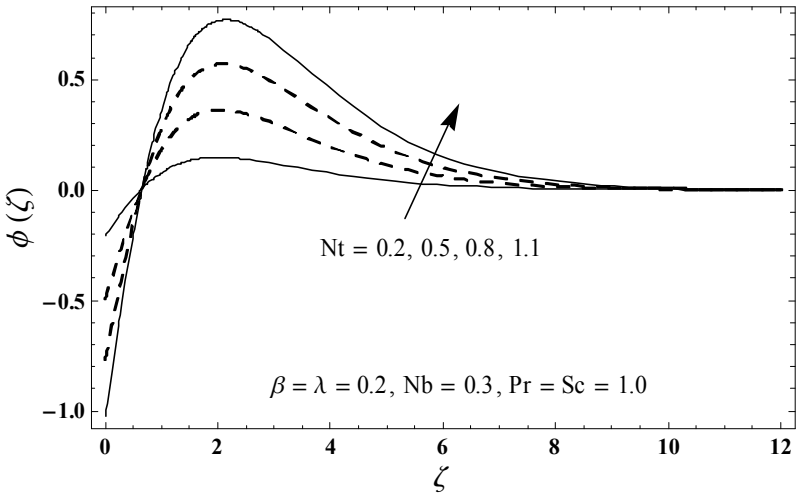

Fig. 6.8. Plots of $\phi(\zeta)$ for Nt.

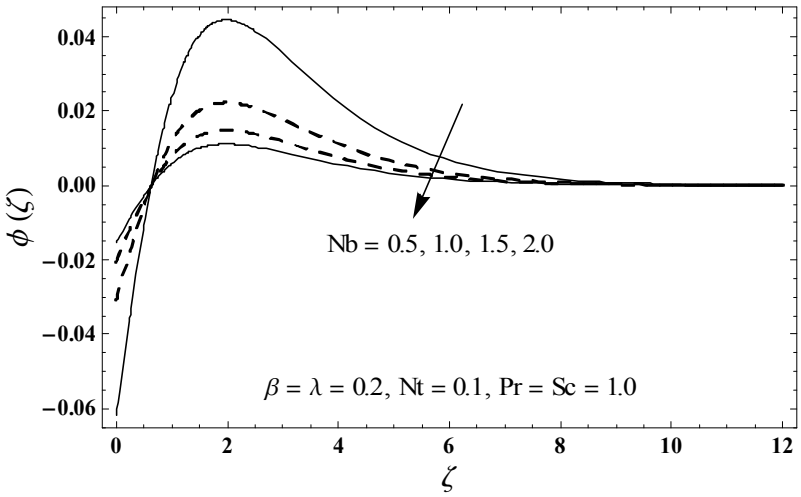

Fig. 6.9. Plots of $\phi(\zeta)$ for Nb.

Table 6.2. Comparative estimations of $-f''(0)$ for various estimations of β when $\lambda = 0$.

β	OHAM	Megahed [70]
0.0	1.0000	0.999978
0.2	1.0519	1.051945
0.4	1.1019	1.101848
0.6	1.1501	1.150160
0.8	1.1967	1.196690
1.2	1.2853	1.285253
1.6	1.3686	1.368641
2.0	1.4476	1.447616

Table 6.3. Numeric data for Nusselt number $\left(-\theta'(0)\right)$ for several estimations of Nt, β, Nb, λ, Sc and Pr.

β	λ	Nt	Nb	Pr	Sc	$-\theta'(0)$
0.0	0.2	0.1	0.3	1.0	1.0	0.5583
0.2						0.5390
0.5						0.5115
0.2	0.0	0.1	0.3	1.0	1.0	0.5580
	0.2					0.5390
	0.4					0.5025
0.2	0.2	0.0	0.3	1.0	1.0	0.5467
		0.3				0.5235
		0.5				0.5082
0.2	0.2	0.1	0.3	1.0	1.0	0.5390
			0.7			0.5390
			1.0			0.5390
0.2	0.2	0.1	0.3	0.5	1.0	0.3205
				1.0		0.5390
				1.5		0.7153
0.2	0.2	0.1	0.3	1.0	0.5	0.5329
					1.0	0.5390
					1.5	0.5394

Chapter 7

Three dimensional rotating flow of Maxwell nanofluid

This chapter investigates three dimensional rotating flow of Maxwell nanoliquid. Flow made is a result of an exponentially extending surface. Optimal homotopic scheme is executed for arrangement of governing relation. Optimal estimations of auxiliary variables are figured. The optimal arrangement articulations of concentration and temperature are explained by means of plots by utilizing the different estimations of included variables. Physical amounts like Sherwood and Nusselt numbers are portrayed by numeric esteems. Here we watched that temperature and its associated thickness of layer emerge for expanding estimations of local Deborah parameter while it decays for bigger temperature exponent.

7.1 Formulation

We mean to expound three dimension rotating flow of Maxwell nanoliquid due to an exponentially extending surface. Nanoliquid relation portrays Brownian movement and thermophoresis. Liquid and surface are in condition of rigid body rotation. We taken liquid in space $z \geq 0$. The surface is expected to extend in $x-$direction with U_0. Also the liquid rotates consistently about $z-$axis with constant angular velocity Ω. The corresponding conditions for Maxwell nanoliquid flow in a rotating frame are

$$\frac{\partial u}{\partial x} + \frac{\partial v}{\partial y} + \frac{\partial w}{\partial z} = 0, \tag{7.1}$$

$$u\frac{\partial u}{\partial x}+v\frac{\partial u}{\partial y}+w\frac{\partial u}{\partial z}-2\Omega v=\nu\frac{\partial^2 u}{\partial z^2}-\lambda_1\left(\begin{array}{c} u^2\frac{\partial^2 u}{\partial x^2}+v^2\frac{\partial^2 u}{\partial y^2}+w^2\frac{\partial^2 u}{\partial z^2} \\ +2uv\frac{\partial^2 u}{\partial x\partial y}+2vw\frac{\partial^2 u}{\partial y\partial z}+2uw\frac{\partial^2 u}{\partial x\partial z} \\ -2\Omega\left(u\frac{\partial v}{\partial x}+v\frac{\partial v}{\partial y}+w\frac{\partial v}{\partial z}\right)+2\Omega\left(v\frac{\partial u}{\partial x}-u\frac{\partial u}{\partial y}\right) \end{array}\right), \quad (7.2)$$

$$u\frac{\partial v}{\partial x}+v\frac{\partial v}{\partial y}+w\frac{\partial v}{\partial z}+2\Omega u=\nu\frac{\partial^2 v}{\partial z^2}-\lambda_1\left(\begin{array}{c} u^2\frac{\partial^2 v}{\partial x^2}+v^2\frac{\partial^2 v}{\partial y^2}+w^2\frac{\partial^2 v}{\partial z^2} \\ +2uv\frac{\partial^2 v}{\partial x\partial y}+2vw\frac{\partial^2 v}{\partial y\partial z}+2uw\frac{\partial^2 v}{\partial x\partial z} \\ +2\Omega\left(u\frac{\partial u}{\partial x}+v\frac{\partial u}{\partial y}+w\frac{\partial u}{\partial z}\right)+2\Omega\left(v\frac{\partial v}{\partial x}-u\frac{\partial v}{\partial y}\right) \end{array}\right), \quad (7.3)$$

$$u\frac{\partial T}{\partial x}+v\frac{\partial T}{\partial y}+w\frac{\partial T}{\partial z}=\alpha\left(\frac{\partial^2 T}{\partial z^2}\right)+\frac{(\rho c)_p}{(\rho c)_f}\left(D_B\left(\frac{\partial T}{\partial z}\frac{\partial C}{\partial z}\right)+\frac{D_T}{T_\infty}\left(\frac{\partial T}{\partial z}\right)^2\right), \quad (7.4)$$

$$u\frac{\partial C}{\partial x}+v\frac{\partial C}{\partial y}+w\frac{\partial C}{\partial z}=D_B\left(\frac{\partial^2 C}{\partial z^2}\right)+\frac{D_T}{T_\infty}\left(\frac{\partial^2 T}{\partial z^2}\right). \quad (7.5)$$

Here one has the following prescribed conditions:

$$u=U_w(x)=U_0\exp(x/L),\ v=0,\ w=0,\ T=T_w,\ C=C_w \text{ at } z=0, \quad (7.6)$$

$$u\to 0,\quad v\to 0,\quad T\to T_\infty,\quad C\to C_\infty \text{ as } z\to\infty. \quad (7.7)$$

Here u, v and w stand for velocities in $x-$, $y-$ and $z-$directions, $\nu=\mu/\rho_f$ for kinematic viscosity, T for temperature, ρ_f for density, $\alpha=k/(\rho c)_f$ for thermal diffusivity, μ for dynamic viscosity, T_w for wall temperature, k for thermal conductivity, $(\rho c)_p$ for effective heat potential of nanoparticles, C for concentration, $(\rho c)_f$ for heat potential of liquid, D_B for Brownian movement, λ_1 for liquid relaxation time, D_T for thermophoretic diffusion, C_w for wall concentration, T_∞ for ambient temperature, C_∞ for ambient concentration, L for characteristic length and U_0 for reference velocity. Selecting

$$\left.\begin{array}{c} u=U_0\exp(x/L)\,f'(\zeta),\ v=U_0\exp(x/L)\,g(\zeta), \\ w=-\sqrt{\frac{\nu U_0}{2L}}\exp(x/2L)\,(f+\zeta f'),\ \zeta=z\sqrt{\frac{U_0}{2\nu L}}\exp(x/2L), \\ T=T_\infty+T_0\exp(Ax/2L)\,\theta(\zeta),\ C=C_\infty+C_0\exp(Bx/2L)\,\phi(\zeta). \end{array}\right\} \quad (7.8)$$

Expression (7.1) is identically verified while Eqs. (7.2) − (7.7) give

$$f''' + ff'' - 2f'^2 + \lambda\left(4g - 2\beta\left(fg' + \zeta f''g\right)\right) - \frac{\beta}{2}\left(4f'^3 - \zeta f'^2 f'' + f^2 f''' - 6ff'f''\right) = 0\,, \tag{7.9}$$

$$g'' + fg' - 2f'g + 4\lambda\left(-f' + \beta\left(-f'^2 - g^2 - \frac{\zeta}{2}gg' + \frac{1}{2}ff''\right)\right) - \frac{\beta}{2}\left(4f'^2 g - \zeta f'^2 g' + f^2 g'' - 6ff'g'\right) = 0\,, \tag{7.10}$$

$$\theta'' + \Pr\left(f\theta' - Af'\theta + Nb\theta'\phi' + Nt\theta'^2\right) = 0, \tag{7.11}$$

$$\phi'' + Sc\left(f\phi' - Bf'\phi\right) + \frac{Nt}{Nb}\theta'' = 0, \tag{7.12}$$

$$f(0) = g(0) = 0,\ f'(0) = 1,\ \theta(0) = 1,\ \phi(0) = 1, \tag{7.13}$$

$$f'(\infty) \to 0,\ g(\infty) \to 0,\ \theta(\infty) \to 0,\ \phi(\infty) \to 0. \tag{7.14}$$

Here Nb stands for Brownian movement number, β for local Deborah parameter, λ for local rotation parameter, Nt for thermophoresis number, Pr for Prandtl parameter, A for temperature exponent, B for concentration exponent and Sc for Schmidt parameter. These variables can be specified by employing the definitions given below:

$$\left.\begin{array}{c} \lambda = \frac{\Omega L}{U_w},\ \beta = \frac{\lambda_1 U_w}{L},\ \Pr = \frac{\nu}{\alpha}, \\ Nb = \frac{(\rho c)_p D_B (C_w - C_\infty)}{(\rho c)_f \nu},\ Nt = \frac{(\rho c)_p D_T (T_w - T_\infty)}{(\rho c)_f \nu T_\infty},\ Sc = \frac{\nu}{D_B}. \end{array}\right\} \tag{7.15}$$

Local Nusselt (Nu_x) and Sherwood (Sh_x) numbers are

$$Nu_x = -\frac{x}{(T_w - T_\infty)}\left.\frac{\partial T}{\partial z}\right|_{z=0} = -\frac{x}{L}\sqrt{\frac{\mathrm{Re}_x}{2}}\theta'(0)\,, \tag{7.16}$$

$$Sh_x = -\frac{x}{(C_w - C_\infty)}\left.\frac{\partial C}{\partial z}\right|_{z=0} = -\frac{x}{L}\sqrt{\frac{\mathrm{Re}_x}{2}}\phi'(0)\,, \tag{7.17}$$

where $\mathrm{Re}_x = U_w L/\nu$ exhibits local Reynolds parameter.

7.2 Solutions by OHAM

The optimal series arrangements of Eqs. (7.9) − (7.12) through (7.13) and (7.14) have been developed by utilizing optimal homotopic analysis technique (OHAM). Initial deformations and linear operators have been selected as follows:

$$\left.\begin{aligned} f_0(\zeta) = 1 - \exp(-\zeta),\ g_0(\zeta) = 0, \\ \theta_0(\zeta) = \exp(-\zeta),\ \phi_0(\zeta) = \exp(-\zeta), \end{aligned}\right\} \tag{7.18}$$

$$\left.\begin{aligned} \mathcal{L}_f = \tfrac{d^3 f}{d\zeta^3} - \tfrac{df}{d\zeta},\quad \mathcal{L}_g = \tfrac{d^2 g}{d\zeta^2} - g, \\ \mathcal{L}_\theta = \tfrac{d^2 \theta}{d\zeta^2} - \theta,\quad \mathcal{L}_\phi = \tfrac{d^2 \phi}{d\zeta^2} - \phi. \end{aligned}\right\} \tag{7.19}$$

The above linear operators obey

$$\left.\begin{aligned} \mathcal{L}_f\left[F_1^{**} + F_2^{**}\exp(\zeta) + F_3^{**}\exp(-\zeta)\right] = 0, \\ \mathcal{L}_g\left[F_4^{**}\exp(\zeta) + F_5^{**}\exp(-\zeta)\right] = 0, \\ \mathcal{L}_\theta\left[F_6^{**}\exp(\zeta) + F_7^{**}\exp(-\zeta)\right] = 0, \\ \mathcal{L}_\phi\left[F_8^{**}\exp(\zeta) + F_9^{**}\exp(-\zeta)\right] = 0, \end{aligned}\right\} \tag{7.20}$$

in which F_j^{**} $(j = 1 - 9)$ stand for arbitrary constants. Problems for zeroth and mth-order deformations are easily formulated in the view of above operators. The deformation issues are solved by BVPh2.0 of Mathematica software.

7.3 Convergence analysis

We have solved the momentum, energy and concentration expressions with the help of BVPh2.0. These expressions contain unknown variables $\hbar_f$, $\hbar_g$, $\hbar_\theta$ and $\hbar_\phi$. We can compute the minimum estimation of these variables by taking total error small. In the frame of HAM, these variables play a vital role. That is why these variables refer to as convergence-control parameter which differs HAM from other analytical approximation methods. In order to reduce the CPU time, we have employed average residual errors at the mth-oder of approximation which are defined

by

$$\varepsilon_m^f = \frac{1}{k+1}\sum_{j=0}^{k}\left[\mathcal{N}_f\left(\sum_{i=0}^{m}\hat{f}(\zeta),\sum_{i=0}^{m}\hat{g}(\zeta)\right)_{\zeta=j\delta\zeta}\right]^2, \tag{7.21}$$

$$\varepsilon_m^g = \frac{1}{k+1}\sum_{j=0}^{k}\left[\mathcal{N}_g\left(\sum_{i=0}^{m}\hat{f}(\zeta),\sum_{i=0}^{m}\hat{g}(\zeta)\right)_{\zeta=j\delta\zeta}\right]^2, \tag{7.22}$$

$$\varepsilon_m^\theta = \frac{1}{k+1}\sum_{j=0}^{k}\left[\mathcal{N}_\theta\left(\sum_{i=0}^{m}\hat{f}(\zeta),\sum_{i=0}^{m}\hat{g}(\zeta),\sum_{i=0}^{m}\hat{\theta}(\zeta),\sum_{i=0}^{m}\hat{\phi}(\zeta)\right)_{\zeta=j\delta\zeta}\right]^2, \tag{7.23}$$

$$\varepsilon_m^\phi = \frac{1}{k+1}\sum_{j=0}^{k}\left[\mathcal{N}_\phi\left(\sum_{i=0}^{m}\hat{f}(\zeta),\sum_{i=0}^{m}\hat{g}(\zeta),\sum_{i=0}^{m}\hat{\theta}(\zeta),\sum_{i=0}^{m}\hat{\phi}(\zeta)\right)_{\zeta=j\delta\zeta}\right]^2. \tag{7.24}$$

Here $\mathcal{N}_f$, $\mathcal{N}_g$, $\mathcal{N}_\theta$ and $\mathcal{N}_\phi$ denote the non-linear operators corresponding to Eqs. (7.9) – (7.12) respectively. Following Liao [69] :

$$\varepsilon_m^t = \varepsilon_m^f + \varepsilon_m^g + \varepsilon_m^\theta + \varepsilon_m^\phi, \tag{7.25}$$

where ε_m^t stands for total residual square error, $k = 20$ and $\delta\zeta = 0.5$. Optimal data for auxiliary variables at 2nd order of deformations is $\hbar_f = -0.891408$, $\hbar_g = -1.04506$, $\hbar_\theta = -0.939956$ and $\hbar_\phi = -1.01791$ and $\varepsilon_m^t = 7.26 \times 10^{-4}$. Table 7.1 presents average square residual error at different order of deformations. It has been analyzed that the average residual square errors reduce with higher order deformations.

Table 7.1. Individual average residual square errors employing optimal data of auxiliary variables.

m	ε_m^f	ε_m^g	ε_m^θ	ε_m^ϕ
2	6.69×10^{-5}	4.71×10^{-5}	2.77×10^{-4}	3.35×10^{-4}
6	3.59×10^{-7}	1.50×10^{-7}	1.06×10^{-5}	1.55×10^{-5}
10	3.13×10^{-8}	6.66×10^{-9}	9.70×10^{-7}	1.70×10^{-6}
16	1.03×10^{-9}	6.23×10^{-10}	3.99×10^{-8}	8.76×10^{-8}
20	5.87×10^{-11}	1.63×10^{-10}	7.79×10^{-9}	1.84×10^{-8}
26	7.47×10^{-12}	1.31×10^{-11}	5.35×10^{-10}	1.48×10^{-9}
30	4.68×10^{-12}	1.02×10^{-12}	1.10×10^{-10}	3.24×10^{-10}

7.4 Discussion

This portion explores effects of a few pertinent flow variables like Prandtl parameter Pr, thermophoresis number Nt, local rotation parameter λ, local Deborah parameter β, Schmidt parameter Sc, Brownian movement number Nb, temperature exponent A and concentration exponent B on temperature $\theta(\zeta)$ and concentration $\phi(\zeta)$. Fig. 7.1 presents curves of temperature profile $\theta(\zeta)$ for differing local Deborah parameter β. It has been watched that by improving local Deborah parameter β, penetration depth of $\theta(\zeta)$ elevates. Fig. 7.2 displays the temperature $\theta(\zeta)$ for distinct estimations of local rotation parameter λ. Bigger λ compare to a elevated temperature and more layer of thermal. Fig. 7.3 delineates that how temperature $\theta(\zeta)$ gets influenced with the variety in Prandtl parameter Pr . It is watched that by upgrading Prandtl parameter Pr, temperature $\theta(\zeta)$ and layer of thermal are diminishment. Physically as Prandtl parameter Pr has reverse association with thermal diffusivity, in this way, an addition in Prandtl parameter Pr prompt poor thermal diffusion and subsequently lower penetration depth of $\theta(\zeta)$. Thicker layer of thermal ascribed to bigger Prandtl parameter is went with higher incline of temperature close to the wall. Fig. 7.4 exhibits the bends of temperature $\theta(\zeta)$ for shifting temperature exponential A. It is watched that by improving temperature exponential A, thermal penetration depth winds up lower. Fig. 7.5 exhibits effect of thermophoreis parameter Nt on temperature $\theta(\zeta)$. Bigger Nt relate to a elevated temperature $\theta(\zeta)$ and more layer of thermal. The purpose for this contention is that an augmentation in thermophoreis parameter Nt provides a more grounded thermophoretic constrain on nanoparticles toward the path inverse to forced temperature gradient. This movements nanoparticles towards the icy surrounding liquid because of which layer of thermal elevates. Fig. 7.6 presents variety in temperature $\theta(\zeta)$ for changing Brownian movement number Nb. It has been watched that by expanding Brownian movement number Nb, an improvement happened in temperature $\theta(\zeta)$ and associated layer. Fig. 7.7 presents concentration $\phi(\zeta)$ for differing local Deborah parameter β. Bigger β prompt a elevated concentration and thicker layer of concentration. Fig. 7.8 presents variation in concentration $\phi(\zeta)$ for particular estimations of local rotation parameter λ. It has been watched that by expanding λ, an upgrade showed up in concentration $\phi(\zeta)$ and its associated layer. Fig. 7.9 exhibits that how concentration $\phi(\zeta)$ gets influenced with the variety in Schmidt parameter Sc. It has been watched that the expanding estimations of Schmidt parameter prompt a lower

concentration $\phi(\zeta)$. Schmidt parameter depends on Brownian diffusivity. Bigger estimations of Schmidt parameter Sc provide poor Brownian diffusivity. Such poor Brownian diffusivity compares to bring down concentration $\phi(\zeta)$ and less layer of concentration. Fig. 7.10 presents bends of concentration $\phi(\zeta)$ for changing concentration exponent B. It has been watched that by improving B, penetration depth of $\phi(\zeta)$ ends up thinner. Fig. 7.11 exhibits the concentration $\phi(\zeta)$ for particular estimations of thermophoreis parameter Nt. It has been watched that higher Nt compares to more concentration $\phi(\zeta)$ and its associated layer. Fig. 7.12 exhibits that expanding estimations of Brownian movement number Nb portrays decrease in concentration $\phi(\zeta)$ and associated layer thickness. Table 7.2 is figured to approve present outcomes with previous published outcomes in a limiting situation. From this Table, we saw that present OHAM arrangements have great concurrence with numerical arrangements of Mustafa et al. [16] in a limiting situation. Table 7.3 presents numeric calculations of Nusselt number $\left(-\theta'(0)\right)$ and Sherwood number $\left(-\phi'(0)\right)$ for a few estimations of Nt, Nb, β, Pr, λ, Sc, A and B. Here we watched that Nusselt and Sherwood numbers have bring down qualities for bigger β, λ and Nt. In addition the Nusselt and Sherwood numbers appear inverse practices for bigger Pr.

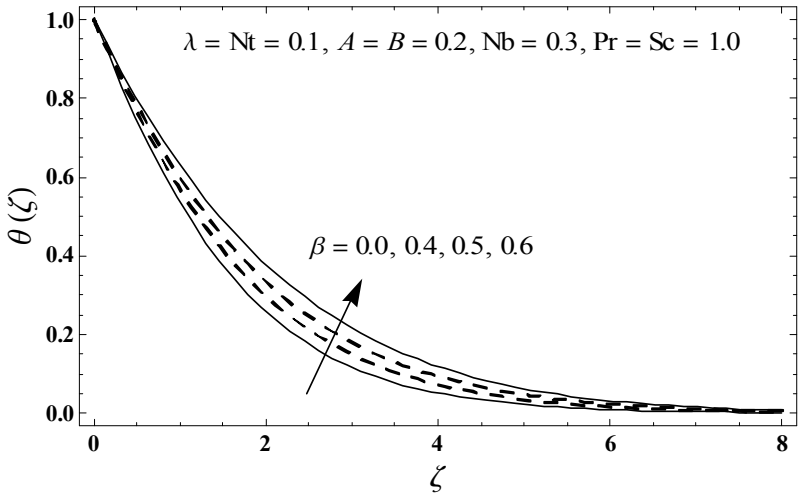

Fig. 7.1. Plots of $\theta(\zeta)$ for β.

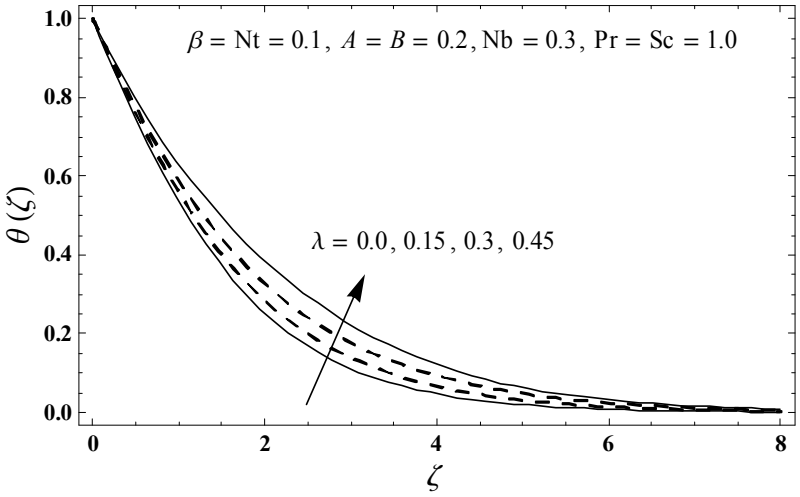

Fig. 7.2. Plots of $\theta(\zeta)$ for λ.

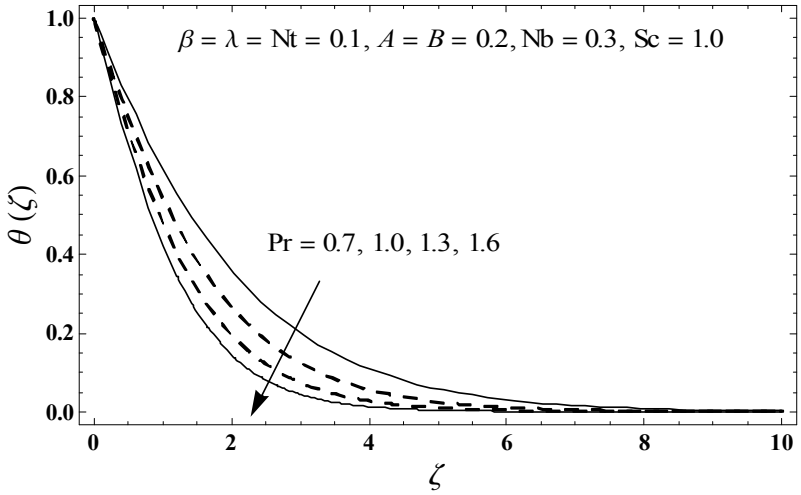

Fig. 7.3. Plots of $\theta(\zeta)$ for Pr.

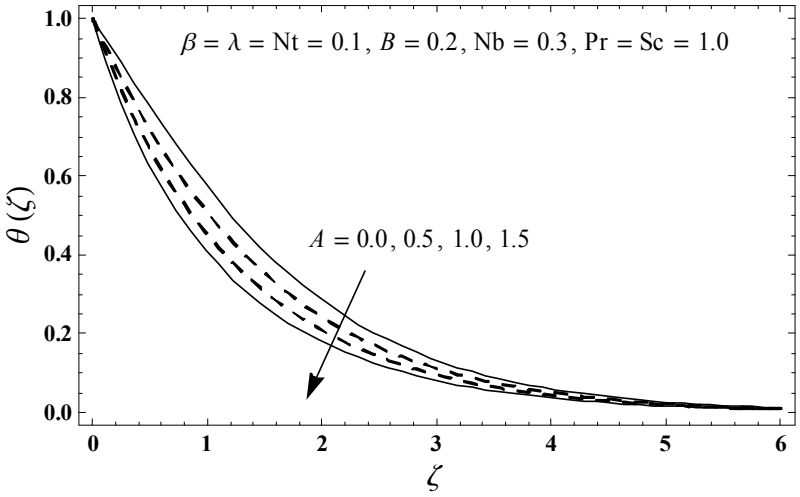

Fig. 7.4. Plots of $\theta(\zeta)$ for A.

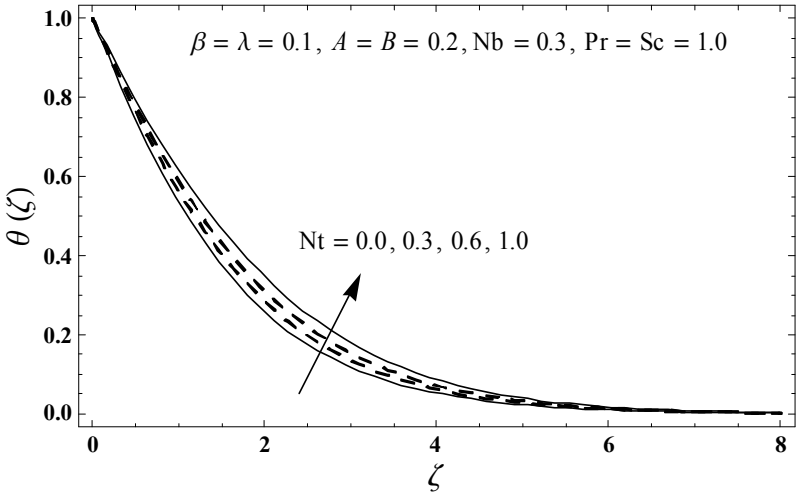

Fig. 7.5. Plots of $\theta(\zeta)$ for Nt.

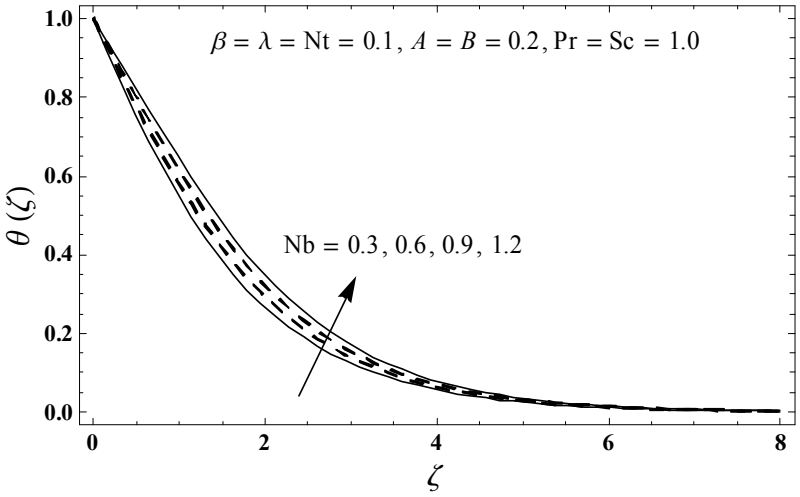

Fig. 7.6. Plots of $\theta(\zeta)$ for Nb.

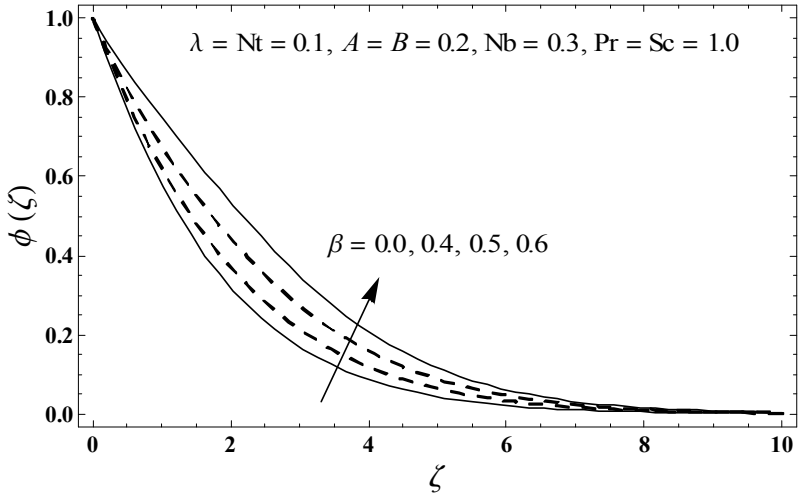

Fig. 7.7. Plots of $\phi(\zeta)$ for β.

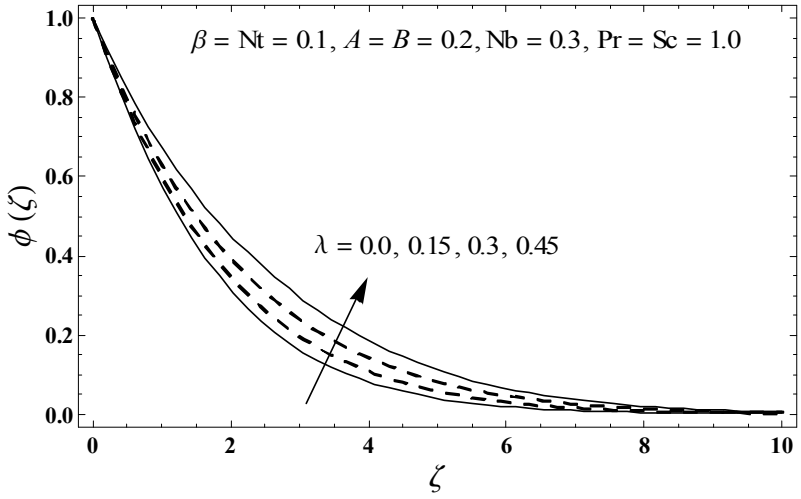

Fig. 7.8. Plots of $\phi(\zeta)$ for λ.

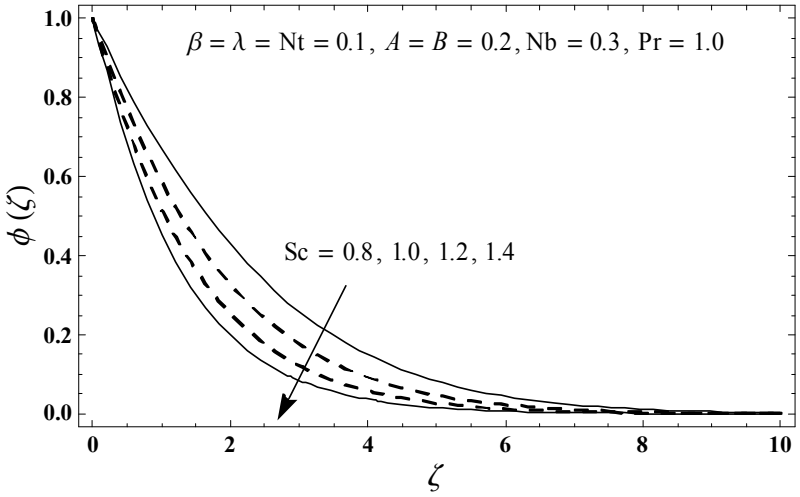

Fig. 7.9. Plots of $\phi(\zeta)$ for Sc.

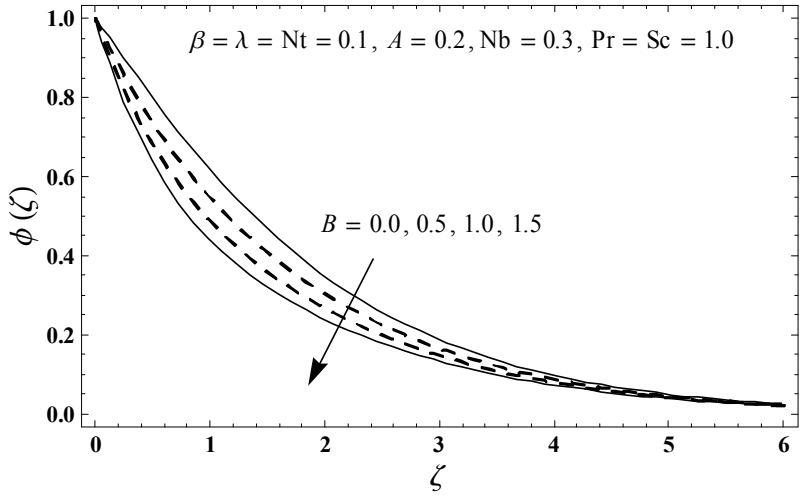

Fig. 7.10. Plots of $\phi(\zeta)$ for B.

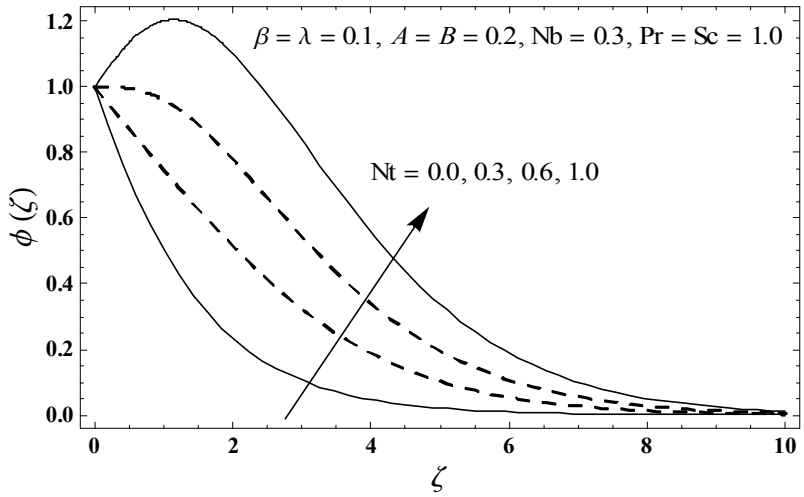

Fig. 7.11. Plots of $\phi(\zeta)$ for Nt.

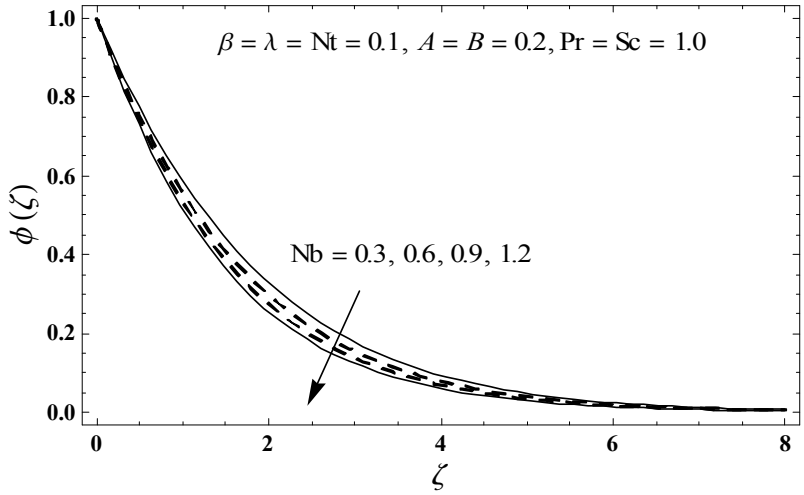

Fig. 7.12. Plots of $\phi(\zeta)$ for Nb.

Table 7.2. Comparative estimations of $-f''(0)$ and $-g'(0)$ for several estimations of λ when $\beta = 0$.

λ	$-f''(0)$		$-g'(0)$	
	OHAM	Numerical [16]	OHAM	Numerical [16]
0.2	1.34742	1.3474203	0.37015	0.3701525
0.5	1.51942	1.5194195	0.76251	0.7625142
1.0	1.80248	1.8024749	1.21796	1.2179573
2.0	2.28281	2.2828127	1.84850	1.8485032
5.0	3.34446	3.3444611	3.06092	3.0609164

Table 7.3. Numeric data for Nusselt number $\left(-\theta'(0)\right)$ and Sherwood number $\left(-\phi'(0)\right)$ for a few estimations of Sc, A, Pr, Nt, Nb, β, λ and B.

β	λ	Nt	Nb	Pr	Sc	A	B	$-\theta'(0)$	$-\phi'(0)$
0.0	0.1	0.1	0.3	1.0	1.0	0.2	0.2	0.5323	0.5040
0.1								0.5239	0.4943
0.2								0.5172	0.4858
0.1	0.0	0.1	0.3	1.0	1.0	0.2	0.2	0.5358	0.5107
	0.1							0.5239	0.4943
	0.2							0.4988	0.4609
0.1	0.1	0.0	0.3	1.0	1.0	0.2	0.2	0.5370	0.6152
		0.1						0.5239	0.4943
		0.3						0.4990	0.2705
0.1	0.1	0.1	0.3	1.0	1.0	0.2	0.2	0.5239	0.4943
			0.5					0.4774	0.5501
			0.8					0.4145	0.5811
0.1	0.1	0.1	0.3	0.5	1.0	0.2	0.2	0.3340	0.5398
				1.0				0.5239	0.4943
				1.5				0.6637	0.4590
0.1	0.1	0.1	0.3	1.0	0.7	0.2	0.2	0.5420	0.2788
					1.0			0.5239	0.4943
					1.5			0.5071	0.7449
0.1	0.1	0.1	0.3	1.0	1.0	0.0	0.2	0.4368	0.5195
						0.2		0.5239	0.4943
						0.5		0.6465	0.4585
0.1	0.1	0.1	0.3	1.0	1.0	0.2	0.0	0.5270	0.3987
							0.2	0.5239	0.4943
							0.5	0.5196	0.6283

Chapter 8

Impact of magnetic field in three-dimensional flow of an Oldroyd-B nanofluid

This chapter explores three dimension boundary layer flow of MHD Oldroyd-B nanoliquid. Flow induced is because of bi-directional extending surface. Brownian movement and thermophoresis impacts are explored. Newly proposed constraint requiring zero nanoparticles flux is utilized. The governing nonlinear boundary-layer expressions through appropriate transformations are diminished into nonlinear ordinary differential frameworks. The resulting nonlinear framework has been solved for velocities, concentration and temperature. The contributions of various interesting variables are studied graphically. Nusselt number is tabulated and analyzed.

8.1 Formulation

We examine three dimension flow of an Oldroyd-B nanoliquid. Flow caused is because of bi-directional extending surface. Liquid is taken electrically conducting subject to constant B_0 applied in $z-$direction. Hall and electric field impacts are disregarded. Impacts of Brownian movement and thermophoresis are considered. We employ Cartesian coordinate framework such that $x-$ and $y-$axes are taken in direction of motion and $z-$axis is normal to it. Surface at $z = 0$ is extended in $x-$ and $y-$directions having velocities U_w and V_w. Boundary layer

expressions governing the flow of an Oldroyd-B liquid are

$$\frac{\partial u}{\partial x}+\frac{\partial v}{\partial y}+\frac{\partial w}{\partial z}=0, \tag{8.1}$$

$$\begin{aligned}&u\frac{\partial u}{\partial x}+v\frac{\partial u}{\partial y}+w\frac{\partial u}{\partial z}+\lambda_1\left(\begin{array}{c}u^2\frac{\partial^2 u}{\partial x^2}+v^2\frac{\partial^2 u}{\partial y^2}+w^2\frac{\partial^2 u}{\partial z^2}\\+2uv\frac{\partial^2 u}{\partial x\partial y}+2vw\frac{\partial^2 u}{\partial y\partial z}+2uw\frac{\partial^2 u}{\partial x\partial z}\end{array}\right)\\&=\nu\left(\frac{\partial^2 u}{\partial z^2}+\lambda_2\left(\begin{array}{c}u\frac{\partial^3 u}{\partial x\partial z^2}+v\frac{\partial^3 u}{\partial y\partial z^2}+w\frac{\partial^3 u}{\partial z^3}\\-\frac{\partial u}{\partial x}\frac{\partial^2 u}{\partial z^2}-\frac{\partial u}{\partial y}\frac{\partial^2 v}{\partial z^2}-\frac{\partial u}{\partial z}\frac{\partial^2 w}{\partial z^2}\end{array}\right)\right)-\frac{\sigma B_0^2}{\rho_f}\left(u+\lambda_1 w\frac{\partial u}{\partial z}\right),\end{aligned} \tag{8.2}$$

$$\begin{aligned}&u\frac{\partial v}{\partial x}+v\frac{\partial v}{\partial y}+w\frac{\partial v}{\partial z}+\lambda_1\left(\begin{array}{c}u^2\frac{\partial^2 v}{\partial x^2}+v^2\frac{\partial^2 v}{\partial y^2}+w^2\frac{\partial^2 v}{\partial z^2}\\+2uv\frac{\partial^2 v}{\partial x\partial y}+2vw\frac{\partial^2 v}{\partial y\partial z}+2uw\frac{\partial^2 v}{\partial x\partial z}\end{array}\right)\\&=\nu\left(\frac{\partial^2 v}{\partial z^2}+\lambda_2\left(\begin{array}{c}u\frac{\partial^3 v}{\partial x\partial z^2}+v\frac{\partial^3 v}{\partial y\partial z^2}+w\frac{\partial^3 v}{\partial z^3}\\-\frac{\partial v}{\partial x}\frac{\partial^2 v}{\partial z^2}-\frac{\partial v}{\partial y}\frac{\partial^2 v}{\partial z^2}-\frac{\partial v}{\partial z}\frac{\partial^2 w}{\partial z^2}\end{array}\right)\right)-\frac{\sigma B_0^2}{\rho_f}\left(v+\lambda_1 w\frac{\partial v}{\partial z}\right),\end{aligned} \tag{8.3}$$

$$u\frac{\partial T}{\partial x}+v\frac{\partial T}{\partial y}+w\frac{\partial T}{\partial z}=\alpha\frac{\partial^2 T}{\partial z^2}+\frac{(\rho c)_p}{(\rho c)_f}\left(D_B\left(\frac{\partial T}{\partial z}\frac{\partial C}{\partial z}\right)+\frac{D_T}{T_\infty}\left(\frac{\partial T}{\partial z}\right)^2\right), \tag{8.4}$$

$$u\frac{\partial C}{\partial x}+v\frac{\partial C}{\partial y}+w\frac{\partial C}{\partial z}=D_B\left(\frac{\partial^2 C}{\partial z^2}\right)+\frac{D_T}{T_\infty}\left(\frac{\partial^2 T}{\partial z^2}\right). \tag{8.5}$$

Here one has the following prescribed conditions:

$$u=U_w(x)=ax,\ v=V_w(y)=by,\ w=0,\ T=T_w(x),\ D_B\frac{\partial C}{\partial z}+\frac{D_T}{T_\infty}\frac{\partial T}{\partial z}=0 \text{ at } z=0, \tag{8.6}$$

$$u\to 0,\quad v\to 0,\quad T\to T_\infty,\quad C\to C_\infty\quad \text{as } z\to\infty. \tag{8.7}$$

Here u, v and w stand for velocities in $x-$, $y-$ and $z-$directions, μ for dynamic viscosity, $\nu\left(=\mu/\rho_f\right)$ for kinematic viscosity, D_B for Brownian movement, ρ_f for density, λ_1 for relaxation time, λ_2 for retardation time, D_T for thermophoretic diffusion, σ for electrical conductivity, $(\rho c)_f$ for heat potential of liquid, T for temperature, $\alpha=k/(\rho c)_f$ for thermal diffusivity, k for thermal conductivity, $(\rho c)_p$ for effective heat potential of nanoparticles, C for concentration, T_w and T_∞ for wall and ambient temperatures and C_∞ for ambient concentration. Here we

assumes that surface stretching velocities and temperature are

$$U_w(x) = ax,\ V_w(y) = by,\ T_w(x) = T_\infty + T_0 x, \tag{8.8}$$

where a, b and T_0 are positive constants. Selecting

$$\left.\begin{aligned} u = axf'(\eta),\ v = ayg'(\eta),\ w = -(a\nu)^{1/2}(f(\eta)+g(\eta)), \\ \theta(\eta) = \tfrac{T-T_\infty}{T_w-T_\infty},\ \phi(\eta) = \tfrac{C-C_\infty}{C_\infty},\ \eta = \left(\tfrac{a}{\nu}\right)^{1/2} z. \end{aligned}\right\} \tag{8.9}$$

Eq. (8.1) is automatically verified while Eqs. $(8.2)-(8.8)$ become

$$\begin{aligned} &f''' + \left(M^2\beta_1 + 1\right)(f+g)f'' - f'^2 + \beta_1\left(2(f+g)f'f'' - (f+g)^2 f'''\right) \\ &+ \beta_2\left(\left(f''+g''\right)f'' - (f+g)f^{iv}\right) - M^2 f' = 0\,, \end{aligned} \tag{8.10}$$

$$\begin{aligned} &g''' + \left(M^2\beta_1 + 1\right)(f+g)g'' - g'^2 + \beta_1\left(2(f+g)g'g'' - (f+g)^2 g'''\right) \\ &+ \beta_2\left(\left(f''+g''\right)g'' - (f+g)g^{iv}\right) - M^2 g' = 0\,, \end{aligned} \tag{8.11}$$

$$\theta'' + \Pr\left((f+g)\theta' - f'\theta + Nb\theta'\phi' + Nt\theta'^2\right) = 0, \tag{8.12}$$

$$\phi'' + Le\Pr(f+g)\phi' + \frac{Nt}{Nb}\theta'' = 0, \tag{8.13}$$

$$f(0) = g(0) = 0,\ f'(0) = 1,\ g'(0) = c,\ \theta(0) = 1,\ Nb\phi'(0) + Nt\theta'(0) = 0, \tag{8.14}$$

$$f'(\infty) \to 0,\ g'(\infty) \to 0,\ \theta(\infty) \to 0,\ \phi(\infty) \to 0. \tag{8.15}$$

Here β_1 and β_2 stand for Deborah parameters in terms of relaxation and retardation times respectively, Nb for Brownian movement number, Pr for Prandtl parameter, c for ratio of extending rates, M for magnetic number, Le for Lewis parameter and Nt for thermophoresis number. These variables can be specified by employing the definitions given below:

$$\left.\begin{aligned} \beta_1 = \lambda_1 a,\ \beta_2 = \lambda_2 a,\ M^2 = \tfrac{\sigma B_0^2}{\rho_f a}\ c = \tfrac{b}{a},\ \Pr = \tfrac{\nu}{\alpha}, \\ Nb = \tfrac{(\rho c)_p D_B C_\infty}{(\rho c)_f \nu},\ Nt = \tfrac{(\rho c)_p D_T (T_w - T_\infty)}{(\rho c)_f \nu T_\infty},\ Le = \tfrac{\alpha}{D_B}. \end{aligned}\right\} \tag{8.16}$$

Local Nusselt number Nu_x is

$$Nu_x = -\frac{x}{(T_w - T_\infty)} \left.\frac{\partial T}{\partial z}\right|_{z=0} = -\left(\mathrm{Re}_x\right)^{1/2} \theta'(0). \tag{8.17}$$

It is watched that mass flux represented by Sherwood number is now identically vanishes and $\mathrm{Re}_x = U_w x/\nu$ is for local Reynolds parameter.

8.2 Solutions by HAM

The series arrangements of Eqs. $(8.10) - (8.13)$ through (8.14) and (8.15) have been developed by utilizing homotopic analysis technique (HAM). The linear operators and initial deformations have been selected as follows:

$$f_0(\eta) = 1 - e^{-\eta}, \quad g_0(\eta) = c(1 - e^{-\eta}), \quad \theta_0(\eta) = e^{-\eta}, \quad \phi_0(\eta) = -\frac{Nt}{Nb} e^{-\eta}, \tag{8.18}$$

$$\mathcal{L}_f = f''' - f', \quad \mathcal{L}_g = g''' - g', \quad \mathcal{L}_\theta = \theta'' - \theta, \quad \mathcal{L}_\phi = \phi'' - \phi. \tag{8.19}$$

The above linear operators obey

$$\left.\begin{array}{cc} \mathcal{L}_f \left[F_1^{**} + F_2^{**} e^{\eta} + F_3^{**} e^{-\eta}\right] = 0, & \mathcal{L}_g \left[F_4^{**} + F_5^{**} e^{\eta} + F_6^{**} e^{-\eta}\right] = 0, \\ \mathcal{L}_\theta \left[F_7^{**} e^{\eta} + F_8^{**} e^{-\eta}\right] = 0, & \mathcal{L}_\phi \left[F_9^{**} e^{\eta} + F_{10}^{**} e^{-\eta}\right] = 0, \end{array}\right\} \tag{8.20}$$

in which F_j^{**} $(j = 1 - 10)$ stand for arbitrary constants. Problems for zeroth and mth-order deformations are easily formulated in the view of above operators. The deformation issues are computed by Mathematica software.

8.3 Convergence analysis

Here series arrangements involve auxiliary variables $\hbar_f$, $\hbar_g$, $\hbar_\theta$ and $\hbar_\phi$. These variables are helpful for convergence of homotopic series arrangements. Proper estimations of such variables play a vital role to construct convergent arrangements through homotopic analysis technique (HAM). To get suitable estimations of $\hbar_f$, $\hbar_g$, $\hbar_\theta$ and $\hbar_\phi$, the $\hbar-$plots are sketched at 15th order of deformations. Figs. 8.1 and 8.2 clearly show that convergence zone lies within the ranges

$-1.55 \leq \hbar_f \leq -0.15$, $-1.60 \leq \hbar_g \leq -0.20$, $-1.55 \leq \hbar_\theta \leq -0.50$ and $-1.60 \leq \hbar_\phi \leq -0.35$. Table 8.1 exhibits that 27th order of deformations is sufficient for convergent series arrangements.

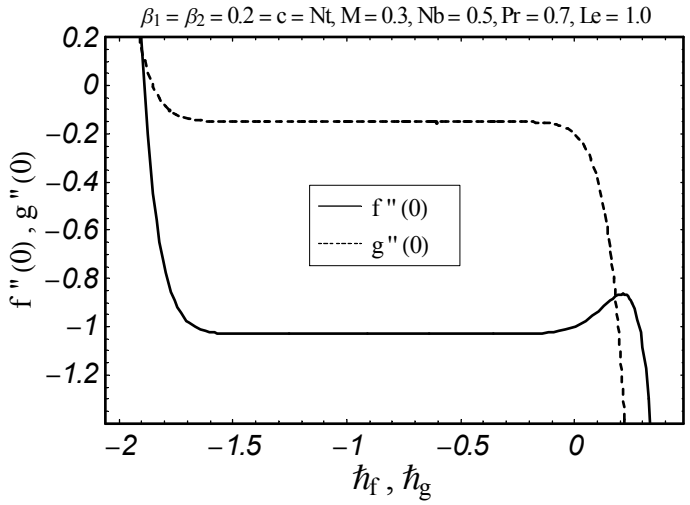

Fig. 8.1. The $\hbar-$plots for $f(\eta)$ and $g(\eta)$.

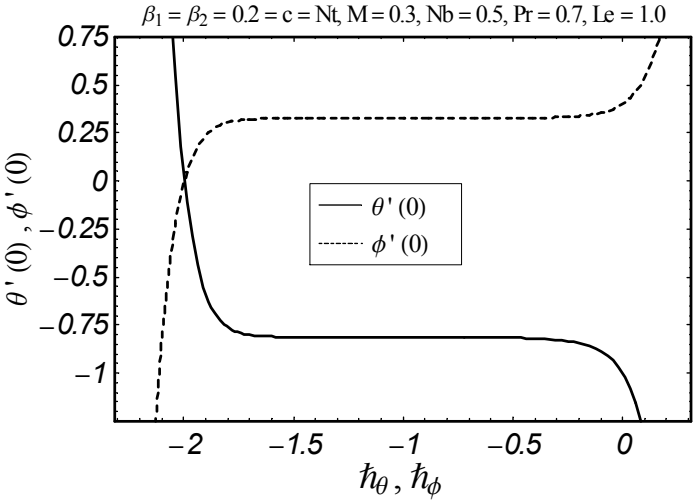

Fig. 8.2. The $\hbar-$plots for $\theta(\eta)$ and $\phi(\eta)$.

Table 8.1. HAM arrangements convergence when $\beta_1 = \beta_2 = 0.2 = c = Nt$, $M = 0.3$, $Nb = 0.5$, $\Pr = 0.7$ and $Le = 1.0$.

Order of deformations	$-f''(0)$	$-g''(0)$	$-\theta'(0)$	$\phi'(0)$
1	1.02593	0.14545	0.87333	0.34933
5	1.03095	0.15090	0.82041	0.32816
10	1.03103	0.15083	0.81353	0.32541
15	1.03103	0.15083	0.81214	0.32486
20	1.03103	0.15083	0.81177	0.32471
27	1.03103	0.15083	0.81163	0.32465
35	1.03103	0.15083	0.81163	0.32465
50	1.03103	0.15083	0.81163	0.32465

8.4 Discussion

This section addresses contributions of various influential variables like Deborah parameter by means of relaxation time β_1, Deborah parameter by means of retardation time β_2, magnetic number M, ratio number c, Prandtl parameter Pr, Brownian movement number Nb, thermophoresis number Nt and Lewis parameter Le on concentration and temperature. Influence of Deborah parameter β_1 on temperature is dipicted in Fig. 8.3. It is watched that temperature and corresponding layer are higher for bigger estimations of β_1. Fig. 8.4 describes that temperature and layer of thermal are decayed via β_2. A comparison of Figs. 8.3 and 8.4 clearly exhibits that β_1 and β_2 have quite reverse effects on temperature field. Here β_1 depends on relaxation time while β_2 involves retardation time. bigger relaxation time corresponds to elevated temperature while higher retardation time creates a diminishment in temperature. Hence an improvement in β_1 leads to an improvement in temperature while bigger β_2 exhibits lower temperature. Further $\beta_2 = 0$ leads to Maxwell liquid flow situation. Fig. 8.5 illustrates variations in temperature for a few estimations of magnetic number. Here $M \neq 0$ is for hydro-magnetic flow and $M = 0$ corresponds to hydro-dynamic flow situation. We watched that temperature and layer of thermal are higher for hydro-magnetic flow in comparison to hydro-dynamic situation. Magnetic number depends upon Lorentz force. Bigger magnetic number has stronger

Lorentz force. Such stronger Lorentz force creates an improvement in temperature and layer of thermal. Fig. 8.6 exhibits that bigger ratio number creates a diminishment in temperature profile and layer of thermal. For $c = 0$, two dimension flow situation is acquired. Here we watched that layer of thermal is more for two dimension situation when compared with three dimension flow. Impact of Prandtl parameter on temperature profile is sketched in Fig. 8.7. Temperature profile is diminished when we improvement estimations of Prandtl parameter. Physically bigger Prandtl fluids have poor thermal diffusivity and small Prandtl fluids have stronger thermal diffusivity. Such variation in thermal diffusivity leads to a diminishment in temperature and corresponding layer of thermal. Fig. 8.8 presents variations of thermophoresis number Nt on temperature profile $\theta(\eta)$. We watched that temperature $\theta(\eta)$ and associated layer of thermal are elevated when we improvement thermophoresis number. In fact presence of nanoparticles elevates thermal conductivity of liquid. An improvement in thermophoresis number exhibits stronger thermal conductivity. Such stronger thermal conductivity elevates temperature and layer of thermal. Influence of β_1 on concentration profile $\phi(\eta)$ is shown in Fig. 8.9. Here concentration $\phi(\eta)$ and associated layer thickness are higher for bigger β_1. Effect of β_2 on concentration profile $\phi(\eta)$ is plotted in Fig. 8.10. Concentration $\phi(\eta)$ and corresponding layer thickness are diminished for higher estimations of β_2. Concentration $\phi(\eta)$ is elevated for bigger magnetic number (see Fig. 8.11). Concentration $\phi(\eta)$ elevates for bigger magnetic number. Variation in concentration ϕ corresponding to a few estimations of ratio number is plotted in Fig. 8.12. We have watched that bigger estimations of ratio number creates a diminishment in concentration and associated layer. Fig. 8.13 illustrates that concentration is poor for higher Lewis parameter. Lewis parameter depends on Brownian movement. Higher Lewis parameter corresponds to a poor Brownian movement which exhibits a poor concentration. Fig. 8.14 exhibits that concentration is diminished via Prandtl parameter. Figs. 8.15 and 8.16 exhibit influences of thermophoresis and Brownian movement on concentration $\phi(\eta)$. Here an improvement in Nt gives rise to concentration but opposite trend is watched for Brownian movement number. Table 8.2 exhibits the comparison for different estimations of c with exact arrangement. Table 8.2 demonstrates an excellent agreement of HAM arrangement with existing exact arrangement in limiting situation. Table 8.3 is computed to investigate transfer of heat rate for different estimations of c, Nt, Nb, β_1, β_2, M, Le and $\Pr$. For $\beta_2 = 0$ the situation

of Maxwell liquid flow is recovered. It is clearly exhibits that estimations of transfer of heat rate for an Oldroyd-B liquid are more than Maxwell liquid. Transfer of heat rate is independent for variations in Brownian movement number. Effects of Lewis and Prandtl parameters on transfer of heat rate are very reverse.

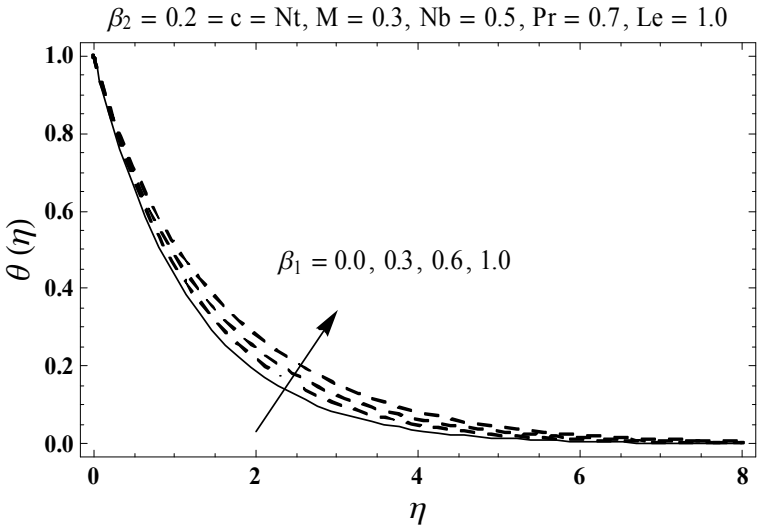

Fig. 8.3. Plots of $\theta(\eta)$ for β_1.

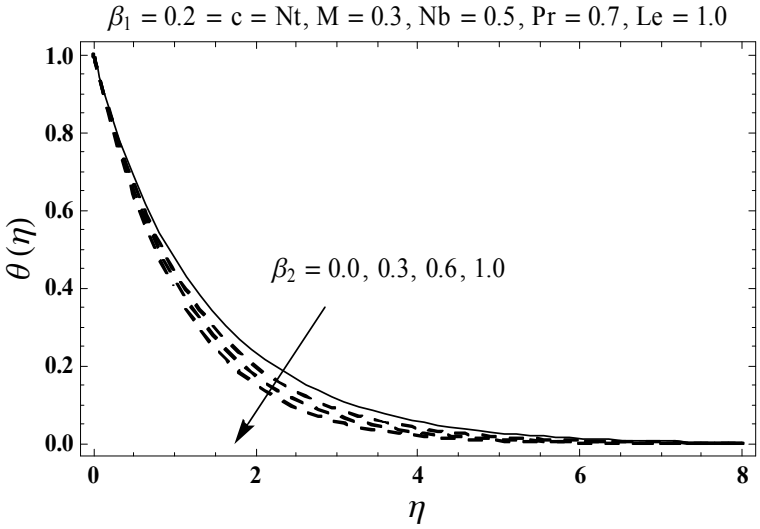

Fig. 8.4. Plots of $\theta(\eta)$ for β_2.

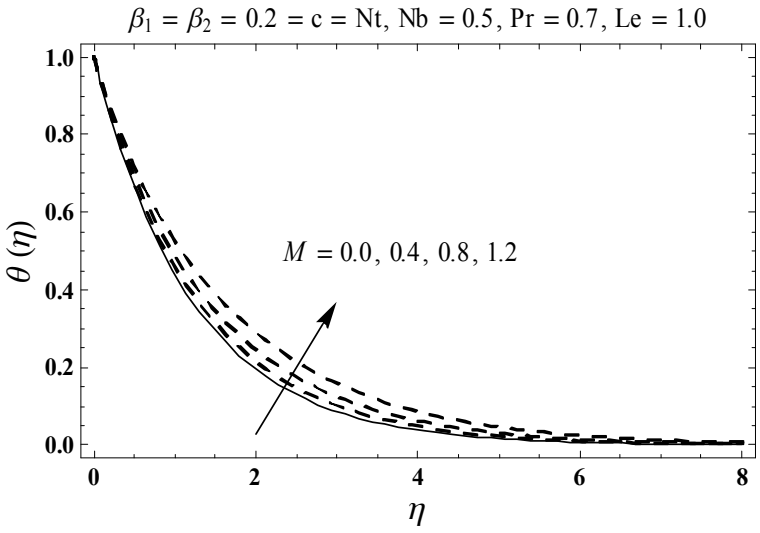

Fig. 8.5. Plots of $\theta(\eta)$ for M.

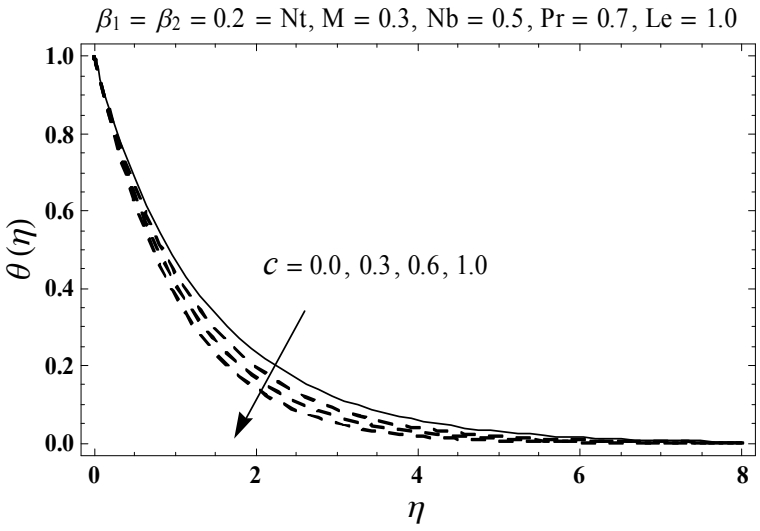

Fig. 8.6. Plots of $\theta(\eta)$ for c.

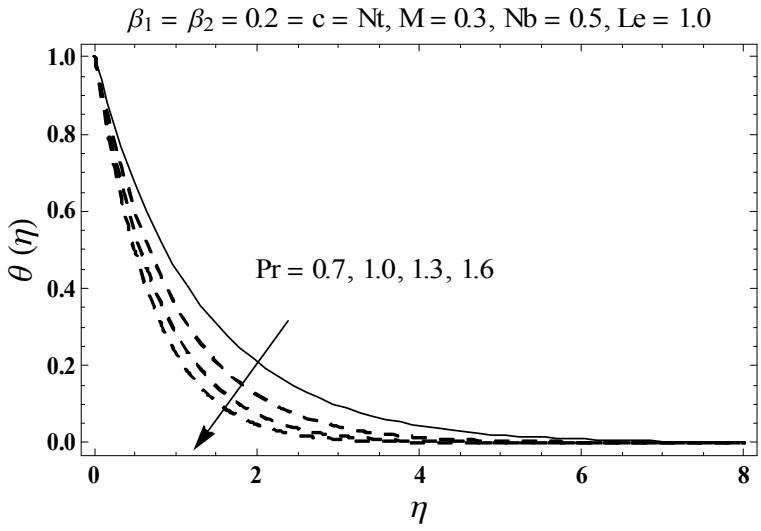

Fig. 8.7. Plots of $\theta(\eta)$ for Pr .

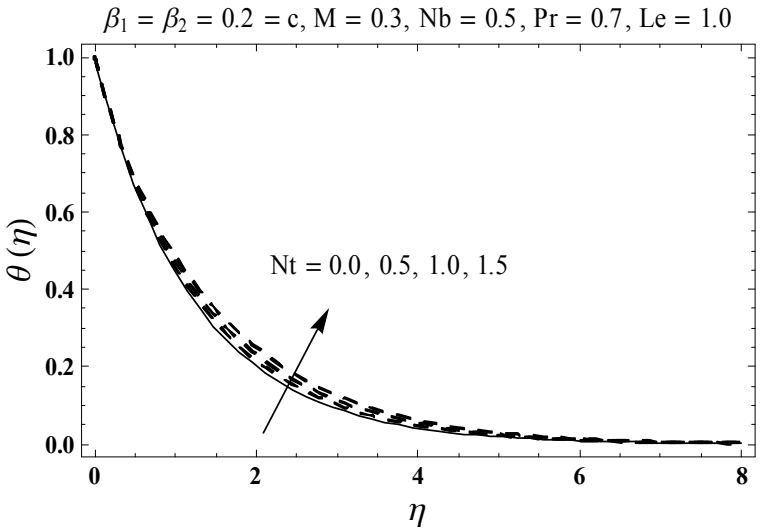

Fig. 8.8. Plots of $\theta(\eta)$ for Nt.

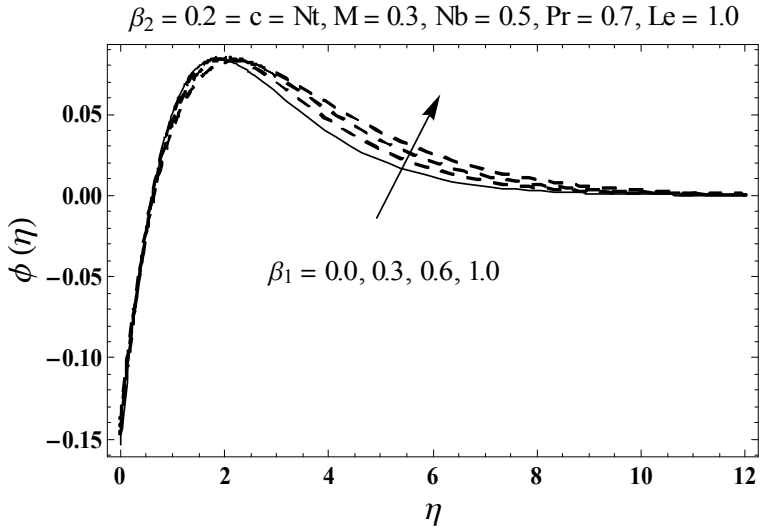

Fig. 8.9. Plots of $\phi(\eta)$ for β_1.

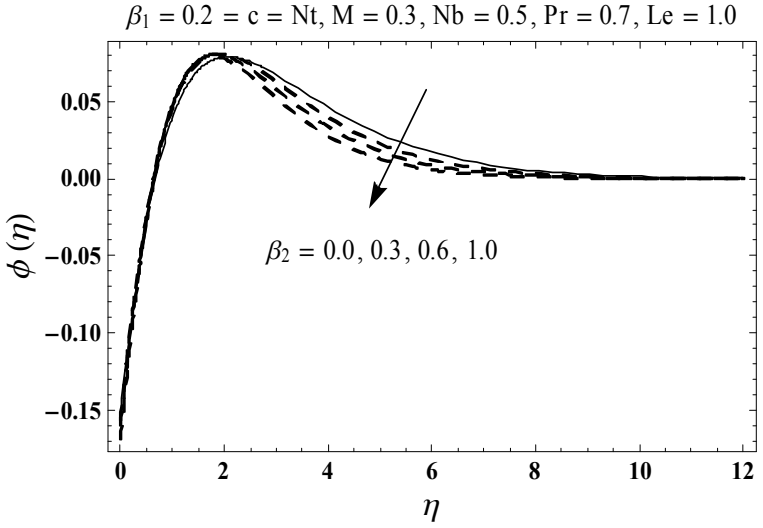

Fig. 8.10. Plots of $\phi(\eta)$ for β_2.

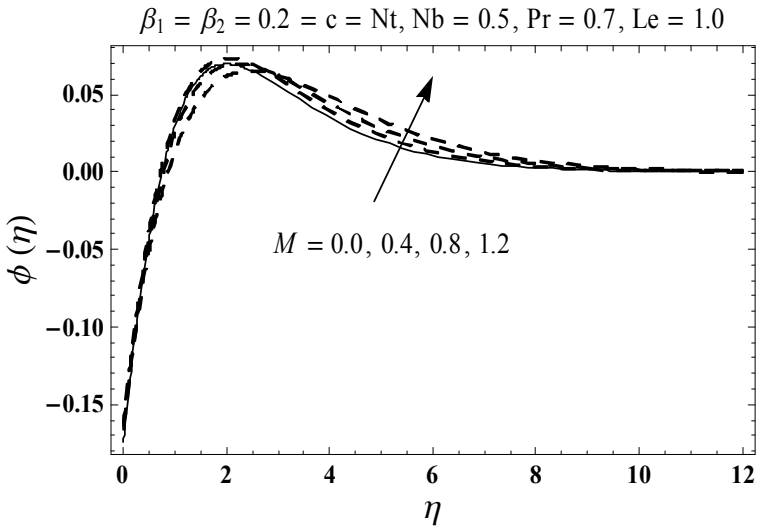

Fig. 8.11. Plots of $\phi(\eta)$ for M.

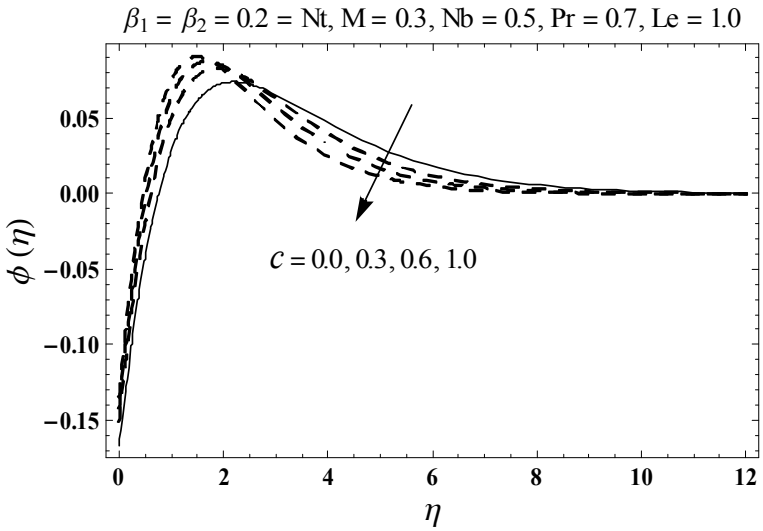

Fig. 8.12. Plots of $\phi(\eta)$ for c.

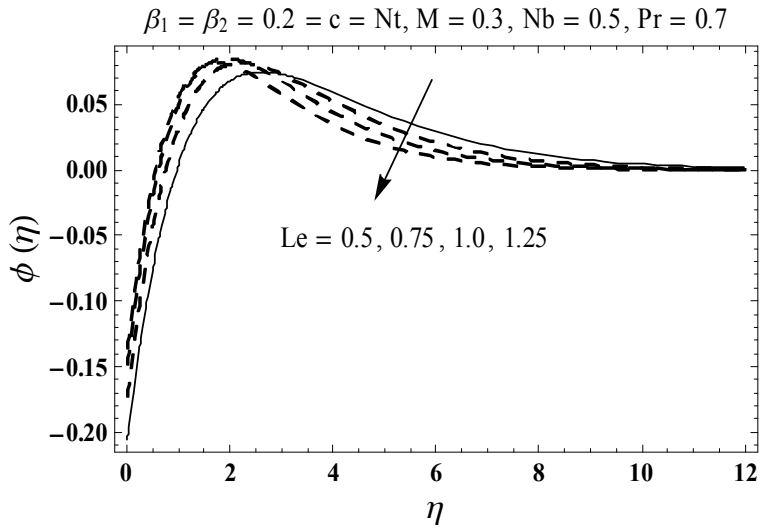

Fig. 8.13. Plots of $\phi(\eta)$ for Le.

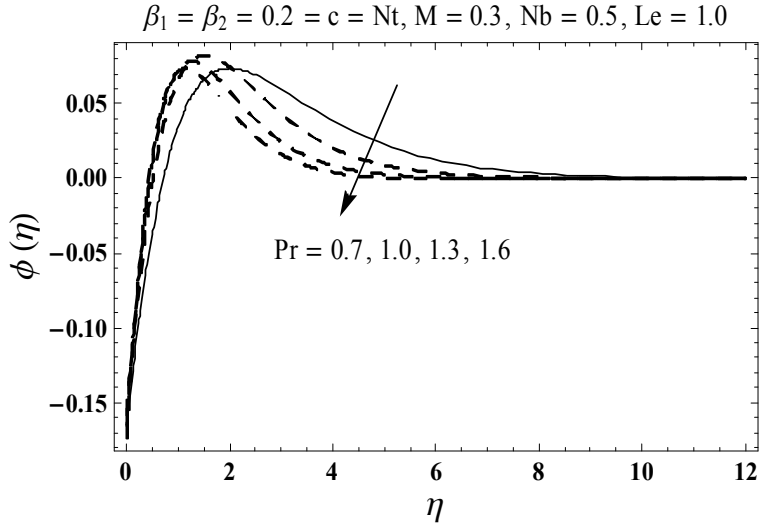

Fig. 8.14. Plots of $\phi(\eta)$ for Pr.

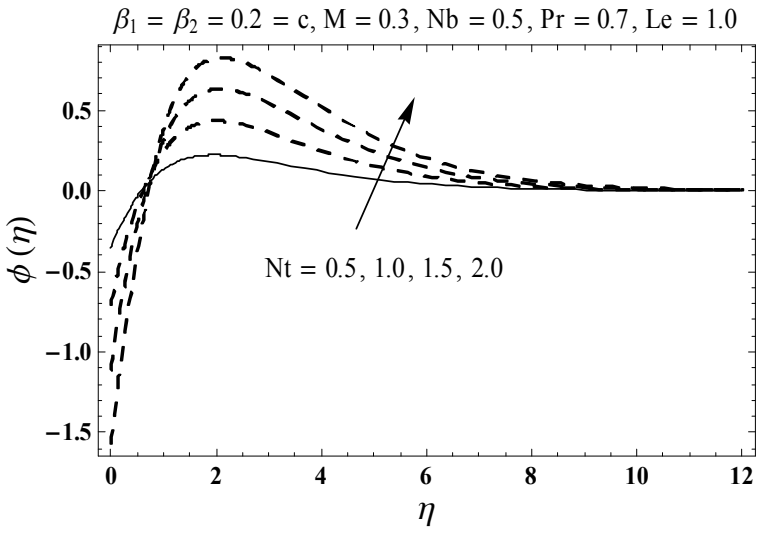

Fig. 8.15. Plots of $\phi(\eta)$ for Nt.

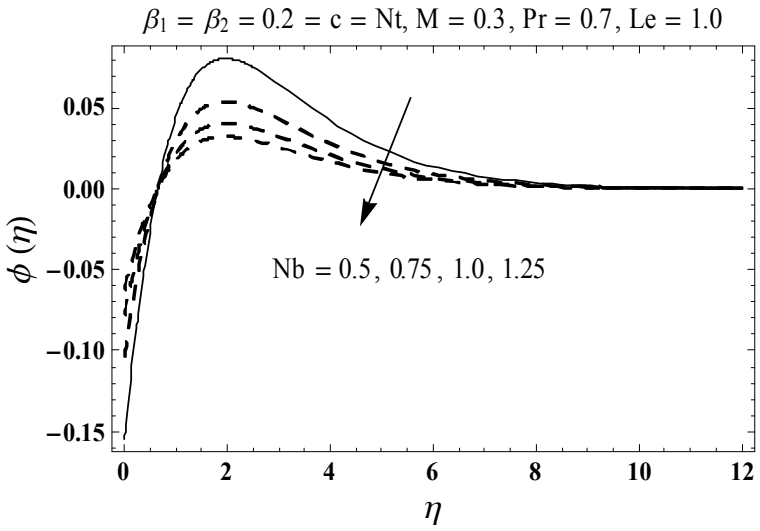

Fig. 8.16. Plots of $\phi(\eta)$ for Nb.

Table 8.2. Comparative estimations of $-f''(0)$ and $-g''(0)$ for several estimations of c when $\beta_1 = \beta_2 = M = 0$.

c	$-f''(0)$		$-g''(0)$	
	HAM	Exact [38]	HAM	Exact [38]
0	1	1	0	0
0.25	1.048811	1.048813	0.194564	0.194564
0.50	1.093095	1.093097	0.465205	0.465205
0.75	1.134486	1.134485	0.794618	0.794622
1.0	1.173722	1.173720	1.173722	1.173720

Table 8.3. Numeric data of Nusselt number $Nu_x\,(\mathrm{Re}_x)^{-1/2}$ for a few estimations of β_1, β_2, M, c, Nt, Nb, Le and Pr.

β_1	β_2	M	c	Nt	Nb	Le	Pr	$-\theta'(0)$
0.0	0.2	0.3	0.2	0.2	0.5	1.0	0.7	0.8358
0.2								0.8117
0.5								0.7780
0.2	0.0	0.3	0.2	0.2	0.5	1.0	0.7	0.7801
	0.2							0.8117
	0.5							0.8458
0.2	0.2	0.0	0.2	0.2	0.5	1.0	0.7	0.8219
		0.3						0.8117
		0.5						0.7948
0.2	0.2	0.3	0.0	0.2	0.5	1.0	0.7	0.7806
			0.2					0.8117
			0.5					0.8539
0.2	0.2	0.3	0.2	0.0	0.5	1.0	0.7	0.8189
				0.5				0.8011
				1.0				0.7838
0.2	0.2	0.3	0.2	0.2	0.5	1.0	0.7	0.8117
					1.0			0.8117
					1.5			0.8117
0.2	0.2	0.3	0.2	0.2	0.5	0.5	0.7	0.8149
						1.0		0.8117
						1.5		0.8098
0.2	0.2	0.3	0.2	0.2	0.5	1.0	0.5	0.6452
							1.0	1.0223
							1.5	1.3094

Chapter 9

An analytical solution for magnetohydrodynamic Oldroyd-B nanofluid flow induced by a stretching surface with heat generation/absorption

This chapter provides an investigation of magnetohydrodynamic (MHD) three dimension (3D) flow of an Oldroyd-B nanoliquid. Heat absorption/generation and convective boundary condition are studied. Flow induced is because of extending surface. Brownian movement and thermophoresis are examined. Oldroyd-B liquid is taken conducting through uniform applied magnetic field. A condition associated with nanoparticles mass flux at surface is utilized. Problem formulation is made for boundary-layer and low magnetic Reynolds parameter approximations. Suitable transformations are employed to construct nonlinear ordinary differential expressions. The strongly nonlinear differential expressions are solved through optimal homotopic analysis technique (OHAM). Impacts of different intriguing variables on concentration and temperature are considered. Nusselt number is also computed and analyzed. Our computations reveal that temperature has direct relation with Biot parameter and magnetic number.

9.1 Formulation

We explore three dimension (3D) flow of an Oldroyd-B nanoliquid by a convectively heated surface. Flow induced is due to a bidirectional extending surface. The liquid is taken conducting via uniform B_0 applied in $z-$direction. Also electric field and Hall impacts are disregarded. Induced magnetic field is not taken for low magnetic Reynolds parameter. Brownian movement, thermophoresis and heat generation/absorption effects are accounted. We employ Cartesian coordinate framework such that $x-$ and $y-$axes brought the extending surface in course of movement and $z-$axis is normal to it. Let $U_w(x) = ax$ and $V_w(y) = by$ be the velocities of extending surface along $x-$ and $y-$directions. Temperature at extending surface is managed by a convective heating phenomenon which is described via coefficient of heat transfer h_f and hot liquid temperature T_f under the surface. The governing boundary layer expressions for three dimension (3D) flow of an Oldroyd-B nanoliquid are

$$\frac{\partial u}{\partial x}+\frac{\partial v}{\partial y}+\frac{\partial w}{\partial z}=0, \tag{9.1}$$

$$\begin{aligned}
&u\frac{\partial u}{\partial x}+v\frac{\partial u}{\partial y}+w\frac{\partial u}{\partial z}+\lambda_1\left(\begin{array}{c} u^2\frac{\partial^2 u}{\partial x^2}+v^2\frac{\partial^2 u}{\partial y^2}+w^2\frac{\partial^2 u}{\partial z^2} \\ +2uv\frac{\partial^2 u}{\partial x\partial y}+2vw\frac{\partial^2 u}{\partial y\partial z}+2uw\frac{\partial^2 u}{\partial x\partial z}\end{array}\right) \\
&=\nu\left(\frac{\partial^2 u}{\partial z^2}+\lambda_2\left(\begin{array}{c} u\frac{\partial^3 u}{\partial x\partial z^2}+v\frac{\partial^3 u}{\partial y\partial z^2}+w\frac{\partial^3 u}{\partial z^3} \\ -\frac{\partial u}{\partial x}\frac{\partial^2 u}{\partial z^2}-\frac{\partial u}{\partial y}\frac{\partial^2 v}{\partial z^2}-\frac{\partial u}{\partial z}\frac{\partial^2 w}{\partial z^2}\end{array}\right)\right)-\frac{\sigma B_0^2}{\rho_f}\left(u+\lambda_1 w\frac{\partial u}{\partial z}\right),
\end{aligned} \tag{9.2}$$

$$\begin{aligned}
&u\frac{\partial v}{\partial x}+v\frac{\partial v}{\partial y}+w\frac{\partial v}{\partial z}+\lambda_1\left(\begin{array}{c} u^2\frac{\partial^2 v}{\partial x^2}+v^2\frac{\partial^2 v}{\partial y^2}+w^2\frac{\partial^2 v}{\partial z^2} \\ +2uv\frac{\partial^2 v}{\partial x\partial y}+2vw\frac{\partial^2 v}{\partial y\partial z}+2uw\frac{\partial^2 v}{\partial x\partial z}\end{array}\right) \\
&=\nu\left(\frac{\partial^2 v}{\partial z^2}+\lambda_2\left(\begin{array}{c} u\frac{\partial^3 v}{\partial x\partial z^2}+v\frac{\partial^3 v}{\partial y\partial z^2}+w\frac{\partial^3 v}{\partial z^3} \\ -\frac{\partial v}{\partial x}\frac{\partial^2 v}{\partial z^2}-\frac{\partial v}{\partial y}\frac{\partial^2 v}{\partial z^2}-\frac{\partial v}{\partial z}\frac{\partial^2 w}{\partial z^2}\end{array}\right)\right)-\frac{\sigma B_0^2}{\rho_f}\left(v+\lambda_1 w\frac{\partial v}{\partial z}\right),
\end{aligned} \tag{9.3}$$

$$u\frac{\partial T}{\partial x}+v\frac{\partial T}{\partial y}+w\frac{\partial T}{\partial z} = \alpha_m\frac{\partial^2 T}{\partial z^2}+\frac{Q}{(\rho c)_f}(T-T_\infty) + \frac{(\rho c)_p}{(\rho c)_f}\left(D_B\left(\frac{\partial T}{\partial z}\frac{\partial C}{\partial z}\right)+\frac{D_T}{T_\infty}\left(\frac{\partial T}{\partial z}\right)^2\right), \tag{9.4}$$

$$u\frac{\partial C}{\partial x}+v\frac{\partial C}{\partial y}+w\frac{\partial C}{\partial z}=D_B\left(\frac{\partial^2 C}{\partial z^2}\right)+\frac{D_T}{T_\infty}\left(\frac{\partial^2 T}{\partial z^2}\right). \tag{9.5}$$

Here one has the following prescribed conditions:

$$u=ax,\ v=by,\ w=0,\ -k\frac{\partial T}{\partial z}=h_f\left(T_f-T\right),\ D_B\frac{\partial C}{\partial z}+\frac{D_T}{T_\infty}\frac{\partial T}{\partial z}=0 \text{ at } z=0, \tag{9.6}$$

$$u\to 0,\ \ v\to 0,\ \ T\to T_\infty,\ \ C\to C_\infty \ \text{ as } z\to\infty. \tag{9.7}$$

Here u, v and w stand for velocities in $x-$, $y-$ and $z-$directions, μ for dynamic viscosity, $\nu\left(=\mu/\rho_f\right)$ for kinematic viscosity, $(\rho c)_p$ for effective heat potential of nanoparticles, λ_1 for relaxation time, ρ_f for density, λ_2 for retardation time, σ for electrical conductivity, T for temperature, $\alpha_m=k/(\rho c)_f$ for thermal diffusivity, D_B for Brownian movement, k for thermal conductivity, $(\rho c)_f$ for heat potential of liquid, Q for heat generation/absorption coefficient, C for concentration, D_T for thermophoretic diffusion, T_∞ for ambient temperature, C_∞ for ambient concentration and a and b for positive constants. Selecting

$$\begin{gathered} u=axf'(\eta),\ v=ayg'(\eta),\ w=-\left(a\nu\right)^{1/2}\left(f(\eta)+g(\eta)\right), \\ \theta(\eta)=\tfrac{T-T_\infty}{T_f-T_\infty},\ \phi(\eta)=\tfrac{C-C_\infty}{C_\infty},\ \eta=\left(\tfrac{a}{\nu}\right)^{1/2}z. \end{gathered} \tag{9.8}$$

Now expression (9.1) is automatically satisfied and Eqs. $(9.2)-(9.7)$ provide

$$\begin{aligned} &f'''+\left(M^2\beta_1+1\right)(f+g)f''-f'^2+\beta_1\left(2\left(f+g\right)f'f''-\left(f+g\right)^2f'''\right) \\ &+\beta_2\left(\left(f''+g''\right)f''-\left(f+g\right)f^{iv}\right)-M^2f'=0\,, \end{aligned} \tag{9.9}$$

$$\begin{aligned} &g'''+\left(M^2\beta_1+1\right)(f+g)g''-g'^2+\beta_1\left(2\left(f+g\right)g'g''-\left(f+g\right)^2g'''\right) \\ &+\beta_2\left(\left(f''+g''\right)g''-\left(f+g\right)g^{iv}\right)-M^2g'=0\,, \end{aligned} \tag{9.10}$$

$$\theta'' + \Pr\left((f+g)\theta' + S\theta + Nb\theta'\phi' + Nt\theta'^2\right) = 0, \tag{9.11}$$

$$\phi'' + Sc(f+g)\phi' + \frac{Nt}{Nb}\theta'' = 0, \tag{9.12}$$

$$f = g = 0,\ f' = 1,\ g' = \alpha,\ \theta' = -\gamma\left(1 - \theta\left(0\right)\right),\ Nb\phi' + Nt\theta' = 0 \text{ at } \eta = 0, \tag{9.13}$$

$$f' \to 0,\ \ g' \to 0,\ \ \theta \to 0,\ \ \phi \to 0 \text{ as } \eta \to \infty. \tag{9.14}$$

Here M stands for magnetic number, Nb for Brownian movement number, β_1 and β_2 for Deborah parameters by mean of relaxation and retardation times, α for ratio number, Pr for Prandtl parameter, Le for Lewis parameter, Nt for thermophoresis number, γ for Biot parameter and S for heat generation/absorption parameter. These variables can be specified by employing the definitions given below:

$$\left.\begin{array}{l} \beta_1 = \lambda_1 a,\ \beta_2 = \lambda_2 a,\ M^2 = \frac{\sigma B_0^2}{\rho_f a},\ \alpha = \frac{b}{a},\ \Pr = \frac{\nu}{\alpha_m},\ S = \frac{Q}{a(\rho c)_f}, \\ Nb = \frac{(\rho c)_p D_B C_\infty}{(\rho c)_f \nu},\ Nt = \frac{(\rho c)_p D_T\left(T_f - T_\infty\right)}{(\rho c)_f \nu T_\infty},\ \gamma = \frac{h_f}{k}\sqrt{\frac{\nu}{a}},\ Le = \frac{\alpha_m}{D_B}. \end{array}\right\} \tag{9.15}$$

The local Nusselt number Nu_x is defined by

$$Nu_x = -\frac{x}{(T_w - T_\infty)}\left.\frac{\partial T}{\partial z}\right|_{z=0} = -\left(\mathrm{Re}_x\right)^{1/2}\theta'(0). \tag{9.16}$$

It is watched that mass flux denoted by Sherwood number is now identically vanishes and $\mathrm{Re}_x = U_w x/\nu$ exhibits local Reynolds parameter.

9.2 Solutions by OHAM

The optimal series arrangements of Eqs. (9.9) – (9.12) through (9.13) and (9.14) have been developed by utilizing optimal homotopic analysis technique (OHAM). The linear operators and initial deformations have been selected as follows:

$$f_0(\eta) = 1 - e^{-\eta},\ g_0(\eta) = \alpha(1 - e^{-\eta}),\ \theta_0(\eta) = \frac{\gamma}{1+\gamma}e^{-\eta},\ \phi_0(\eta) = -\frac{\gamma}{1+\gamma}\frac{Nt}{Nb}e^{-\eta}, \tag{9.17}$$

$$\mathcal{L}_f = f''' - f',\ \ \mathcal{L}_g = g''' - g',\ \ \mathcal{L}_\theta = \theta'' - \theta,\ \ \mathcal{L}_\phi = \phi'' - \phi. \tag{9.18}$$

The above linear operators obey

$$\left.\begin{array}{cc} \mathcal{L}_f\left[F_1^{**}+F_2^{**}e^{\eta}+F_3^{**}e^{-\eta}\right]=0, & \mathcal{L}_g\left[F_4^{**}+F_5^{**}e^{\eta}+F_6^{**}e^{-\eta}\right]=0, \\ \mathcal{L}_\theta\left[F_7^{**}e^{\eta}+F_8^{**}e^{-\eta}\right]=0, & \mathcal{L}_\phi\left[F_9^{**}e^{\eta}+F_{10}^{**}e^{-\eta}\right]=0, \end{array}\right\} \tag{9.19}$$

in which F_j^{**} $(j=1-10)$ stand for arbitrary constants. Problems for zeroth and mth-order deformations are easily formulated in the view of above operators. The deformation issues are solved by BVPh2.0 of Mathematica software.

9.3 Convergence analysis

We have solved the momentum, energy and concentration expressions with the help of BVPh2.0. These expressions contain unknown variables $\hbar_f$, $\hbar_g$, $\hbar_\theta$ and $\hbar_\phi$. We can compute the minimum estimation of these variables by taking total error small. In the frame of HAM, these variables play a vital role. That is why these variables refer to as convergence-control parameter which differs HAM from other analytical approximation methods. In order to reduce the CPU time, we have employed average residual errors at the mth-oder of approximation which are defined by

$$\varepsilon_m^f=\frac{1}{k+1}\sum_{j=0}^{k}\left[\mathcal{N}_f\left(\sum_{i=0}^{m}\hat{f}(\eta),\ \sum_{i=0}^{m}\hat{g}(\eta)\right)_{\eta=j\delta\eta}\right]^2, \tag{9.20}$$

$$\varepsilon_m^g=\frac{1}{k+1}\sum_{j=0}^{k}\left[\mathcal{N}_g\left(\sum_{i=0}^{m}\hat{f}(\eta),\ \sum_{i=0}^{m}\hat{g}(\eta)\right)_{\eta=j\delta\eta}\right]^2, \tag{9.21}$$

$$\varepsilon_m^\theta=\frac{1}{k+1}\sum_{j=0}^{k}\left[\mathcal{N}_\theta\left(\sum_{i=0}^{m}\hat{f}(\eta),\ \sum_{i=0}^{m}\hat{g}(\eta),\ \sum_{i=0}^{m}\hat{\theta}(\eta),\ \sum_{i=0}^{m}\hat{\phi}(\eta),\right)_{\eta=j\delta\eta}\right]^2, \tag{9.22}$$

$$\varepsilon_m^\phi=\frac{1}{k+1}\sum_{j=0}^{k}\left[\mathcal{N}_\phi\left(\sum_{i=0}^{m}\hat{f}(\eta),\ \sum_{i=0}^{m}\hat{g}(\eta),\ \sum_{i=0}^{m}\hat{\theta}(\eta),\ \sum_{i=0}^{m}\hat{\phi}(\eta),\right)_{\eta=j\delta\eta}\right]^2. \tag{9.23}$$

Here $\mathcal{N}_f$, $\mathcal{N}_g$, $\mathcal{N}_\theta$ and $\mathcal{N}_\phi$ denote the non-linear operators corresponding to Eqs. (9.9) – (9.12) respectively. Following Liao [69] :

$$\varepsilon_m^t=\varepsilon_m^f+\varepsilon_m^g+\varepsilon_m^\theta+\varepsilon_m^\phi, \tag{9.24}$$

where ε_m^t stands for total residual square error, $k = 20$ and $\delta\eta = 0.5$. Optimal data for auxiliary variables at 2nd order of deformations is $\hbar_f = -0.92591$, $\hbar_g = -0.905895$, $\hbar_\theta = -1.25056$ and $\hbar_\phi = -1.68203$ and $\varepsilon_m^t = 5.43 \times 10^{-5}$. Table 9.1 presents average square residual error at different order of deformations. It has been analyzed that the average residual square errors reduce with higher order deformations.

Table 9.1. Individual average residual square errors employing optimal data of auxiliary variables.

m	ε_m^f	ε_m^g	ε_m^θ	ε_m^ϕ
2	7.61×10^{-7}	3.80×10^{-7}	2.12×10^{-5}	3.19×10^{-5}
6	7.03×10^{-10}	1.28×10^{-9}	3.06×10^{-9}	5.05×10^{-7}
10	7.76×10^{-12}	1.26×10^{-11}	5.79×10^{-11}	1.76×10^{-8}
16	2.95×10^{-14}	2.86×10^{-14}	1.16×10^{-14}	1.47×10^{-10}
20	2.27×10^{-14}	1.55×10^{-14}	2.16×10^{-16}	6.27×10^{-12}

9.4 Discussion

The present section examines effects of various interesting variables like Deborah parameters by mean of relaxation and retardation times β_1 and β_2 respectively, Lewis parameter Le, magnetic number M, Biot parameter γ, ratio number α, heat generation/absorption parameter S, thermophoresis number Nt, Prandtl parameter Pr and Brownian movement number Nb on temperature and concentration. Fig. 9.1 displays impact of Deborah parameter β_1 on temperature $\theta(\eta)$. Here temperature θ and layer of thermal are higher for expanding estimations of Deborah parameter β_1. Fig. 9.2 presents that an improvement in Deborah parameter β_2 exhibits a decay in temperature $\theta(\eta)$ and corresponding layer of thermal. A comparative study of Figs. 9.1 and 9.2 clearly presents that β_1 and β_2 have quite opposite effects on temperature. Here β_1 involves relaxation time while β_2 depends on retardation time. An improvement in β_1 and β_2 corresponds to bigger relaxation and retardation times respectively. Bigger relaxation time leads to a stronger temperature profile while bigger retardation time corresponds to a poor temperature profile. Further present results diminishes to Maxwell liquid flow situation when $\beta_2 = 0$. Effect of magnetic number M on temperature θ is plotted in Fig. 9.3. Both temperature θ and layer of thermal are upgraded for expanding estimations of magnetic number M.

Magnetic number M includes Lorentz force. Bigger M prompts a more grounded Lorentz force which causes an improvement in temperature and corresponding layer of thermal. Here $M = 0$ corresponds to a hydro-dynamic flow situation. Fig. 9.4 exhibits that an improvement in ratio number α lead to a poor temperature θ and less layer of thermal. For $\alpha = 0$, the two dimension flow situation is achieved. Variation in temperature θ for various estimations of Biot parameter γ is outlined in Fig. 9.5. Here temperature $\theta(\eta)$ and layer of thermal show expanding conduct for bigger Biot parameter γ. Fig. 9.6 exhibits variations in temperature $\theta(\eta)$ for various estimations of heat generation/absorption parameter S. Here $S > 0$ corresponds to heat generation and $S < 0$ leads to heat absorption. It is clearly watched that temperature θ and layer of thermal are higher for heat generation situation in comparison to heat absorption situation. Fig. 9.7 presents that temperature $\theta(\eta)$ and layer of thermal are diminishing elements of Pr. Prandtl parameter Pr has an opposite association with thermal diffusivity. An expansion in Prandtl parameter Pr prompt poor thermal diffusivity which causes a rot in temperature and layer of thermal. Fig. 9.8 delineates conduct of Nt on temperature $\theta(\eta)$. Both temperature θ and layer of thermal are upgraded for expanding estimations of thermophoresis number Nt. Fig. 9.9 presents impact of Deborah parameter β_1 on concentration profile $\phi(\eta)$. Bigger Deborah parameter β_1 causes an improvement in concentration profile. Variation in concentration field $\phi(\eta)$ for various estimations of Deborah parameter β_2 is sketched in Fig. 9.10. Here concentration ϕ and layer of concentration are lower for expanding estimation of Deborah parameter β_2. Fig. 9.11 exhibits that bigger magnetic number M leads to elevated concentration profile and more layer of concentration. Impact of ratio number α on concentration $\phi(\eta)$ is displayed in Fig. 9.12. An improvement in ratio number α causes a decay in concentration profile. Fig. 9.13 displays impact of Biot parameter γ on concentration $\phi(\eta)$. Here concentration $\phi(\eta)$ and layer of concentration are expanding functions of Biot parameter γ. Fig. 9.14 exhibits that an improvement in Lewis parameter Le exhibits a decay in concentration $\phi(\eta)$. Lewis parameter has an inverse relationship with Brownian movement coefficient. Bigger Lewis parameter Le corresponds to poor Brownian movement coefficient which causes a diminishment in concentration distribution. Fig. 9.15 exhibits that bigger Prandtl parameter Pr leads to lower concentration distribution $\phi(\eta)$. Impact of thermophoresis number Nt on concentration $\phi(\eta)$ is plotted in Fig. 9.16. Both concentration and associated thickness are higher for expanding

estimations of thermophoresis number Nt. Fig. 9.17 presents that bigger Brownian movement number Nb relates to a poor concentration ϕ and less layer of concentration. Table 9.2 exhibits the comparison for different estimations of α with exact arrangement. Table 9.2 demonstrates an excellent agreement of OHAM arrangement with existing exact arrangement in limiting situation. Table 9.3 elucidates local Nusselt number $-\theta'(0)$ for β_1, β_2, α, S, γ, Nt, Nb, Le, Pr and M. Obviously Nusselt number is higher for expanding estimations of Biot γ and Prandtl Pr numbers while inverse conduct is watched for thermophoresis number Nt. It is additionally watched that impacts of β_1 and β_2 on Nusselt number are very invert. Furthermore estimations of Nusselt number are higher for hydro-dynamic flow situation ($M = 0$) when compared with hydro-magnetic flow situation ($M \neq 0$).

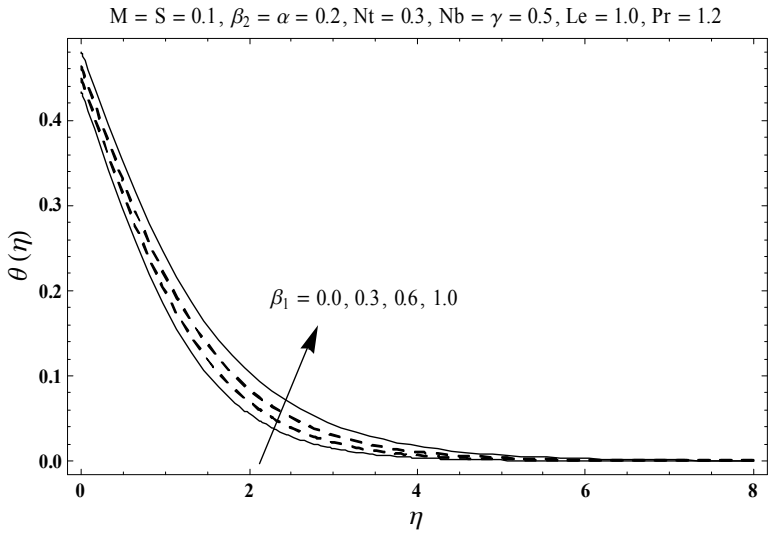

Fig. 9.1. Plots of $\theta(\eta)$ for β_1.

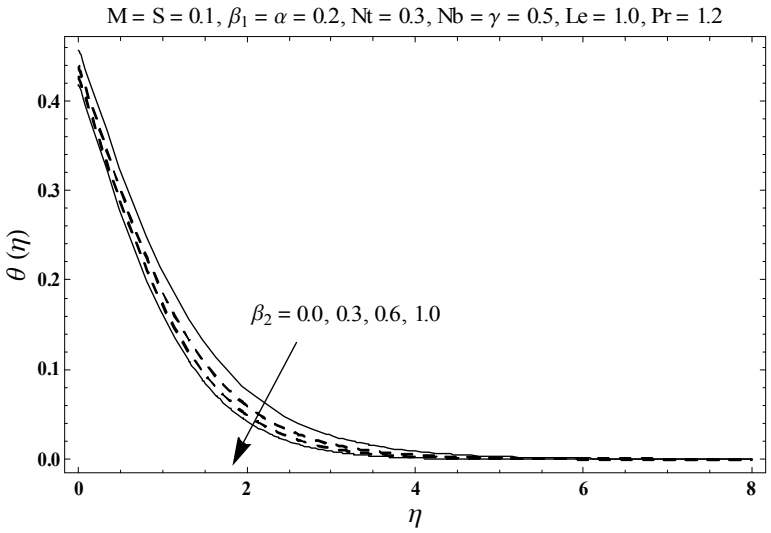

Fig. 9.2. Plots of $\theta(\eta)$ for β_2.

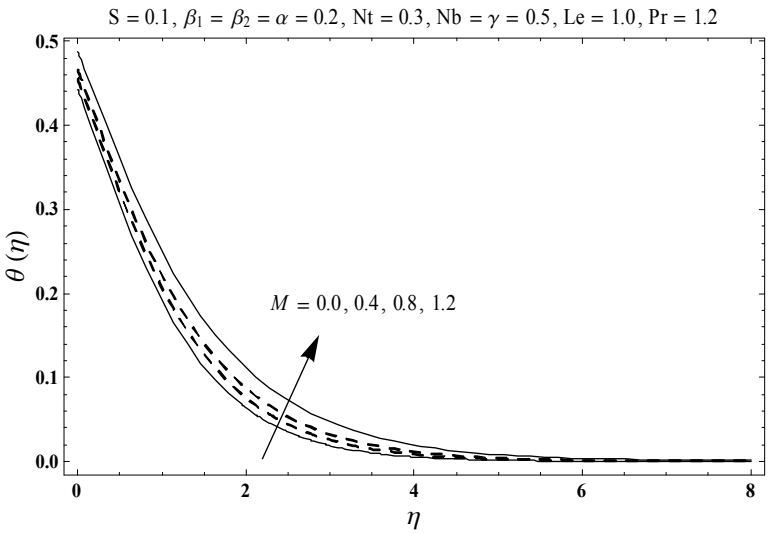

Fig. 9.3. Plots of $\theta(\eta)$ for M.

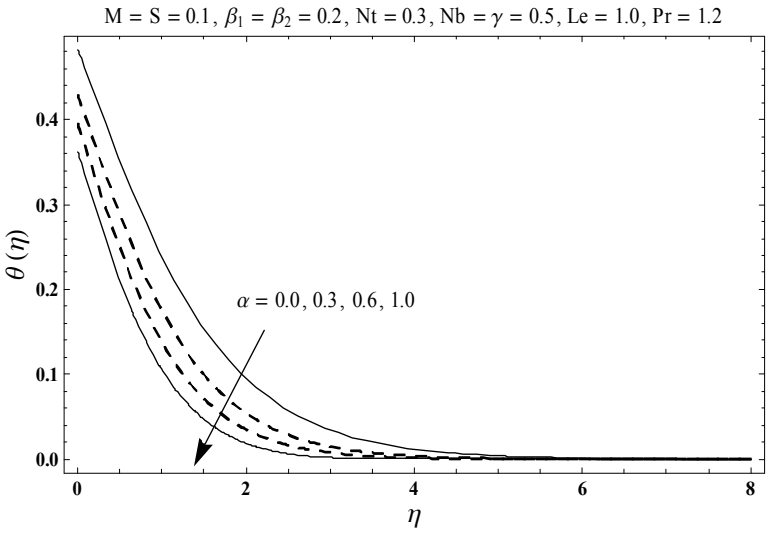

Fig. 9.4. Plots of $\theta(\eta)$ for α.

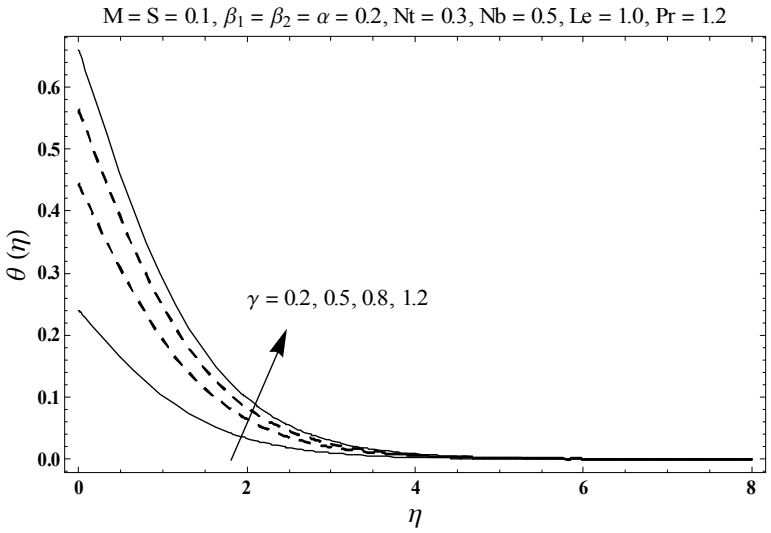

Fig. 9.5. Plots of $\theta(\eta)$ for γ.

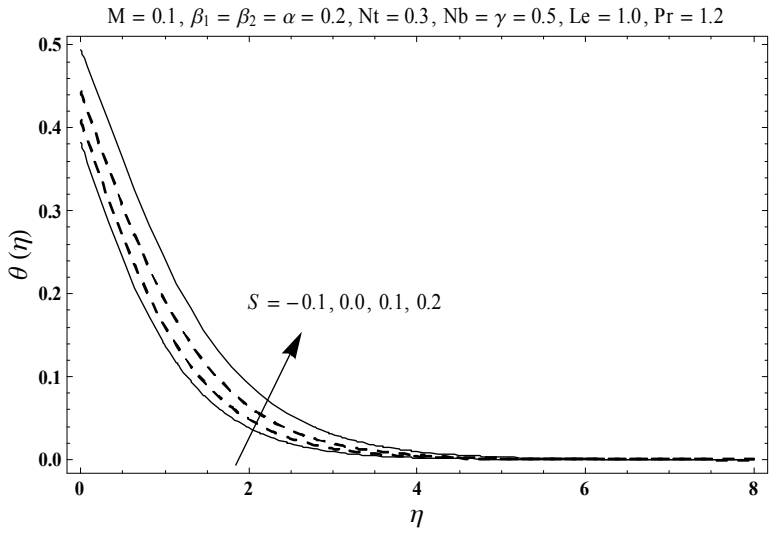

Fig. 9.6. Plots of $\theta(\eta)$ for S.

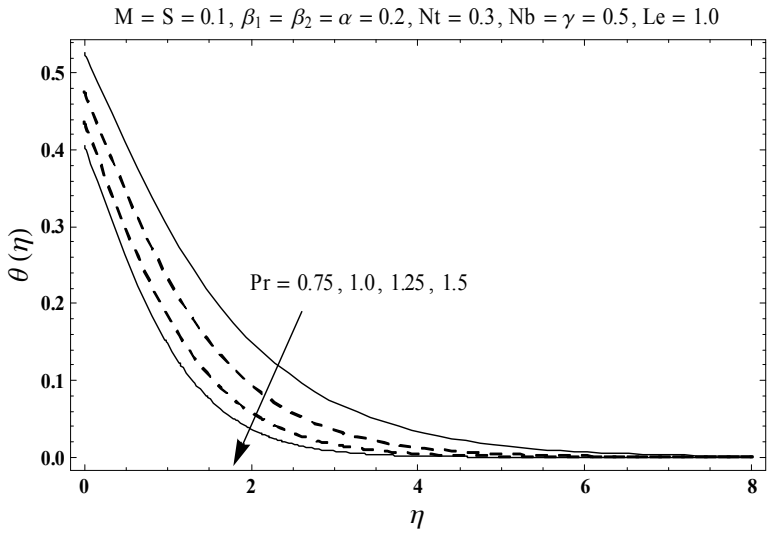

Fig. 9.7. Plots of $\theta(\eta)$ for Pr.

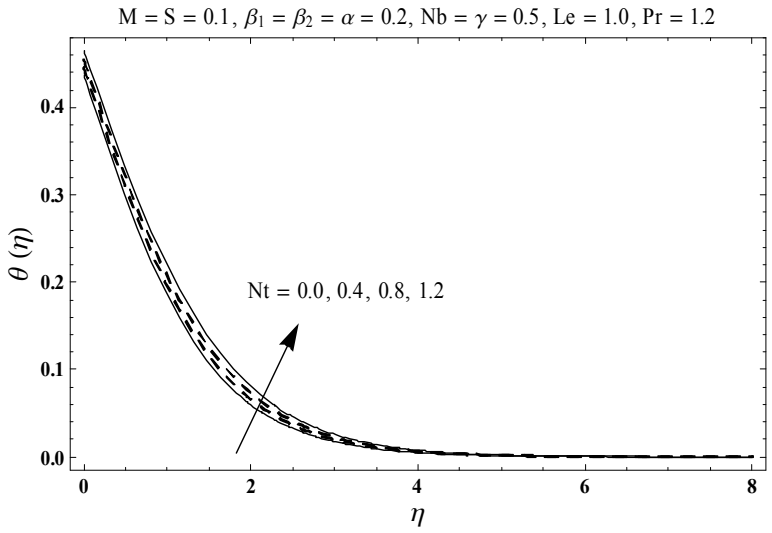

Fig. 9.8. Plots of $\theta(\eta)$ for Nt.

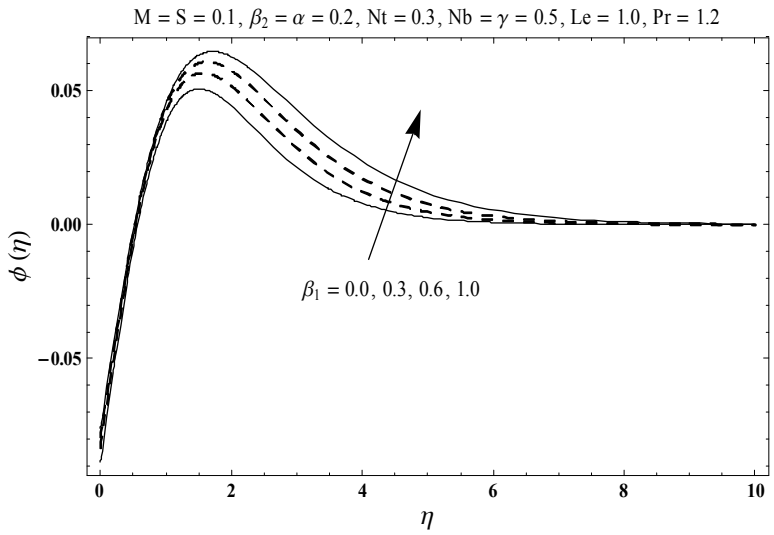

Fig. 9.9. Plots of $\phi(\eta)$ for β_1.

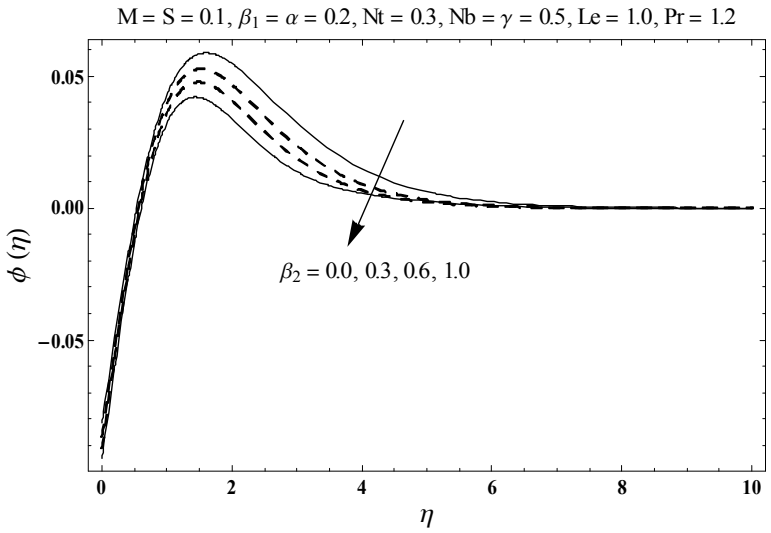

Fig. 9.10. Plots of $\phi(\eta)$ for β_2.

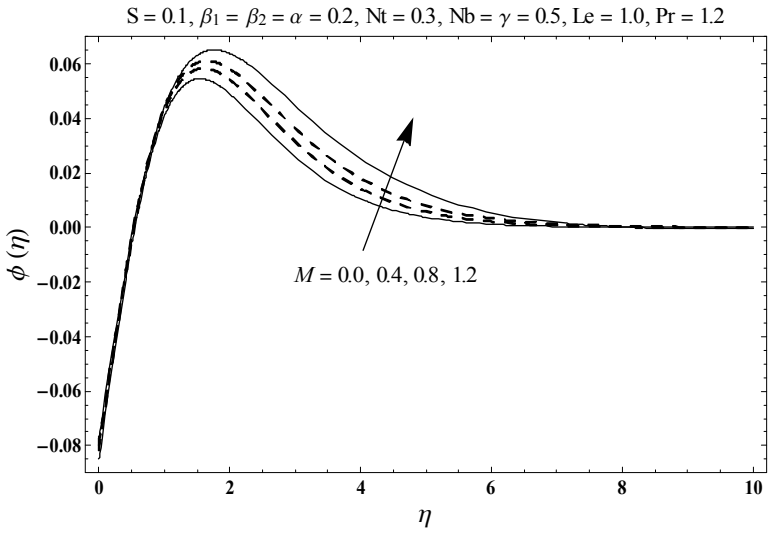

Fig. 9.11. Plots of $\phi(\eta)$ for M.

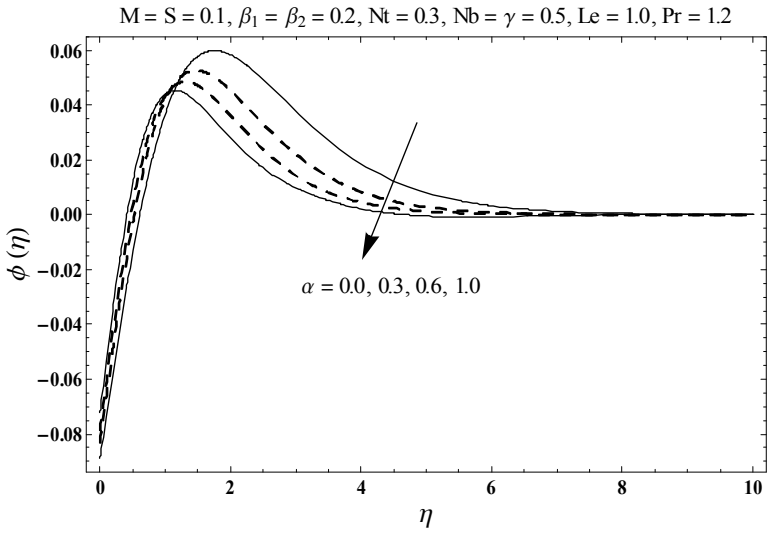

Fig. 9.12. Plots of $\phi(\eta)$ for α.

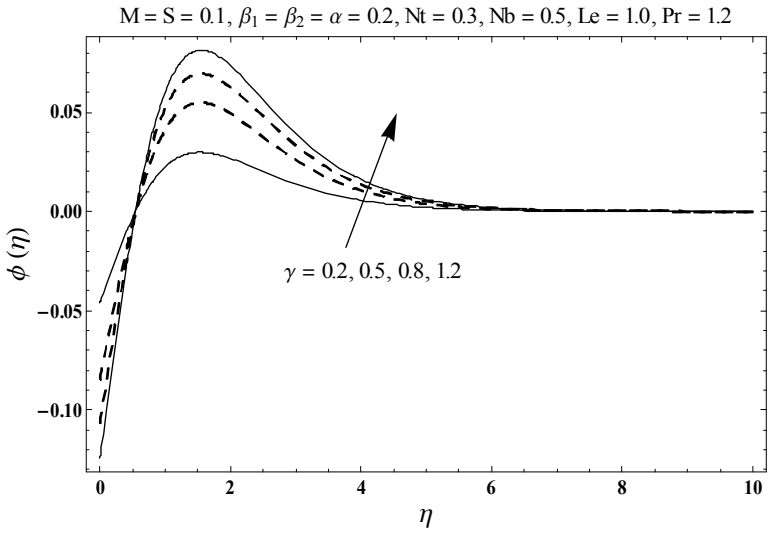

Fig. 9.13. Plots of $\phi(\eta)$ for γ.

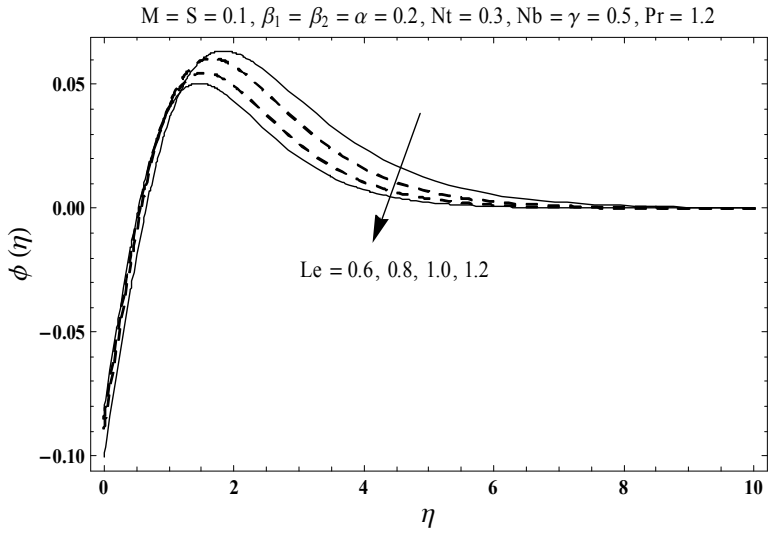

Fig. 9.14. Plots of $\phi(\eta)$ for Le.

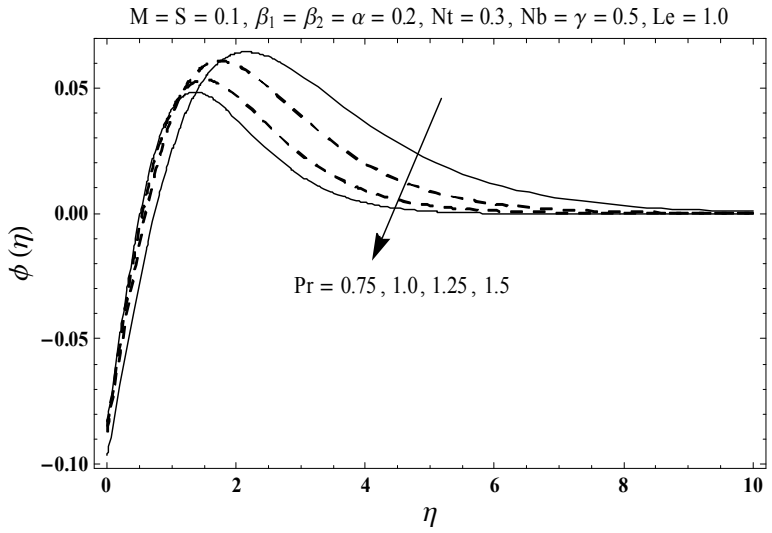

Fig. 9.15. Plots of $\phi(\eta)$ for Pr.

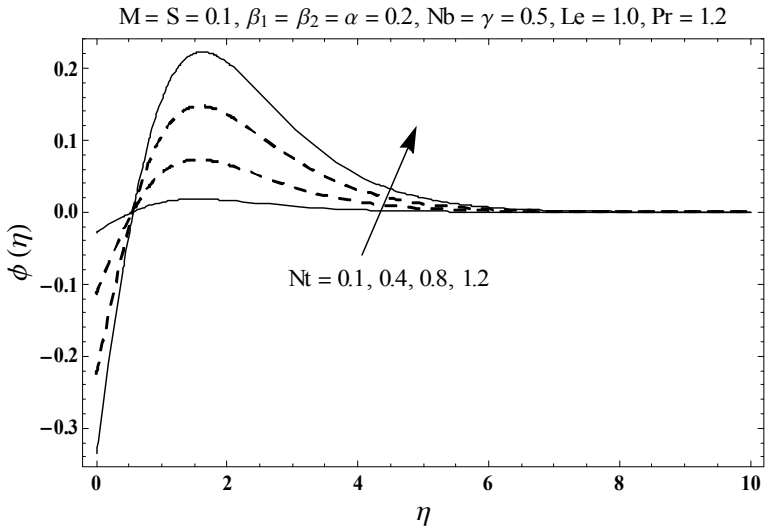

Fig. 9.16. Plots of $\phi(\eta)$ for Nt.

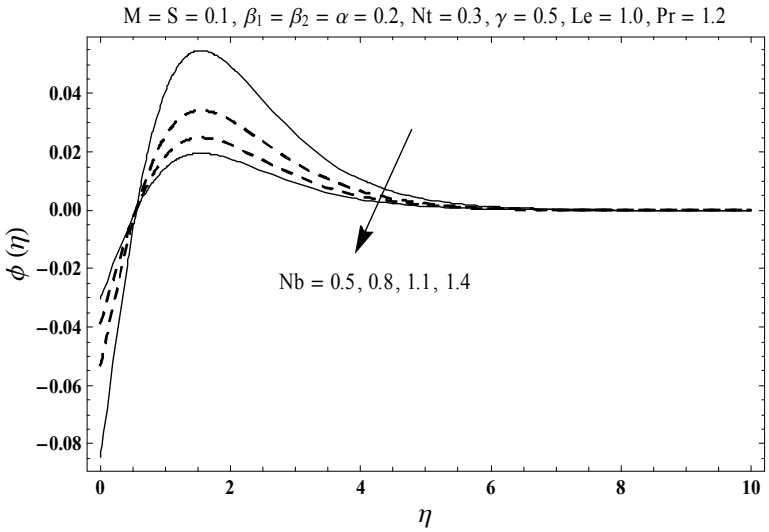

Fig. 9.17. Plots of $\phi(\eta)$ for Nb.

Table 9.2. Comparative estimations of $-f''(0)$ and $-g''(0)$ for various estimations of α when $\beta_1 = \beta_2 = M = 0$.

α	$-f''(0)$		$-g''(0)$	
	OHAM	Exact [38]	OHAM	Exact [38]
0	1	1	0	0
0.25	1.048811	1.048813	0.194564	0.194564
0.50	1.093095	1.093097	0.465205	0.465205
0.75	1.134486	1.134485	0.794618	0.794622
1.0	1.173722	1.173720	1.173722	1.173720

Table 9.3. Numeric data for Nusselt number $\left(-\theta'(0)\right)$ for various estimations of β_1, β_2, α, S, γ, Nt, Nb, Le, Pr and M.

β_1	β_2	α	S	γ	Nt	Nb	Le	Pr	$-\theta'(0)$	
									$M = 0.0$	$M = 0.5$
0.0	0.2	0.2	0.1	0.5	0.3	0.5	1.0	1.2	0.2833	0.2777
0.2									0.2785	0.2723
0.4									0.2737	0.2667
0.2	0.0	0.2	0.1	0.5	0.3	0.5	1.0	1.2	0.2719	0.2643
	0.2								0.2785	0.2724
	0.4								0.2832	0.2778
0.2	0.2	0.0	0.1	0.5	0.3	0.5	1.0	1.2	0.2589	0.2504
		0.5							0.2980	0.2935
		1.0							0.3217	0.3160
0.2	0.2	0.2	0.0	0.5	0.3	0.5	1.0	1.2	0.2958	0.2918
			0.1						0.2785	0.2723
			0.2						0.2532	0.2415
0.2	0.2	0.2	0.1	0.2	0.3	0.5	1.0	1.2	0.1522	0.1504
				0.5					0.2785	0.2723
				0.8					0.3507	0.3407
0.2	0.2	0.2	0.1	0.5	0.0	0.5	1.0	1.2	0.2818	0.2758
					0.3				0.2785	0.2723
					0.5				0.2763	0.2698
0.2	0.2	0.2	0.1	0.5	0.3	0.5	1.0	1.2	0.2785	0.2723
						0.7			0.2785	0.2723
						1.0			0.2785	0.2723
0.2	0.2	0.2	0.1	0.5	0.3	0.5	0.5	1.2	0.2798	0.2738
							1.0		0.2785	0.2723
							1.5		0.2778	0.2714
0.2	0.2	0.2	0.1	0.5	0.3	0.5	1.0	0.5	0.1918	0.1812
								1.0	0.2620	0.2546
								1.5	0.2976	0.2923

Chapter 10

A mathematical study for three-dimensional boundary layer flow of Jeffrey nanofluid

Here we investigated characteristics of Brownian movement and thermophoresis in magneto-hydrodynamic (MHD) three dimension flow of Jeffrey liquid. Flow generated is because of bi-directional extending surface. Mathematical formulation of considered flow problem is made through boundary-layer approach. Newly developed constraint requiring zero nanoparticle flux is employed in flow analysis of Jeffrey liquid. The governing nonlinear boundary layer expressions are diminished into nonlinear ordinary differential frameworks through appropriate transformations. The resulting frameworks have been solved for velocities, concentration and temperature. The importance of various interesting variables is studied graphically. The estimations of Nusselt number are computed and examined.

10.1 Formulation

We examine three dimensional (3D) flow of Jeffrey nanoliquid. Flow made is because of a bidirectional extending surface. Liquid is considered electrically conducting subject to constant B_0 applied in $z-$direction. Also Hall and electric field impacts are disregarded. Brownian movement and thermophoresis impacts are examined. We employ Cartesian coordinate framework

such that $x-$ and $y-$axes are taken along extending surface toward movement and $z-$axis is normal to it. Surface at $z=0$ is extended in $x-$ and $y-$directions with velocities U_w and V_w. The subjected boundary layer expressions for Jeffrey liquid are written below:

$$\frac{\partial u}{\partial x}+\frac{\partial v}{\partial y}+\frac{\partial w}{\partial z}=0, \tag{10.1}$$

$$u\frac{\partial u}{\partial x}+v\frac{\partial u}{\partial y}+w\frac{\partial u}{\partial z}=\frac{\nu}{1+\lambda_1}\left(\frac{\partial^2 u}{\partial z^2}+\lambda_2\left(\begin{array}{c} u\frac{\partial^3 u}{\partial x\partial z^2}+v\frac{\partial^3 u}{\partial y\partial z^2}+w\frac{\partial^3 u}{\partial z^3} \\ +\frac{\partial u}{\partial z}\frac{\partial^2 u}{\partial x\partial z}+\frac{\partial v}{\partial z}\frac{\partial^2 u}{\partial y\partial z}+\frac{\partial w}{\partial z}\frac{\partial^2 u}{\partial z^2}\end{array}\right)\right)-\frac{\sigma B_0^2}{\rho_f}u, \tag{10.2}$$

$$u\frac{\partial v}{\partial x}+v\frac{\partial v}{\partial y}+w\frac{\partial v}{\partial z}=\frac{\nu}{1+\lambda_1}\left(\frac{\partial^2 v}{\partial z^2}+\lambda_2\left(\begin{array}{c} u\frac{\partial^3 v}{\partial x\partial z^2}+v\frac{\partial^3 v}{\partial y\partial z^2}+w\frac{\partial^3 v}{\partial z^3} \\ +\frac{\partial u}{\partial z}\frac{\partial^2 v}{\partial x\partial z}+\frac{\partial v}{\partial z}\frac{\partial^2 v}{\partial y\partial z}+\frac{\partial w}{\partial z}\frac{\partial^2 v}{\partial z^2}\end{array}\right)\right)-\frac{\sigma B_0^2}{\rho_f}v, \tag{10.3}$$

$$u\frac{\partial T}{\partial x}+v\frac{\partial T}{\partial y}+w\frac{\partial T}{\partial z}=\alpha\frac{\partial^2 T}{\partial z^2}+\frac{(\rho c)_p}{(\rho c)_f}\left(D_B\left(\frac{\partial T}{\partial z}\frac{\partial C}{\partial z}\right)+\frac{D_T}{T_\infty}\left(\frac{\partial T}{\partial z}\right)^2\right), \tag{10.4}$$

$$u\frac{\partial C}{\partial x}+v\frac{\partial C}{\partial y}+w\frac{\partial C}{\partial z}=D_B\left(\frac{\partial^2 C}{\partial z^2}\right)+\frac{D_T}{T_\infty}\left(\frac{\partial^2 T}{\partial z^2}\right). \tag{10.5}$$

Here one has the following prescribed conditions:

$$u=U_w(x)=ax,\ v=V_w(y)=by,\ w=0,\ T=T_w(x),\ D_B\frac{\partial C}{\partial z}+\frac{D_T}{T_\infty}\frac{\partial T}{\partial z}=0 \text{ at } z=0, \tag{10.6}$$

$$u\to 0,\quad v\to 0,\quad T\to T_\infty,\quad C\to C_\infty \quad \text{as } z\to\infty. \tag{10.7}$$

Here u, v and w stand for velocities in $x-$, $y-$ and $z-$directions, μ for dynamic viscosity, $\nu\left(=\mu/\rho_f\right)$ for kinematic viscosity, k for thermal conductivity, ρ_f for density, λ_1 for ratio of relaxation and retardation times, D_T for thermophoretic diffusion, λ_2 for retardation time, $(\rho c)_p$ for effective heat potential of nanoparticles, σ for electrical conductivity, T for temperature, $\alpha=k/(\rho c)_f$ for thermal diffusivity, $(\rho c)_f$ for heat potential of the liquid, D_B for Brownian movement, C for concentration, T_w and T_∞ for wall and ambient temperatures and C_∞ for ambient concentration. Here we assumes that surface extending velocities and temperature are

$$U_w(x)=ax,\ V_w(y)=by,\ T_w(x)=T_\infty+T_0x, \tag{10.8}$$

where a, b and T_0 are positive constants. Selecting

$$\left.\begin{array}{c} u = axf'(\eta),\ v = ayg'(\eta),\ w = -\left(a\nu\right)^{1/2}\left(f(\eta)+g(\eta)\right), \\ \theta(\eta) = \frac{T-T_\infty}{T_w-T_\infty},\ \phi(\eta) = \frac{C-C_\infty}{C_\infty},\ \eta = \left(\frac{a}{\nu}\right)^{1/2} z. \end{array}\right\} \tag{10.9}$$

Expression (10.1) is automatically satisfied and Eqs. $(10.2)-(10.8)$ have the following forms

$$f''' + (1+\lambda_1)\left((f+g)f'' - f'^2\right) + \beta\left(f''^2 - (f+g)\,f^{iv} - g'f'''\right) - (1+\lambda_1)\,M^2 f' = 0, \tag{10.10}$$

$$g''' + (1+\lambda_1)\left((f+g)g'' - g'^2\right) + \beta\left(g''^2 - (f+g)\,g^{iv} - f'g'''\right) - (1+\lambda_1)\,M^2 g' = 0, \tag{10.11}$$

$$\theta'' + \Pr\left((f+g)\theta' - f'\theta + Nb\theta'\phi' + Nt\theta'^2\right) = 0, \tag{10.12}$$

$$\phi'' + Le\Pr(f+g)\phi' + \frac{Nt}{Nb}\theta'' = 0, \tag{10.13}$$

$$f = 0,\ g = 0,\ f' = 1,\ g' = c,\ \theta = 1,\ Nb\phi' + Nt\theta' = 0 \text{ at } \eta = 0, \tag{10.14}$$

$$f' \to 0,\ g' \to 0,\ \theta \to 0,\ \phi \to 0 \text{ as } \eta \to \infty. \tag{10.15}$$

Here Pr stands for Prandtl parameter, β for Deborah parameter, Nb for Brownian movement number, M for magnetic number, Le for Lewis parameter, Nt for thermophoresis number and c for ratio of extending rates. These variables can be specified by employing the definitions given below:

$$\left.\begin{array}{c} \beta = \lambda_2 a,\ M^2 = \frac{\sigma B_0^2}{\rho_f a},\ c = \frac{b}{a},\ \Pr = \frac{\nu}{\alpha}, \\ Nb = \frac{(\rho c)_p D_B C_\infty}{(\rho c)_f \nu},\ Nt = \frac{(\rho c)_p D_T (T_w - T_\infty)}{(\rho c)_f \nu T_\infty},\ Le = \frac{\alpha}{D_B}. \end{array}\right\} \tag{10.16}$$

The local Nusselt number Nu_x is defined as

$$Nu_x = -\frac{x}{(T_w - T_\infty)}\left.\frac{\partial T}{\partial z}\right|_{z=0} = -\left(\mathrm{Re}_x\right)^{1/2}\theta'(0). \tag{10.17}$$

It is watched that mass flux represented by Sherwood number is now identically vanishes and $\mathrm{Re}_x = U_w x/\nu$ is for local Reynolds parameter.

10.2 Solutions by HAM

The series arrangements of Eqs. (10.10) − (10.13) through (10.14) and (10.15) have been developed by utilizing homotopic analysis technique (HAM). The linear operators and initial deformations have been selected as follows:

$$f_0(\eta) = 1 - e^{-\eta}, \quad g_0(\eta) = c(1 - e^{-\eta}), \quad \theta_0(\eta) = e^{-\eta}, \quad \phi_0(\eta) = -\frac{Nt}{Nb}e^{-\eta}, \tag{10.18}$$

$$\mathcal{L}_f = f''' - f', \quad \mathcal{L}_g = g''' - g', \quad \mathcal{L}_\theta = \theta'' - \theta, \quad \mathcal{L}_\phi = \phi'' - \phi. \tag{10.19}$$

The above linear operators obey

$$\left.\begin{array}{c} \mathcal{L}_f\left[F_1^{**} + F_2^{**}e^{\eta} + F_3^{**}e^{-\eta}\right] = 0, \quad \mathcal{L}_g\left[F_4^{**} + F_5^{**}e^{\eta} + F_6^{**}e^{-\eta}\right] = 0, \\ \mathcal{L}_\theta\left[F_7^{**}e^{\eta} + F_8^{**}e^{-\eta}\right] = 0, \quad \mathcal{L}_\phi\left[F_9^{**}e^{\eta} + F_{10}^{**}e^{-\eta}\right] = 0, \end{array}\right\} \tag{10.20}$$

in which F_j^{**} $(j = 1 - 10)$ stand for arbitrary constants. Problems for zeroth and mth-order deformations are easily formulated in the view of above operators. The deformation issues are computed by Mathematica software.

10.3 Convergence analysis

The homotopic series arrangements have auxiliary variables $\hbar_f$, $\hbar_g$, $\hbar_\theta$ and $\hbar_\phi$. Such variables are helpful for convergence of homotopic series arrangements. Proper estimations of such variables play a vital role to construct convergent homotopic arrangements via homotopic analysis technique (HAM). To get suitable estimations of $\hbar_f$, $\hbar_g$, $\hbar_\theta$ and $\hbar_\phi$, the $\hbar-$plots are depicted at 20th order of deformations. Figs. 10.1 and 10.2 clearly show that convergence area lies within the ranges $-1.35 \leq \hbar_f \leq -0.15$, $-1.45 \leq \hbar_g \leq -0.10$, $-1.40 \leq \hbar_\theta \leq -0.45$ and $-1.40 \leq \hbar_\phi \leq -0.25$. Table 10.1 exhibits that 34th order of deformations is sufficient for

convergent homotopic series arrangements.

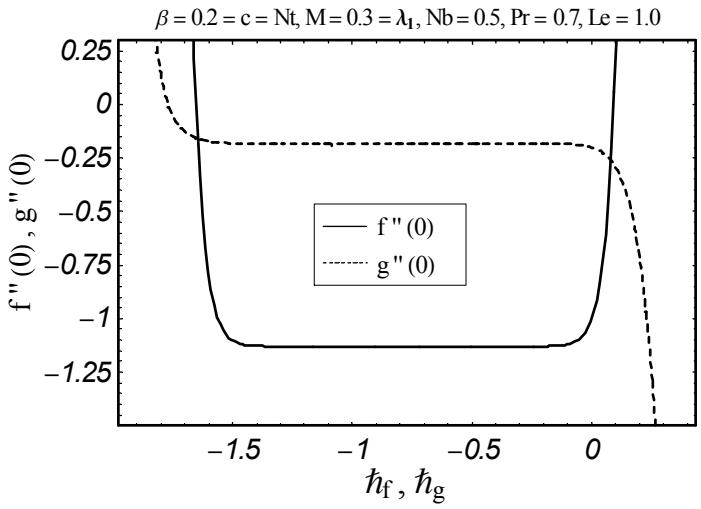

Fig. 10.1. The $\hbar-$plots for $f(\eta)$ and $g(\eta)$.

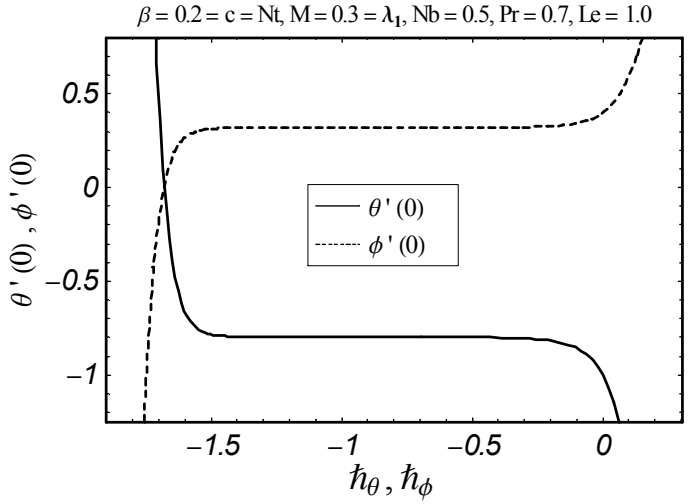

Figs 10.2. The $\hbar-$plots for $\theta(\eta)$ and $\phi(\eta)$.

Table 10.1. HAM arrangements convergence when $\beta = 0.2 = c = Nt$, $M = 0.3 = \lambda_1$, $Nb = 0.5$, $\Pr = 0.7$ and $Le = 1.0$.

Order of deformations	$-f''(0)$	$-g''(0)$	$-\theta'(0)$	$\phi'(0)$
1	1.15850	0.18370	0.87333	0.34933
5	1.12932	0.18471	0.80614	0.32245
10	1.12918	0.18474	0.79790	0.31916
15	1.12918	0.18474	0.79613	0.31845
25	1.12918	0.18474	0.79544	0.31817
34	1.12918	0.18474	0.79535	0.31814
45	1.12918	0.18474	0.79535	0.31814
60	1.12918	0.18474	0.79535	0.31814

10.4 Discussion

The motivation behind this segment is to investigate the contributions of several influential variables including Brownian movement number Nb, Lewis parameter Le, ratio of relaxation to retardation times λ_1, ratio number c, Prandtl parameter Pr, magnetic number M, thermophoresis number Nt and Deborah parameter β on concentration and temperature. Fig. 10.3 exhibits that an improvement in ratio of relaxation to retardation times creates an improvement in temperature $\theta(\eta)$ and layer of thermal. The situation $\lambda_1 = 0$ compares to least temperature and thinner layer of thermal. Physically large λ_1 prompts increment in relaxation time and a lessening in retardation time. This adjustment in relaxation and retardation times makes a elevated temperature and thicker layer of thermal. The variety in temperature $\theta(\eta)$ because of Deborah parameter β is shown in Fig. 10.4. It is watched from Fig. 10.4 that an expansion in β exhibits a decrease in temperature $\theta(\eta)$ and corresponding layer of thermal. Fig. 10.5 exhibits that temperature $\theta(\eta)$ and layer of thermal are higher for bigger magnetic number. Here $M > 0$ is for hydro-magnetic flow and $M = 0$ corresponds to hydro-dynamic flow situation. We watched that temperature and layer of thermal are higher for hydro-magnetic flow in comparison to hydro-dynamic situation. Magnetic number depends upon Lorentz force. Bigger magnetic number has stronger Lorentz force. Such stronger Lorentz force is responsible to im-

provement the temperature in nanoliquid motion. Consequently the layer of thermal becomes thicker for stronger magnetic field. Influence of ratio number on temperature θ is displayed in Fig. 10.6. Temperature and layer of thermal are diminishing functions of ratio number. For $c = 0$, two dimensional flow circumstance is recuperated. Here we watched that layer of thermal is more for two dimensional situation in contrast with three dimensional flow. Thermophoresis number Nt is key number for dissecting temperature in nanoliquid flow. Influence of Nt on temperature is presented in Fig. 10.7. With the expansion in Nt, temperature of liquid increments. An expansion in Nt creates an upgrade in thermophoresis constrain which tends to shift nanoparticles from hot to icy territories and therefore it improves temperature θ and corresponding layer of thermal. Effect of Pr on temperature $\theta(\eta)$ is depicted in Fig. 10.8. An augmentation in Prandtl parameter makes real impact on temperature $\theta(\eta)$ and layer of thermal. Layer of thermal diminishes with Prandtl parameter and it occurs due to decrease of thermal diffusivity for higher Prandtl parameter. Fig. 10.9 plainly delineates that concentration $\phi(\eta)$ and corresponding layer are expanding elements of λ_1. A comparison of Figs. 10.3 and 10.9 obviously portrays that effects of ratio of relaxation to retardation times on concentration and temperature very comparative. Impact of Deborah parameter β on $\phi(\eta)$ is plotted in Fig. 10.10. Here concentration and corresponding layer thickness are diminishment when Deborah parameter increments. Concentration $\phi(\eta)$ is an expanding potential of magnetic number (see Fig. 10.11). As magnetic number elevates, concentration $\phi(\eta)$ improves. variation in $\phi(\eta)$ comparing to various estimations of ratio number is inspected in Fig. 10.12. We have watched that bigger ratio number makes a decrease in concentration and corresponding layer thickness. Fig. 10.13 exhibits that concentration is diminished by means of Lewis parameter. Lewis parameter relies upon Brownian movement. Higher Lewis parameter leads to poor Brownian movement which exhibits a poor concentration. Influence of Pr for concentration is depicted in Fig. 10.14. Bigger Prandtl parameter exhibits a diminishment of concentration. Concentration exhibits overshoot close to the surface for bigger estimations of Pr, however the nanoparticle volume layer thickness diminishes. Effect of thermophoresis number Nt on concentration $\phi(\eta)$ is displayed in Fig. 10.15. Concentration and corresponding layer thickness are expanding elements of Nt. An expansion in Nt makes an improvement in thermophoresis compel which tends to improvement concentration and corresponding layer thickness. Impact of Brownian movement

number Nb on concentration $\phi(\eta)$ is sketched via Fig. 10.16. Concentration diminishes with expanding estimations of Nb. In nanoliquid framework, because of the nearness of nanoparticles, Brownian movement happens and with expansion in Nb the Brownian movement is influenced and thusly layer of concentration diminishes. Table 10.2 exhibits the comparison for different estimations of c with exact arrangement. Table 10.2 presents an excellent agreement of HAM arrangement with existing exact arrangement in a limiting situation. Table 10.3 is tabulated to investigate transfer of heat rate for β, λ_1, M, c, Nt, Nb, Le and $\Pr$. Rate of heat transfer is independent for variations in Brownian movement number. Effects of Lewis and Prandtl parameters on transfer of heat rate are very reverse.

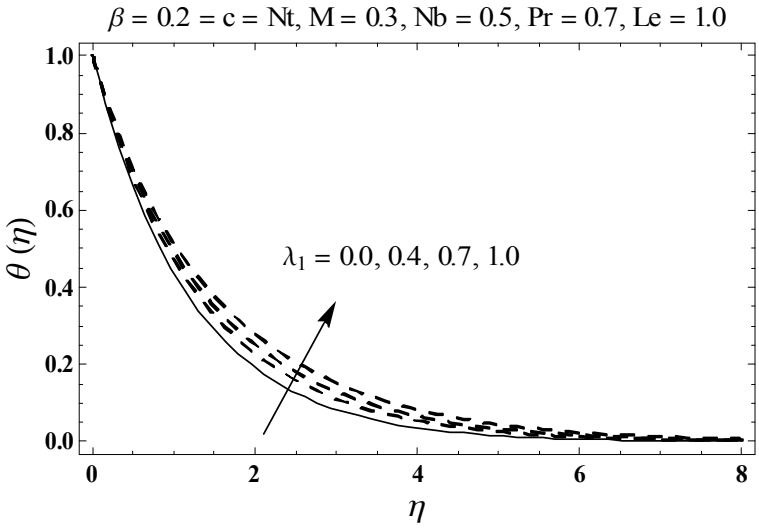

Fig. 10.3. Plots of $\theta(\eta)$ for λ_1.

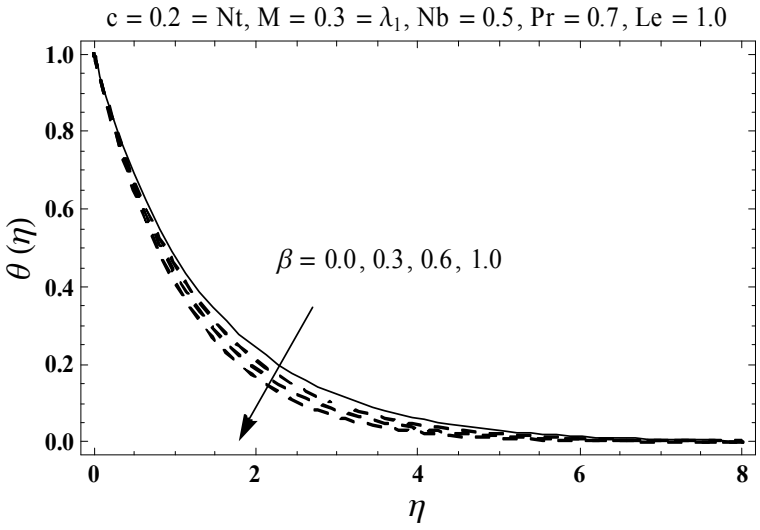

Fig. 10.4. Plots of $\theta(\eta)$ for β.

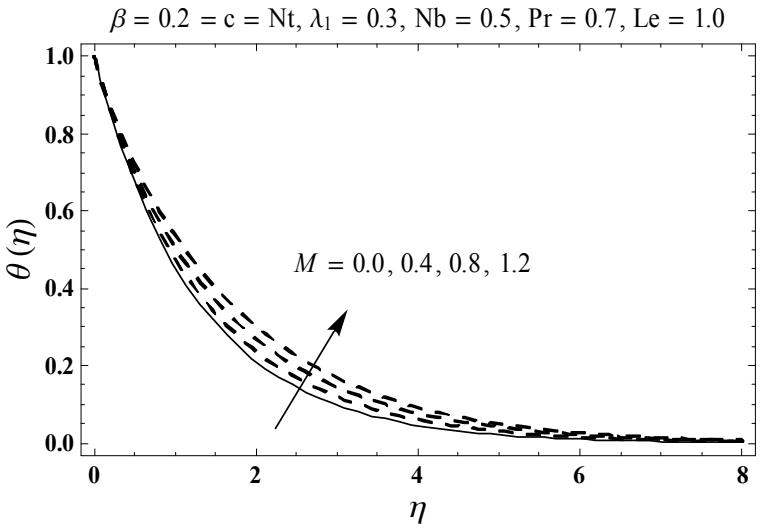

Fig. 10.5. Plots of $\theta(\eta)$ for M.

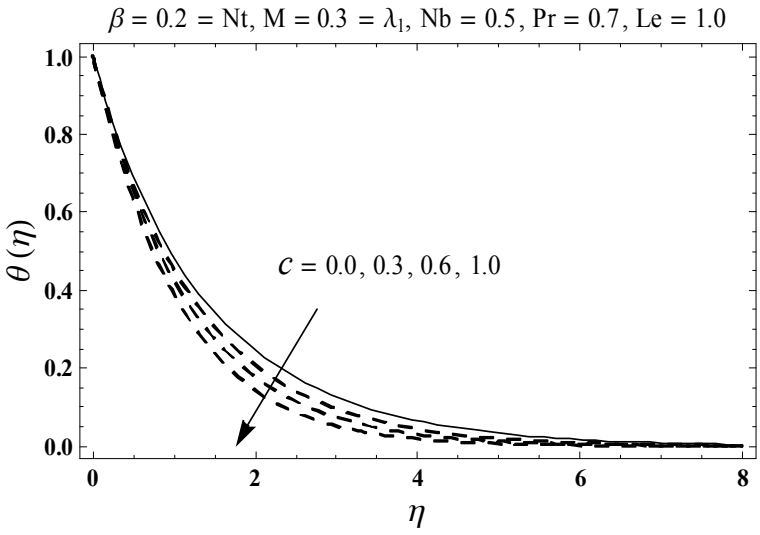

Fig. 10.6. Plots of $\theta(\eta)$ for c.

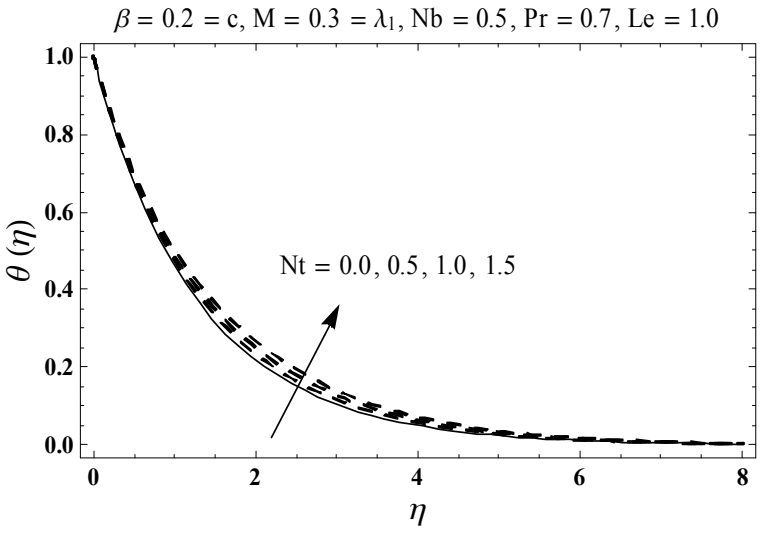

Fig. 10.7. Plots of $\theta(\eta)$ for Nt.

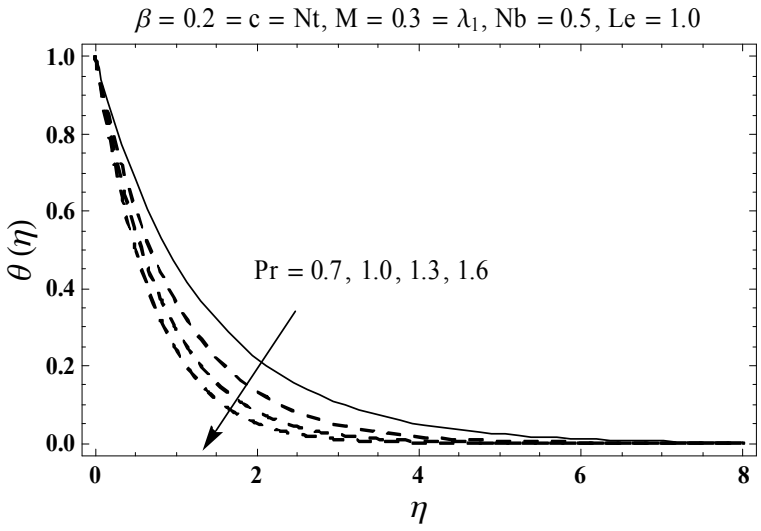

Fig. 10.8. Plots of $\theta(\eta)$ for Pr.

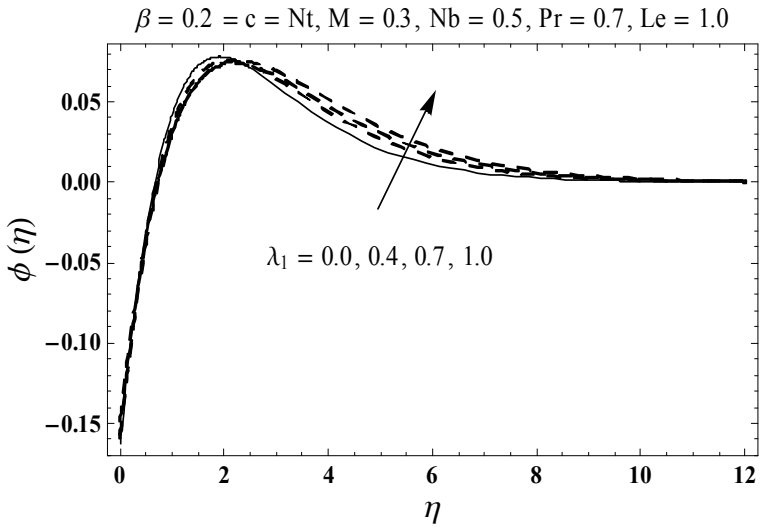

Fig. 10.9. Plots of $\phi(\eta)$ for λ_1.

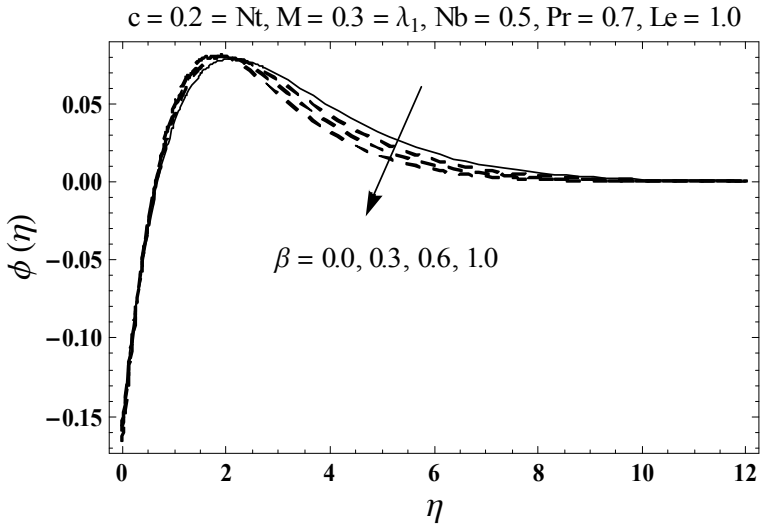

Fig. 10.10. Plots of $\phi(\eta)$ for β.

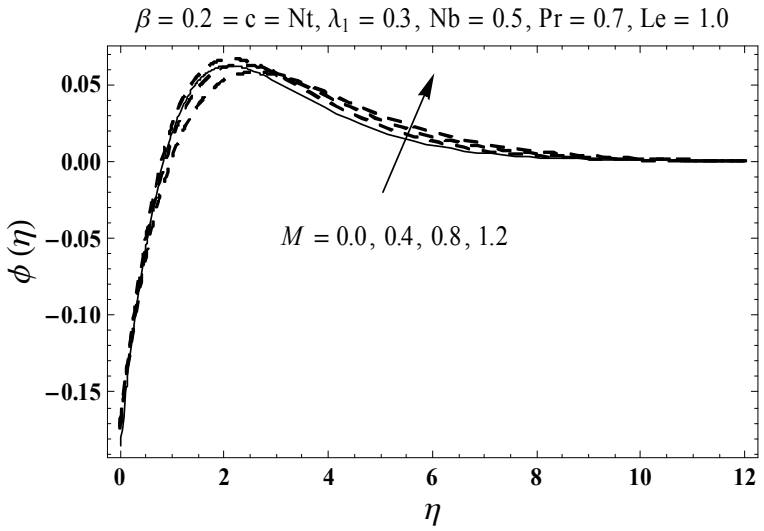

Fig. 10.11. Plots of $\phi(\eta)$ for M.

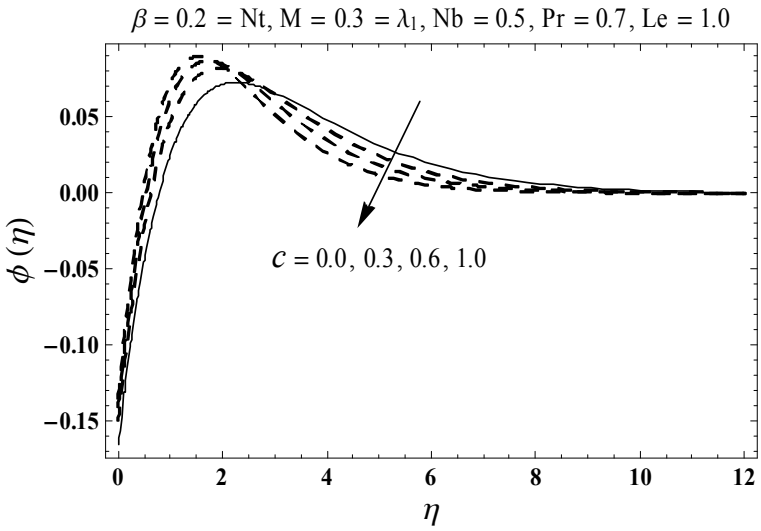

Fig. 10.12. Plots of $\phi(\eta)$ for c.

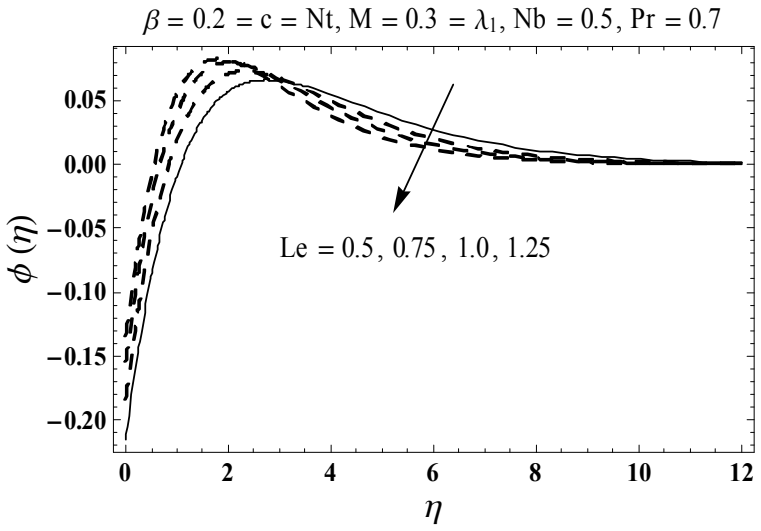

Fig. 10.13. Plots of $\phi(\eta)$ for Le.

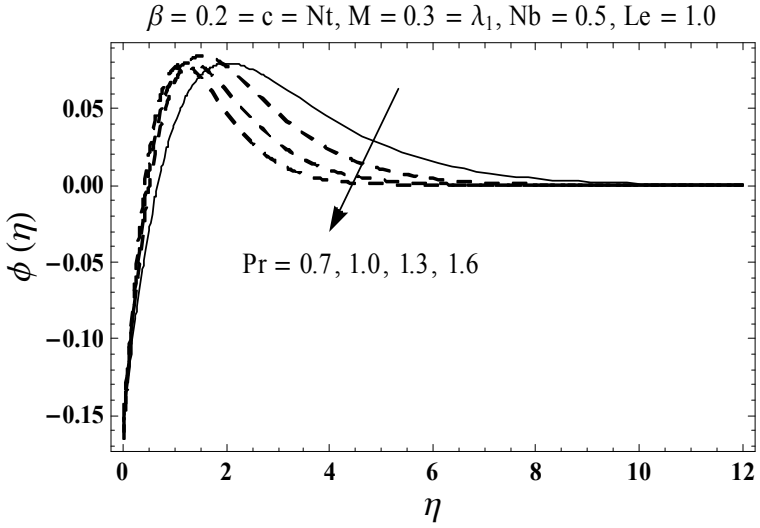

Fig. 10.14. Plots of $\phi(\eta)$ for Pr .

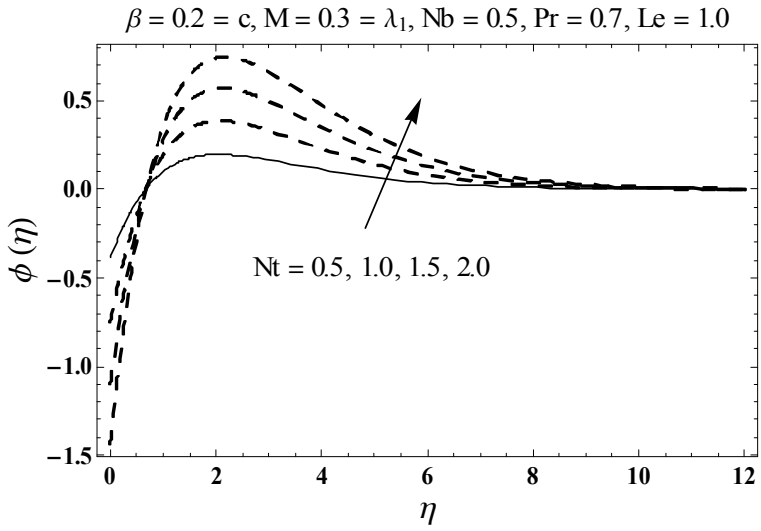

Fig. 10.15. Plots of $\phi(\eta)$ for Nt.

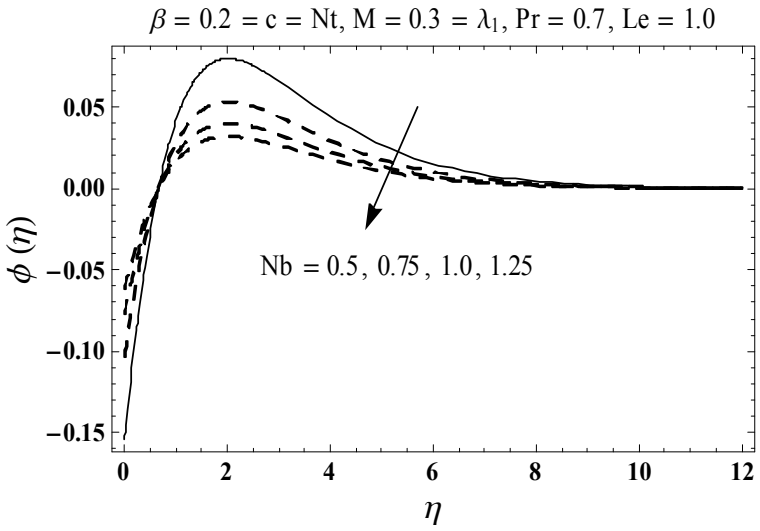

Fig. 10.16. Plots of $\phi(\eta)$ for Nb.

Table 10.2. Comparative estimations of $-f''(0)$ and $-g''(0)$ for several estimations of c when $\beta = \lambda_1 = M = 0$.

c	$-f''(0)$		$-g''(0)$	
	HAM	Exact [38]	HAM	Exact [38]
0	1	1	0	0
0.25	1.048811	1.048813	0.194564	0.194564
0.50	1.093095	1.093097	0.465205	0.465205
0.75	1.134486	1.134485	0.794618	0.794622
1.0	1.173722	1.173720	1.173722	1.173720

Table 10.3. Numeric data of Nusselt number $Nu_x\,(\mathrm{Re}_x)^{-1/2}$ for various estimations of β, λ_1, M, c, Nt, Nb, Le and Pr.

β	λ_1	M	c	Nt	Nb	Le	Pr	$-\theta'(0)$
0.0	0.3	0.3	0.2	0.2	0.5	1.0	0.7	0.7674
0.2								0.7954
0.5								0.8268
0.2	0.0	0.3	0.2	0.2	0.5	1.0	0.7	0.8317
	0.3							0.7954
	0.5							0.7740
0.2	0.3	0.0	0.2	0.2	0.5	1.0	0.7	0.8064
		0.3						0.7954
		0.5						0.7769
0.2	0.3	0.3	0.0	0.2	0.5	1.0	0.7	0.7650
			0.5					0.8378
			1.0					0.9065
0.2	0.3	0.3	0.2	0.0	0.5	1.0	0.7	0.8026
				0.5				0.7848
				1.0				0.7674
0.2	0.3	0.3	0.2	0.2	0.5	1.0	0.7	0.7954
					1.0			0.7954
					1.5			0.7954
0.2	0.3	0.3	0.2	0.2	0.5	0.5	0.7	0.7985
						1.0		0.7954
						1.5		0.7934
0.2	0.3	0.3	0.2	0.2	0.5	1.0	0.5	0.6304
							1.0	1.0047
							1.5	1.2904

Chapter 11

Three-dimensional flow of Jeffrey nanofluid with a new mass flux condition

Three dimensional flow of Jeffrey nanoliquid with convectively heated surface is analyzed. Flow induced is due to a bidirectional extending surface. Impacts of thermophoresis and Brownian movement are explored. Newly developed constraint with zero nanoparticles flux is employed. Similarity variables have been employed for conversion of partial differential frameworks into nonlinear ordinary differential frameworks. The subsequent nonlinear ordinary differential conditions have been tackled for velocities, concentration and temperature. Diagrams are sketched to look at concentration and temperature. Numeric estimations of Nusselt number are tabulated and analyzed. Effects of Biot parameter on concentration and temperature are quite similar. Both concentration and temperature are elevated for bigger Biot parameter.

11.1 Formulation

Consider three dimensional (3D) flow of Jeffrey nanoliquid. Flow generated is due to a bidirectional extending surface at $z = 0$. Flow possesses the area $z > 0$. Effects of thermophoresis and Brownian movement are explored. Temperature at extending surface is controlled by convective heating process which is characterized via coefficient of heat transfer h_f and hot liquid

temperature T_f below the extending surface. Flow under boundary layer approximations are presented by the following expressions:

$$\frac{\partial u}{\partial x}+\frac{\partial v}{\partial y}+\frac{\partial w}{\partial z}=0, \tag{11.1}$$

$$u\frac{\partial u}{\partial x}+v\frac{\partial u}{\partial y}+w\frac{\partial u}{\partial z}=\frac{\nu}{1+\lambda_1}\left(\frac{\partial^2 u}{\partial z^2}+\lambda_2\left(\begin{array}{c} u\frac{\partial^3 u}{\partial x\partial z^2}+v\frac{\partial^3 u}{\partial y\partial z^2}+w\frac{\partial^3 u}{\partial z^3} \\ +\frac{\partial u}{\partial z}\frac{\partial^2 u}{\partial x\partial z}+\frac{\partial v}{\partial z}\frac{\partial^2 u}{\partial y\partial z}+\frac{\partial w}{\partial z}\frac{\partial^2 u}{\partial z^2}\end{array}\right)\right), \tag{11.2}$$

$$u\frac{\partial v}{\partial x}+v\frac{\partial v}{\partial y}+w\frac{\partial v}{\partial z}=\frac{\nu}{1+\lambda_1}\left(\frac{\partial^2 v}{\partial z^2}+\lambda_2\left(\begin{array}{c} u\frac{\partial^3 v}{\partial x\partial z^2}+v\frac{\partial^3 v}{\partial y\partial z^2}+w\frac{\partial^3 v}{\partial z^3} \\ +\frac{\partial u}{\partial z}\frac{\partial^2 v}{\partial x\partial z}+\frac{\partial v}{\partial z}\frac{\partial^2 v}{\partial y\partial z}+\frac{\partial w}{\partial z}\frac{\partial^2 v}{\partial z^2}\end{array}\right)\right), \tag{11.3}$$

$$u\frac{\partial T}{\partial x}+v\frac{\partial T}{\partial y}+w\frac{\partial T}{\partial z}=\alpha\frac{\partial^2 T}{\partial z^2}+\frac{(\rho c)_p}{(\rho c)_f}\left(D_B\left(\frac{\partial T}{\partial z}\frac{\partial C}{\partial z}\right)+\frac{D_T}{T_\infty}\left(\frac{\partial T}{\partial z}\right)^2\right), \tag{11.4}$$

$$u\frac{\partial C}{\partial x}+v\frac{\partial C}{\partial y}+w\frac{\partial C}{\partial z}=D_B\left(\frac{\partial^2 C}{\partial z^2}\right)+\frac{D_T}{T_\infty}\left(\frac{\partial^2 T}{\partial z^2}\right). \tag{11.5}$$

Here one has the following prescribed conditions:

$$u=ax,\ v=by,\ w=0,\ -k\frac{\partial T}{\partial z}=h_f\left(T_f-T\right),\ D_B\frac{\partial C}{\partial z}+\frac{D_T}{T_\infty}\frac{\partial T}{\partial z}=0 \text{ at } z=0, \tag{11.6}$$

$$u\to 0,\quad v\to 0,\quad T\to T_\infty,\quad C\to C_\infty \quad \text{as } z\to\infty. \tag{11.7}$$

Here u, v and w stand for velocities in $x-$, $y-$ and $z-$directions, k for thermal conductivity, μ for dynamic viscosity, λ_2 for retardation time, $(\rho c)_f$ for heat potential of liquid, $\nu\left(=\mu/\rho_f\right)$ for kinematic viscosity, $(\rho c)_p$ for effective heat potential of nanoparticles, ρ_f for density, D_B for Brownian movement, λ_1 for ratio of relaxation and retardation times, T for temperature, $\alpha=k/(\rho c)_f$ for thermal diffusivity, C for concentration, D_T for thermophoretic diffusion, T_∞ for ambient temperature, C_∞ for ambient concentration and a and b for positive constants. Selecting

$$\begin{array}{c} u=axf'(\eta),\ v=ayg'(\eta),\ w=-\left(a\nu\right)^{1/2}\left(f(\eta)+g(\eta)\right), \\ \theta(\eta)=\frac{T-T_\infty}{T_f-T_\infty},\ \phi(\eta)=\frac{C-C_\infty}{C_\infty},\ \eta=\left(\frac{a}{\nu}\right)^{1/2}z. \end{array} \tag{11.8}$$

Eq. (11.1) is automatically verified while Eqs. (11.2) − (11.7) have the following forms:

$$f''' + (1+\lambda_1)\left((f+g)f'' - f'^2\right) + \beta\left(f''^2 - (f+g)\,f^{iv} - g'f'''\right) = 0, \tag{11.9}$$

$$g''' + (1+\lambda_1)\left((f+g)g'' - g'^2\right) + \beta\left(g''^2 - (f+g)\,g^{iv} - f'g'''\right) = 0, \tag{11.10}$$

$$\theta'' + \Pr\left((f+g)\theta' + Nb\theta'\phi' + Nt\theta'^2\right) = 0, \tag{11.11}$$

$$\phi'' + Le\Pr(f+g)\phi' + \frac{Nt}{Nb}\theta'' = 0, \tag{11.12}$$

$$f = 0,\ g = 0,\ f' = 1,\ g' = c,\ \theta' = -\gamma\left(1-\theta\left(0\right)\right),\ Nb\phi' + Nt\theta' = 0 \text{ at } \eta = 0, \tag{11.13}$$

$$f' \to 0,\ g' \to 0,\ \theta \to 0,\ \phi \to 0 \text{ as } \eta \to \infty. \tag{11.14}$$

Here Nt stands for thermophoresis number, γ for Biot parameter, β for Deborah parameter, Nb for Brownian movement number, c for ratio of extending rates, Pr for Prandtl parameter and Le for Lewis parameter. These variables can be specified by employing the definitions given below:

$$\left.\begin{array}{c} \beta = \lambda_2 a,\ c = \frac{b}{a},\ \Pr = \frac{\nu}{\alpha},\ Nb = \frac{(\rho c)_p D_B C_\infty}{(\rho c)_f \nu}, \\ Nt = \frac{(\rho c)_p D_T\left(T_f - T_\infty\right)}{(\rho c)_f \nu T_\infty},\ \gamma = \frac{h_f}{k}\sqrt{\frac{\nu}{a}},\ Le = \frac{\alpha}{D_B}. \end{array}\right\} \tag{11.15}$$

The local Nusselt number Nu_x is defined as by

$$Nu_x = -\frac{x}{(T_w - T_\infty)}\left.\frac{\partial T}{\partial z}\right|_{z=0} = -\left(\mathrm{Re}_x\right)^{1/2}\theta'(0). \tag{11.16}$$

It is watched that mass flux represented by Sherwood number is now identically vanishes and $\mathrm{Re}_x = u_w x/\nu$ is for local Reynolds parameter.

11.2 Solutions by HAM

The series arrangements of Eqs. (11.9) − (11.12) through (11.13) and (11.14) have been developed by utilizing homotopic analysis technique (HAM). The linear operators and initial

deformations have been selected as follows:

$$f_0(\eta) = 1 - e^{-\eta}, \quad g_0(\eta) = c(1 - e^{-\eta}), \quad \theta_0(\eta) = \frac{\gamma}{1+\gamma} e^{-\eta}, \quad \phi_0(\eta) = -\frac{\gamma}{1+\gamma} \frac{Nt}{Nb} e^{-\eta}, \tag{11.17}$$

$$\mathcal{L}_f = f''' - f', \quad \mathcal{L}_g = g''' - g', \quad \mathcal{L}_\theta = \theta'' - \theta, \quad \mathcal{L}_\phi = \phi'' - \phi. \tag{11.18}$$

The above linear operators obey

$$\left.\begin{array}{cc} \mathcal{L}_f \left[F_1^{**} + F_2^{**} e^{\eta} + F_3^{**} e^{-\eta}\right] = 0, & \mathcal{L}_g \left[F_4^{**} + F_5^{**} e^{\eta} + F_6^{**} e^{-\eta}\right] = 0, \\ \mathcal{L}_\theta \left[F_7^{**} e^{\eta} + F_8^{**} e^{-\eta}\right] = 0, & \mathcal{L}_\phi \left[F_9^{**} e^{\eta} + F_{10}^{**} e^{-\eta}\right] = 0, \end{array}\right\} \tag{11.19}$$

in which F_j^{**} $(j = 1 - 10)$ stand for arbitrary constants. Problems for zeroth and mth-order deformations are easily formulated in the view of above operators. The deformation issues are computed by Mathematica software.

11.3 Convergence analysis

The homotopic series arrangements have auxiliary variables $\hbar_f$, $\hbar_g$, $\hbar_\theta$ and $\hbar_\phi$. Such variables are helpful for convergence of acquired homotopic series arrangements. Proper estimations of such variables play a vital role to construct convergent homotopic arrangements via homotopic analysis technique (HAM). To get suitable estimations of $\hbar_f$, $\hbar_g$, $\hbar_\theta$ and $\hbar_\phi$, the $\hbar-$plots are depicted at 15th order of deformations. Figs. 11.1 and 11.2 clearly show that convergence area lies within the ranges $-1.50 \leq \hbar_f \leq -0.10$, $-1.45 \leq \hbar_g \leq -0.10$, $-1.50 \leq \hbar_\theta \leq -0.15$ and $-1.50 \leq \hbar_\phi \leq -0.05$. Table 11.1 exhibits that 13th order of deformations is sufficient for

convergent homotopic series arrangements.

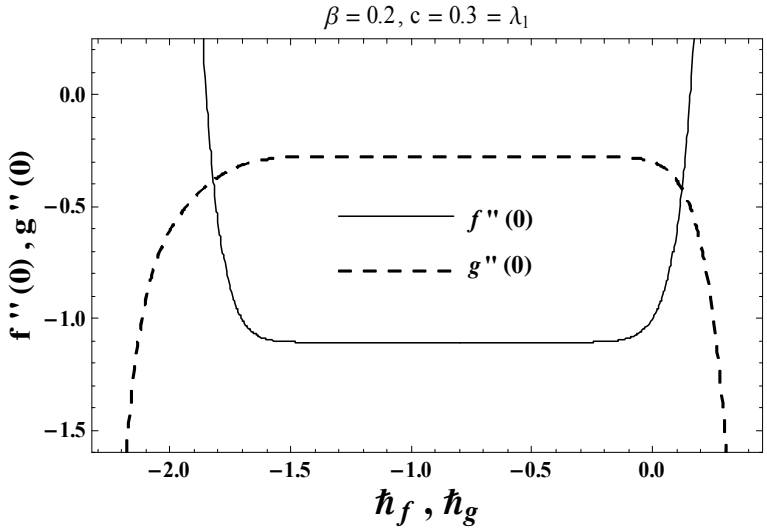

Fig. 11.1. The $\hbar-$plots for $f(\eta)$ and $g(\eta)$.

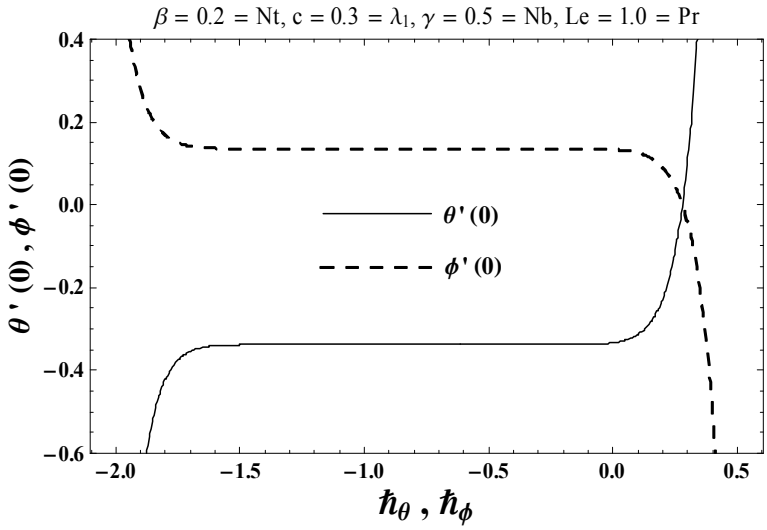

Fig. 11.2. The $\hbar-$plots for $\theta(\eta)$ and $\phi(\eta)$.

Table 11.1. HAM arrangements convergence when $\beta = 0.2 = Nt$, $c = 0.3 = \lambda_1$, $\gamma = 0.5 = Nb$ and $Le = 1.0 = \Pr$.

Order of deformations	$-f''(0)$	$-g''(0)$	$-\theta'(0)$	$\phi'(0)$
1	1.12500	0.27450	0.33889	0.13556
5	1.10643	0.27728	0.33802	0.13521
13	1.10643	0.27737	0.33790	0.13516
20	1.10643	0.27737	0.33790	0.13516
30	1.10643	0.27737	0.33790	0.13516
40	1.10643	0.27737	0.33790	0.13516
50	1.10643	0.27737	0.33790	0.13516

11.4 Discussion

Impacts of ratio number c, ratio of relaxation to retardation times λ_1, Deborah parameter β, Biot parameter γ, Lewis parameter Le, Prandtl parameter Pr, thermophoresis number Nt and Brownian movement number Nb on temperature $\theta(\eta)$ and concentration $\phi(\eta)$ are shown in Figs. $11.3 - 11.16$. Fig. 11.3 presents that an improvement in ratio of relaxation to retardation times λ_1 causes an improvement in temperature $\theta(\eta)$ and layer of thermal. An increment in λ_1 creates an improvement in relaxation time and a diminishment in retardation time. Due to such fact there is an increment in temperature $\theta(\eta)$ and layer of thermal via λ_1. Fig. 11.4 elucidates influence of Deborah parameter β on temperature $\theta(\eta)$. Here temperature $\theta(\eta)$ and layer of thermal are lower for bigger Deborah parameter. Fig. 11.5 presents that bigger ratio number c exhibits a diminishment in temperature $\theta(\eta)$ and layer of thermal. For $c = 0$, the two dimension flow situation is achieved. We watched that layer of thermal is more in two dimension flow when compared with three dimension flow. Fig. 11.6 exhibits impact of Biot parameter γ on temperature $\theta(\eta)$. Here bigger Biot parameter causes a higher convection at the extending surface which provides a stronger temperature $\theta(\eta)$ and thicker layer of thermal. Fig. 11.7 is plotted to see variations in temperature corresponding to different estimations of Prandtl parameter Pr. Temperature $\theta(\eta)$ and layer of thermal are diminished when we improvement Prandtl parameter. Physically bigger Prandtl liquids have poor thermal diffusivity and small

Prandtl liquids have stronger thermal diffusivity. Such variation in thermal diffusivity causes a diminishment in temperature and corresponding layer of thermal. Effect of thermophoresis number Nt on temperature is depicted in Fig. 11.8. Here temperature $\theta(\eta)$ and layer of thermal are higher for bigger thermophoresis number. An improvement in Nt creates an improvement in thermophoresis force which provides a elevated temperature profile and thicker layer of thermal. Fig. 11.9 exhibits that concentration $\phi(\eta)$ and its corresponding layer thickness are elevated for bigger ratio of relaxation to retardation times λ_1. Here $\lambda_1 = 0$ corresponds to minimum concentration $\phi(\eta)$ and thinner layer of concentration. Fig. 11.10 exhibits influence of Deborah parameter β on concentration $\phi(\eta)$. Concentration $\phi(\eta)$ and corresponding layer are diminishing functions of Deborah parameter β. Importance of ratio number c on concentration $\phi(\eta)$ is depicted in Fig. 11.11. Here it is watched that concentration $\phi(\eta)$ is diminishment when we improvement ratio number. Fig. 11.12 presents variations in concentration $\phi(\eta)$ for different estimations of Biot parameter γ. We watched that an improvement in Biot parameter γ causes an improvement in concentration $\phi(\eta)$ and its corresponding layer thickness. Influence of Lewis parameter Le on concentration $\phi(\eta)$ is plotted in Fig. 11.13. Concentration $\phi(\eta)$ and its associated layer thickness are diminished for bigger Lewis parameter. Higher Lewis parameter corresponds to poor Brownian movement coefficient which exhibits a poor concentration and its corresponding layer. Fig. 11.14 presents that concentration $\phi(\eta)$ is diminished for Prandtl parameter Pr. Concentration exhibits overshoot near extending surface for bigger Prandtl parameter Pr which exhibits a diminishment in layer of concentration. Fig. 11.15 exhibits that an increment in thermophoresis number Nt causes a elevated concentration and its associated layer thickness. Importance of Brownian movement number Nb on concentration $\phi(\eta)$ is depicted in Fig. 11.16. Concentration $\phi(\eta)$ and corresponding layer are diminishing functions of Brownian movement number Nb. In nanoliquid flow, due to the existence of nanoparticles, the Brownian movement takes place and with improvement in Nb the Brownian movement is affected and thus layer of concentration diminishes. Table 11.2 exhibits the comparison for different estimations of c with exact arrangement. Table 11.2 presents an excellent agreement of HAM arrangement with existing exact arrangement in limiting situation. Table 11.3 indicates Numeric data of Nusselt number $\left(-\theta'(0)\right)$ for $\lambda_1,\ \beta,\ c,\ \gamma,\ Le,\ \mathrm{Pr},\ Nt$ and Nb. From this Table we watched that Nusselt number $\left(-\theta'(0)\right)$ is higher for bigger Biot parameter γ. However

impact of Brownian movement number Nb on local Nusselt number $\left(-\theta'(0)\right)$ is constant.

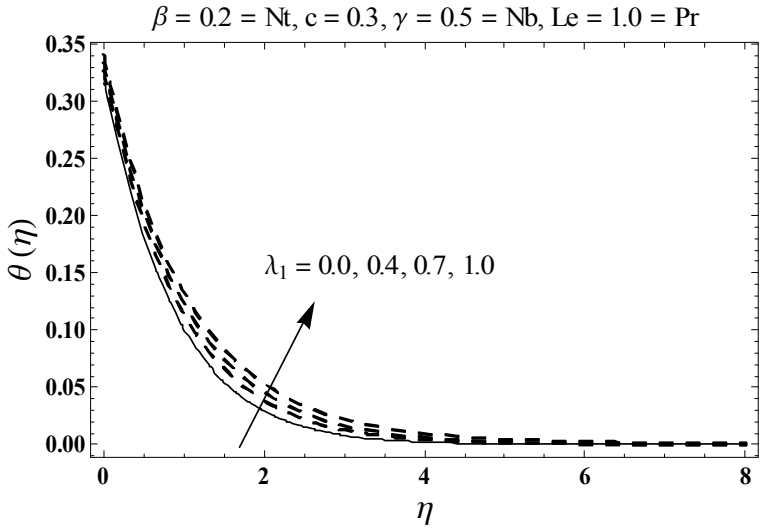

Fig. 11.3. Plots of $\theta(\eta)$ for λ_1.

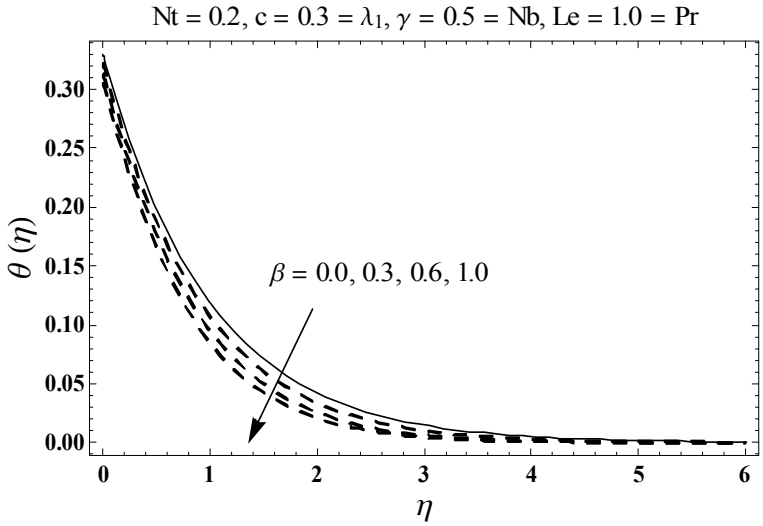

Fig. 11.4. Plots of $\theta(\eta)$ for β.

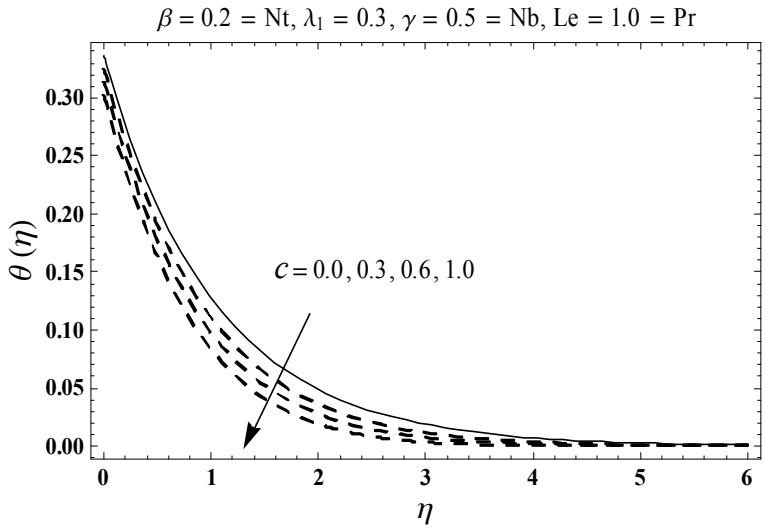

Fig. 11.5. Plots of $\theta(\eta)$ for c.

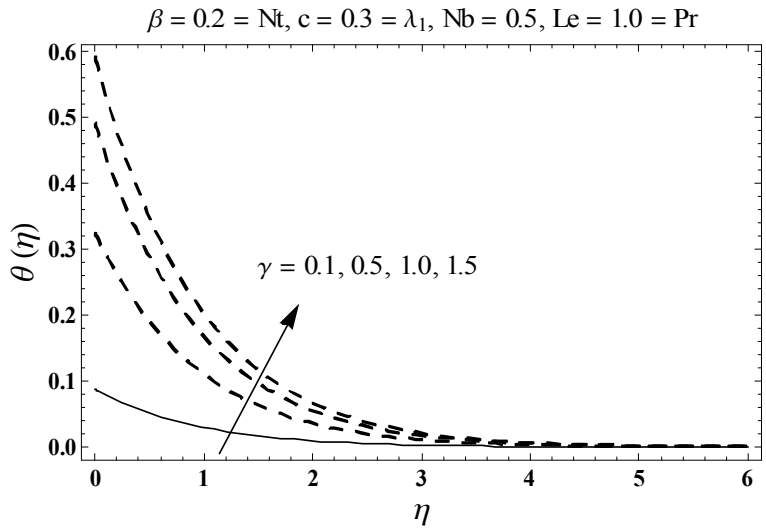

Fig. 11.6. Plots of $\theta(\eta)$ for γ.

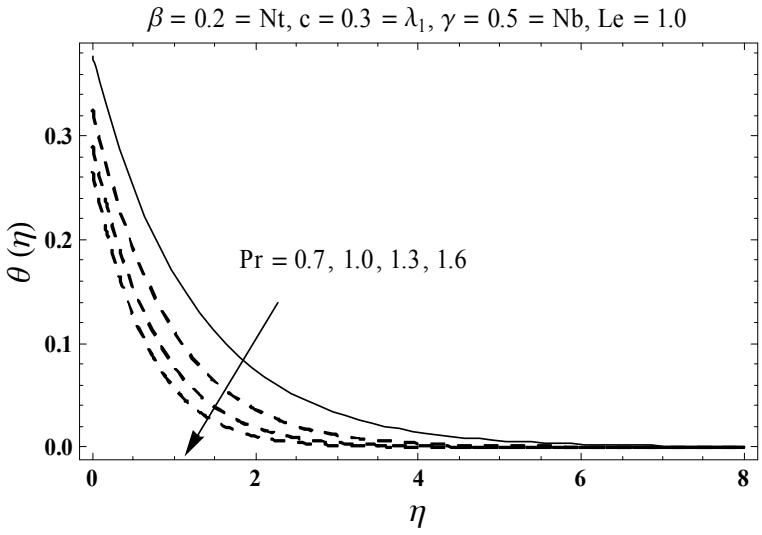

Fig. 11.7. Plots of $\theta(\eta)$ for Pr.

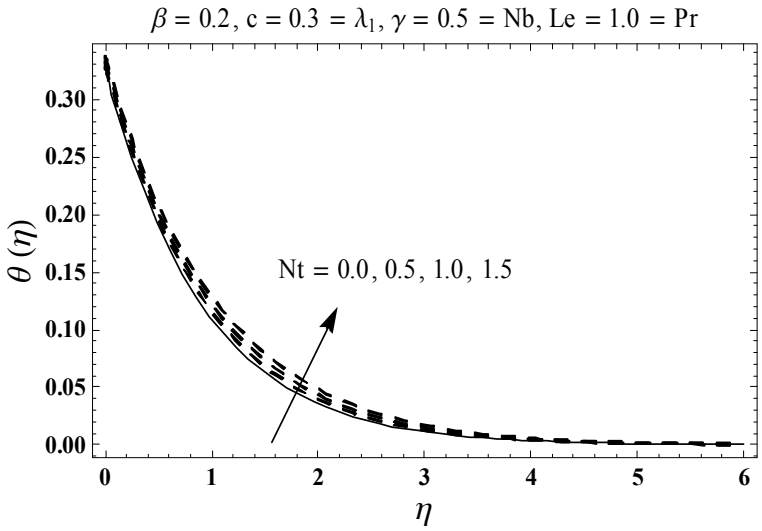

Fig. 11.8. Plots of $\theta(\eta)$ for Nt.

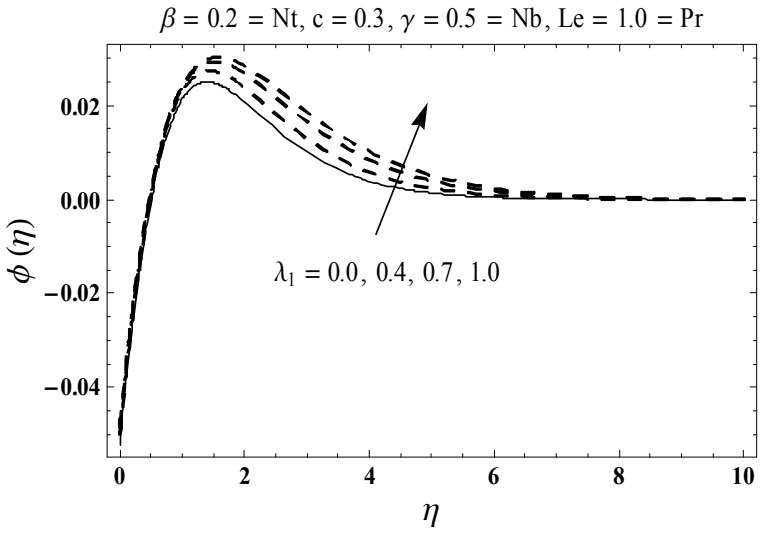

Fig. 11.9. Plots of $\phi(\eta)$ for λ_1.

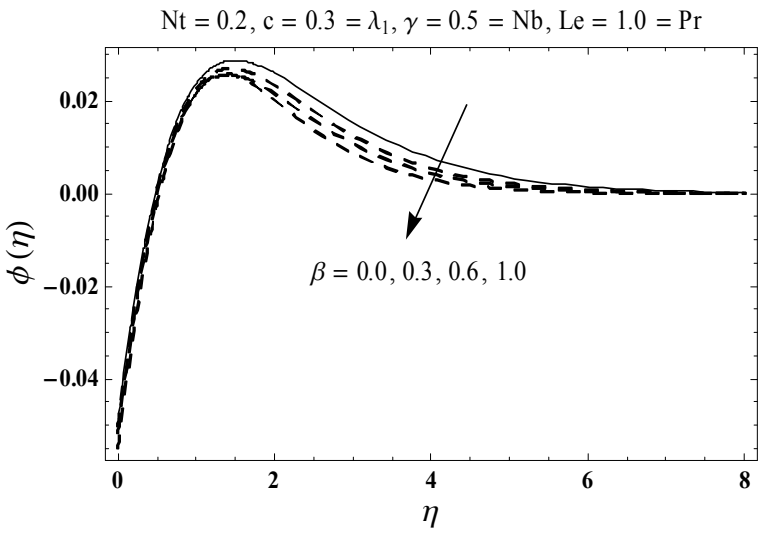

Fig. 11.10. Plots of $\phi(\eta)$ for β.

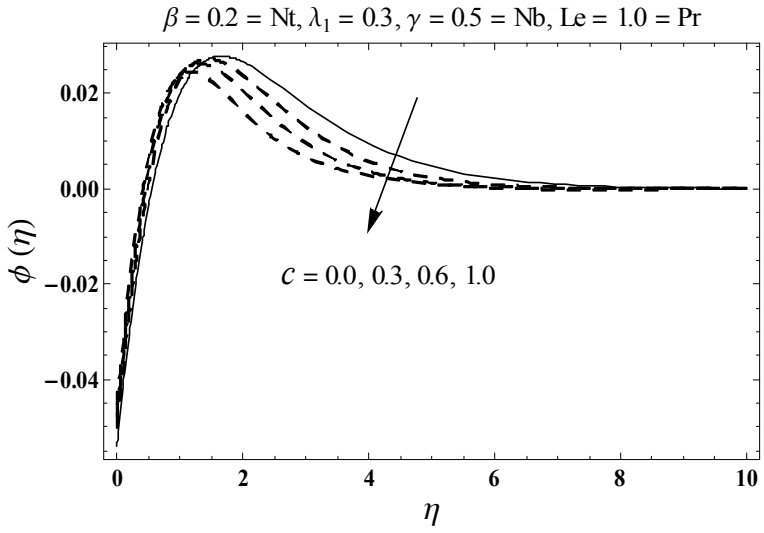

Fig. 11.11. Plots of $\phi(\eta)$ for c.

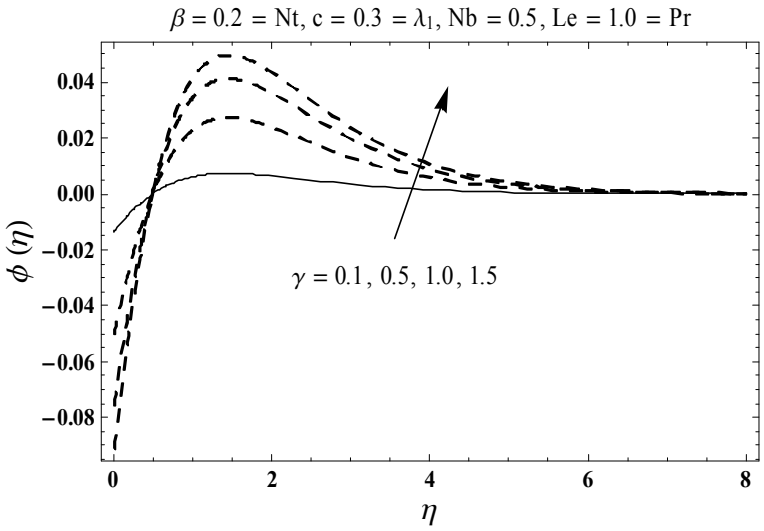

Fig. 11.12. Plots of $\phi(\eta)$ for γ.

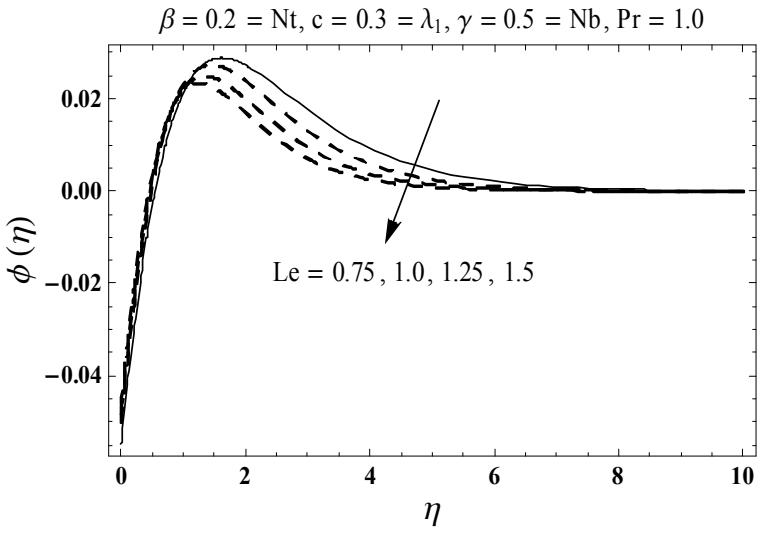

Fig. 11.13. Plots of $\phi(\eta)$ for Le.

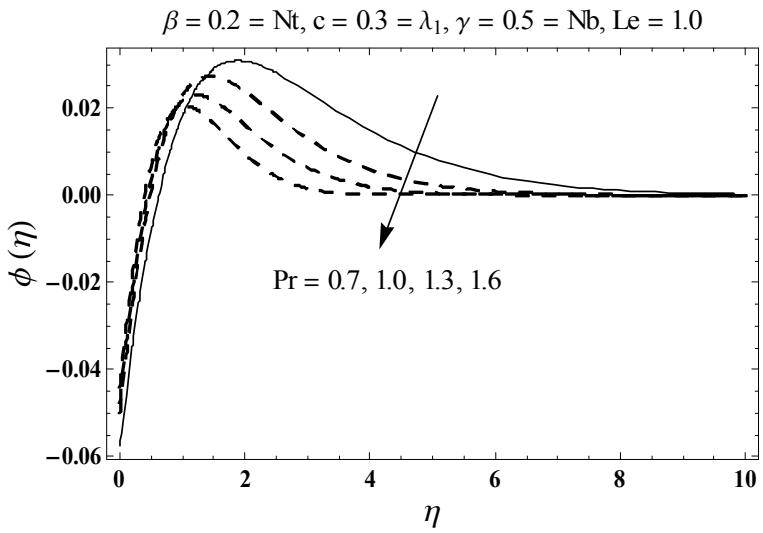

Fig. 11.14. Plots of $\phi(\eta)$ for Pr .

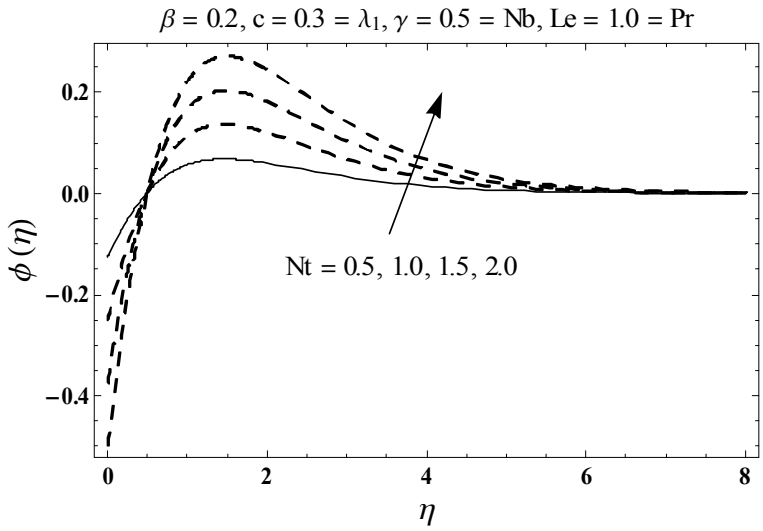

Fig. 11.15. Plots of $\phi(\eta)$ for Nt.

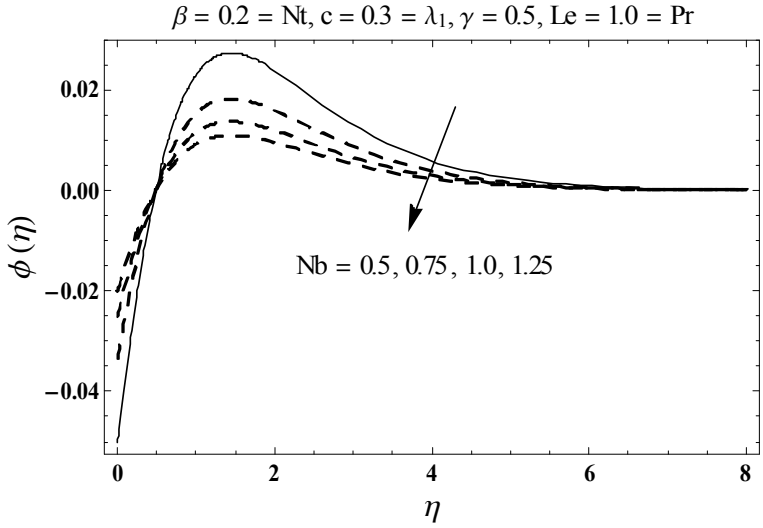

Fig. 11.16. Plots of $\phi(\eta)$ for Nb.

Table 11.2. Comparative estimations of $-f''(0)$ and $-g''(0)$ for various estimations of c when $\beta = \lambda_1 = 0$.

c	$-f''(0)$		$-g''(0)$	
	HAM	Exact [38]	HAM	Exact [38]
0	1	1	0	0
0.25	1.048811	1.048813	0.194564	0.194564
0.50	1.093095	1.093097	0.465205	0.465205
0.75	1.134486	1.134485	0.794618	0.794622
1.0	1.173722	1.173720	1.173722	1.173720

Table 11.3. Numeric data for Nusselt number $\left(-\theta'(0)\right)$ for various estimations of λ_1, β, c, γ, Le, Pr, Nt and Nb.

λ_1	β	c	γ	Le	Pr	Nt	Nb	$-\theta'(0)$
0.0	0.2	0.3	0.5	1.0	1.0	0.2	0.5	0.3416
0.5								0.3356
1.0								0.3302
0.3	0.0	0.3	0.5	1.0	1.0	0.2	0.5	0.3349
	0.3							0.3391
	0.5							0.3411
0.3	0.2	0.0	0.5	1.0	1.0	0.2	0.5	0.3317
		0.5						0.3415
		1.0						0.3493
0.3	0.2	0.3	0.1	1.0	1.0	0.2	0.5	0.0913
			0.7					0.4186
			1.5					0.6138
0.3	0.2	0.3	0.5	0.5	1.0	0.2	0.5	0.3382
				1.0				0.3379
				1.5				0.3378
0.3	0.2	0.3	0.5	1.0	0.5	0.2	0.5	0.2836
					1.0			0.3379
					1.5			0.3642
0.3	0.2	0.3	0.5	1.0	1.0	0.0	0.5	0.3383
						0.5		0.3373
						1.0		0.3362
0.3	0.2	0.3	0.5	1.0	1.0	0.2	0.5	0.3379
							1.0	0.3379
							1.5	0.3379

Chapter 12

On three-dimensional boundary layer flow of Sisko nanofluid with magnetic field effects

This chapter models effects of magnetic field and nanoparticles in three dimensional flow of Sisko liquid. Flow caused is due to a bi-directional extending surface. Effects of Brownian movement and thermophoresis in nanoliquid relation are considered. Sisko liquid is taken electrically conducted via constant applied magnetic field. Mathematical development in boundary layer regime is presented for weak magnetic Reynolds parameter. Newly constructed boundary condition subject to zero nanoparticles mass flux is employed. Nonlinear differential frameworks are solved for convergent arrangements. Effects of several physical variables are studied. Skin frictions and Nusselt number are tabulated and explored. It is watched that effects of Brownian motion and thermophoresis variables on concentration are quite opposite. Further concentration and temperature are elevated for bigger magnetic number.

12.1 Formulation

Consider three dimensional (3D) flow of Sisko nanoliquid by bi-directional extending surface. Sisko liquid is employed electrically conducting. Magnetic field B_0 is taken in $z-$direction. Furthermore the electric field and Hall impacts are disregarded. Brownian movement and

thermophoresis impacts are additionally present. Cartesian coordinate framework is embraced such that $x-$ and $y-$axes are brought the extending surface and $z-$axis is opposite to it. Let U_w and V_w denote surface extending velocities along $x-$ and $y-$directions. The subjected boundary layer expressions for considered flow are expressed as follows:

$$\frac{\partial u}{\partial x}+\frac{\partial v}{\partial y}+\frac{\partial w}{\partial z}=0, \tag{12.1}$$

$$u\frac{\partial u}{\partial x}+v\frac{\partial u}{\partial y}+w\frac{\partial u}{\partial z}=\frac{a}{\rho_f}\frac{\partial^2 u}{\partial z^2}-\frac{b}{\rho_f}\frac{\partial}{\partial z}\left(-\frac{\partial u}{\partial z}\right)^n-\frac{\sigma B_0^2}{\rho_f}u, \tag{12.2}$$

$$u\frac{\partial v}{\partial x}+v\frac{\partial v}{\partial y}+w\frac{\partial v}{\partial z}=\frac{a}{\rho_f}\frac{\partial^2 v}{\partial z^2}+\frac{b}{\rho_f}\frac{\partial}{\partial z}\left(-\frac{\partial u}{\partial z}\right)^{n-1}\frac{\partial v}{\partial z}-\frac{\sigma B_0^2}{\rho_f}v, \tag{12.3}$$

$$u\frac{\partial T}{\partial x}+v\frac{\partial T}{\partial y}+w\frac{\partial T}{\partial z}=\alpha_m\frac{\partial^2 T}{\partial z^2}+\frac{(\rho c)_p}{(\rho c)_f}\left(D_B\left(\frac{\partial T}{\partial z}\frac{\partial C}{\partial z}\right)+\frac{D_T}{T_\infty}\left(\frac{\partial T}{\partial z}\right)^2\right), \tag{12.4}$$

$$u\frac{\partial C}{\partial x}+v\frac{\partial C}{\partial y}+w\frac{\partial C}{\partial z}=D_B\left(\frac{\partial^2 C}{\partial z^2}\right)+\frac{D_T}{T_\infty}\left(\frac{\partial^2 T}{\partial z^2}\right). \tag{12.5}$$

Here one has the following prescribed conditions:

$$u=U_w(x)=cx,\ v=V_w(y)=dy,\ w=0,\ T=T_w,\ D_B\frac{\partial C}{\partial z}+\frac{D_T}{T_\infty}\frac{\partial T}{\partial z}=0 \text{ at } z=0, \tag{12.6}$$

$$u\to 0,\quad v\to 0,\quad T\to T_\infty,\quad C\to C_\infty \quad \text{as } z\to\infty. \tag{12.7}$$

Here u, v and w stand for velocities in $x-$, $y-$ and $z-$directions, k for thermal conductivity, ρ_f for density, $(\rho c)_p$ for effective heat potential of nanoparticles, σ for electrical conductivity, a, b and n $(n\geq 0)$ for material constants, T for temperature, $\alpha_m=k/(\rho c)_f$ for thermal diffusivity, $(\rho c)_f$ for heat potential of the liquid, D_B for Brownian movement, C for concentration, D_T for thermophoretic diffusion, T_w and T_∞ for wall and ambient temperatures, C_∞ for ambient concentration and c and d for positive constants. Selecting

$$\left.\begin{aligned} u=cxf'(\eta),\ v=dyg'(\eta),\ w=-c\left(\tfrac{c^{n-2}}{\rho_f/b}\right)^{1/(n+1)}\left(\tfrac{2n}{n+1}f+\tfrac{1-n}{1+n}\eta f'+g\right)x^{(n-1)/(n+1)},\\ \theta(\eta)=\tfrac{T-T_\infty}{T_w-T_\infty},\ \phi(\eta)=\tfrac{C-C_\infty}{C_\infty},\ \eta=z\left(\tfrac{c^{2-n}}{b/\rho_f}\right)^{1/(n+1)}x^{(1-n)/(1+n)}. \end{aligned}\right\} \tag{12.8}$$

Expression (12.1) is now satisfied and Eqs. $(12.2)-(12.7)$ have the following expressions

$$Af'''-\left(f'\right)^2+gf''+n\left(-f''\right)^{n-1}f'''+\left(\frac{2n}{n+1}\right)ff''-M^2f'=0, \tag{12.9}$$

$$Ag'''-\left(g'\right)^2+gg''+\left(-f''\right)^{n-1}g'''-(n-1)\,g''f'''\left(-f''\right)^{n-2}+\left(\frac{2n}{n+1}\right)fg''-M^2g'=0, \tag{12.10}$$

$$\theta''+\Pr\left(\left(\frac{2n}{n+1}\right)f\theta'+g\theta'+Nt\left(\theta'\right)^2+Nb\theta'\phi'\right)=0, \tag{12.11}$$

$$\phi''+Le\Pr\left(\left(\frac{2n}{n+1}\right)f\phi'+g\phi'\right)+\left(\frac{Nt}{Nb}\right)\theta''=0, \tag{12.12}$$

$$f(0)=g(0)=0,\ f'(0)=1,\ g'(0)=\alpha,\ \theta(0)=1,\ Nb\phi'(0)+Nt\theta'(0)=0, \tag{12.13}$$

$$f'(\infty)\to 0,\ g'(\infty)\to 0,\ \theta(\infty)\to 0,\ \phi(\infty)\to 0. \tag{12.14}$$

Here Pr is for Prandtl parameter, α for ratio number, M for magnetic number, A for material parameter, Nb for Brownian movement number, Le for Lewis parameter and Nt for thermophoresis number. Such variables can be specified by employing the definitions given below:

$$\left.\begin{array}{c} A=\frac{\mathrm{Re}_b^{2/(n+1)}}{\mathrm{Re}_a},\ M^2=\frac{\sigma B_0^2}{\rho_f c},\ \alpha=\frac{d}{c},\ \Pr=\frac{xU_w\,\mathrm{Re}_b^{-2/(n+1)}}{\alpha_m}, \\ Nb=\frac{(\rho c)_p D_B C_\infty}{(\rho c)_f a/\rho_f},\ Nt=\frac{(\rho c)_p D_T(T_w-T_\infty)}{(\rho c)_f T_\infty a/\rho_f},\ Le=\frac{\alpha_m}{D_B}. \end{array}\right\} \tag{12.15}$$

Skin frictions and Nusselt number are given by

$$\left.\begin{array}{c} C_{fx}\,\mathrm{Re}_b^{1/(n+1)}=Af''(0)-\left(-f''(0)\right)^n, \\ C_{fy}\,\mathrm{Re}_b^{1/(n+1)}=\frac{V_w}{U_w}\left(Ag''(0)+\left(-f''(0)\right)^{n-1}g''(0)\right), \\ Nu_x\,\mathrm{Re}_b^{-1/(n+1)}=-\theta'(0), \end{array}\right\} \tag{12.16}$$

It is watched that $\mathrm{Re}_a=\rho_f U_w x/a$ and $\mathrm{Re}_b=\rho_f U_w^{2-n}x^n/b$ denote local Reynolds parameters and Sherwood number Sh_x is now identically zero.

12.2 Solutions by OHAM

The optimal series arrangements of Eqs. $(12.9)-(12.12)$ through (12.13) and (12.14) have been developed by utilizing optimal homotopic analysis technique (OHAM). The linear operators

and initial deformations have been selected as follows:

$$f_0(\eta) = 1 - e^{-\eta}, \quad g_0(\eta) = \alpha(1 - e^{-\eta}), \quad \theta_0(\eta) = e^{-\eta}, \quad \phi_0(\eta) = -\frac{Nt}{Nb}e^{-\eta}, \tag{12.17}$$

$$\mathcal{L}_f = f''' - f', \quad \mathcal{L}_g = g''' - g', \quad \mathcal{L}_\theta = \theta'' - \theta, \quad \mathcal{L}_\phi = \phi'' - \phi. \tag{12.18}$$

The above linear operators obey

$$\left.\begin{array}{c} \mathcal{L}_f\left[F_1^{**} + F_2^{**}e^{\eta} + F_3^{**}e^{-\eta}\right] = 0, \quad \mathcal{L}_g\left[F_4^{**} + F_5^{**}e^{\eta} + F_6^{**}e^{-\eta}\right] = 0, \\ \mathcal{L}_\theta\left[F_7^{**}e^{\eta} + F_8^{**}e^{-\eta}\right] = 0, \quad \mathcal{L}_\phi\left[F_9^{**}e^{\eta} + F_{10}^{**}e^{-\eta}\right] = 0, \end{array}\right\} \tag{12.19}$$

in which F_j^{**} $(j = 1 - 10)$ stand for arbitrary constants. Problems for zeroth and mth-order deformations are easily formulated in the view of above operators. The deformation issues are solved by BVPh2.0 of Mathematica software.

12.3 Convergence analysis

We have solved the momentum, energy and concentration expressions with the help of BVPh2.0. These expressions contain unknown variables $\hbar_f$, $\hbar_g$, $\hbar_\theta$ and $\hbar_\phi$. We can compute the minimum estimation of these variables by taking total error small. In the frame of HAM, these variables play a vital role. That is why these variables refer to as convergence-control parameter which differs HAM from other analytical approximation methods. In order to reduce the CPU time, we have employed average residual errors at the mth-oder of approximation which are defined by

$$\varepsilon_m^f = \frac{1}{k+1}\sum_{j=0}^{k}\left[\mathcal{N}_f\left(\sum_{i=0}^{m}\hat{f}(\eta),\ \sum_{i=0}^{m}\hat{g}(\eta)\right)_{\eta=j\delta\eta}\right]^2, \tag{12.20}$$

$$\varepsilon_m^g = \frac{1}{k+1}\sum_{j=0}^{k}\left[\mathcal{N}_g\left(\sum_{i=0}^{m}\hat{f}(\eta),\ \sum_{i=0}^{m}\hat{g}(\eta)\right)_{\eta=j\delta\eta}\right]^2, \tag{12.21}$$

$$\varepsilon_m^\theta = \frac{1}{k+1}\sum_{j=0}^{k}\left[\mathcal{N}_\theta\left(\sum_{i=0}^{m}\hat{f}(\eta),\ \sum_{i=0}^{m}\hat{g}(\eta),\ \sum_{i=0}^{m}\hat{\theta}(\eta),\ \sum_{i=0}^{m}\hat{\phi}(\eta),\right)_{\eta=j\delta\eta}\right]^2, \tag{12.22}$$

$$\varepsilon_m^{\phi} = \frac{1}{k+1}\sum_{j=0}^{k}\left[\mathcal{N}_{\phi}\left(\sum_{i=0}^{m}\hat{f}(\eta),\ \sum_{i=0}^{m}\hat{g}(\eta),\ \sum_{i=0}^{m}\hat{\theta}(\eta),\ \sum_{i=0}^{m}\hat{\phi}(\eta),\right)_{\eta=j\delta\eta}\right]^2. \tag{12.23}$$

Here $\mathcal{N}_f, \mathcal{N}_g, \mathcal{N}_\theta$ and $\mathcal{N}_\phi$ denote the non-linear operators corresponding to Eqs. $(12.9)-(12.12)$ respectively. Following Liao [69] :

$$\varepsilon_m^t = \varepsilon_m^f + \varepsilon_m^g + \varepsilon_m^\theta + \varepsilon_m^\phi, \tag{12.24}$$

where ε_m^t stands for total residual square error, $k = 20$ and $\delta\eta = 0.5$. Optimal data for auxiliary variables at 4th order of deformations is $\hbar_f = -0.575281$, $\hbar_g = -0.806452$, $\hbar_\theta = -0.873621$ and $\hbar_\phi = -1.16577$ and $\varepsilon_m^t = 2.81 \times 10^{-4}$. Table 12.1 presents average square residual error at different order of deformations. It has been analyzed that the average residual square errors reduce with higher order deformations.

Table 12.1. Individual average residual square errors employing optimal data of auxiliary variables.

m	ε_m^f	ε_m^g	ε_m^θ	ε_m^ϕ
2	1.11×10^{-3}	2.14×10^{-5}	4.69×10^{-5}	7.61×10^{-5}
6	8.38×10^{-5}	1.13×10^{-6}	1.34×10^{-5}	6.65×10^{-6}
10	3.36×10^{-5}	3.87×10^{-7}	7.72×10^{-7}	3.12×10^{-7}
16	1.76×10^{-5}	1.11×10^{-7}	4.65×10^{-9}	3.46×10^{-9}
20	1.22×10^{-5}	5.90×10^{-8}	6.63×10^{-9}	2.37×10^{-9}
26	7.59×10^{-6}	2.64×10^{-8}	3.98×10^{-10}	5.39×10^{-10}
30	5.68×10^{-6}	1.64×10^{-8}	6.12×10^{-10}	3.53×10^{-10}

12.4 Discussion

Effects of various physical variables like thermophoresis number Nt, Prandtl parameter Pr, Sisko liquid parameter A, Brownian movement number Nb, magnetic number M, ratio number α and Lewis parameter Le on temperature θ and concentration ϕ are displayed in Figs. $12.1 - 12.12$. Impact of Sisko liquid parameter A on temperature $\theta(\eta)$ is plotted in Fig. 12.1. Here temperature $\theta(\eta)$ and layer of thermal are diminishment when Sisko liquid parameter upgrades. Fig. 12.2 presents that bigger magnetic number M compares to elevated temperature

and more layer of thermal. Here $M = 0$ prompts hydro-dynamic flow and $M \neq 0$ for hydro-magnetic flow situation. It is watched that temperature is higher for hydro-magnetic flow when contrasted with hydro-dynamic flow circumstance. Fig. 12.3 exhibits effect of ratio number α on temperature $\theta(\eta)$. Temperature and layer thickness are diminishing elements of ratio number. For $\alpha = 0$ the two dimensional flow circumstance is accomplished. Here we watched that temperature is more grounded for two dimension flow in contrast with three dimension flow. Fig. 12.4 presents variations in temperature $\theta(\eta)$ for different estimations of Prandtl parameter $\Pr$. Here temperature and layer of thermal are less for bigger Prandtl parameter. Prandtl parameter has a reverse association with thermal diffusivity. An expansion in Prandtl parameter prompts poor thermal diffusivity. Such poor thermal diffusivity causes a lessening in temperature and layer of thermal. Variations in temperature $\theta(\eta)$ relating to various estimations of thermophoresis number Nt is appeared in Fig. 12.5. Here an upgrade in thermophoresis number offers ascend to temperature and associated layer thickness. An expansion in thermophoresis number Nt causes an upgrade in thermophoresis constrain which exhibits a more grounded temperature and more layer of thermal. Fig. 12.6 exhibits variations in concentration $\phi(\eta)$ for various estimations of Sisko liquid parameter A. It is watched that an expansion in Sisko liquid parameter exhibits a diminishment in concentration profile $\phi(\eta)$. Fig. 12.7 presents that bigger magnetic number M creates an improvement in concentration and associated layer. Effect of ratio number α on concentration ϕ is displayed in Fig. 12.8. Here concentration ϕ and layer of concentration are diminishing elements of ratio number. Fig. 12.9 exhibits effect of Lewis parameter Le on concentration $\phi(\eta)$. This Fig. clearly exhibits that bigger Lewis parameter Le causes a diminishment in concentration $\phi(\eta)$. Lewis parameter involves Brownian movement. An expansion in Lewis parameter prompts poor Brownian movement which exhibits a decrease in concentration and layer of concentration. Fig. 12.10 presents that bigger Prandtl parameter Pr relates to poor concentration ϕ and less layer of concentration. Fig. 12.11 portrays impact of Brownian movement number Nb on concentration ϕ. Here an upgrade in Brownian movement number prompt poor concentration and associated layer of concentration. Fig. 12.12 exhibits effect of thermophoresis number Nt on concentration ϕ. Here concentration is improved when thermophoresis number increments. Table 12.2 exhibits comparison for different estimations of α with exact arrangement. Table 12.2 presents an excellent agreement of OHAM arrangement

with existing exact arrangement in limiting situation. Table 12.3 presents numeric data of skin frictions $-C_{fx}\,\mathrm{Re}_b^{1/(n+1)}$ and $-C_{fy}\,\mathrm{Re}_b^{1/(n+1)}$ for various estimations of M, A and α. It is clearly watched that skin frictions are higher for bigger magnetic number M, Sisko liquid parameter A and ratio number α. Table 12.4 is processed to investigate Nusselt number $-\theta'(0)$ for various estimations of α, Le, Pr, A, Nb, M and Nt. Here it is watched that impacts of Lewis and Prandtl parameters on Nusselt number are very inverse. Nusselt number is found constant when we increment Brownian movement number.

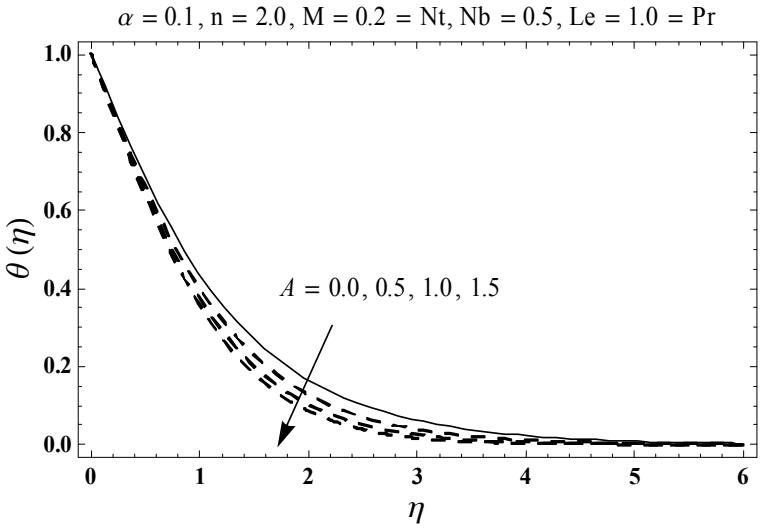

Fig. 12.1. Plots of $\theta(\eta)$ for A.

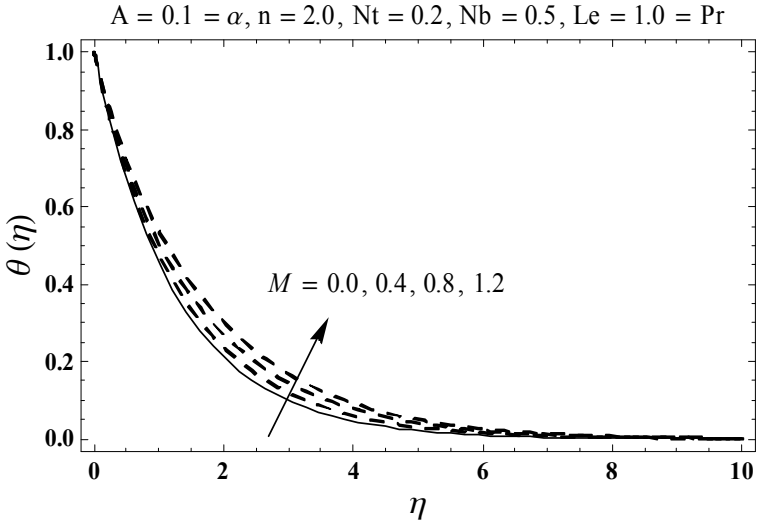

Fig. 12.2. Plots of $\theta(\eta)$ for M.

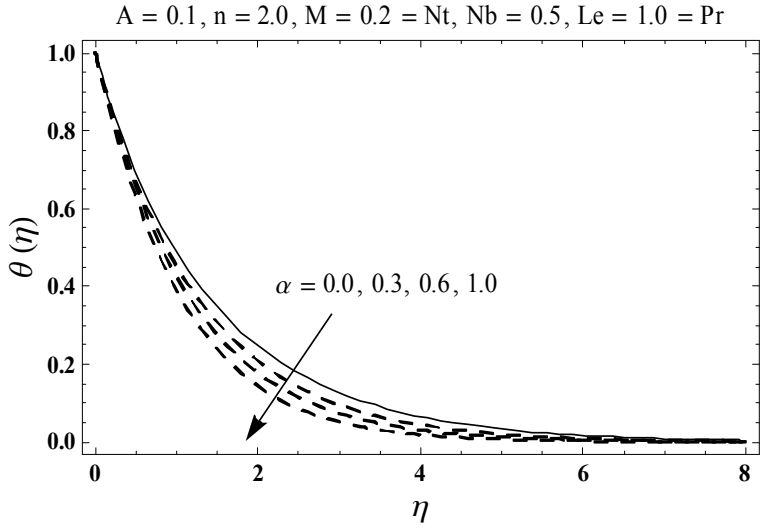

Fig. 12.3. Plots of $\theta(\eta)$ for α.

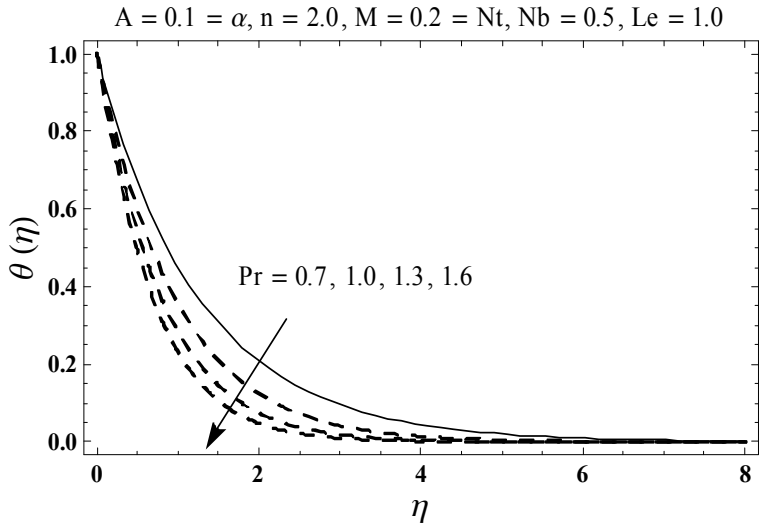

Fig. 12.4. Plots of $\theta(\eta)$ for Pr.

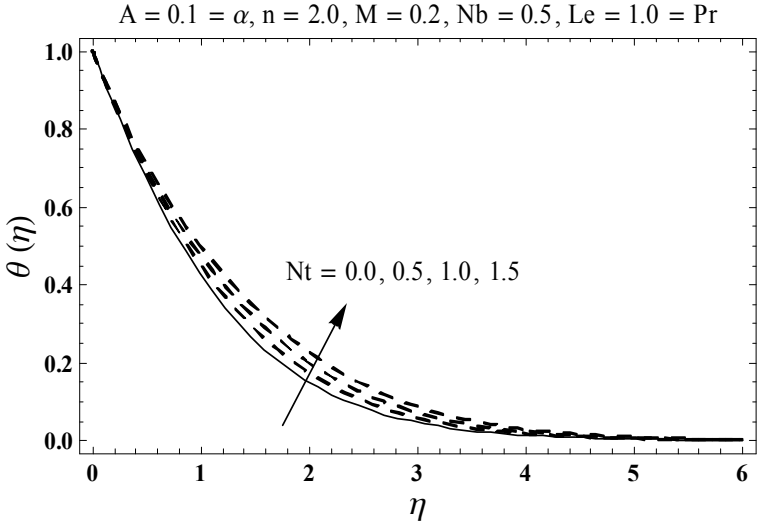

Fig. 12.5. Plots of $\theta(\eta)$ for Nt.

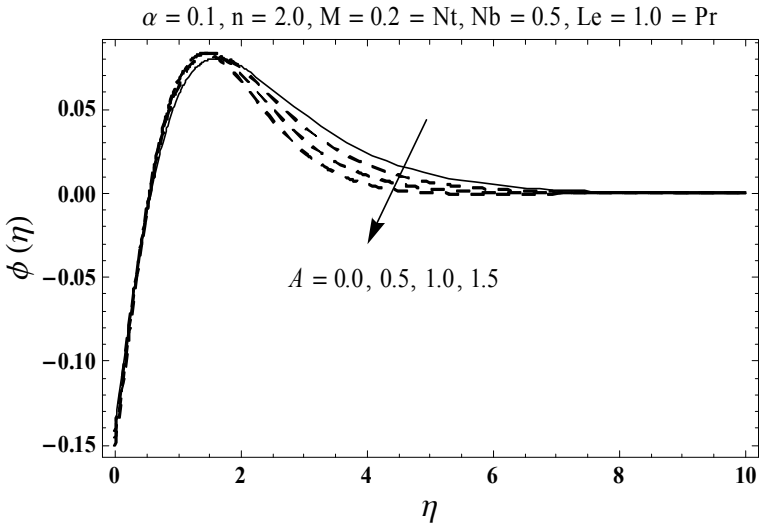

Fig. 12.6. Plots of $\phi(\eta)$ for A.

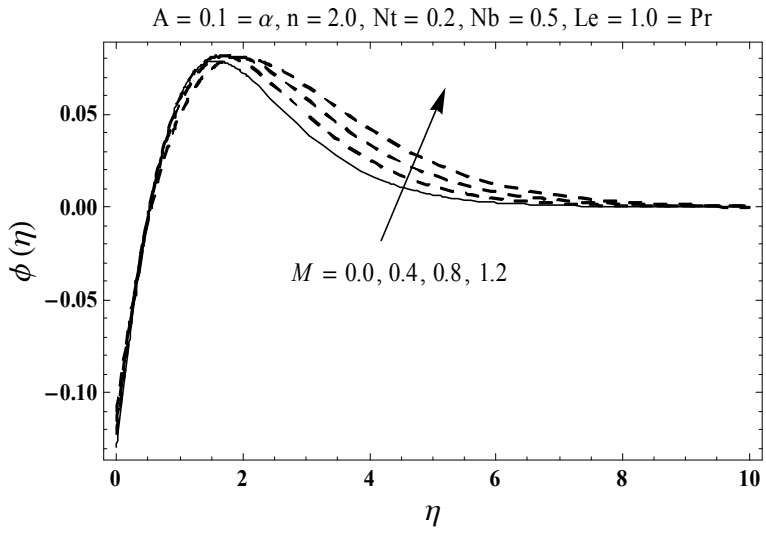

Fig. 12.7. Plots of $\phi(\eta)$ for M.

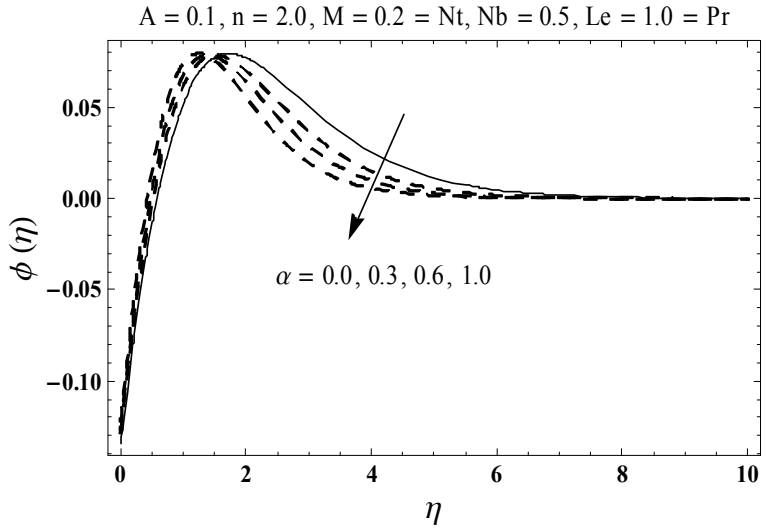

Fig. 12.8. Plots of $\phi(\eta)$ for α.

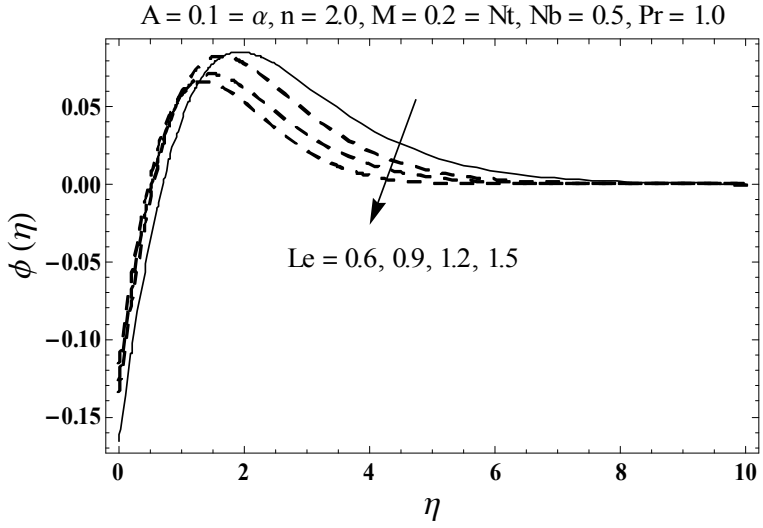

Fig. 12.9. Plots of $\phi(\eta)$ for Le.

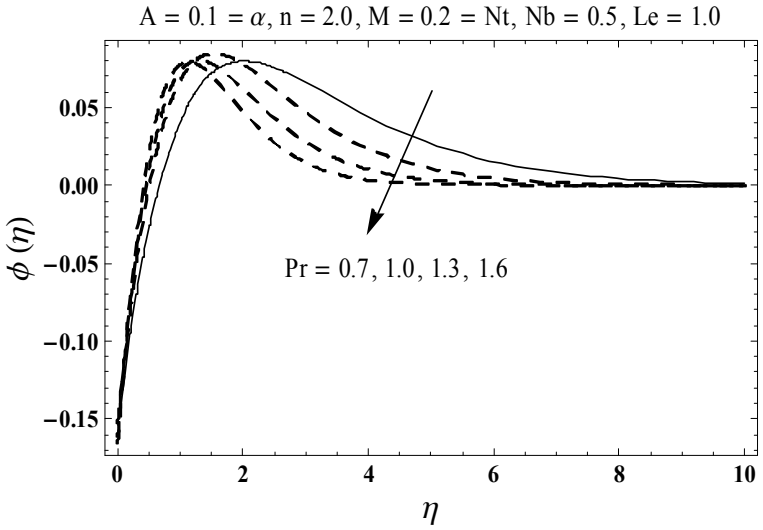

Fig. 12.10. Plots of $\phi(\eta)$ for Pr .

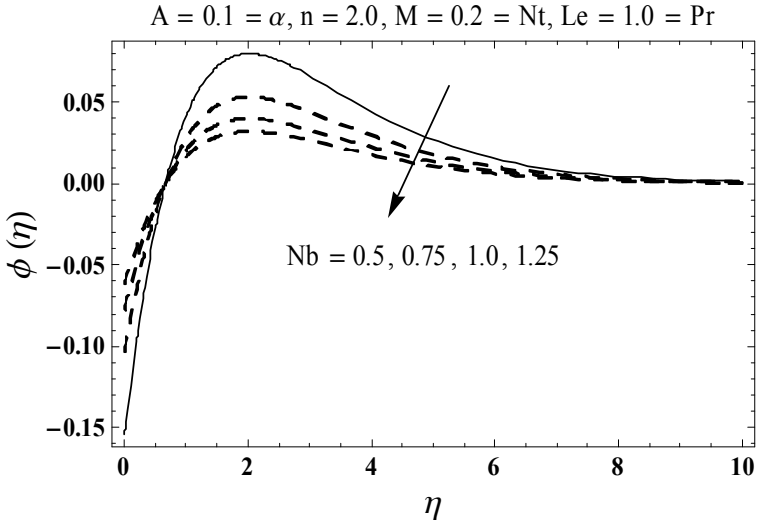

Fig. 12.11. Plots of $\phi(\eta)$ for Nb.

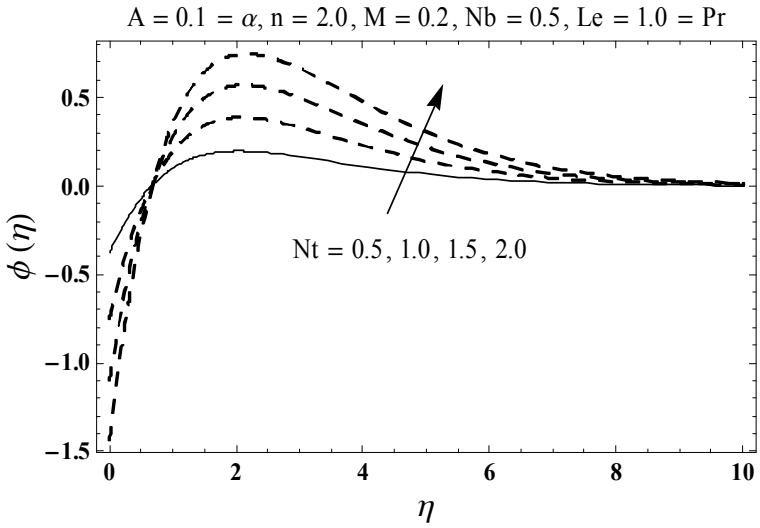

Fig. 12.12. Plots of $\phi(\eta)$ for Nt.

Table 12.2. Comparative estimations of $-f''(0)$ and $-g''(0)$ for various estimations of α when $n = 1$ and $A = M = 0$.

α	$-f''(0)$		$-g''(0)$	
	OHAM	Exact [38]	OHAM	Exact [38]
0	1	1	0	0
0.25	1.048811	1.048813	0.194564	0.194564
0.50	1.093095	1.093097	0.465205	0.465205
0.75	1.134486	1.134485	0.794618	0.794622
1.0	1.173722	1.173720	1.173722	1.173720

Table 12.3. Numeric data of skin frictions $-C_{fx}\,\mathrm{Re}_b^{1/(n+1)}$ and $-C_{fy}\,\mathrm{Re}_b^{1/(n+1)}$ for different estimations of A, M and α.

A	M	α	$-C_{fx}\,\mathrm{Re}_b^{1/(n+1)}$		$-C_{fy}\,\mathrm{Re}_b^{1/(n+1)}$	
			$n = 1.0$	$n = 2.0$	$n = 1.0$	$n = 2.0$
0.0	0.2	0.1	1.0394	1.0050	0.0698	0.0703
0.5			1.2730	1.2076	0.0855	0.0850
1.0			1.4700	1.4714	0.0986	0.1060
0.1	0.0	0.1	1.0700	1.0264	0.0702	0.0709
	0.5		1.1907	1.1483	0.0873	0.0854
	1.0		1.4967	1.4824	0.1257	0.1233
0.1	0.2	0.0	1.0696	1.0210	0.0000	0.0000
		0.5	1.1650	1.1415	0.4987	0.4935
		1.0	1.2482	1.2497	1.2482	1.2497

Table 12.4. Numeric data of Nusselt number for different estimations of Pr, α, A, Nb, Le, M and Nt.

A	M	α	Le	Pr	Nb	Nt	$-\theta'(0)$	
							$n = 1.0$	$n = 2.0$
0.0	0.2	0.1	1.0	1.0	0.5	0.2	0.5980	0.6577
0.5							0.6388	0.7142
1.0							0.6638	0.7481
0.1	0.0	0.1	1.0	1.0	0.5	0.2	0.6120	0.6741
	0.5						0.5888	0.6595
	1.0						0.5335	0.6235
0.1	0.2	0.0	1.0	1.0	0.5	0.2	0.5727	0.6401
		0.5					0.7244	0.7806
		1.0					0.8402	0.8949
0.1	0.2	0.1	0.5	1.0	0.5	0.2	0.6160	0.6795
			1.0				0.6082	0.6716
			1.5				0.6040	0.6668
0.1	0.2	0.1	1.0	0.5	0.5	0.2	0.3812	0.4056
				1.0			0.6081	0.6716
				1.5			0.7829	0.8796
0.1	0.2	0.1	1.0	1.0	0.5	0.2	0.6081	0.6715
					1.0		0.6081	0.6715
					1.5		0.6081	0.6715
0.1	0.2	0.1	1.0	1.0	0.5	0.0	0.6241	0.6907
						0.5	0.5845	0.6430
						1.0	0.5456	0.5970

Chapter 13

Impact of magnetic field in three-dimensional flow of Sisko nanofluid with convective condition

This chapter addresses magnetohydrodynamic (MHD) three dimension flow of Sisko nanoliquid with convectively heated extending surface. Nanoliquid relation includes Brownian movement and thermophoresis impacts. Heat transfer via convective process is discussed. Developed constraint with zero nanoparticles flux at boundary is employed. The subjected problems with boundary layer approach are computed for convergent homotopic series arrangements. Effects of interesting flow variables on concentration and temperature are studied. Skin frictions and Nusselt number are computed and explored.

13.1 Formulation

Magnetohydrodynamic (MHD) three dimension (3D) flow of Sisko nanoliquid by bidirectional extending surface is examined. Sisko liquid is taken electrically conducting through a constant B_0 applied in $z-$direction. Moreover electric field and Hall impacts are disregarded. Mass and heat transfer are investigated via Brownian movement and thermophoresis. We employ Cartesian coordinate framework such that surface agrees with $xy-$plane and liquid possesses space $z \geq 0$. Let $U_w(x) = cx$ and $V_w(y) = dy$ depict surface extending velocities in $x-$

and $y-$directions. Temperature at extending surface is administered by convective heating procedure which is portrayed by coefficient of heat transfer h_f and hot liquid temperature T_f below extending surface. Subjected boundary-layer expressions for considered flow are

$$\frac{\partial u}{\partial x}+\frac{\partial v}{\partial y}+\frac{\partial w}{\partial z}=0, \tag{13.1}$$

$$u\frac{\partial u}{\partial x}+v\frac{\partial u}{\partial y}+w\frac{\partial u}{\partial z}=\frac{a}{\rho_f}\frac{\partial^2 u}{\partial z^2}-\frac{b}{\rho_f}\frac{\partial}{\partial z}\left(-\frac{\partial u}{\partial z}\right)^n-\frac{\sigma B_0^2}{\rho_f}u, \tag{13.2}$$

$$u\frac{\partial v}{\partial x}+v\frac{\partial v}{\partial y}+w\frac{\partial v}{\partial z}=\frac{a}{\rho_f}\frac{\partial^2 v}{\partial z^2}+\frac{b}{\rho_f}\frac{\partial}{\partial z}\left(-\frac{\partial u}{\partial z}\right)^{n-1}\frac{\partial v}{\partial z}-\frac{\sigma B_0^2}{\rho_f}v, \tag{13.3}$$

$$u\frac{\partial T}{\partial x}+v\frac{\partial T}{\partial y}+w\frac{\partial T}{\partial z}=\alpha_m\frac{\partial^2 T}{\partial z^2}+\frac{(\rho c)_p}{(\rho c)_f}\left(D_B\left(\frac{\partial T}{\partial z}\frac{\partial C}{\partial z}\right)+\frac{D_T}{T_\infty}\left(\frac{\partial T}{\partial z}\right)^2\right), \tag{13.4}$$

$$u\frac{\partial C}{\partial x}+v\frac{\partial C}{\partial y}+w\frac{\partial C}{\partial z}=D_B\left(\frac{\partial^2 C}{\partial z^2}\right)+\frac{D_T}{T_\infty}\left(\frac{\partial^2 T}{\partial z^2}\right). \tag{13.5}$$

Here one has the following prescribed conditions:

$$u=U_w(x),\ v=V_w(y),\ w=0,\ -k\frac{\partial T}{\partial z}=h_f(T_f-T),\ D_B\frac{\partial C}{\partial z}+\frac{D_T}{T_\infty}\frac{\partial T}{\partial z}=0 \text{ at } z=0, \tag{13.6}$$

$$u\to 0,\quad v\to 0,\quad T\to T_\infty,\quad C\to C_\infty \quad \text{as } z\to\infty. \tag{13.7}$$

Here u, v and w stand for velocities in $x-$, $y-$ and $z-$directions, k for thermal conductivity, $(\rho c)_p$ for effective heat potential of nanoparticles, σ for electrical conductivity, D_B for Brownian movement, ρ_f for density, a, b and n $(n\geq 0)$ for material constants, T for temperature, $(\rho c)_f$ for heat potential of liquid, $\alpha_m=k/(\rho c)_f$ for thermal diffusivity, C for concentration, D_T for thermophoretic diffusion, T_∞ for ambient temperature, C_∞ for ambient concentration and c and d for positive constants. Selecting

$$\left.\begin{aligned} u=cxf'(\eta),\ v=dyg'(\eta),\ w=-c\left(\tfrac{c^{n-2}}{\rho_f/b}\right)^{1/(n+1)}\left(\tfrac{2n}{n+1}f+\tfrac{1-n}{1+n}\eta f'+g\right)x^{(n-1)/(n+1)},\\ \theta(\eta)=\tfrac{T-T_\infty}{T_f-T_\infty},\ \phi(\eta)=\tfrac{C-C_\infty}{C_\infty},\ \eta=z\left(\tfrac{c^{2-n}}{b/\rho_f}\right)^{1/(n+1)}x^{(1-n)/(1+n)}. \end{aligned}\right\} \tag{13.8}$$

Expression (13.1) is now satisfied and Eqs. $(13.2)-(13.7)$ have the following forms:

$$Af'''-\left(f'\right)^2+gf''+n\left(-f''\right)^{n-1}f'''+\left(\frac{2n}{n+1}\right)ff''-M^2f'=0, \tag{13.9}$$

$$Ag'''-\left(g'\right)^2+gg''+\left(-f''\right)^{n-1}g'''-(n-1)\,g''f'''\left(-f''\right)^{n-2}+\left(\frac{2n}{n+1}\right)fg''-M^2g'=0, \tag{13.10}$$

$$\theta''+\Pr\left(\left(\frac{2n}{n+1}\right)f\theta'+g\theta'+Nt\left(\theta'\right)^2+Nb\theta'\phi'\right)=0, \tag{13.11}$$

$$\phi''+Le\Pr\left(\left(\frac{2n}{n+1}\right)f\phi'+g\phi'\right)+\left(\frac{Nt}{Nb}\right)\theta''=0, \tag{13.12}$$

$$f(0)=g(0)=0,\ f'(0)=1,\ g'(0)=\alpha,\ \theta'=-\gamma\left(1-\theta(0)\right),\ Nb\phi'(0)+Nt\theta'(0)=0, \tag{13.13}$$

$$f'(\infty)\to 0,\ g'(\infty)\to 0,\ \theta(\infty)\to 0,\ \phi(\infty)\to 0. \tag{13.14}$$

Here Pr stands for Prandtl parameter, γ for Biot parameter, A for material parameter, Nb for Brownian movement number, M for magnetic number, Le for Lewis parameter, Nt for thermophoresis number and α for ratio number. These variables can be specified by employing the definitions given below:

$$\left.\begin{array}{c} A=\frac{\mathrm{Re}_b^{2/(n+1)}}{\mathrm{Re}_a},\ \alpha=\frac{d}{c},\ M^2=\frac{\sigma B_0^2}{\rho_f c},\ \Pr=\frac{xU_w\,\mathrm{Re}_b^{-2/(n+1)}}{\alpha_m}, \\ Nb=\frac{(\rho c)_p D_B C_\infty}{(\rho c)_f a/\rho_f},\ Nt=\frac{(\rho c)_p D_T\left(T_f-T_\infty\right)}{(\rho c)_f T_\infty a/\rho_f},\ \gamma=\frac{h_f}{k}x\,\mathrm{Re}_b^{-1/(n+1)},\ Le=\frac{\alpha_m}{D_B}. \end{array}\right\} \tag{13.15}$$

Skin frictions and Nusselt number are

$$\left.\begin{array}{c} C_{fx}\,\mathrm{Re}_b^{1/(n+1)}=Af''(0)-\left(-f''(0)\right)^n, \\ C_{fy}\,\mathrm{Re}_b^{1/(n+1)}=\frac{V_w}{U_w}\left(Ag''(0)+\left(-f''(0)\right)^{n-1}g''(0)\right), \\ Nu_x\,\mathrm{Re}_b^{-1/(n+1)}=-\theta'(0), \end{array}\right\} \tag{13.16}$$

It is watched that $\mathrm{Re}_a=\rho_f U_w x/a$ and $\mathrm{Re}_b=\rho_f U_w^{2-n}x^n/b$ show local Reynolds parameters and Sherwood number Sh_x is now identically zero.

13.2 Solutions by HAM

The series arrangements of Eqs. (13.9) – (13.12) through (13.13) and (13.14) have been developed by utilizing homotopy analysis technique (HAM). The linear operators and initial deformations have been selected as follows:

$$f_0(\eta) = 1 - e^{-\eta}, \quad g_0(\eta) = \alpha(1 - e^{-\eta}), \quad \theta_0(\eta) = \frac{\gamma}{1+\gamma} e^{-\eta}, \quad \phi_0(\eta) = -\frac{\gamma}{1+\gamma} \frac{Nt}{Nb} e^{-\eta}, \tag{13.17}$$

$$\mathcal{L}_f = f''' - f', \quad \mathcal{L}_g = g''' - g', \quad \mathcal{L}_\theta = \theta'' - \theta, \quad \mathcal{L}_\phi = \phi'' - \phi. \tag{13.18}$$

The above linear operators obey

$$\left.\begin{array}{c} \mathcal{L}_f \left[F_1^{**} + F_2^{**} e^{\eta} + F_3^{**} e^{-\eta}\right] = 0, \quad \mathcal{L}_g \left[F_4^{**} + F_5^{**} e^{\eta} + F_6^{**} e^{-\eta}\right] = 0, \\ \mathcal{L}_\theta \left[F_7^{**} e^{\eta} + F_8^{**} e^{-\eta}\right] = 0, \quad \mathcal{L}_\phi \left[F_9^{**} e^{\eta} + F_{10}^{**} e^{-\eta}\right] = 0, \end{array}\right\} \tag{13.19}$$

in which F_j^{**} $(j = 1 - 10)$ stand for arbitrary constants. Problems for zeroth and mth-order deformations are easily formulated in the view of above operators. The deformation issues are computed by Mathematica software.

13.3 Convergence analysis

Most likely series arrangements are subject to non-zero auxiliary variables $\hbar_f$, $\hbar_g$, $\hbar_\theta$ and $\hbar_\phi$. Reasonable estimations of these variables are imperative to get convergent series arrangements. The $\hbar-$curves for velocities, concentration and temperature are outlined at 20th order of deformations. Figs. 13.1 and 13.2 clearly portray that zones of convergence for f, g, θ and ϕ are $[-0.71, \ -0.22]$, $[-0.76, \ -0.11]$, $[-0.91, \ -0.24]$ and $[-0.91, \ -0.11]$. Table 13.1 exhibits that 12th order of deformations is essential for convergent homotopic series arrangements of f,

g, θ and ϕ.

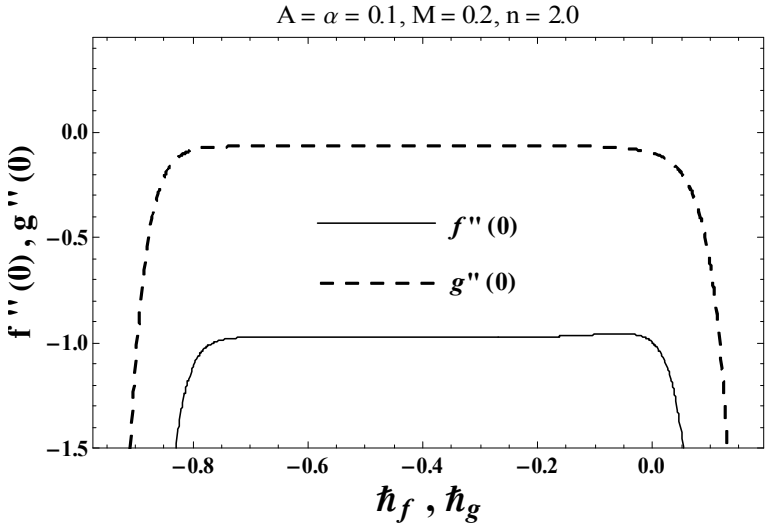

Fig. 13.1. The $\hbar-$plots for $f(\eta)$ and $g(\eta)$.

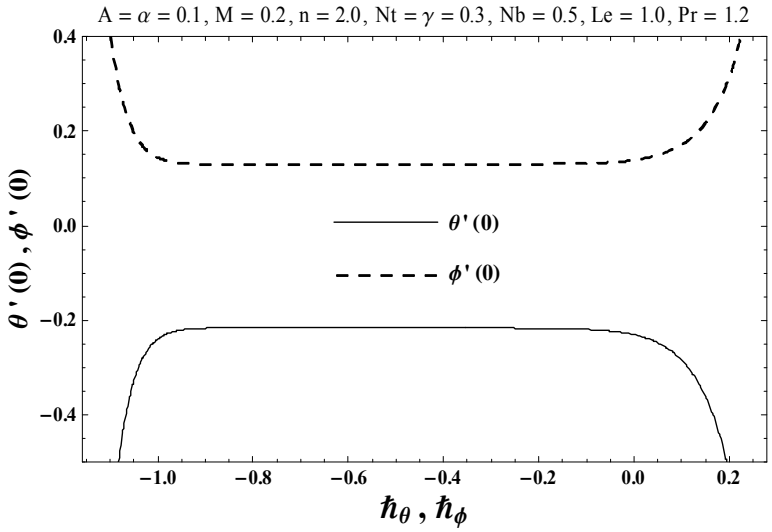

Fig. 13.2. The $\hbar-$plots for $\theta(\eta)$ and $\phi(\eta)$.

Table 13.1. HAM arrangements convergence when $A = \alpha = 0.1,\ Nt = \gamma = 0.3,\ M = 0.2,\ Nb = 0.5,\ n = 2.0,\ \Pr = 1.2$ and $Le = 1.0$.

Order of deformations	$-f''(0)$	$-g''(0)$	$-\theta'(0)$	$\phi'(0)$
1	0.9379	0.0787	0.2250	0.1352
5	0.9675	0.0670	0.2183	0.1308
13	0.9747	0.0685	0.2164	0.1297
20	0.9747	0.0685	0.2164	0.1297
35	0.9747	0.0685	0.2164	0.1297
50	0.9747	0.0685	0.2164	0.1297

13.4 Discussion

Effects of several physical variables like Prandtl parameter Pr, ratio number α, Lewis parameter Le, Sisko liquid parameter A, thermophoresis number Nt, Biot parameter γ, Brownian movement number Nb and magnetic number M on temperature θ and concentration ϕ are displayed in Figs. $13.3 - 13.16$. Fig. 13.3 presents effect of Sisko liquid parameter A on temperature θ. It is watched that an expansion in Sisko liquid parameter A makes a diminishment in temperature and associated thickness of layer. Fig. 13.4 delineates varieties in temperature θ for various estimations of M. Here temperature θ and layer of thermal are expanding elements of magnetic number. Here $M = 0$ compares to hydro-dynamic flow situation and $M \neq 0$ for hydro-magnetic flow. It is additionally watched that temperature is more grounded for hydro-magnetic flow when contrasted with hydro-dynamic flow. Fig. 13.5 delineates that bigger ratio number α prompts bring down temperature θ and less layer of thermal. Two dimension (2D) flow circumstance is recouped when ratio number $\alpha = 0$. Fig. 13.6 exhibits impact of Biot parameter γ on temperature θ. Here bigger Biot parameter γ causes a elevated temperature and more layer of thermal. Physically an upgrade in γ makes a more grounded convection which prompts elevated temperature. Fig. 13.7 presents that an expansion in Prandtl parameter Pr gives decrease in temperature θ. Prandtl parameter includes thermal diffusivity. Bigger Prandtl parameter prompts bring down thermal diffusivity. Such poor thermal diffusivity causes a poor temperature and less layer of thermal. Fig. 13.8 exhibits impact of thermophoresis number

Nt on temperature θ. Here temperature θ and subjected thickness of layer are upgraded when we increment thermophoresis number. Bigger thermophoresis number prompts more grounded thermophoresis constrain which exhibits an improvement in temperature. Fig. 13.9 presents effect of Sisko liquid parameter A on concentration ϕ. Concentration ϕ and associated layer thickness are diminishment when we upgrade Sisko liquid parameter. Fig. 13.10 delineates that bigger magnetic number M exhibits upgrade in concentration ϕ. Effect of ratio number α on concentration ϕ is shown in Fig. 13.11. Here we watched that bigger ratio number compares to bring down concentration and less layer of concentration. Fig. 13.12 delineates impact of Biot parameter γ on concentration ϕ. Concentration and associated layer thickness are expanding elements of Biot parameter. Fig. 13.13 delineates that bigger Lewis parameter Le prompts poor concentration ϕ and less layer thickness. Lewis parameter has a backwards association with Brownian movement. Bigger Lewis parameter corresponds to poor Brownian movement. Such poor Brownian movement exhibits a diminishment in concentration field. Fig. 13.14 exhibits varieties in concentration ϕ for Prandtl parameter Pr. Here bigger Prandtl parameter demonstrate a poor concentration. Fig. 13.15 portrays that an expansion in Brownian movement number Nb causes a poor concentration and less layer thickness. Effect of thermophoresis number Nt on concentration ϕ is plotted in Fig. 13.16. Here concentration ϕ and associated layer thickness are improved for bigger thermophoresis number. Table 13.2 exhibits the comparison for different estimations of α with exact arrangement. Table 13.2 presents an excellent agreement of HAM arrangement with existing exact arrangement in limiting situation. Table 13.3 is figured to investigate skin frictions $-C_{fx}\,\mathrm{Re}_b^{1/(n+1)}$ and $-C_{fy}\,\mathrm{Re}_b^{1/(n+1)}$ for different estimations of M, A and α. Skin frictions are higher for bigger magnetic number M, Sisko liquid parameter A and ratio number α. Table 13.4 exhibits Nusselt number $-\theta'(0)$ for different estimations of Pr, M, γ, Le, A, α, Nt and Nb. We watched that Nusselt number is independent for bigger Brownian movement number. It is additionally watched that impacts of Biot parameter and

magnetic number on Nusselt number have been very inverse.

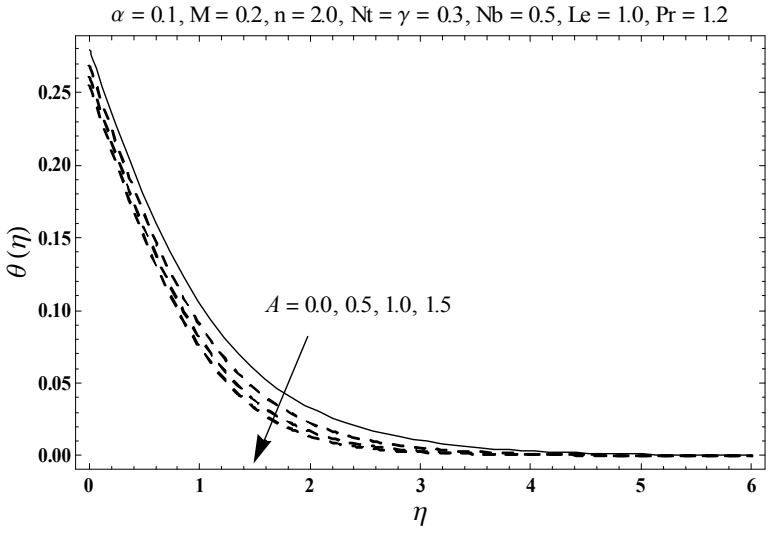

Fig. 13.3. Plots of $\theta(\eta)$ for A.

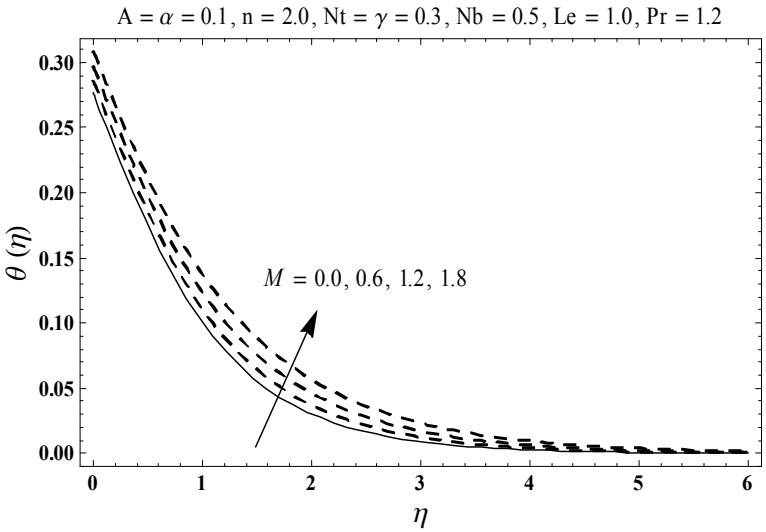

Fig. 13.4. Plots of $\theta(\eta)$ for M.

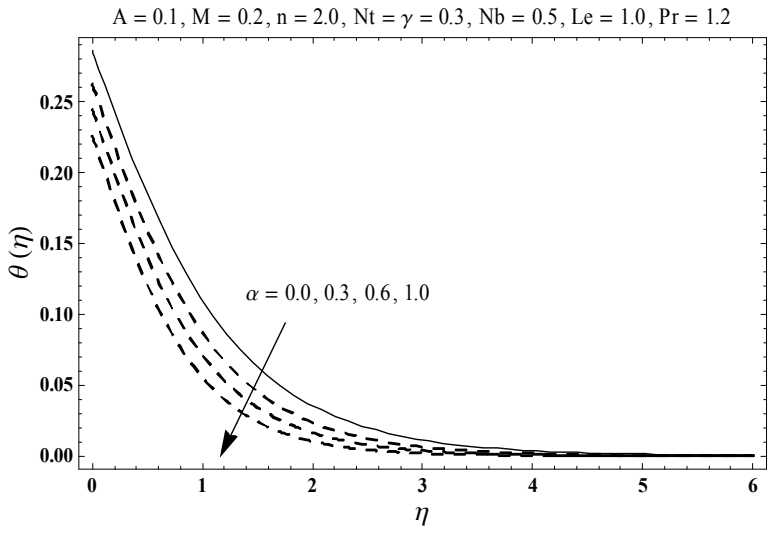

Fig. 13.5. Plots of $\theta(\eta)$ for α.

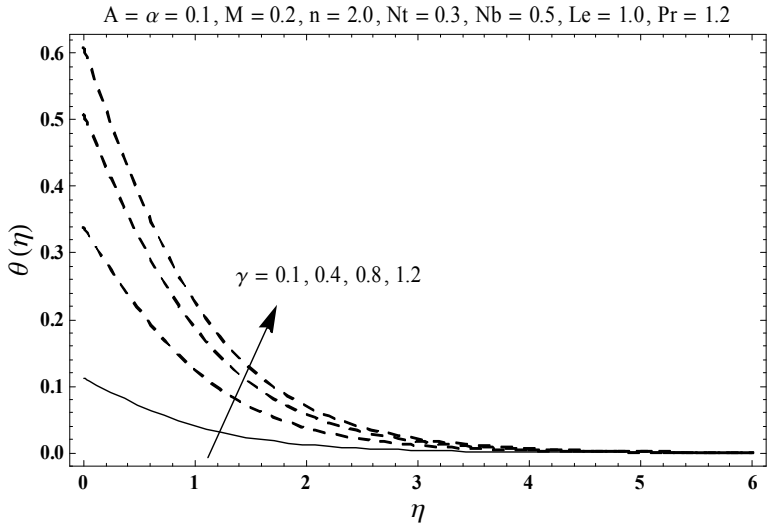

Fig. 13.6. Plots of $\theta(\eta)$ for γ.

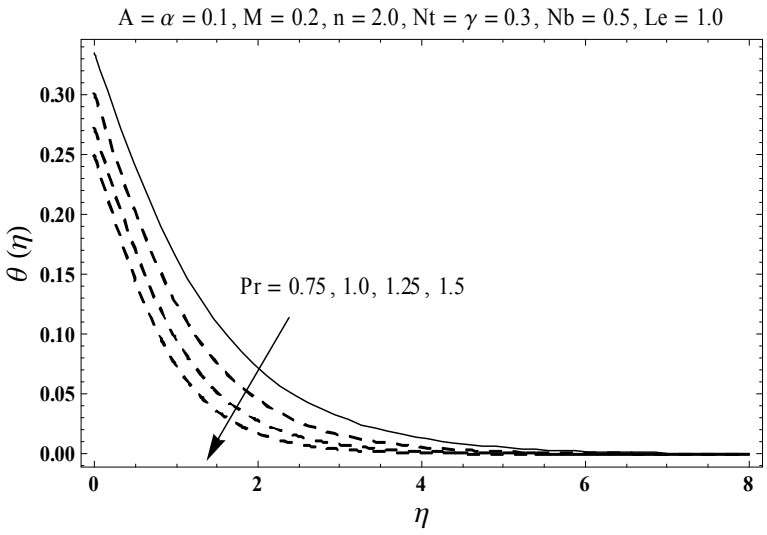

Fig. 13.7. Plots of $\theta(\eta)$ for Pr.

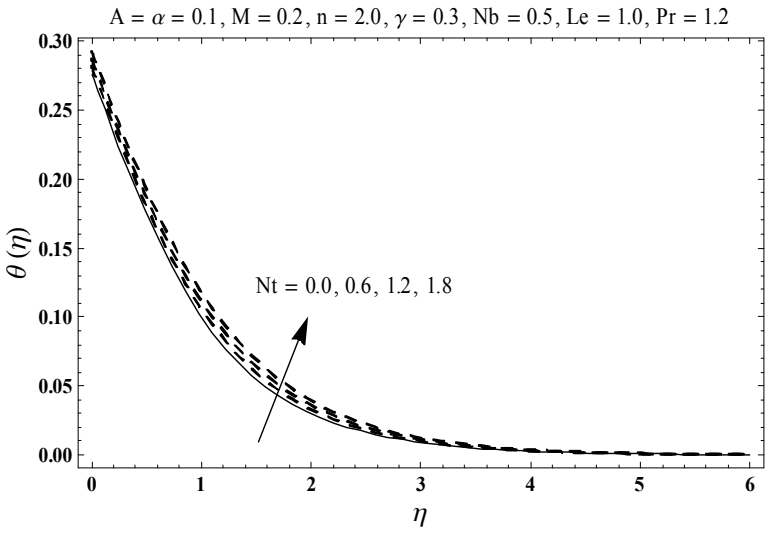

Fig. 13.8. Plots of $\theta(\eta)$ for Nt.

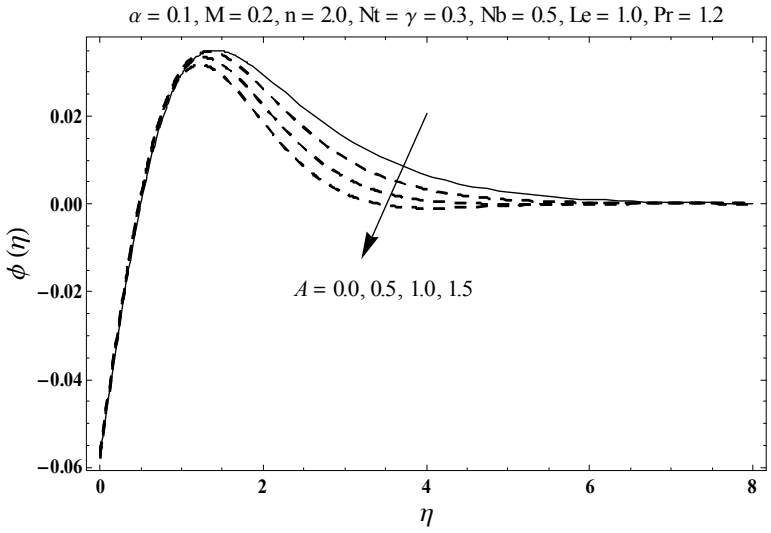

Fig. 13.9. Plots of $\phi(\eta)$ for A.

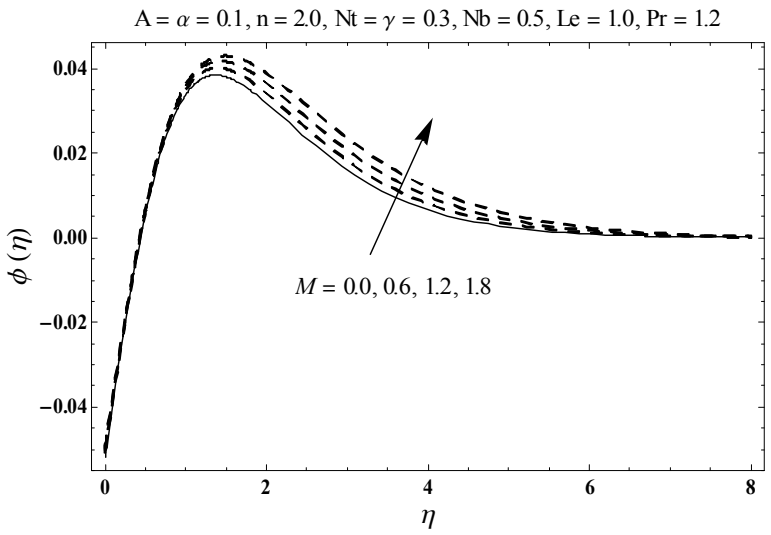

Fig. 13.10. Plots of $\phi(\eta)$ for M.

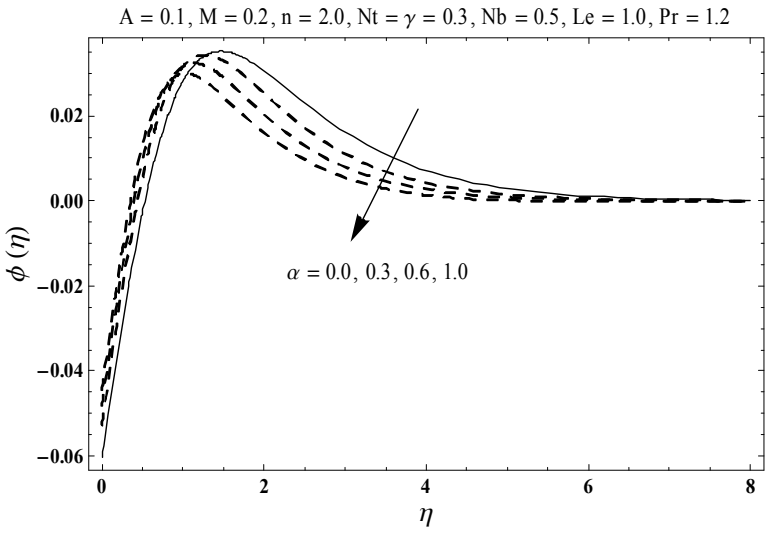

Fig. 13.11. Plots of $\phi(\eta)$ for α.

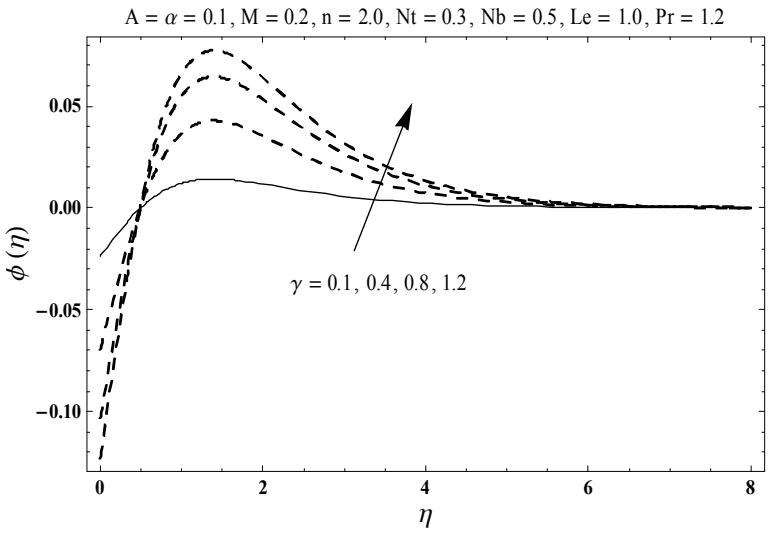

Fig. 13.12. Plots of $\phi(\eta)$ for γ.

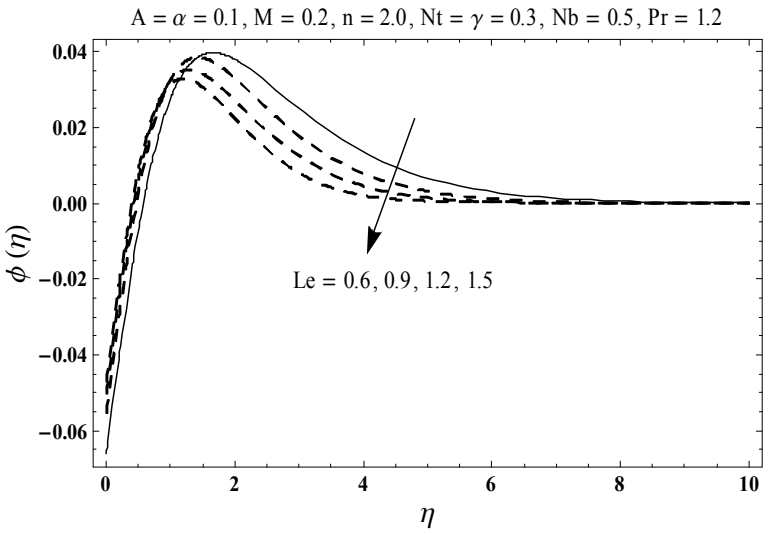

Fig. 13.13. Plots of $\phi(\eta)$ for Le.

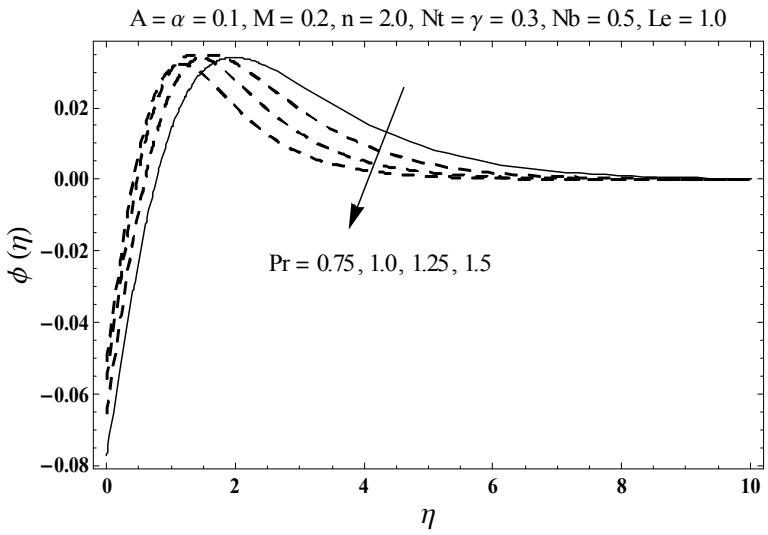

Fig. 13.14. Plots of $\phi(\eta)$ for Pr.

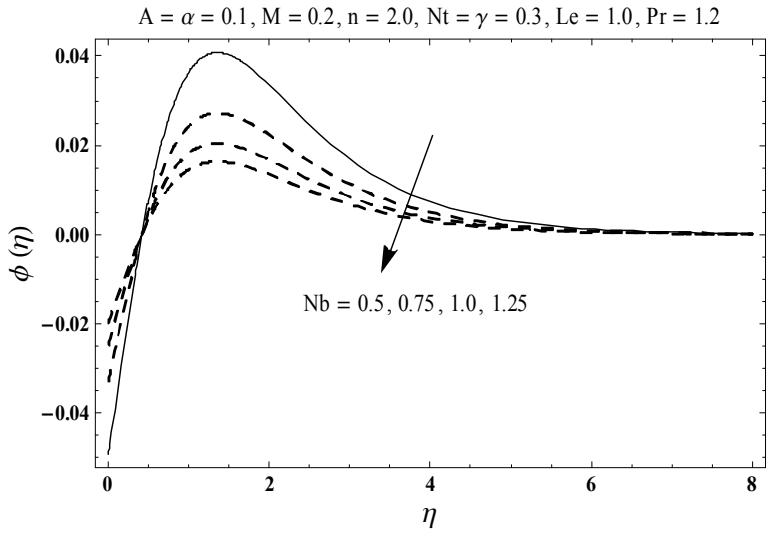

Fig. 13.15. Plots of $\phi(\eta)$ for Nb.

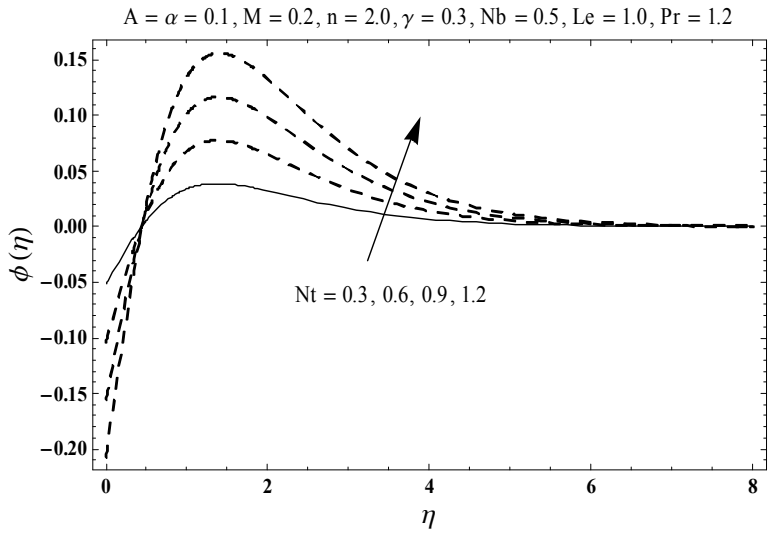

Fig. 13.16. Plots of $\phi(\eta)$ for Nt.

Table 13.2. Comparative estimations of $-f''(0)$ and $-g''(0)$ for several estimations of α when $n = 1$ and $A = M = 0$.

α	$-f''(0)$		$-g''(0)$	
	HAM	Exact [38]	HAM	Exact [38]
0	1	1	0	0
0.25	1.048811	1.048813	0.194564	0.194564
0.50	1.093095	1.093097	0.465205	0.465205
0.75	1.134486	1.134485	0.794618	0.794622
1.0	1.173722	1.173720	1.173722	1.173720

Table 13.3. Skin frictions $-C_{fx}\,\mathrm{Re}_b^{1/(n+1)}$ and $-C_{fy}\,\mathrm{Re}_b^{1/(n+1)}$ for various estimations of M, A and α.

A	M	α	$-C_{fx}\,\mathrm{Re}_b^{1/(n+1)}$		$-C_{fy}\,\mathrm{Re}_b^{1/(n+1)}$	
			$n = 1.0$	$n = 2.0$	$n = 1.0$	$n = 2.0$
0.0	0.2	0.1	1.0394	1.0050	0.0698	0.0703
0.5			1.2730	1.2076	0.0855	0.0850
1.0			1.4700	1.4714	0.0986	0.1060
0.1	0.0	0.1	1.0700	1.0264	0.0702	0.0709
	0.5		1.1907	1.1483	0.0873	0.0854
	1.0		1.4967	1.4824	0.1257	0.1233
0.1	0.2	0.0	1.0696	1.0210	0.0000	0.0000
		0.5	1.1650	1.1415	0.4987	0.4935
		1.0	1.2482	1.2497	1.2482	1.2497

Table 13.4. Numeric data of Nusselt number for various estimations of Pr, M, γ, Le, A, α, Nt and Nb.

A	M	α	γ	Le	Pr	Nb	Nt	$-\theta'(0)$	
								$n = 1.0$	$n = 2.0$
0.0	0.2	0.1	0.3	1.0	1.2	0.5	0.3	0.20870	0.21530
0.5								0.21230	0.21940
1.0								0.21440	0.22180
0.1	0.0	0.1	0.3	1.0	1.2	0.5	0.3	0.20990	0.21650
	0.7							0.20600	0.21430
	1.5							0.19440	0.20820
0.1	0.2	0.0	0.3	1.0	1.2	0.5	0.3	0.20570	0.21350
		0.5						0.22020	0.22500
		1.0						0.22860	0.23230
0.1	0.2	0.1	0.2	1.0	1.2	0.5	0.3	0.15540	0.15930
			0.7					0.34720	0.36620
			1.2					0.43580	0.46630
0.1	0.2	0.1	0.3	0.5	1.2	0.5	0.3	0.20990	0.21670
				1.0				0.20950	0.21650
				1.5				0.20920	0.21610
0.1	0.2	0.1	0.3	1.0	0.5	0.5	0.3	0.16880	0.17450
					1.0			0.20180	0.20850
					1.5			0.21820	0.22510
0.1	0.2	0.1	0.3	1.0	1.2	0.5	0.3	0.20960	0.21630
						1.0		0.20960	0.21630
						1.5		0.20960	0.21630
0.1	0.2	0.1	0.3	1.0	1.2	0.5	0.0	0.21030	0.21710
							0.5	0.20910	0.21580
							1.0	0.20750	0.21430

Chapter 14

Conclusions

The exploration performed in the present thesis is finished up through chapters two to thirteen. The prime target of every one of these chapters is to analyze the magnetohydrodynamic three dimensional (3D) boundary-layer flow of viscous and non-Newtonian nanoliquids due to extending surface. Analysis is carried out in both fixed and rotating frames. Buongiorno relation is adopted which includes the novel parts of Brownian dispersion and thermophoresis. Thermal convective and zero nanoparticles mass flux conditions are implemented at the boundary. Boundary-layer and low magnetic Reynolds parameter approximations are summoned to improve the governing arrangement of partial differential expressions. Appropriate transformations are introduced to nondimensionalize the relevant boundary-layer expressions. Uniformly valid convergent arrangement expressions are developed by means of homotopy analysis method (HAM) and optimal homotopy analysis method (OHAM). Importance of physical variables is described through the plots. Moreover the physical quantities like skin friction and Nusselt number are characterized by numerical estimations. Major outcomes of the presented research are summarized as follows:

- Concentration and temperature fields show expanding conduct for bigger magnetic number.
- Higher ratio number depict diminishing conduct for concentration and temperature.
- Bigger porosity and Forchheimer variables show expanding trend for concentration and temperature fields.

- Bigger Biot parameter causes an improvement in concentration and temperature fields.
- By improving thermophoresis number, an increment is watched in both concentration and temperature fields.
- Concentration field is diminished with an upgrade in Brownian movement number.
- There is decay in temperature and associated layer corresponding to Prandtl parameter.
- Concentration field and corresponding layer thickness are diminishing functions of Lewis parameter.
- Skin frictions are elevated when we upgrade estimations of magnetic number.
- Nusselt number is diminishment with an upgrade in thermophoresis number while it is independent of Brownian movement number.
- Both mass and heat transfer rates are higher for bigger concentration and thermal relaxation variables.

All chapters considered in this thesis examine the three dimensional (3D) flow problems of viscous and non-Newtonian nanoliquids due to extending surface. These problems can be extended to explore the more complicated situations in connection with three dimensional flow and extending surface. Some possible extensions of present thesis are given below.

- Three dimensional flow of nanoliquids in region of stagnation-point towards extending surface.
- Melting heat transfer effects on three dimensional flow of nanoliquids.
- Three dimensional flow problems of different non-Newtonian nanoliquids in the presence of mass and heat flux boundary conditions.
- Binary chemical reaction and activation energy aspects on three dimensional flow of non-Newtonian nanoliquids.
- Importance of homogeneous and heterogeneous reactions on three dimensional flow of non-Newtonian nanoliquids.

Bibliography

[1] S.U.S. Choi and J.A. Eastman, Enhancing thermal conductivity of fluids with nanoparticles, ASME International Mechanical Engineering Congress & Exposisition, American Society of Mechanical Engineers, San Francisco (1995).

[2] J. Buongiorno, Convective transport in nanoliquids, ASME J. Heat Transfer, 128(3) (2006) 240-250.

[3] O.D. Makinde and A. Aziz, boundary-layer flow of a nanoliquid past a extending surface with a convective boundary condition, Int. J. Thermal Sci., 50(7) (2011) 1326-1332.

[4] K.L. Hsiao, nanoliquid flow with multimedia physical features for conjugate mixed convection and radiation, Comp. Fluids, 104 (2014) 1-8.

[5] A.V. Kuznetsov and D.A. Nield, Natural convective boundary-layer flow of a nanoliquid past a vertical plate: A revised relation, Int. J. Thermal Sci., 77 (2014) 126-129.

[6] T. Hayat, T. Muhammad, A. Alsaedi and M.S. Alhuthali, Magnetohydrodynamic three dimensional flow of viscoelastic nanoliquid in the presence of nonlinear thermal radiation, J. Magn. Magn. Mater., 385 (2015) 222-229.

[7] A. Chamkha, S. Abbasbandy and A.M. Rashad, Non-Darcy natural convection flow for non-Newtonian nanoliquid over cone saturated in porous medium with uniform heat and volume fraction fluxes, Int. J. Numer. Methods Heat liquid Flow, 25(2) (2015) 422-437.

[8] T. Hayat, T. Muhammad, A. Qayyum, A. Alsaedi and M. Mustafa, On squeezing flow of nanoliquid in the presence of magnetic field effects, J. Mol. Liq., 213 (2016) 179-185.

[9] A. Malvandi, S. Heysiattalab and D.D. Ganji, Thermophoresis and Brownian motion effects on heat transfer improvement at film boiling of nanoliquids over a vertical cylinder, J. Mol. Liq., 216 (2016) 503-509.

[10] N. Shehzad, A. Zeeshan, R. Ellahi and K. Vafai, Convective heat transfer of nanoliquid in a wavy channel: Buongiorno's mathematical relation, J. Mol. Liq., 222 (2016) 446-455.

[11] M. Sheikholeslami, D.D. Ganji and M.M. Rashidi, Magnetic field effect on unsteady nanoliquid flow and heat transfer using Buongiorno relation, J. Magn. Magn. Mater., 416 (2016) 164-173.

[12] T. Hayat, T. Abbas, M. Ayub, T. Muhammad and A. Alsaedi, On squeezed flow of Jeffrey nanoliquid between two parallel disks, Appl. Sci., 6(11) (2016) 346.

[13] B.J. Gireesha, B. Mahanthesh, I.S. Shivakumara and K.M. Eshwarappa, Melting heat transfer in boundary layer stagnation-point flow of nanofluid toward a stretching sheet with induced magnetic field, Int. J. Eng. Sci. Tech., 19(1) (2016) 313-321.

[14] M.R. Eid, Chemical reaction effect on MHD boundary-layer flow of two-phase nanofluid model over an exponentially stretching sheet with a heat generation, J. Mol. Liq., 220 (2016) 718-725.

[15] M. Turkyilmazoglu, Condensation of laminar film over curved vertical walls using single and two-phase nanoliquid models, European J. Mech.-B/Fluids, 65 (2017) 184-191.

[16] M. Mustafa, M. Wasim, T. Hayat and A. Alsaedi, A revised relation to study the rotating flow of nanoliquid over an exponentially deforming surface: Numerical arrangements, J. Mol. Liq., 225 (2017) 320-327.

[17] T. Hayat, F. Haider, T. Muhammad and A. Alsaedi, On Darcy-Forchheimer flow of viscoelastic nanoliquids: A comparative study, J. Mol. Liq., 233 (2017) 278-287.

[18] T. Hayat, R. Sajjad, A. Alsaedi, T. Muhammad and R. Ellahi, On squeezed flow of couple stress nanofluid between two parallel plates, Results Phys., 7 (2017) 553-561.

[19] M. Sheikholeslami, T. Hayat, A. Alsaedi and S. Abelman, Numerical analysis of EHD nanofluid force convective heat transfer considering electric field dependent viscosity, Int. J. Heat Mass Transfer, 108 (2017) 2558-2565.

[20] T. Hayat, A. Aziz, T. Muhammad and A. Alsaedi, A revised model for Jeffrey nanofluid subject to convective condition and heat generation/absorption, Plos One, 12(2) (2017) e0172518.

[21] T. Hayat, A. Aziz, T. Muhammad and A. Alsaedi, Darcy-Forchheimer three-dimensional flow of Williamson nanofluid over a convectively heated nonlinear stretching surface, Commun. Theor. Phys., 68(3) (2017) 387-394.

[22] T. Hayat, A. Aziz, T. Muhammad and A. Alsaedi, Three-dimensional flow of nanofluid with heat and mass flux boundary conditions, Chinese J. Phys., 55(4) (2017) 1495-1510.

[23] A. Aziz, A. Alsaedi, T. Muhammad and T. Hayat, Numerical study for heat generation/absorption in flow of nanofluid by a rotating disk, Results Phys., 8 (2018) 785-792.

[24] M. Sheikholeslami, T. Hayat, T. Muhammad and A. Alsaedi, MHD forced convection flow of nanofluid in a porous cavity with hot elliptic obstacle by means of Lattice Boltzmann method, Int. J. Mech. Sci., 135 (2018) 532-540.

[25] M.R. Eid, K.L. Mahny, T. Muhammad and M. Sheikholeslami, Numerical treatment for Carreau nanofluid flow over a porous nonlinear stretching surface, Results Phys., 8 (2018) 1185-1193.

[26] M.J. Uddin, O.A. Beg and N. Amin, hydro-magnetic transport phenomena from a extending or shrinking nonlinear nanomaterial surface with Navier slip and convective heating: A relation for bio-nano-materials processing, J. Magn. Magn. Mater., 368 (2014) 252-261.

[27] Y. Lin, L. Zheng, X. Zhang, L. Ma and G. Chen, MHD pseudo-plastic nanoliquid unsteady flow and heat transfer in a finite thin film over extending surface with internal heat generation, Int. J. Heat Mass Transfer, 84 (2015) 903-911.

[28] M. Sheikholeslami, M.M. Rashidi, T. Hayat and D.D. Ganji, Free convection of magnetic nanoliquid considering MFD viscosity effect, J. Mol. Liq., 218 (2016) 393-399.

[29] F.M. Abbasi, S.A. Shehzad, T. Hayat and B. Ahmad, Doubly stratified mixed convection flow of Maxwell nanoliquid with heat generation/absorption, J. Magn. Magn. Mater., 404 (2016) 159-165.

[30] T. Hayat, T. Muhammad, S.A. Shehzad and A. Alsaedi, On three dimensional boundary-layer flow of Sisko nanoliquid with magnetic field effects, Adv. Powder Tech., 27(2) (2016) 504-512.

[31] S. Heysiattalab, A. Malvandi and D.D. Ganji, Anisotropic conduct of magnetic nanoliquids (MNFs) at filmwise condensation over a vertical plate in presence of a uniform parameter-directional magnetic field, J. Mol. Liq., 219 (2016) 875-882.

[32] T. Hayat, A. Aziz, T. Muhammad and A. Alsaedi, On magnetohydrodynamic three dimensional flow of nanoliquid over a convectively heated nonlinear extending surface, Int. J. Heat Mass Transfer, 100 (2016) 566-572.

[33] T. Hayat, M. Waqas, M.I. Khan and A. Alsaedi, Analysis of thixotropic nanomaterial in a doubly stratified medium considering magnetic field effects, Int. J. Heat Mass Transfer, 102 (2016) 1123-1129.

[34] A. Malvandi, A. Ghasemi and D.D. Ganji, Thermal performance analysis of hydro-magnetic Al_2O_3-water nanoliquid flows inside a concentric microannulus considering nanoparticle migration and asymmetric heating, Int. J. Thermal Sci., 109 (2016) 10-22.

[35] T. Hayat, T. Muhammad, S.A. Shehzad and A. Alsaedi, An analytical arrangement for magnetohydrodynamic Oldroyd-B nanoliquid flow induced by a extending surface with heat generation/absorption, Int. J. Thermal Sci., 111 (2017) 274-288.

[36] B.C. Sakiadis, boundary-layer behaviour on continuous solid surfaces: II. The boundary-layer on a continuous flat surface, AIChE J., 7(2) (1961) 221-225.

[37] L.J. Crane, Flow past a extending plate, Z. Angew. Math. Phys., 21(4) (1970) 645-647.

[38] C.Y. Wang, The three dimensional flow due to a extending flat surface, Phys. Fluids, 27(8) (1984) 1915-1917.

[39] P.D. Ariel, The three dimensional flow past a extending surface and the homotopy perturbation method, Comput. Math. Appl., 54(7-8) (2007) 920-925.

[40] H. Xu, S.J. Liao and I. Pop, Series arrangements of unsteady three dimensional MHD flow and heat transfer in the boundary-layer over an impulsively extending plate, Eur. J. Mech. B/Fluids, 26(1) (2007) 15-27.

[41] T. Hayat, M. Qasim and Z. Abbas, Homotopy arrangement for the unsteady three dimensional MHD flow and mass transfer in a porous space, Commun. Nonlinear Sci. Numer. Simul., 15(9) (2010) 2375-2387.

[42] I.C. Liu, H.H. Wang and Y.F. Peng, Flow and heat transfer for three dimensional flow over an exponentially extending surface, Chem. Eng. Comm., 200(2) (2013) 253-268.

[43] T. Hayat, T. Muhammad, A. Alsaedi and B. Ahmad, three dimensional flow of nanoliquid with Cattaneo-Christov double diffusion, Results Phys., 6 (2016) 897-903.

[44] W. Tan, W. Pan and M. Xu, A note on unsteady flows of a viscoelastic liquid with the fractional Maxwell relation between two parallel plates, Int. J. Non-Linear Mech., 38(5) (2003) 645-650.

[45] W.C. Tan and T. Masuoka, Stokes first problem for an Oldroyd-B liquid in a porous half space, Phys. Fluids, 17(2) (2005) 023101.

[46] L.B. Bergstrom, Transient growth of small disturbances in a Jeffrey liquid flowing through a pipe, liquid Dynamics Research, 32(1-2) (2003) 29-44.

[47] M. Sajid and T. Hayat, Wire coating analysis by withdrawal from a bath of Sisko liquid, Appl. Math. Comput., 199(1) (2008) 13-22.

[48] H. Darcy, Les Fontaines Publiques De La Ville De Dijon, Victor Dalmont, Paris, 1856.

[49] P. Forchheimer, Wasserbewegung durch boden, Zeitschrift, Ver D. Ing. 45 (1901) 1782-1788.

[50] M. Muskat, The Flow of Homogeneous Fluids through Porous Media, Edwards, MI, 1946.

[51] M.A. Seddeek, Influence of viscous dissipation and thermophoresis on Darcy-Forchheimer mixed convection in a liquid saturated porous media, J. Colloid Interface Sci., 293(1) (2006) 137-142.

[52] D. Pal and H. Mondal, Radiation effects on combined convection over a vertical flat plate embedded in a porous medium of parameter porosity, Meccanica, 44(2) (2009) 133-144.

[53] D. Pal and S. Chatterjee, mass and heat transfer in MHD non-Darcian flow of a micropolar liquid over a extending surface embedded in a porous media with non-uniform heat source and thermal radiation, Commun. Nonlinear Sci. Numer. Simulat., 15(7) (2010) 1843-1857.

[54] A.K. Singh, R. Kumar, U. Singh, N.P. Singh and A.K. Singh, Unsteady hydro-magnetic convective flow in a vertical channel using Darcy-Brinkman-Forchheimer extended relation with heat generation/absorption: analysis with asymmetric heating/cooling of the channel walls, Int. J. Heat Mass Transfer, 54(25-26) (2011) 5633-5642.

[55] B.J. Gireesha, B. Mahanthesh, P.T. Manjunatha and R.S.R. Gorla, Numerical arrangement for hydro-magnetic boundary-layer flow and heat transfer past a extending surface embedded in non-Darcy porous medium with liquid-particle suspension, J. Nig. Math. Soc., 34(3) (2015) 267-285

[56] T. Hayat, T. Muhammad, S. Al-Mezal and S.J. Liao, Darcy-Forchheimer flow with parameter thermal conductivity and Cattaneo-Christov heat flux, Int. J. Numer. Methods Heat liquid Flow, 26(8) (2016) 2355-2369.

[57] S.A. Shehzad, F.M. Abbasi, T. Hayat and A. Alsaedi, Cattaneo-Christov heat flux relation for Darcy-Forchheimer flow of an Oldroyd-B liquid with parameter conductivity and nonlinear convection, J. Mol. Liq., 224 (2016) 274-278.

[58] T. Hayat, F. Haider, T. Muhammad and A. Alsaedi, An optimal study for Darcy-Forchheimer flow with generalized Fourier's and Fick's laws, Results Phys., 7 (2017) 2878-2885.

[59] M.A. Sadiq, M. Waqas and T. Hayat, Importance of Darcy-Forchheimer relation in chemically reactive radiating flow towards convectively heated surface, J. Mol. Liq., 248 (2017) 1071-1077.

[60] T. Muhammad, A. Alsaedi, S.A. Shehzad and T. Hayat, A revised model for Darcy-Forchheimer flow of Maxwell nanofluid subject to convective boundary condition, Chinese J. Phys., 55(3) (2017) 963-976.

[61] T. Hayat, S. Farooq, B. Ahmad and A. Alsaedi, Peristalsis of Eyring-Powell magneto nanomaterial considering Darcy-Forchheimer relation, Int. J. Heat Mass Transfer, 115 (2017) 694-702.

[62] T. Hayat, F. Haider, T. Muhammad and A. Alsaedi, Darcy-Forchheimer flow due to a curved stretching surface with Cattaneo-Christov double diffusion: A numerical study, Results Phys., 7 (2017) 2663-2670.

[63] T. Hayat, R.S. Saif, R. Ellahi, T. Muhammad and B. Ahmad, Numerical study for Darcy-Forchheimer flow due to a curved stretching surface with Cattaneo-Christov heat flux and homogeneous-heterogeneous reactions, Results Phys., 7 (2017) 2886-2892.

[64] J.C. Umavathi, O. Ojjela and K. Vajravelu, Numerical analysis of natural convective flow and heat transfer of nanofluids in a vertical rectangular duct using Darcy-Forchheimer-Brinkman model, Int. J. Thermal Sci., 111 (2017) 511-524.

[65] T. Hayat, K. Rafique, T. Muhammad, A. Alsaedi and M. Ayub, Carbon nanotubes significance in Darcy-Forchheimer flow, Results Phys., 8 (2018) 26-33.

[66] T. Hayat, F. Haider, T. Muhammad and A. Alsaedi, Numerical study for Darcy-Forchheimer flow of nanofluid due to an exponentially stretching curved surface, Results Phys., 8 (2018) 764-771.

[67] J. Harris, Rheology and Non-Newtonian Flow, Longman, London, 1977.

[68] H. Schlichting, boundary-layer Theory, 6th ed. Mc-Graw Hill, New York, 1964.

[69] S.J. Liao, An optimal homotopy-analysis approach for strongly nonlinear differential expressions, Commun. Nonlinear Sci. Numer. Simulat., 15(8) (2010) 2003-2016.

[70] A.M. Megahed, parameter liquid properties and parameter heat flux effects on the flow and heat transfer in a non-Newtonian Maxwell liquid over an unsteady extending surface with slip velocity, Chin. Phys. B, 22(9) (2013) 094701.

Turnitin Originality Report

Three dimensional nonlinear flow problems in the presence of nanoparticles by Taseer Muhammad

From IRs (Institutional Repository)

Processed on 05-Mar-2018 14:32 PKT
ID: 925331477
Word Count: 37638

Similarity Index	Similarity by Source	
16%	Internet Sources:	4%
	Publications:	12%
	Student Papers:	7%

sources:

1 4% match (student papers from 19-Sep-2015)
Submitted to Higher Education Commission Pakistan on 2015-09-19

2 1% match (publications)
Hayat, T., Taseer Muhammad, S.A. Shehzad, M.S. Alhuthali, and Jinhu Lu. "Impact of magnetic field in three-dimensional flow of an Oldroyd-B nanofluid", Journal of Molecular Liquids, 2015.

3 1% match (publications)
Hayat, Tasawar, Taseer Muhammad, Sabir Ali Shehzad, and Ahmed Alsaedi. "Three-Dimensional Flow of Jeffrey Nanofluid with a New Mass Flux Condition", Journal of Aerospace Engineering, 2015.

4 1% match (publications)
Tasawar Hayat, Arsalan Aziz, Taseer Muhammad, Ahmed Alsaedi. "Darcy–Forchheimer Three-Dimensional Flow of Williamson Nanofluid over a Convectively Heated Nonlinear Stretching Surface", Communications in Theoretical Physics, 2017

5 1% match (publications)
Hayat, T., Taseer Muhammad, S.A. Shehzad, G.Q. Chen, and Ibrahim A. Abbas. "Interaction of magnetic field in flow of Maxwell nanofluid with convective effect", Journal of Magnetism and Magnetic Materials, 2015

6 1% match (publications)
Hayat, T., T. Muhammad, S. A. Shehzad, and A. Alsaedi. "Three-dimensional boundary layer flow of Maxwell nanofluid: mathematical model", Applied Mathematics and Mechanics, 2015.

7 < 1% match (Internet from 05-Oct-2017)
http://prr.hec.gov.pk/Thesis/2927S.pdf

8 < 1% match (student papers from 20-Dec-2017)
Submitted to Higher Education Commission Pakistan on 2017-12-20

9 < 1% match (publications)

Focal Person (Turnitin)
Quaid-i-Azam University
Islamabad

05/03/18